MODULATING SURFACE DIPOLES

IN FLUORINATED THIN FILMS

A Dissertation Presented to

the Faculty of the Department of Chemistry

University of Houston

In Partial Fulfillment

of the Requirements for the Degree of

Doctor of Philosophy

By

María De Jesús Márquez

December 2017

MODULATING SURFACE DIPOLES

IN FLUORINATED THIN FILMS

_____

María De Jesús Márquez

APPROVED:

_____

Dr. T. Randall Lee, Chairman

_____

Dr. Eva Harth

_____

Dr. Ognjen Š. Miljanić

_____

Dr. Steven Baldelli

_____

Dr. Ramon Colorado

_____

Dean, College of Natural Sciences
and Mathematics

Dedicated to my parents, husband, and sisters,

Lorenzo Márquez, Carlota García, Adrian Campa, Karina and Ileana Márquez

For the love and the outstanding support during my

Academic endeavor.

ACKNOWLEDGMENTS

First and foremost, I am deeply grateful to my research advisor Professor T. Randall Lee for giving me the opportunity to join the group and grow as a scientist. I would also like to extend my gratitude to my committee members Dr. Steven Baldelli, Dr. Ognjen Š. Miljanić, Dr. Eva Harth, and Dr. Ramon Colorado for the time taken out of their busy day to review this dissertation.

My deepest appreciation goes to Dr. Oussama Zenasni for his friendship and mentorship throughout my time at the University of Houston. I would also like to thank my editorial team, Dr. Oussama Zenasni and Daniela Rodriguez, for sacrificing their sleep to catch any "sprios" that might have slipped through and to make sense of this dissertation. I would like to thank my laboratory colleagues for their aid in some of the experimental procedures included in this dissertation: Dr. Oussama Zenasni for the synthesis of the F1H16SH, F1H17SH, H1F6H10SH, H1F6H11SH, H3F6H11SH, H4F6H11SH and H5F6H11SH adsorbates; Dr. Han Ju Lee for his help in the synthesis of the F1H18SH and F1H19SH adsorbates; and Daniela Rodriguez for the electrochemical deposition of silver monolayers used in Chapters 4 and 5. I would also like to thank Dr. Arkadiusz Czader for the molecular modeling of the H1F6HnSH and HnF6H11SH molecules.

My experience in graduate school would not have been as great as it was without the awesome members of the Lee group and their shenanigans. First of all, I would like to thank Johnson for just being Johnson; there are no words to capture his persona. My desk neighbors Tingting and Riddhiman for keeping the lab up to date on sports, even

during the stressful writing of this dissertation. Ploy for keeping everyone "cool" throughout the day and reminding everyone that "everything will be ok". Yi-Ting "Princess" for her royal presence and friendly advice. Sammy for his humor and encouragement in stressful situations. "Mr. Long" for ordering all of my chemicals and helping me with reaction workups and purifications, including the purification of "precious". Lydia and Youngblood (Will) for their wittiness and support. I would also like to thank previous members of the Lee group: Dr. Chien-Hung Li (Henry), Dr. Chul Soon Park, Dr. Amin Shakiba, Dr. Arati Kolhatkar, Dr. Orawan Khantamat, Dr. Da Hye Lee, and Diego. I would also like to thank Alan and Mohammed for the random conversations we have had throughout the years during our lunch / coffee breaks.

I would not have been able to finish my studies if it were not from the support of my husband, my family, and my cats. I want to especially thank Adrian, my husband, for his patience, cleaning the house, and meal prep during these hectic days. I am also grateful to my cats, Thor and Loki, for the emotional support, though they have no idea how helpful petting them really was for me. And finally, my parents for their endless love, support, and encouragement throughout my academic endeavor, an experience they did not have the luxury to experience themselves.

Mamá y Papá muchas gracias por todo el apoyo que me han brindado durante estos diez años de estudio.

Maria

MODULATING SURFACE DIPOLES

IN FLUORINATED THIN FILMS

An Abstract of a Dissertation

Presented to

the Faculty of the Department of Chemistry

University of Houston

In Partial Fulfillment

of the Requirements for the Degree of

Doctor of Philosophy

By

María De Jesús Márquez

December 2017

ABSTRACT

This dissertation investigates the effect a surface dipole has on the interfacial properties of partially fluorinated self-assembled monolayers (FSAMs). In the first study, the synthesis of a new type of partially fluorinated adsorbate of the form $CH_3(CF_2)_6(CH_2)_nSH$ where n = 10–13 was performed. On the surface, these adsorbates generate a novel hydrocarbon-fluorocarbon (HC-FC) dipole at the interface of the SAMs that has a profound effect on the wettability of the surfaces with various contacting liquids; specifically, the inverse odd-even effect observed with regard to the wettability of polar protic and aprotic liquids. Additionally, the properties of the HC-FC dipole were compared to those of a FC-HC (fluorocarbon-hydrocarbon) dipole derived from CF_3-termianted alkanethiols.

In efforts to understand further the effect of the new HC-FC dipole, an additional series of alkyl-terminated alkanethiols of the form $H(CH_2)_n(CF_2)_6(CH_2)_{11}SH$, where n = 1–7, was synthesized and used to form SAMs. In this study, the dipole was systematically buried in the film and analyzed with several contacting liquids. The effect of the dipole in these types of FSAMs appears to have a diminished effect after 3 hydrocarbons, after which an odd-even effect in the wettability was observed. The odd-even effects observed in the FSAMs were the opposite of that observed with normal alkanethiols of the same carbon length, which suggests that the orientation of the terminal methyl group is different from the normal alkanethiol.

Finally, to explore further the effect of the direction of the FC-HC and HC-FC dipoles, evaporated gold surfaces were electrochemically modified with a monolayer of

silver via underpotential deposition (UPD). The monolayer of silver has an effect on the structural features of the films caused by the different binding geometries of the sulfur on gold and silver. The structural difference between the two substrates inverts the odd-even effects for SAMs with a FC-HC dipole. For SAMs possessing a HC-FC dipole, the presence of silver on the gold surface also changes the orientation of the molecules on the different metals, influencing the physical and interfacial properties of the resulting films.

TABLE OF CONTENTS

LIST OF FIGURES

LIST OF SCHEMES

LIST OF TABLES

Chapter 1: Homogeneously Mixed Monolayers: Emergence of Compositionally Conflicted Interfaces

1.1. Introduction

Intermolecular interactions such as van der Waals or London dispersion forces govern much of the interfacial properties of materials that give rise to commonly observed behaviors such as the well known "like dissolves like" phenomenon that we utilize on a daily basis. For chemists, such rules have enabled the development of an array of tools, specialty materials, and purification processes that provide unquestionable benefits to society. While such intermolecular forces are generally applied to the three-dimensional world, they are also relevant to two-dimensional systems; for example, the structural quality of organic thin films of molecules assembled on solid substrates is greatly impacted by intermolecular van der Waals interactions.[1] More specifically, self-assembled monolayers (SAMs) composed of a blend of two chemically or structurally different adsorbates tend to undergo phase separation during film formation.[2-4] The resulting phase domains represent the degree of incompatibility between the different molecular components. Thus, the domain size, shape, and structural continuity reflect the relative presence of each component in the film and the interactions at their phase boundaries and with the interface.[2-4] Furthermore, forces exerted by these surfaces (attractive or repulsive) toward contacting matter are dictated by the relative exposure of these patches and their chemical compositions. Note that, the applicability of such forces relies on the ability to control the phase behavior of dissimilar molecular structures on the surfaces.

One goal of our recent research efforts in the area of mixed SAMs has been to generate and study unique nanoscale interfaces comprised of phase-incompatible chemical entities or other types of dissimilar molecular architectures by means of either designing molecular adsorbates bearing bifunctional moieties or thermodynamic conditions to yield such SAMs, as illustrated in Figure 1.1.[5,6] For this particular mixed-chain system, we concluded that the intimate blending of the oligoethylene glycol-terminated (OEG-terminated) chain with a hydrocarbon-terminated chain produced films that were more resistant to protein adsorption than that of a thin film exposing only the hydrocarbon chains, but less resistant than a film exposing only the OEG-terminated chains.[5]

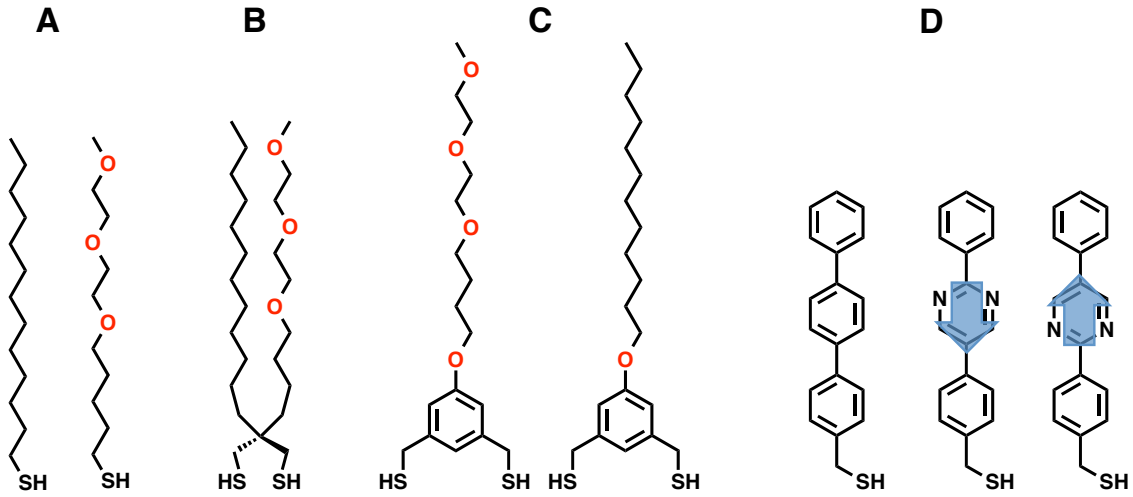

Figure 1.1. Illustration of adsorbates used for generating mixed SAMs from A) single-tailed adsorbates, B) a double-tailed adsorbate with a bidentate headgroup, C) single-tailed adsorbates with bidentate headgroups, and D) terphenyl-methanethiol molecules bearing a 2,5-pyrimidine moiety. Molecules shown in B and C represent means for producing a surface with an intimately mixed interface of phase-incompatible chains. Adapted from references 5, 6, and 25. Copyright 2016 American Chemical Society.

Tailoring SAM composition is essential for monolayer thin-film applications in areas such as protein adhesion/resistance in biological and medical applications,[7-12] friction reduction in microelectromechanical systems (MEMS),[13,14] nanoparticle coatings for colloidal stability,[15,16] controlled topological formation in mixed-adsorbate films,[17,18] and the mimicking of biochemical and biological processes.[19] Alkanethiols decorated with polar functional groups have been mixed with normal alkanethiols in order to dilute the presence of the active terminal group. For example, this technique has been used to improve click reactions of azido-terminated SAMs in efforts to install a maleimide group with the ultimate goal of creating a poly(L-lysine) interface,[20] to generate a biomimetic protein surface,[21] to incorporate ferrocene groups,[22] and to reduce steric hindrance in the photoswitching of azobenzenes.[23-25] Separately, the formation of mixed monolayer films via successive immersion of biomolecule-functionalized surfaces (e.g., DNA) in a secondary thiol solution is an effective tool for minimizing nonspecific adsorption in sensing applications.[26-28] Further, the recently reported work on terphenyl-methanethiol based SAMs, where the molecules bear a 2,5-pyrimidine moiety in the up and down orientation (Figure 1.1D), showed that the generation of mixed monolayers of these two adsorbates allows for a controlled tuning of the work function of the metal electrode while simultaneously eliminating any phase separation in the films, (i.e., consistent with a homogenous monolayer film).[25]

Additionally, incorporating the chemical functionalities of two separate adsorbates into one molecular structure influences the interfacial properties of the generated monolayer thin-films. For example, our group reported on the ability of a double-chained monothiol linactant -- a line-active adsorbate having an unsubstituted

hydrocarbon chain and a terminally perfluorinated chain segment -- to influence domain formation in binary SAMs.[29] By controlling the ratios of the adsorbates present in the deposition solution, a mixed SAM can be prepared from a combination of the double-tailed linactant and a *n*-alkanethiol, where the mixture forms single-dimensional patterns of the fluorinated chains embedded in the hydrocarbon matrix, as shown in Figure 1.2.

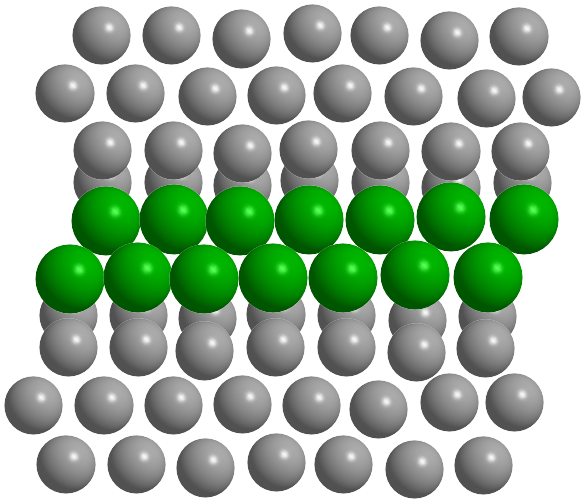

Figure 1.2. Illustration of a mixed SAM as viewed from above showing how adsorbates with two dissimilar chains avoid the formation of large domains (terminally fluorinated chains are represented by filled green circles). Reproduced with permission from reference 29. Copyright 2012 American Chemical Society.

This article seeks to highlight methods used to produce compositionally mixed interfaces derived from thiol-based adsorbates. In addition, we discuss both structural and systematic designs used to overcome incompatibility challenges encountered in nanoscale mixing. Hopefully, these efforts will inspire others to consider this new and exciting approach to the study and development of compositionally conflicted interfaces.

1.2. The Pursuit of Uniquely Blended Interfaces

1.2.1. Background

Prior reports describing the intimate blending of phase incompatible or structurally dissimilar motifs generally involved combining separate adsorbates for each of the surface chains, which led to a loss of homogeneity in the resulting film.[3,4,30,31] Efforts to resolve such problems in our laboratories have primarily involved the design and synthesis of multidentate adsorbates bearing a mixture of interfacial chains -- an approach to adsorbate design that enhances the stability and homogeneity of the resulting monolayer films. For monolayer films that have produced an interface of phase incompatible chains, the chains in conflict with each other generally have involved a combination of hydrocarbon chains versus fluorocarbon chains or chains terminated with polar groups such as oligoethylene glycol moieties (OEG).[3,32-35] However, other forms of dissimilarities have also been investigated, with a goal of achieving control over the interfacial characteristics for the resulting films.[36-38] This new emphasis on mixed-component thin-film design builds on more than two decades of fundamental research, which has revealed the challenges encountered in attempting to blend two dissimilar components in a single heterogeneous thin-film assembly.

1.2.2. Hydrocarbon Chains

Many of the initial systematic studies of self-assembled monolayers involved the use of a homologous series of normal alkanethiols; this history arose largely due to the commercial or synthetic accessibility of *n*-alkanethiols and their ability to generate well-ordered films. Therefore, initial attempts at creating and investigating homogeneously

mixed SAMs have pursued a number of routes towards film formation starting with normal alkanethiol chains mixed with either methyl or polar termini; some examples include: (1) the co-adsorption of different alkanethiols in a single solution,[39-43] (2) the immersion of an alkanethiolate film into the solution of a second alkanethiol in either an exchange or a backfilling process,[33,44,45] and (3) the adsorption of unsymmetrical disulfides.[46,47] With the preparation of binary SAMs from a mixed-thiol solution, several authors have noted that the composition of the adsorbate within the fully formed film departs from those in solution due to a number of factors that include: ongoing exchange processes with the solution phase, surface migration of the adsorbates (and the associated domain formation, which typically favors adsorption of one adsorbate over another), and differences in adsorbate solubility. Bain et al. noted that for mixed adsorbate SAMs formed from *n*-alkanethiols of different chain lengths, $CH_3(CH_2)_nSH$ (n = 11, 15, and 21) and $HO(CH_2)_mSH$ (m = 11 and 19), the longer chains preferentially adsorb over the shorter chains.[41] Furthermore, nanoscale phase separation can occur between molecules of the same chain length bearing different chemical functionality at their termini (i.e., different tailgroups).[2,4,30,31,36] Mixed SAMs derived from methyl- and methyl ester-terminated thiols having the same alkyl chain length, $CH_3(CH_2)_{15}SH$ and $CH_3O_2C(CH_2)_{15}SH$ for example, experience similar intermolecular interactions between the alkyl chains, yet still phase separate into two-dimensional assemblies to form separate domains.[30]

Several studies have investigated the factors that control the formation of domains in these types of mixed films. For example, Tamada et al. demonstrated that the deposition conditions can be controlled to form mixed films from *n*-alkanethiols having

significantly different chain lengths (4 and 18 carbon difference) so that the adsorbates separate into nanometer-scale domains ranging in size from 10 to 20 nm.[31] In a separate study by Chen et al. involving mixed *n*-alkanethiols with similar chain dynamics (4 to 10 carbon difference), the authors concluded that phase separation and preferential adsorption (where one adsorbate is preferred over the other) can also be attributed to defects in the gold substrate or to defects that occur as a consequence of the deposition temperature.[48] The authors also suggested that deposition at higher temperatures (e.g., 50 °C or higher) follows a kinetically controlled process, whereas at lower temperatures (e.g., room temperature or lower), it follows a thermodynamically controlled process. In the latter (occurring at low temperatures), the rapid formation of the SAM can lead to either an incomplete film or a film with defects caused by the underlying gold surface. Therefore, adsorbates having shorter chain lengths in such a SAM are readily exchanged by longer chain adsorbates in solution. In contrast, the kinetically controlled process (occurring at high temperatures), leads to a SAM with few defects (i.e., a compact monolayer) unable to undergo exchange with thiols in solution.

In a frictional-force microscopy study of mixed *n*-alkanethiol monolayers that was accompanied by STM imaging, Zuo et al. were able to correlate gauche defects in the film and lubricity.[49] They concluded that there is an enhancement in lubricity when the two *n*-alkanethiol chains have only small differences in chain length (i.e., two methylenes) and fail to phase separate into islands larger than a few molecules, rather than an anticipated increase in friction (see Figure 1.3). The friction-versus-load graphs in Figure 1.3d depict this trend on mixed SAMs formed from an equimolar solution of C14 with C15, C16, or C18. Mixed monolayers formed from adsorbates with small

difference in chain length (e.g., C14 and C15) showed a reduction in the friction as the load was increased when compared to SAMs derived from only C14. In contrast, when the difference in chain length was large (e.g., C14 with C18) an increase in the friction was observed. In addition, their observations led them to conclude that there is a competition between entropy (random ordering) and energy (van der Waals attractions) in which binary mixtures of adsorbate chain lengths with a two methylene chain difference favor homogeneous mixing, whereas the thiolate mixtures with a larger difference in chain length (four methylenes) are inclined to phase segregate, a result that is visible in the STM images in Figure 1.3. With the increase in domain size, the frictional properties of the resulting mixed film seemed to align with that of a single-component film. The effect of the surface composition of a mixed SAM on the frictional properties is also evident in Figure 1.3e, where a large difference in the solution concentration of adosrbates, for example 9:1 and 1:9 C14:C16, gave rise to SAMs predominantly composed of a single type of adsorbate, with frictional properties similar to those of a single-component SAM. In contrast, mixed solution compositions of 3:7, 7:3, or equimolar C14:C16 led to the formation of monolayers with lower frictional responses than that of a single-component SAM. These results were interpreted to indicate that, in addition to the often-encountered phase separation in mixed monolayers formed from the solution-based co-adsorption of thiols, the surface composition of adsorbates in the generated mixed-SAMs also differed from the ratio of adsorbate molecules in solution.[40,50-55] Thus, homogeneously mixed binary SAMs of monothiols are difficult to obtain from a simple solution-phase co-deposition process.

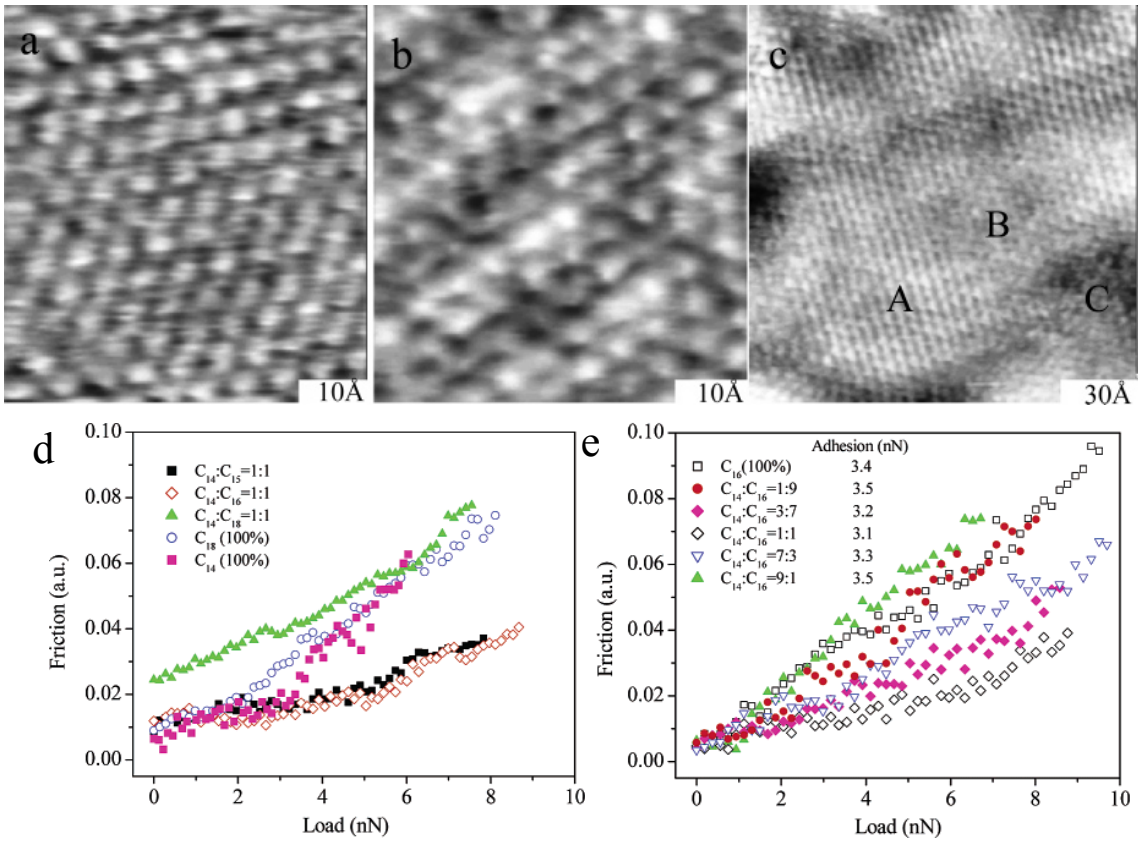

Figure 1.3. STM images of mixed SAMs formed from (a) $CH_3(CH_2)_5SH$ (C6), (b) mixture of $CH_3(CH_2)_5SH$ (C6) and $CH_3(CH_2)_7SH$ (C8), and (c) mixture of $CH_3(CH_2)_5SH$ (C6) and $CH_3(CH_2)_9SH$ (C10) with A, B, and C indicating the presence of C10, a mixture C6 and C10, and C6, respectively. Friction-versus-load curves are shown for (d) equimolar mixtures of C14 with C15, C16, and C18 and (e) C14 mixed with C16 at various concentrations. Reproduced with permission from reference 49. Copyright American Chemical Society 2005.

An alternative procedure for forming mixed SAMs takes advantage of exchange processes between surface-bound thiols and those dissolved in solution. In this approach, a preformed monolayer is dipped into a solution containing a different thiol to replace some of the adsorbates in the original monolayer and generate a new mixed-adsorbate film. The rate at which a thiol-based adsorbate on gold is replaced depends on the quality/packing of the initial SAM.[3,56,57] Chidsey et al. found that the replacement of bound thiols occurs rapidly at defect sites, concluding that the exchange (replacement)

rate depends on the packing characteristics of the molecules on the surface, as determined using electrochemical techniques.[56] Separately, Chung et al. quantified the replacement of compact and non-compact monolayers using Fourier transform infrared (FT-IR) spectroscopy.[57] In the case of a compact monolayer, $CH_3(CH_2)_{19}SH$, being replaced by its deuterated analog, $CD_3(CH_2)_{19}SH$, a fast replacement of ~25% of the monolayer was observed within a 15-min window (see Figure 1.4A). On the other hand, when a non-compact monolayer derived from ferrocene-terminated alkanethiols was replaced with an alkanethiol of the same hydrocarbon chain length, $CH_3(CH_2)_{11}SH$, a rapid exchange occurred in which ~55% of the monolayer was replaced within 15 minutes (see Figure 1.4B).

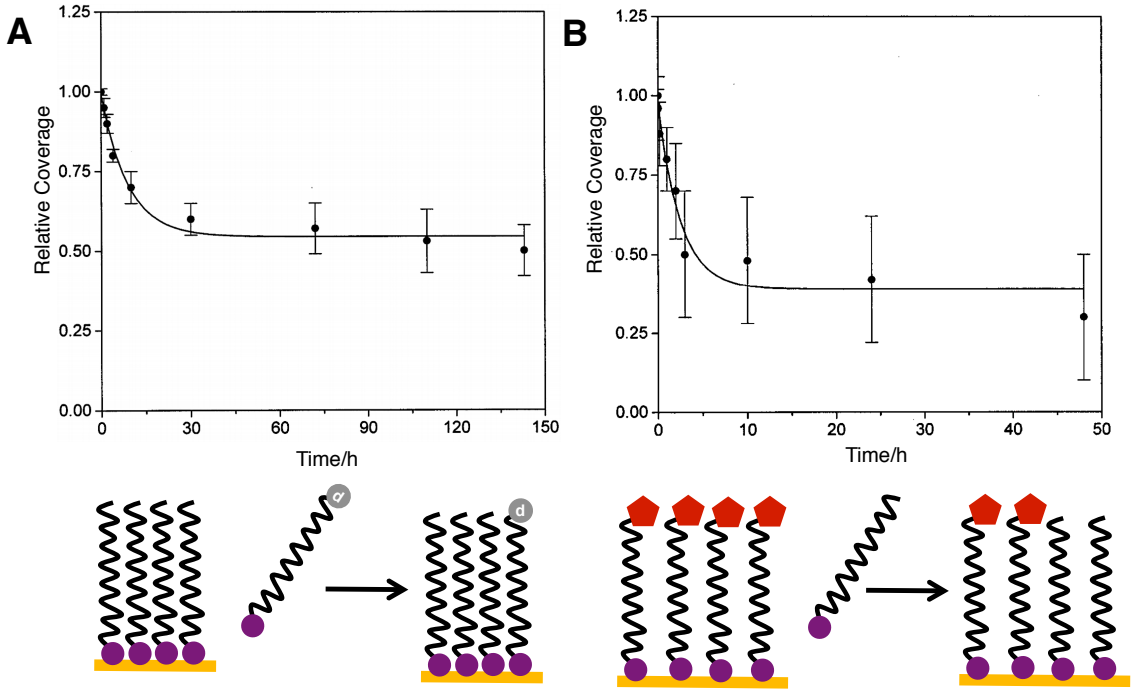

Figure 1.4. Relative coverage of (A) $CH_3(CH_2)_{19}SH$ in a SAM dipped in a $CD_3(CH_2)_{19}SH$ solution and (B) ferrocene-terminated thiols in a SAM dipped in $CH_3(CH_2)_{11}SH$ solution over time. Adapted with permission from reference 57. Copyright Elsevier 1999.

Intermolecular forces have also been attributed to exert an effect on the rate of replacement in SAMs. For example, replacement of *n*-alkanethiolates by carboxy-terminated alkanethiols (i.e., two adsorbates with phase-incompatible termini: $CH_3(CH_2)_{15}SH$ and $HO_2C(CH_2)_{11}SH$) has been described as having first-order kinetics and occurring domain-wise rather than randomly.[3] In this type of system, the solubility of the carboxylic acid-terminated adsorbates within the ordered alkanethiolate matrix is low. When the opposite process was tested -- a SAM formed from carboxy-terminated adsorbates dipped in a normal alkanethiol solution -- the authors found that the adsorbate exchange was much slower. The authors attributed this result to intermolecular H-bonding between the carboxylic acid termini in the existing monolayer. Additional studies using this technique have revealed that exchange processes occur mainly at domain boundaries and gold-defect sites, which limits the effectiveness of this procedure for generating homogeneously blended binary SAMs.[37,38,58]

Another means of generating mixed films is the backfilling method. Spencer and co-workers demonstrated this procedure, which involves the insertion of a gold-coated slide into an initial deposition solution containing one thiol, followed by a slow withdrawal of the slide from the solution.[33] This process produces a thin monolayer film that is sparsely populated with adsorbates at the end of the slide that was first withdrawn, but densely populated at the end that is last to leave the solution. A rapid withdrawal and rinsing procedure can produce an initial array of adsorbates that are evenly distributed across the substrate. Subsequent immersion of the gold substrate into a second thiol solution, allows the second thiol to backfill the unoccupied area on the substrate. It is important to note that the backfilling process can also give rise to exchange processes,

which might produce inhomogeneity in the resulting mixed films.

In the 1990s, SAMs formed from linear disulfides (i.e., having no cyclic moiety such as structure **1** in Figure 1.5) were extensively studied and compared to films derived from *n*-alkanethiols. In principle, unsymmetrical disulfides should form homogeneously mixed binary SAMs upon adsorbing to the surface of gold. Investigations by Bain et al. found that films developed from disulfides expose the same chemical termini (functional group) at their interface as SAMs formed from comparable alkanethiols.[46] This particular report also noted a greater presence of disorder in the hydrocarbon segment of disulfide films as compared to films derived from thiols, concluded from measurements of the contact angles of hexadecane. Additionally, the authors described the adsorption of alkanethiols as being faster than that of disulfides, likely due to the steric hindrance of the disulfide headgroup upon approach to the surface of gold as well as the greater bulk of the disulfide structure in general. This assessment was further confirmed in a separate account by the same authors through wettability comparisons.[59] The latter study revealed that films formed from disulfides are more wettable than those formed from thiols, indicating a slightly disordered film of the former adsorbates due to a less efficient film formation process. Chen et al. compared films formed from unsymmetrical and symmetrical disulfides, along with the corresponding thiols, and found that homogenously mixed films formed from the disulfides with low surface coverage (as expected for disulfides), while phase-separated structures were present in the SAMs formed from mixed alkanethiols, although with high surface coverage (as expected for alkanethiols).[60]

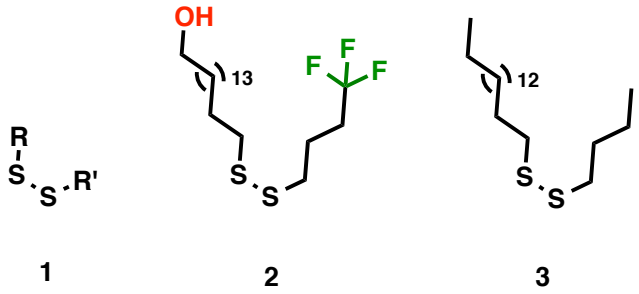

Figure 1.5. Structures of disulfide adsorbates used for fundamental studies for generating monolayer films.[61,62]

Biebuyck et al. examined the adsorption of disulfides, where the length of the two terminally-substituted alkyl chains (R and R') was different (i.e., structure **2** in Figure 1.5).[44] Although XPS results initially revealed approximately equal proportions of the two components on the surface, the authors noted that exposure to an ethanolic solution containing $HS(CH^2)^{16}CN$ led to the preferential displacement of the shorter perfluoromethyl-terminated alkyl chain. Beulen prepared systems involving the adsorption of dialkyl disulfides of different chain lengths (i.e., structure **3** in Figure 1.5), which revealed a preferential adsorption for the longer chain over the shorter chain over time; a phenomena observed in SAMs formed from the adsorption of a mixture of alkanethiols.[47] Considering that each of the disulfides noted above produced mixed SAMs composed of stable adsorbates that are subject to exchange processes with adsorbates in solution, the resulting SAMs were also subject to a loss of homogeneity during monolayer development.

A more precise exchange method that has been investigated in an effort to produce binary mixed interfaces without domain formation starts with single-component SAMs formed from alkanethiolate adsorbates, which are then irradiated with light. This approach, known as the irradiation-promoted exchange reaction (IPER), operates on the

basis of removing adsorbates from the surface using irradiation to degrade some of the chains and promote exchange processes that lead to the insertion of a dissimilar adsorbate into the existing SAM.[63,64] Using this method, mixed films have been successfully produced in which the content of the second adsorbate is controlled by the irradiation dose.[64-66] This process appears to produce surfaces having "conflicted" character, but the resulting thiolate films are assembled with the premise that all of the degraded adsorbates will desorb and be replaced, and after exchange, only pristine adsorbates will remain in the film.

For the systems reviewed in this section, the structural differences between the chains that produced the mixed films are minor, and van der Waals attractions between alkyl chains play a large role in both stabilizing the assembly and limiting the influence of any structural differences upon domain formation; however, it is apparent that binary thiolate SAMs favor the development of domains.[2-4,29-31,34,36,58,60,67] As detailed in the following sections, increasing the contact area for phase-incompatible moieties within mixed-chain assemblies significantly increases the challenges for producing binary SAMs in which the chains are homogeneously intermixed.

1.2.3. Fluorocarbon Chains

The use of fluorinated adsorbates in thin-film technology has enjoyed widespread use in advanced applications due to their (1) hydrophobicity and non adhesiveness, (2) chemical and biological inertness, (3) thermal and nanomechanical stability, (4) resistance to oxidation and corrosion, and (5) ease in the ability to manipulate the structure of the adsorbate synthetically.[68-70] Furthermore, the ability of fluorinated chain

segments to beget structural ordering within mixed films that reflects their phase incompatibility with other organic moieties reveals the rigidity and stability that such a segment imparts to the film.[29,71]

Some of the first studies of mixed fluorocarbon–hydrocarbon monolayers arose from research on Langmuir-Blodgett (LB) films of partially fluorinated or perfluorinated carboxylic acids and phosphonic acids mixed with their hydrocarbon counterparts.[71-73] Studies performed with fatty acids having extended hydrocarbon chains mixed with partially fluorinated carboxylic acids, $CF_3(CF_2)_8(CH_2)_2$-O-$(CH_2)_2COOH$, that incorporated either an ether linkage or ester group, produced domains or "islands" within a continuous phase that could be differentiated by their interfacial frictional properties via atomic force microscopy (AFM), Figure 1.6.[71,72]

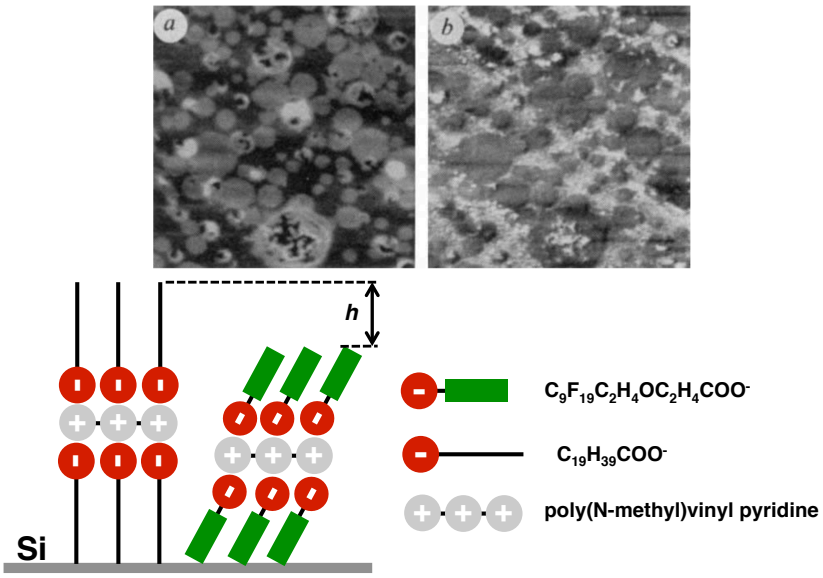

Figure 1.6. AFM images and a schematic of a bilayer surface generated from an equimolar mixture of fluorocarbon and hydrocarbon carboxylates; the difference in height between the two systems is denoted by *h*. (a) Demonstrates the topographical image, where the fluorocarbons are the flat portion and the hydrocarbons the circular structures, and (b) the lateral force image of the same area. The bright areas on the image denote areas of higher friction. Adapted with permission from reference 71. Copyright 1992 Nature Publishing Group.

When the two acids were the same length, phase separation was observed in which the alkylated acid formed circular domains within a sea of the partially fluorinated molecules. As the length of the alkylated acid was decreased, the shape of the circular domains became disordered. The authors explained the phase structures observed in these early studies of mixed alkyl/fluoroalkyl films through the influence of attractive dispersive interactions and entropic effects. With the longer chains, the attractive forces between the chains minimized their surface energy, giving rise to circular islands; whereas with the shorter chains, entropy began to favor disordered structures.[71,72] In addition, the perfluorinated structures in these types of films appeared to be less ordered than their longer hydrocarbon counterparts.[73]

A separate study involving mixtures of non-fluorinated, $CH_3(CH_2)_{n-2}COOH$ where n = 18, 20, 22, 24, and perfluoropolyether (PFPE) point toward phase separation also being dependent upon the chain length of the carboxylic acid along with the surface pressure.[74] Additionally, the size of the domains that can form in LB monolayers from partially fluorinated phosphonic acid adsorbates [$CF_3(CF_2)_7(CH_2)_{11}PO_3H_2$, $CF_3(CF_2)_9(CH_2)_6PO_3H_2$, $CF_3(CF_2)_7(CH_2)_8PO_3H_2$, $CF_3(CF_2)_5(CH_2)_{10}PO_3H_2$] have been shown to depend on the relative length of the fluorocarbon and hydrocarbon chain segments within the molecular structure, and that these adsorbates can form equilibrium phase structures that persist even in the presence of an excess of a nonfluorinated phase.[75] The authors, Trabelsi et al., concluded in a second study that the larger diameter of the overlying perfluorinated chain segments, as compared to the hydrocarbon chain segments (i.e., the alkyl spacers), led to packing arrangements in which the adsorbates splayed to form domain structures of characteristic sizes and dimensions.[18] For all of these partially

fluorinated LB films, the perfluorinated chain segments played an important role in the organization of the resulting monolayer film, including the formation of persistent phase structures.

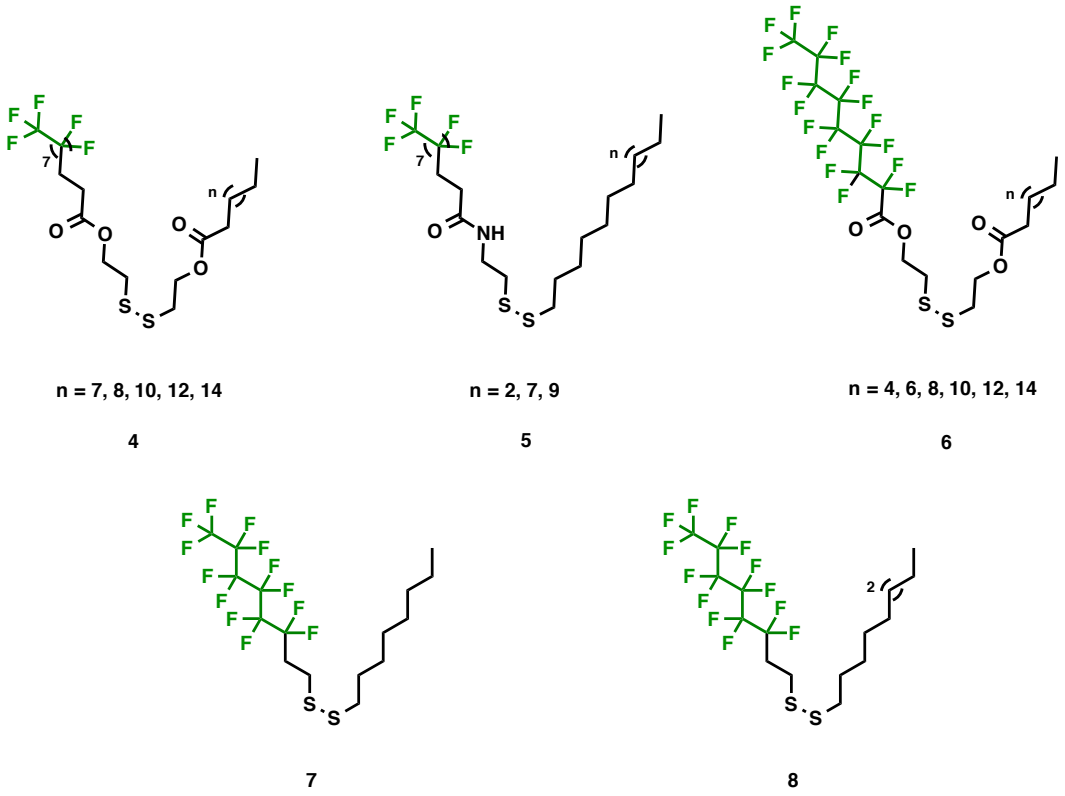

Figure 1.7. Structures of fluorinated disulfide adsorbates used for fundamental studies in the generation of mixed monolayer films.[32,76]

Schönherr et al. studied the adsorption of unsymmetrical disulfides containing terminal alkyl and fluorinated alkane chains and compared the resulting SAMs to monolayers produced from analogous thiols (i.e., structures **4-6** in Figure 1.7).[76] The authors concluded from contact angle studies that the monolayers derived from the mixed-chain disulfides were well packed and displayed wetting properties that were intermediate to those of the single-component SAMs formed from the corresponding *n*-alkanethiols.

Ishida et al. explored the films formed from a series of unsymmetrical disulfides having alkane and fluoroalkane chains (i.e., structure **7** in Figure 1.7).[67] Their study revealed that cleavage of the S-S bond occurs on the surface of the gold, and that the films exhibit phase separation upon annealing for 8 h at 100 °C. Separately, Fujihira and co-workers examined the reductive desorption of mixed-chain disulfides (i.e., structure **8** in Figure 1.7) on Au(111) electrodes using cyclic voltammetry (CV).[62] These authors found that a high concentration (i.e., ranging from 10 to 100 μM) of the disulfide in solution produced a relatively homogenous film, but if the adsorption temperature was too high (i.e., 60 °C maximum), or was elevated for too long, phase separation occurred (i.e., separation was visible at 1 h, 10 h, and 22 h). Thus, both of these studies are consistent with a model of film development that involves an initial homogeneous distribution of chemical heterogeneity on the surface, followed by temperature-induced surface rearrangement of the adsorbates leading to phase separation.

As with mixed SAMs of alkanethiols having different chain lengths, mixtures of fluoroalkane and normal alkanethiols [$CF_3(CF_2)_7CONH(CH_2)_2SH$ with $C_nH_{(2n+1)}SH$ where n = 12, 16, 18] produced phase-separated structures, even when developed in solutions with equimolar concentrations.[32] The contributing factors for the resulting film compositions for these mixed-thiolate SAMs are the same as those for mixtures of alkanethiols of different chain lengths (vide supra). Furthermore, such a competitive adsorption phenomenon was also observed in mixed films where both components were terminated with fluorinated alkane chains in which the longer chain was preferentially adsorbed over the shorter chain, $CF_3(CF_2)_7(CH_2)_{11}SH$ and $CF_3(CF_2)_7(CH_2)_2SH$.[77] Similarities between mixed-adsorbate films incorporating only non-fluorinated thiolates

versus those including chains with extended fluorinated segments also include the ability to produce homogeneously blended binary SAMs from disulfides, as described in a report by Tsao et al.[32] However, such films are subject to the same exchange/adsorbate migration processes that were noted above. An investigation of the exchange reactions of an alkanethiol SAM, $CH_3(CH_2)_7SH$, by a partially fluorinated thiol, $CF_3(CF_2)_6(CH_2)_2SH$, and vice versa, gives insight into island formation for each process. First, the replacement of a fluorinated thiolate in a single-component SAM by a normal alkanethiol is a slow process and occurs via the formation of an ordered array, likely due to the lack of domain boundaries in such SAMs. Second, the opposite dynamic, replacement of an alkanethiolate in a single-component SAM by a fluorinated thiol, is a much faster process that occurs mainly at domain boundaries. Third, due to the larger size of the fluorinated molecule, fluorinated domains were not observed embedded in the hydrocarbon matrix, and a more homogeneous distribution of the embedded adsorbate was observed.[34]

1.2.4. OEG-Terminated Chains

Mixed films that incorporate the OEG moiety into the chain terminus with other organic molecules have been shown to have anti-adhesive character toward biomolecules or can be tailored for specific adsorption of certain proteins for use as biosensors, giving promising applications in biomedical research.[7,8,12,35,78-80] The amount of OEG present on the surface plays an important role in the anti-adhesive character of these types of films. In a specific example, Prime and co-workers examined the adsorption of several proteins on mixed SAMs composed of an OEG-terminated alkanethiol and a hydroxyl-terminated alkanethiol.[78] The films with a higher concentration of OEG-terminated alkanethiols demonstrated higher resistance to the kinetically irreversible, nonspecific protein

adsorption. For the films possessing longer OEG moieties, resistance to protein adsorption was achieved even at lower concentration in the films.

The previously described techniques, co-adsorption, backfilling, and photolithography, have been used to produce mixed-films containing the OEG moiety. Montague et al. used scanning

near-field photolithography to pattern a surface and then covalently attach proteins to it.[81] The technique works by generating sulfonates that are formed rapidly followed by immersion into the second component, but the degradation of the OEG chains, a slower but present reaction, can be problematic. A description of the scanning near-field photolithography process can be found in the literature, and is illustrated in Figure 1.8.[82] Additionally, Zharnikov and co-workers have used IPER to generate mixed SAMs designed for the specific adsorption of avidin in which the composition of the OEG-terminated alkanethiol and biotin-terminated alkanethiol can be controlled by the irradiation dose.[80] The IPER technique has also been applied to pattern films using disulfides terminated with an atom transfer radical polymerization (ATRP) initiator in efforts to grow complex polymers on the surface, such as poly(ethylene glycol dimethacrylate), a polymer relevant for use in biomedical devices.[83]

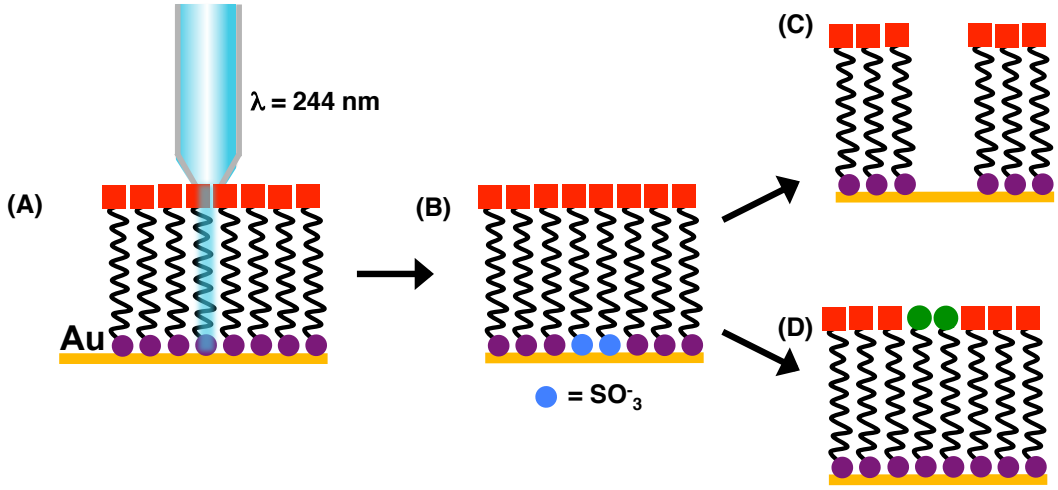

Figure 1.8. Patterning SAMs on gold surfaces using scanning near-field photolithography. This process includes: (A) scanning the SAM using UV light; (B) photochemical oxidation of exposed thiolates to sulfonates; (C) selective etching of gold surfaces; and (D) displacement of the oxidized adsorbate molecule. Reproduced with permission from reference 82. Copyright American Chemical Society 2002.

It is the combination of anti-adhesiveness and hydrophilicity that makes the incorporation of terminal OEG moieties within an adsorbate structure promising for a variety of applications. A recent example where such characteristics have been applied can be found in a recent article by our group, where placing an OEG component between the alkyl spacer of an adsorbate and a terminal maleimide moiety improved aqueous stability for gold nanoparticles decorated with maleimide-terminated SAMs.[84] This enhanced resistance to aggregation provides added flexibility in handling such nanoparticles when conjugating thiol-terminated biomolecules or other bulky molecules to these particles.

Research efforts of mixed OEG films have sought to create surfaces that have the potential to serve as biosensors.[35,79,85] For example, Jeong and co-workers grafted poly(ethylene glycol methacrylate) brushes from the surface of a mixed SAM and determined that the concentration of the initiator molecule in the SAM dictated the lateral

packing density and overall amount of bound streptavidin.[35] Additionally, Clare and co-workers expanded research on OEG-terminated films by covalently attaching OEG monolayers on silicon and diamond surfaces as a potential electronic biosensor.[79] The technique generated high quality monolayers on the surfaces and displayed similar protein resistance as OEG-terminated surfaces on gold. In addition to successfully generating the monolayers, the authors were able to demonstrate the specific adsorption of avidin to surface-immobilized biotin in the presence of a complex mixture of several proteins.

1.2.5. Techniques Used to Characterize Mixed SAMs

Spectroscopy techniques commonly used to characterize mixed SAMs (particularly those outlined in this report) include infrared spectroscopy, UV-Vis spectroscopy, and X-ray photoelectron spectroscopy (XPS).[44,46,57,86] Microscopy techniques such as atomic force microscopy (AFM) and scanning tunneling microscopy (STM) are also widely used to characterize mixed-monolayer films.[49,71,72] For example, Pallavicini et al. employed UV-Vis spectroscopy to determine the fraction of an absorbing 4,4-difluoro-4-bora-3a,4a-diaza-s-indacene (BODIPY)-functionalized alkanethiol mixed with a normal alkanethiol or a PEGylated alkanethiol, both of which are colorless.[86] Using UV-Vis analysis, the authors extracted the exchange constant for the BODIPY alkanethiol and then the constants for the colorless alkanethiols. These constants were then used to calculate the amount of the colorless thiol present on the surface. Separately, Campbell et al. relied on the presence of a fluorescent probe in a binary SAM to gain insight into the surface composition.[87] The approach used by the authors utilized a wet stamping technique to generate a binary SAM from a mixture of a

disulfide functionalized with the fluorescent probe and an alkanethiol bearing a hydroxyl or carboxyl group termini; these groups have the ability to participate in hydrogen bonding. The authors concluded from their studies that the lateral interactions (i.e., hydrogen bonding) have an effect on the composition of the resulting films. In monolayers containing the fluorescent disulfide mixed with the normal alkanethiol, fluorescence was observed in all mixtures containing the disulfide. In contrast, in monolayers containing either the hydroxyl-terminated or carboxyl-termianted adsorbates as part of the mixture, fluorescence was only observed at a certain concentration of disulfide; thus indicating that the ratio of adsorbates on the surface differed from the solution concentration.

Analysis of surface composition has also been studied using electrochemical techniques. The catalytic activity of (2,2,6,6-tetramethylpiperidin-1-yl)oxyl (TEMPO)-terminated mixed SAMs with an alkanethiol has been used to determine the distribution and efficiency of the active moiety.[88,89] The authors used the full width at half maximum (FWHM) and the peak potential from cyclic voltammetry (CV) to determine the distribution of the active centers. A linear dependency of the FWHM and potential revealed a surface that was homogeneously mixed. On the other hand, a non-linear dependency pointed to a phase-separated surface. In the case of the mixed TEMPO-based SAMs, a non-linear relationship was observed. Forster also used CV to monitor the absorption of redox-functionalized bypyridine derivatives on platinum wires; this approach allows for the measurement of the adsorbate ratio.[90] Recently, Capitao et al. were able to achieve a linear dependence between the ratio of adsorbates on the surface and solution using the electro-assisted deposition method detailed by Sahli et al.[91,92] In

addition to creating a surface where the adsorbate ratio is the same as that in solution, one might simultaneously monitor the concentration of the adsorbates on the surface.

1.2.6. The Consequences of Adsorbate Mixing

Apparent in the details outlined above is that any adsorbate system that produces a mixed-chain monolayer film where the component chains are subject to exchange processes or are able to migrate within the monolayer is subject to domain formation, even if initially deposited from an unsymmetrical linear disulfide as a perfectly homogeneous SAM. This situation is exacerbated when the component parts of the mixed-adsorbate film are significantly different, and, like oil and water, naturally phase separate. Therefore, alternative approaches to generating films with such compatibility conflicts have been pursued.

1.3. Multidentate Adsorbates and Interfacial Homogeneity

The stability of ligand-metal complexes can be enhanced through an entropy-driven process know as the "chelate effect".[93] For example, previous studies point toward the entropy change achieved upon substituting two monodentate ligands with an analogous bis-chelating ligand as the primary driving force for such an exchange.[94] Consequently, if the same technique is applied to chelating thiols on gold, a greater stability is achieved as compared to having two individual sulfur-gold bond enthalpies and the concomitant inter-chain van der Waals stabilization.[16,95] Figure 1.9 provides an overview of the different types of multidentate adsorbates/headgroups that have been used to form stable monolayers on gold with the potential to generate homogeneously mixed "conflicted" interfaces.

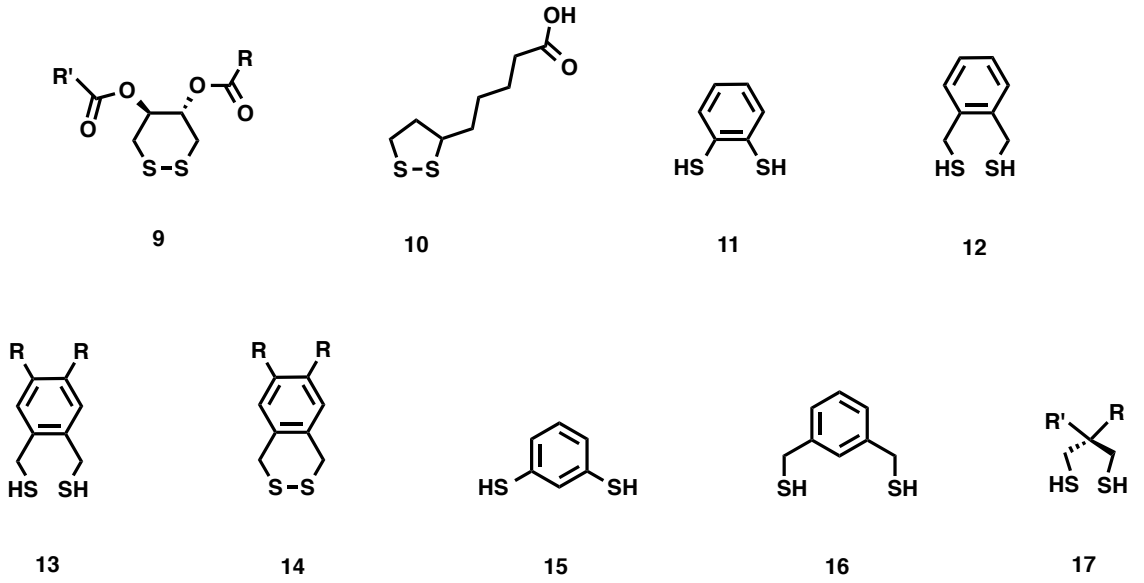

Figure 1.9. Structures of multidentate adsorbates/headgroups used in efforts to generate stable monolayer films on gold.[6,96,112-118]

1.3.1. Cyclic Disulfide Headgroups

Current research involving SAMs on gold was sparked by the work of Nuzzo and Allara over 30 years ago with the adsorption of a series of symmetrical, cyclic disulfides having the framework of molecule **9** in Figure 1.9.[96] Monolayer films derived from these adsorbates led to stable, well packed films;[97] but in these initial studies, the extra stability gained from the chelating character was not considered. In a separate study conducted by Bruening and co-workers, the same dithiane framework was used to create multifunctional films.[98] The authors custom-tailored the dithiane base to incorporate two different functional groups to create surfaces having two different interfacial functionalities within the same molecular assembly.

Other commonly used cyclic disulfide anchoring headgroups are those based on thioctic acid (framework **10** in Figure 1.9). These types of adsorbates have been used as the adhesion layer in bio- or immunosensors,[99-105] molecular electronic applications,[106] as

well as anchors for attaching catenanes on surfaces.[107] A thorough review on the use of thioctic acid and its derivatives to create SAMs as an immobilization platform of biomolecules can be found in the literature.[108] Moreover, researchers have used functionalized thioctic acid derivatives mixed with a diluent alkanethiol to carry out surface reactions, including olefin cross metathesis[109] and glycosylation.[110,111] In these latter reactions, the use of a mixed monolayer improved the overall efficiency of the reaction by reducing the steric interactions around the active site.

1.3.2. Aromatic Dithiol Headgroups: First Generation

Researchers sought an alternative approach toward the development of multidentate thiol-based adsorbates through the exploration of molecules having aromatic-based headgroups (i.e., frameworks **11-16** in Figure 1.9).[112-117,119] Initial work in this area explored the adsorption of 1,2-benzenedithiol (**11** in Figure 1.9) onto gold and silver surfaces.[112] Kinetic studies performed on these types of monolayers revealed a more stable film when compared to the adsorption and desorption rates of octadecanethiol. Using a systematic approach to adsorbate design, our group generated monolayers derived from alkylfunctionalized analogs of adsorbate **12**, framework **13**, and found that the adsorbates generated "chelating" SAMs that were well-packed and highly oriented.[113] However, monolayer films generated from the corresponding disulfide, framework **14**, were less complete and disordered, likely due to constraints introduced by the cyclic disulfide ring.[114] Separate studies by Kim et al. utilized adsorbate **12** to form SAMs on gold surfaces.[115] The authors showed that monolayers formed from **12** yielded highly ordered, well-packed films, and attributed the phenomena to the flexibility of the methylene units. As noted in our previous work,[113] the incorporation of the methylene

units allows the sulfur atoms to bind to the gold in a manner that avoids steric and torsional strain, as shown in molecular modeling of the adsorbate -- the distance between the sulfur atoms can reach 5.0 Å, Figure 1.10.[113]

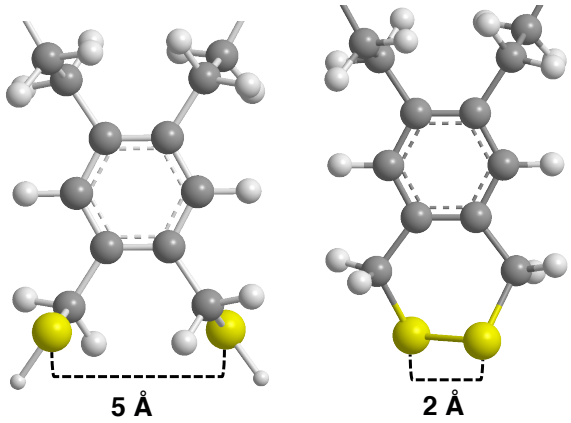

Figure 1.10. Model depicting the distance between the sulfurs of adsorbates **13** and **14**. Model was obtained using MM2 calculations on ChemBio 3D Ultra.

1,3-Benzendithiol **15** and its methylated analog **16** were utilized to form SAMs on both gold and silver nanoparticles.[116,117] The authors found that the coordination of the thiolate groups on the surface (i.e, the number of sulfur atoms per molecule bound to the metal) was highly dependent on the structure and concentration of the adsorbate. Both sulfur atoms of **15** were found to bind to the metal surface regardless of the concentration of the adsorbate in solution. However, a full binding of sulfur atoms to the metal in SAMs derived from **16** occurred only at lower concentrations. At higher concentrations, there was only a single sulfur-metal bond per adsorbate, which led to a more upright conformation.

1.3.3. Spiroalkanedithiols

A second structural design that arose shortly afterward is the bidentate dithiol having structural motif **17**, dubbed "spiroalkanedithiol".[118] In subsequent studies, the spiro headgroup was coupled with dissimilar tailgroups and utilized for the creation of "conflicted" interfaces.[5,120,121] Our research group was the first to report the use of the "spiro" motif to incorporate two alkyl chains of differing lengths to create the first example of a homogenously mixed film at the molecular level.[120] SAMs derived from spiroalkanedithiols (SADTs) bearing both a 10- and a 17-carbon tailgroup (**22**) were compared to those derived from SADTs having two equivalent 10-carbon tailgroups (**18**) and two equivalent 17-carbon tailgroups (**20**) as well as SAMs derived from their individual *n*-alkanethiol counterparts (**19** and **21**) and mixtures of the latter *n*-alkanethiols. All of the characterization techniques employed on the SAMs derived from **22** were consistent with a homogeneously mixed film. For example ellipsometry measurements revealed a thickness for the film derived from **22** in between the thicknesses of the individual films derived from **19** and **21**. Evaluation of the degree of conformational order for the films by polarization-modulation infrared reflection adsorption spectroscopy (PM-IRRAS) showed liquid-like character for the unsymmetrical SADT SAMs when compared to films derived from the *n*-alkanethiols and the symmetrical SADTs; further analysis by PM-IRRAS revealed that the mixed SAMs at solution ratios of 2 and 3 (i.e., ratio = **19** / **21**) were similar to the SAM derived from the unsymmetrical SADT, **22**. Perhaps the most revealing analysis performed was the AFM images (see Figure 1.11). The topographical images offer visual conformation of a homogenously mixed interface for the unsymmetrical SADT SAM (Figure 1.11E),

whereas domain formation is apparent in the SAM derived from the analogous mixture of *n*-alkanethiols (Figure 1.11F).

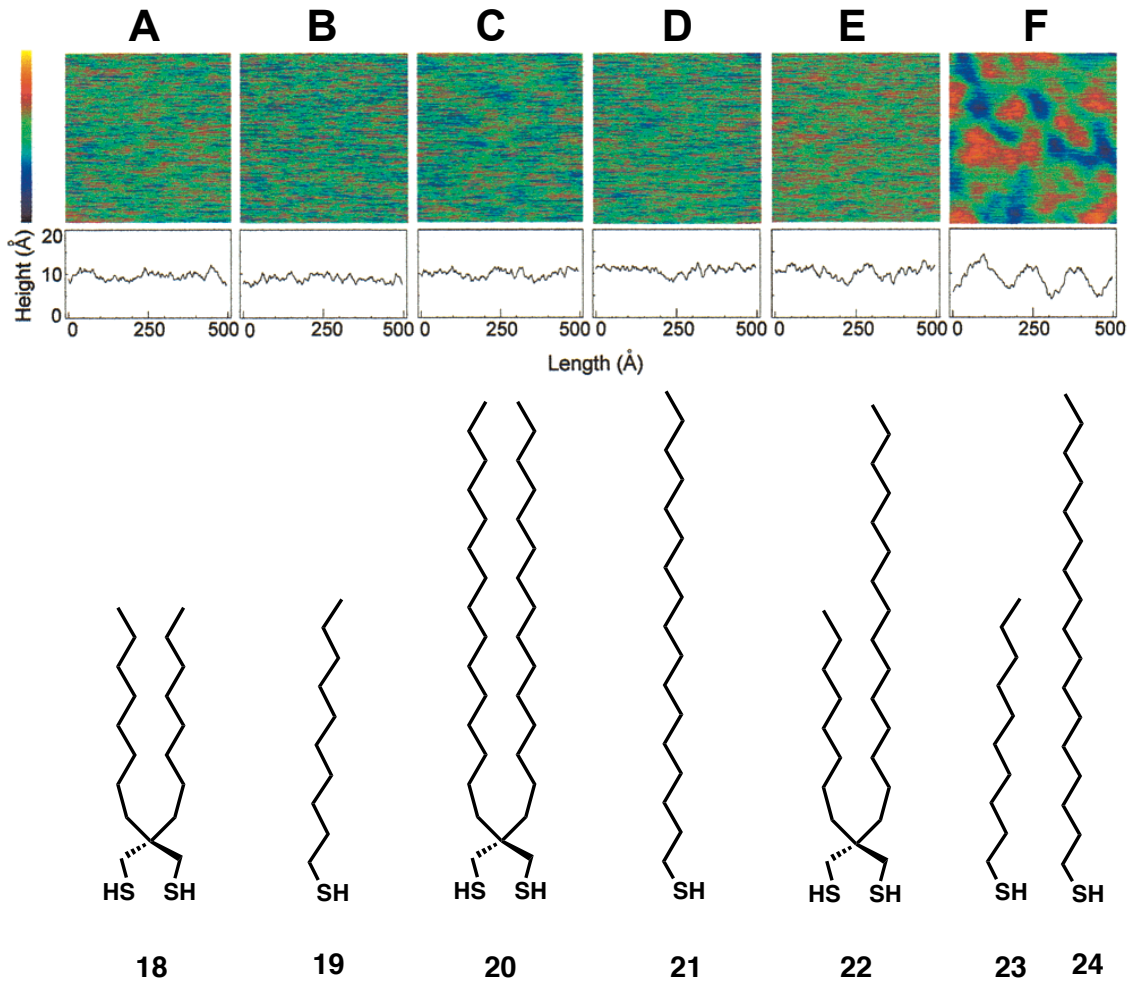

Figure 1.11. AFM images (topographic) of the SADT SAMs (A) C10C10$(SH)_2$ (**18**), (C) C17C17$(SH)_2$ (**20**), and (E) C10C17$(SH)_2$ (**22**) along with the normal alkanethiols (B) C10SH (**19**), (D) C17SH (**21**), and (F) a mixed SAM where [C10SH]/[C17SH] = 2. Reproduced with permission from reference 120. Copyright 2000 American Chemical Society.

In studies related to those outlined in the Introduction,[5] we utilized the spiroalkanedithiol headgroup to study the effects of blending two mutually incompatible tailgroups comprised of hydrocarbon and partially fluorinated chains in efforts to

generate yet another class of "conflicted" interface.[121] Comparison of the SAMs generated from the unsymmetrical SADTs, **27**, to SAMs generated from analogous hydrocarbon, **25**, and partially fluorinated monothiols, **26** (see Figure 1.12) indicates that the custom-designed bidentate adsorbates afford stable monolayers on gold. Furthermore, analysis of these SAMs by XPS showed that the C 1s peak position for the methylene spacers of the SADT SAMs appeared at a higher binding energy (284.7 eV) than that of the SAM derived from **26** (284.5 eV) (see Figure 1.12A), indicating a denser packing of the hydrocarbon chains in the SADT SAMs. However, the hydrocarbon portion of the SADT SAMs was still less densely packed than that of the SAM derived from **25** (285.0 eV). The enhanced packing density of the chains of the SADT SAMs compared to that of **26** SAMs was also evident in the F 1s binding energies; specifically, the F 1s peak position for the **26** SAMs appeared at a lower binding energy compared to that of SADT SAMs. We rationalized such shifts in the binding energies of the SADT films by considering them as better insulators than the **26** films, which translates to a slower discharge of the positive holes generated in the core electron ejection process (inhibition of electron flow from the gold surface to the SAMs).[121] Additionally, the analyses suggested that the fluorinated portions of the SADT films were more tilted than those in the **26** films.[121] Thus, by covalently blending these mutually incompatible chains, we were able to reduce the structural constraints of a well-packed partially fluorinated segment (5.8 Å) on the hydrocarbon segment that arise from differences in the chain diameters (5.8 Å vs 4.2 Å). It is important to note that SAMs derived from mixtures of partially fluorinated alkanethiols and *n*-alkanethiols typically leads to domain formation or "islanding" of the two distinct species within the monolayer film.[29,122]

Nevertheless, this research demonstrates that properly designed molecules can be used to generate mixed monolayers having good interfacial homogeneity and low surface energy. Exploration of the interfacial properties (e.g., adhesion and friction) of these new "conflicted" interfaces are ongoing.

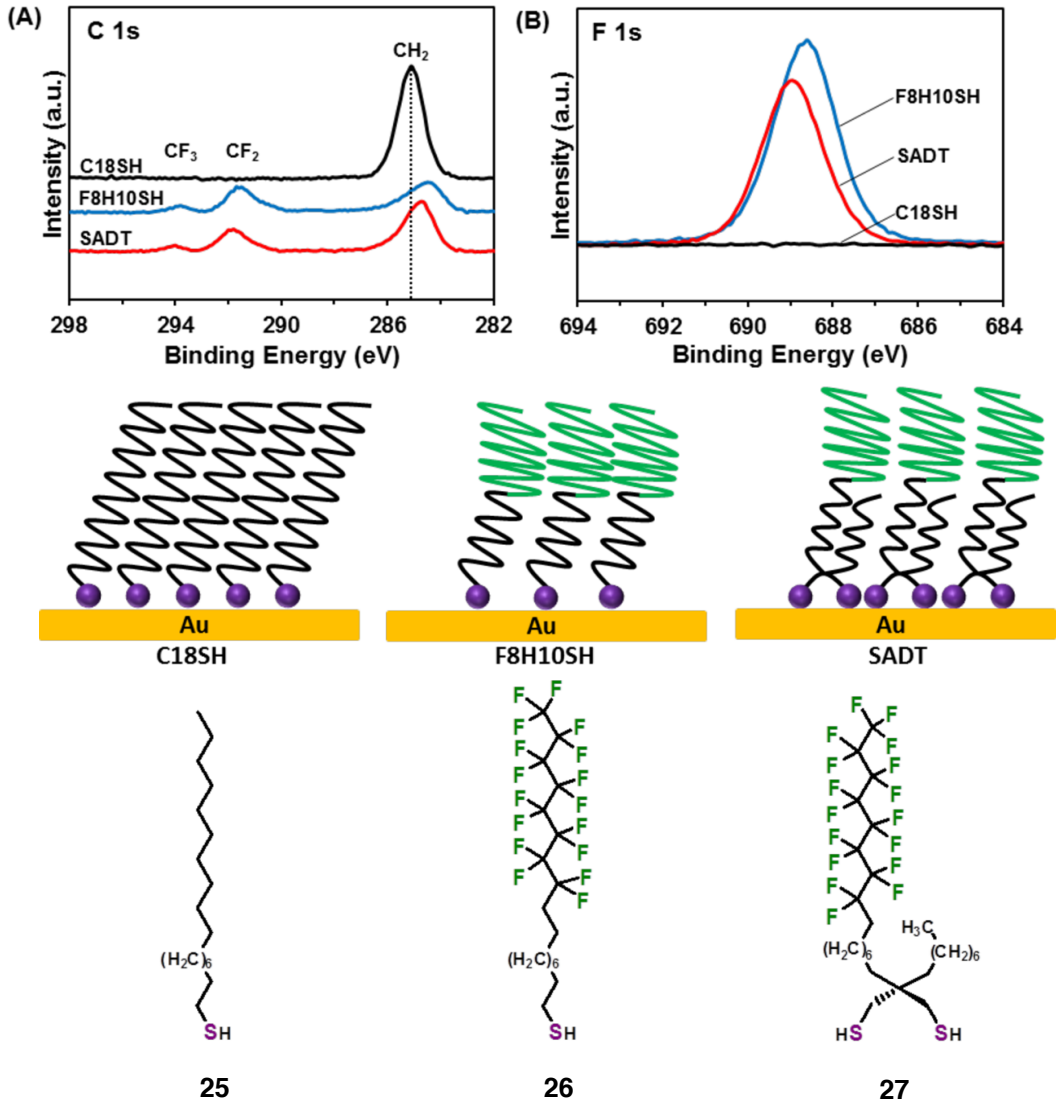

Figure 1.12. Homogeneously mixed multi-component spiro adsorbates for exploring the interfacial properties of surfaces containing well-defined mixtures of hydrocarbons and fluorocarbons. Results of XPS analysis of (A) C 1s and (B) F 1s binding energy regions of normal alkanethiol, partially fluorinated spiroalkanedithiol, and partial fluorinated SAMs. Reproduced with permission from reference 121. Copyright 2015 American Chemical Society.

1.3.4. Dithiocarboxylic Acids and Derivatives

Aliphatic dithiocarboxylic acids (ADTCAs; **28**, Figure 1.13) have also been explored as multidentate adsorbates for generating SAMs on gold.[123,124] Despite the chelating nature of the adsorbate, SAMs formed from **28** were found to be less stable under air, oxygen, and argon when compared to SAMs derived from nalkanethiols.[124] SAMs on gold derived from xanthic acids (NAXAs; **29**) and dithiocarbamic acids (DTCAs **30**) have also been studied.[125,126] Structurally, SAMs formed from NAXAs were found to exhibit reduced conformational order compared to SAMs formed from ADTCAs; in addition, stability tests revealed a less stable film when compared to analogous ADTCA SAMs.[125,126] Eckerman et al. utilized an analogue of **30** that bears two different alkyl groups where one has a ferocene group to study the effect of a mixed monolayer on electron-transfer proceses.[127] The dithiocarbamate moiety in DTCAs has also been employed as an organic layer to lower the work function of electrodes.[128] Notably, the relative ease of removal for these types of adsorbates (i.e., **28–30**) makes them promising candidates as transient protective inks in orthogonal patterning by soft lithography.[124]

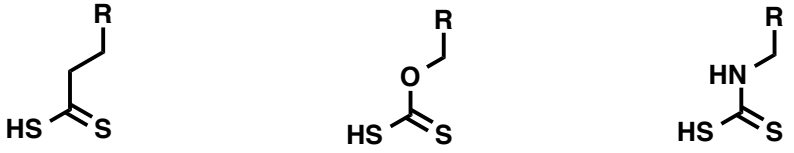

28 **29** **30**

Figure 1.13. Structures of dithiocarboxylic acids, xanthic acids, and dithiocarbamic acid used in efforts to generate stable monolayer films on gold.[123,125,126]

1.3.5. Aromatic Dithiol Headgroups: Second Generation

Combining two of the structural motifs above, our group designed, synthesized, and studied a series of alkyl-terminated aromatic dithiols having a "spiro" headgroup motif, **31**–**33** (see Figure 1.14), to investigate the relationship between tailgroup chains and headgroup packing densities.[129] From these studies, we concluded that increasing the number of alkoxy chains on the ring led to an increased degree of conformational order with increased van der Waals interactions. Moreover, in addition to the chelate effect, the addition of multiple alkoxy chains gave rise to an enhancement in the overall thermal stability of the SAMs. The aromatic ring in this adsorbate provides a unique platform where two or even three dissimilar tailgroups can be incorporated into a single adsorbate (in contrast to the spiroalkanethiols, where the number of dissimilar tailgroups is limited to two).

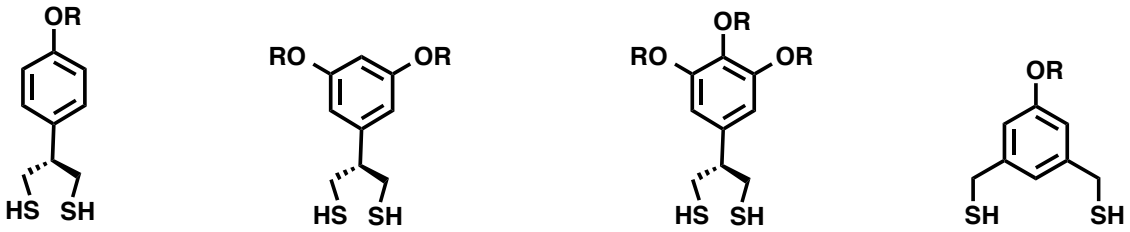

31 **32** **33** **34**

Figure 1.14. Structures of aromatic dithiol-based adsorbates used to generate stable monolayer films on gold.[129]

In recent breakthrough studies[6], our group utilized the unmatched stability of SAMs on gold derived from adsorbates having 1,3-bis(mercaptomethyl)phenyl-based headgroups (see framework **34** in Figure 1.14) to generate conflicted interfaces comprised of alkyl, perfluoro, and OEG moieties. In contrast to mixed monolayers

derived from functionalized monothiols, which show clear deviations from the solution composition, the surface composition of mixed SAMs generated from these unique bidentate molecules reflect the molar solution concentration of the respective molecules -- a reflection of the kinetically controlled film formation process brought about by the above-mentioned chelating effect. Perhaps more importantly, the interfacial properties of these mixed films are consistent with what one would predict from the solution concentration. After quantitatively analyzing the mixed-SAMs by XPS and comparing the XPS data to the wettability data (see Figure 1.15), the results showed that the bidentate system offers a precise way to control the interfacial properties in contrast to the traditional monodentate nalkanethiol system. For the hydrocarbon/OEG-terminated SAMs (right side panels), the change in the contact angle of water on the mixed SAMs formed from the bidentate system (Figure 1.15B) is more gradual than in the monodentate system (Figure 1.15A). The more gradual change observed for the bidentate system vs. the monodentate system arises from the greater (more precise) control of surface composition afforded by the bidentate adsorbates.[6] Furthermore, a stability assessment of mixed-SAMs in the study showed that the monodentate adsorbates (PFT and OEGT) were completely exchanged by hexadecanethiol (HDT) when placed in solutions with high HDT concentration, as indicated from wettability data. In contrast, however, the bidentate system remained intact, showing constant wettability data even after long incubation times in a 10 mM solution of the displacing adsorbate. Using judiciously selected mixtures of these custom-designed bidentate thiols offers the ability to create thin monolayer films with precisely defined and entirely unique interfacial properties.

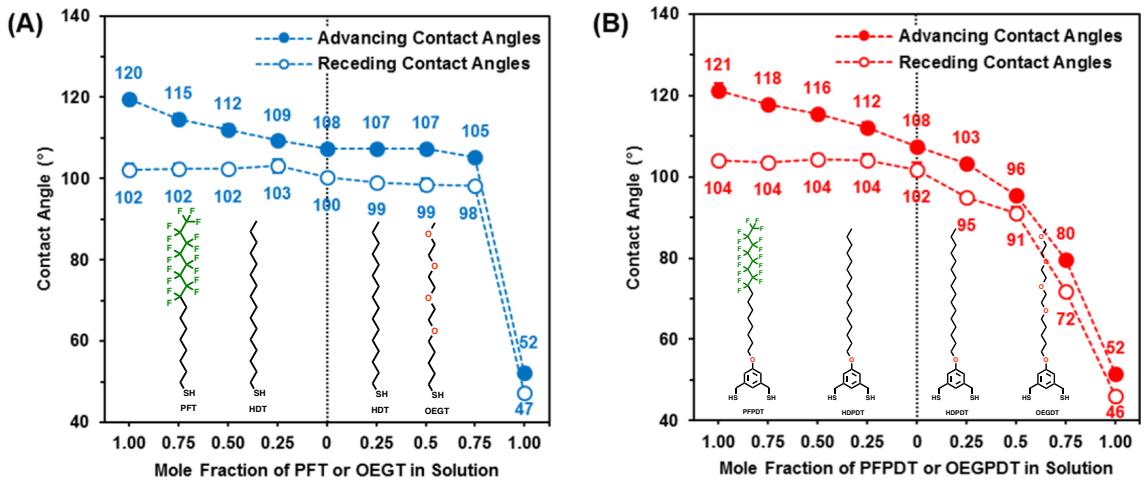

Figure 1.15. Wettability data of mixed monolayers of (A) monodentate systems (PFT/HDT and HDT/OEGT) and (B) homogeneously mixed-SAMs of bidentate systems (PFPDT/HDPDT and HDPDT/OEGPDT). Reproduced with permission from reference 6. Copyright 2016 American Chemical Society

1.3.6. Developing Strategies for Generating Conflicted Interfaces

As described in the preceding section, the use of adsorbates with multidentate headgroups in the form of either aromatic-based or spiro-based dithiols offers a facile strategy for creating homogeneously mixed interfaces having tunable chemical heterogeneity.[5,6,120,121] Moreover, depending on the desired structural features and chemical compositions of the coated surface, mixed SAMs can be prepared simply by designing and synthesizing multidentate adsorbates with suitable architecture and chemical composition. For instance, SADTs with unsymmetrical tailgroups are likely the best choice for generating homogenously mixed SAMs having a 50:50 ratio of chemical functionality.[5,120,121] Such adsorbates allow intimate mixing of chain termini on the surface needed to tune interfacial properties (e.g., wettability, adhesion, and friction) while eliminating the possibility of domain formation.[120,121] Separately, mixed monolayers derived from adsorbates having 1,3- bis(mercaptomethyl)phenyl headgroups

represent an alternative approach to mixed interfaces, where the interfacial properties can be tuned simply by adjusting the relative adsorbate concentrations in solution.[6] Yet, regardless of the type of adsorbate used in generating the SAM (spiro or aromatic dithiol), these monolayer coatings exhibit enhanced stability when compared to their monothiol-based counterparts, (i.e., they are more resistant to ligand exchange, and are more chemically and thermally stable with respect to molecular desorption). Additionally, kinetically controlled film formation from such adsorbates obviates the need for more laborious approaches for the generation of compositionally mixed organic thin films.[33,66]

1.4. Conclusions

This article examines a variety of strategies that have been used to generate stable, compositionally mixed SAMs on gold, including the development of new adsorbates that offer homogenously mixed "conflicted" interfaces. Previous efforts to generate high quality mixed films include the widely studied techniques of the co-adsorption of monothiols, backfilling processes, and the adsorption of disulfides; these commonly used techniques have been shown to yield films with phase-separated domains, where the relative concentration of adsorbates on the surface differs from that in solution, films that show preferential adsorption, and films that are susceptible to exchange processes. In contrast, newly developed strategies such as imbedding an internal dipole within a molecule[25] or designing adsorbates with phase-incompatible tailgroups that are structurally connected into the molecule coupled with the incorporation of a dithiol headgroup have been used to generate films having homogeneous mixtures of phaseincompatible species. Furthermore, capitalizing on the enhanced stability of SAMs

on gold derived from adsorbates having 1,3-bis(mercaptomethyl)phenyl-based headgroups, mixed thin SAMs derived from these custom-designed molecules resist desorption and are stable against exchange processes. These newly developed adsorbates and film-forming strategies will undoubtedly lead to advances in a variety of applications, including surfaces for selective protein adsorption and/or desorption, nanoparticles with extended circulation time in physiological media, and robust non-adhesive films for antifouling applications.

1.5. Acknowledgments

We thank the National Science Foundation (CHE-1411265), the Robert A Welch Foundation (Grant No. E-1320), and the Texas Center for Superconductivity at the University of Houston for generous support of this research.

1.6. References

1. Bain, C. D.; Whitesides, G. M. Molecular-Level Control over Surface Order in Self-Assembled Monolayer Films of Thiols on Gold. *Science* **1988**, *240*, 62–63.
2. Brewer, N. J.; Leggett, G. J. Chemical Force Microscopy of Mixed Self-Assembled Monolayers of Alkanethiols on Gold: Evidence for Phase Separation. *Langmuir* **2004**, *20*, 4109–4115.
3. Kakiuchi, T.; Sato, K.; Iida, M.; Hobara, D.; Imabayashi, S.; Niki, K. Phase Separation of Alkanethiol Self-Assembled Monolayers During the Replacement of Adsorbed Thiolates on Au(111) with Thiols in Solution. *Langmuir* **2000**, *16*, 7238–7244.
4. Stranick, S. J.; Atre, S. V.; Parikh, A. N.; Wood, M. C.; Allara, D. L.; Winograd, N.; Weiss, P. S. Nanometer-Scale Phase Separation in Mixed Composition Self-Assembled Monolayers. *Nanotechnology* **1996**, *7*, 438–442.
5. Chinwangso, P.; Lee, H. J.; Jamison, A. C.; Marquez, M. D.; Park, C. S.; Lee, T. R. Structure, Wettability, and Thermal Stability of Organic Thin Films on Gold

Generated from the Molecular Self-Assembly of Unsymmetrical Oligo(Ethylene Glycol) Spiroalkanedithiols. *Langmuir* **2017**, *33*, 1751–1762.

6. Lee, H. J.; Jamison, A. C.; Lee, T. R. Two Are Better Than One: Bidentate Adsorbates Offer Precise Control of Interfacial Composition and Properties. *Chem. Mater*. **2016**, *28*, 5356–5364.

7. Bethencourt, M. I.; Barriet, D.; Frangi, N. M.; Lee, T. R. Model Glycol-Terminated Surfaces for Adhesion Resistance. *J. Adhes*. **2005**, *81*, 1031–1048.

8. Miller, J. S.; Bethencourt, M. I.; Hahn, M.; Lee, T. R.; West, J. L. Laser-Scanning Lithography (LSL) for the Soft Lithographic Patterning of Cell-Adhesive Self-Assembled Monolayers. *Biotechnol. and Bioeng.* **2006**, *93*, 1060–1068.

9. Jeyachandran, Y. L.; Weber, T.; Terfort, A.; Zharnikov, M. Application of Long Wavelength Ultraviolet Radiation for Modification and Patterning of Protein-Repelling Monolayers. *J. Phys. Chem. C* **2013**, *117*, 5824–5830.

10. Jeyachandran, Y. L.; Terfort, A.; Zharnikov, M. Controlled Modification of Protein- Repelling Self-Assembled Monolayers by Ultraviolet Light: The Effect of the Wavelength. *J. Phys. Chem. C* **2012**, *116*, 9019–9028.

11. Fallah, M. A.; Stanglmair, C.; Pacholski, C.; Hauser, K. Devising Self-Assembled- Monolayers for Surface-Enhanced Infrared Spectroscopy of PH-Driven Poly-L-Lysine Conformational Changes. *Langmuir* **2016**, *32*, 7356–7364.

12. Im, H.; Shao, H.; Park, Y. I.; Peterson, V. M.; Castro, C. M.; Weissleder, R.; Lee, H. Label-Free Detection and Molecular Profiling of Exosomes with a Nano-Plasmonic Sensor. *Nat. Biotechnol.* **2014**, *32*, 490–495.

13. Lee, T. R.; Barriet, D.; Moore, H. J. Structure and Properties of Fluorinated Organic Thin Films: Implications for MEMS Devices. *NDSI Digest* **2005**, *2*, 93.

14. Bhushan, B.; Kasai, T.; Kulik, G.; Barbieri, L.; Hoffmann, P. AFM Study of Perfluoroalkylsilane and Alkylsilane Self-Assembled Monolayers for Anti-Stiction in MEMS/NEMS. *Ultramicroscopy* **2005**, *105*, 176–188.

15. Lee, H. J.; Jamison, A. C.; Yuan, Y.; Li, C.-H.; Rittikulsittichai, S.; Rusakova, I.;

Lee, T. R. Robust Carboxylic Acid-Terminated Organic Thin Films and Nanoparticle Protectants Generated from Bidentate Alkanethiols. *Langmuir* **2013**, *29*, 10432–10439.

16. Srisombat, L.; Jamison, A. C.; Lee, T. R. Stability: A Key Issue for Self-Assembled Monolayers on Gold as Thin-Film Coatings and Nanoparticle Protectants. *Colloids Surf., A* **2011**, *390*, 1–19.

17. Trabelsi, S.; Zhang, Z.; Zhang, S.; Lee, T. R.; Schwartz, D. K. Correlating Linactant Efficiency and Self-Assembly: Structural Basis of Line Activity in Molecular Monolayers. *Langmuir* **2009**, *25*, 8056–8061.

18. Trabelsi, S.; Zhang, S.; Zhang, Z.; Lee, T. R.; Schwartz, D. K. Semi-Fluorinated Phosphonic Acids Form Stable Nanoscale Clusters in Langmuir-Blodgett and Self-Assembled Monolayers. *Soft Matter* **2009**, *5*, 750–758.

19. Yang, H.; Yuan, B.; Zhang, X.; Scherman, O. A. Supramolecular Chemistry at Interfaces: Host–Guest Interactions for Fabricating Multifunctional Biointerfaces. *Acc. Chem. Res.* **2014**, *47*, 2106–2115.

20. Shakiba, A.; Jamison, A. C.; Lee, T. R. Poly(L-Lysine) Interfaces Via Dual Click Reactions on Surface-Bound Custom-Designed Dithiol Adsorbates. *Langmuir* **2015**, *31*, 6154–6163.

21. Dugger, J. W.; Webb, L. J. Preparation and Characterization of Biofunctionalized Inorganic Substrates. *Langmuir* **2015**, *31*, 10331–10340.

22. Collman, J. P.; Devaraj, N. K.; Eberspacher, T. P. A.; Chidsey, C. E. D. Mixed Azide-Terminated Monolayers: A Platform for Modifying Electrode Surfaces. *Langmuir* **2006**, *22*, 2457–2464.

23. Valley, D. T.; Onstott, M.; Malyk, S.; Benderskii, A. V. Steric Hindrance of Photoswitching in Self-Assembled Monolayers of Azobenzene and Alkane Thiols. *Langmuir* **2013**, *29*, 11623–11631.

24. Moldt, T.; Brete, D.; Przyrembel, D.; Das, S.; Goldman, J. R.; Kundu, P. K.; Gahl, C.; Klajn, R.; Weinelt, M. Tailoring the Properties of Surface-Immobilized Azobenzenes by Monolayer Dilution and Surface Curvature. *Langmuir* **2015**, *31*,

1048–1057.

25. Hehn, I.; Schuster, S.; Wächter, T.; Abu-Husein, T.; Terfort, A.; Zharnikov, M.; Zojer, E. Employing X-Ray Photoelectron Spectroscopy for Determining Layer Homogeneity in Mixed Polar Self-Assembled Monolayers. *J. Phys. Chem. Lett.* **2016**, *7*, 2994–3000.

26. Qiu, S.; Zhao, F.; Zenasni, O.; Li, J.; Shih, W.-C. Nanoporous Gold Disks Functionalized with Stabilized G-Quadruplex Moieties for Sensing Small Molecules. *ACS Appl. Mater. Interfaces* **2016**, *8*, 29968–29976.

27. Das, J.; Ivanov, I.; Montermini, L.; Rak, J.; Sargent, E. H.; Kelley, S. O. An Electrochemical Clamp Assay for Direct, Rapid Analysis of Circulating Nucleic Acids in Serum. *Nat. Chem.* **2015**, *7*, 569–575.

28. Wang, S.; Zhang, L.; Wan, S.; Cansiz, S.; Cui, C.; Liu, Y.; Cai, R.; Hong, C.; Teng, I. T.; Shi, M.; Wu, Y.; Dong, Y.; Tan, W. Aptasensor with Expanded Nucleotide Using DNA Nanotetrahedra for Electrochemical Detection of Cancerous Exosomes. *ACS Nano* **2017**, *11*, 3943–3949.

29. Jamison, A. C.; Zhang, S.; Zenasni, O.; Schwartz, D. K.; Lee, T. R. Fibrillar Self-Organization of a Line-Active Partially Fluorinated Thiol within Binary Self-Assembled Monolayers. *Langmuir* **2012**, *28*, 16834–16844.

30. Stranick, S. J.; Parikh, A. N.; Tao, Y. T.; Allara, D. L.; Weiss, P. S. Phase Separation of Mixed-Composition Self-Assembled Monolayers into Nanometer Scale Molecular Domains. *J. Phys. Chem.* **1994**, *98*, 7636–7646.

31. Tamada, K.; Hara, M.; Sasabe, H.; Knoll, W. Surface Phase Behavior of N-Alkanethiol Self-Assembled Monolayers Adsorbed on Au(111): An Atomic Force Microscope Study. *Langmuir* **1997**, *13*, 1558–1566.

32. Tsao, M.-W.; Rabolt, J. F.; Schönherr, H.; Castner, D. G. Semifluorinated/Hydrogenated Alkylthiol Thin Films: A Comparison between Disulfides and Thiol Binary Mixtures. *Langmuir* **2000**, *16*, 1734–1743.

33. Morgenthaler, S.; Lee, S.; Zürcher, S.; Spencer, N. D. A Simple, Reproducible Approach to the Preparation of Surface-Chemical Gradients. *Langmuir* **2003**, *19*,

10459–10462.

34. Patole, S. N.; Baddeley, C. J.; O'Hagan, D.; Richardson, N. V. Reversible Exchange of Self-Assembled Monolayers of Semifluorinated N-Alkanethiols and N-Alkanethiols on Au/Mica Surfaces. *J. Phys. Chem. C* **2008**, *112*, 13997–14000.

35. Jeong, S. P.; Lee, B. S.; Kang, S. M.; Ko, S.; Choi, I. S.; Lee, J. K. Binding Behaviors of Protein on Spatially Controlled Poly[Oligo(Ethylene Glycol) Methacrylate] Brushes Grafted from Mixed Self-Assembled Monolayers on Gold. *Chem. Commun.* **2014**, *50*, 5291–5293.

36. Hayes, W. A.; Kim, H.; Yue, X.; Perry, S. S.; Shannon, C. Nanometer-Scale Patterning of Surfaces Using Self-Assembly Chemistry. 2. Preparation, Characterization, and Electrochemical Behavior of Two-Component Organothiol Monolayers on Gold Surfaces. *Langmuir* **1997**, *13*, 2511–2518.

37. Lüssem, B.; Müller-Meskamp, L.; Karthäuser, S.; Waser, R.; Homberger, M.; Simon, U. STM Study of Mixed Alkanethiol/Biphenylthiol Self-Assembled Monolayers on Au(111). *Langmuir* **2006**, *22*, 3021–3027.

38. Majumdar, N.; Gergel-Hackett, N.; Bean, J. C.; Harriott, L. R.; Pattanaik, G.; Zangari, G.; Yao, Y.; Tour, J. M. The Electrical Behavior of Nitro Oligo(Phenylene Ethynylene)s in Pure and Mixed Monolayers. *J. Electron. Mater.* **2006**, *35*, 140–146.

39. Bain, C. D.; Whitesides, G. M. Formation of Two-Component Surfaces by the Spontaneous Assembly of Monolayers on Gold from Solutions Containing Mixtures of Organic Thiols. *J. Am. Chem. Soc.* **1988**, *110*, 6560–6561.

40. Bain, C. D.; Evall, J.; Whitesides, G. M. Formation of Monolayers by the Coadsorption of Thiols on Gold: Variation in the Head Group, Tail Group, and Solvent. *J. Am. Chem. Soc.* **1989**, *111*, 7155–7164.

41. Bain, C. D.; Whitesides, G. M. Formation of Monolayers by the Coadsorption of Thiols on Gold: Variation in the Length of the Alkyl Chain. *J. Am. Chem. Soc.* **1989**, *111*, 7164–7175.

42. Folkers, J. P.; Laibinis, P. E.; Whitesides, G. M. Self-Assembled Monolayers of Alkanethiols on Gold: Comparisons of Monolayers Containing Mixtures of Short- and Long-Chain Constituents with Methyl and Hydroxymethyl Terminal Groups. *Langmuir* **1992**, *8*, 1330–1341.

43. Laibinis, P. E.; Nuzzo, R. G.; Whitesides, G. M. Structure of Monolayers Formed by Coadsorption of Two N-Alkanethiols of Different Chain Lengths on Gold and Its Relation to Wetting. *J. Phys. Chem.* **1992**, *96*, 5097–5105.

44. Biebuyck, H. A.; Whitesides, G. M. Interchange between Monolayers on Gold Formed from Unsymmetrical Disulfides and Solutions of Thiols: Evidence for Sulfur-Sulfur Bond Cleavage by Gold Metal. *Langmuir* **1993**, *9*, 1766–1770.

45. Folkers, J. P.; Laibinis, P. E.; Whitesides, G. M.; Deutch, J. Phase Behavior of Two-Component Self-Assembled Monolayers of Alkanethiolates on Gold. *J. Phys. Chem.* **1994**, *98*, 563–571.

46. Bain, C. D.; Biebuyck, H. A.; Whitesides, G. M. Comparison of Self-Assembled Monolayers on Gold: Coadsorption of Thiols and Disulfides. *Langmuir* **1989**, *5*, 723–727.

47. Heister, K.; Allara, D. L.; Bahnck, K.; Frey, S.; Zharnikov, M.; Grunze, M. Deviations from 1:1 Compositions in Self-Assembled Monolayers Formed from Adsorption of Asymmetric Dialkyl Disulfides on Gold. *Langmuir* **1999**, *15*, 5440–5443.

48. Chen, S.; Li, L.; Boozer, C. L.; Jiang, S. Controlled Chemical and Structural Properties of Mixed Self-Assembled Monolayers of Alkanethiols on Au(111). *Langmuir* **2000**, *16*, 9287–9293.

49. Zuo, L.; Xiong, Y.; Xie, X.; Xiao, X. Enhanced Lubricity in Mixed Alkanethiol Monolayers. *J. Phys. Chem. B* **2005**, *109*, 22971–22975.

50. Rowe, G. K.; Creager, S. E. Chain Length and Solvent Effects on Competitive Self- Assembly of Ferrocenylhexanethiol and 1-Alkanethiols onto Gold. *Langmuir* **1994**, *10*, 1186–1192.

51. Ma, F.; Lennox, R. B. Potential-Assisted Deposition of Alkanethiols on Au:

Controlled Preparation of Single- and Mixed-Component SAMs. *Langmuir* **2000**, *16*, 6188–6190.

52. Larsen, A. G.; Gothelf, K. V. Electrochemical Properties of Mixed Self-Assembled Monolayers on Gold Electrodes Containing Mercaptooctylhydroquinone and Alkylthiols. *Langmuir* **2005**, *21*, 1015–1021.

53. Lee, L. Y. S.; Sutherland, T. C.; Rucareanu, S.; Lennox, R. B. Ferrocenylalkylthiolates as a Probe of Heterogeneity in Binary Self-Assembled Monolayers on Gold. *Langmuir* **2006**, *22*, 4438–4444.

54. Doneux, T.; Steichen, M.; Bouchta, T.; Buess-Herman, C. Mixed Self-Assembled Monolayers of 2-Mercaptobenzimidazole and 2-Mercaptobenzimidazole-5-Sulfonate: Determination and Control of the Surface Composition. *J. Electroanal. Chem.* **2007**, *599*,241–248.

55. Alévêque, O.; Levillain, E. Electroactive Mixed Self-Assembled Monolayers: Lateral Interactions Model Updated to Interactions between Redox and Non-Redox Species. *Electrochem. Commun.* **2013**, *34*, 165–169.

56. Chidsey, C. E. D.; Bertozzi, C. R.; Putvinski, T. M.; Mujsce, A. M. Coadsorption of Ferrocene-Terminated and Unsubstituted Alkanethiols on Gold: Electroactive Self- Assembled Monolayers. *J. Am. Chem. Soc.* **1990**, *112*, 4301–4306.

57. Chung, C.; Lee, M. Exchange of Self-Assembled Thiol Monolayers on Gold: Characterization by FT-IR External Reflection Spectroscopy. *J. Electroanal. Chem.* **1999**, *468*, 91–97.

58. Xu, G.; Woodruff, D. P.; Bennett, N.; Elliott, M.; Macdonald, J. E. STM Study of Molecule Double-Rows in Mixed Self-Assembled Monolayers of Alkanethiols. *Langmuir* **2010**, *26*, 8174–8179.

59. Biebuyck, H. A.; Bain, C. D.; Whitesides, G. M. Comparison of Organic Monolayers on Polycrystalline Gold Spontaneously Assembled from Solutions Containing Dialkyl Disulfides or Alkanethiols. *Langmuir* **1994**, *10*, 1825–1831.

60. Chen, S.; Li, L.; Boozer, C. L.; Jiang, S. Controlled Chemical and Structural Properties of Mixed Self-Assembled Monolayers by Coadsorption of Symmetric

and Asymmetric Disulfides on Au(111). *J. Phys. Chem. B* **2001**, *105*, 2975–2980.

61. Jaschke, M.; Schönherr, H.; Wolf, H.; Butt, H. J.; Bamberg, E.; Besocke, M. K.; Ringsdorf, H. Structure of Alkyl and Perfluoroalkyl Disulfide and Azobenzenethiol Monolayers on Gold(111) Revealed by Atomic Force Microscopy. *J. Phys. Chem.* **1996**, *100*, 2290–2301.

62. Azehara, H.; Yoshimoto, S.; Hokari, H.; Akiba, U.; Taniguchi, I.; Fujihira, M. Investigation of the Structure of Self-Assembled Monolayers of Asymmetrical Disulfides on Au(111) Electrodes by Electrochemical Desorption. *J. Electroanal. Chem.* **1999**, *473*, 68–74.

63. Ballav, N.; Weidner, T.; Rößler, K.; Lang, H.; Zharnikov, M. A New Approach for the Fabrication of Strongly Heterogeneous Mixed Self-Assembled Monolayers. *ChemPhysChem* **2007**, *8*, 819–822.

64. Ballav, N.; Terfort, A.; Zharnikov, M. Mixing of Nonsubstituted and Partly Fluorinated Alkanethiols in a Binary Self-Assembled Monolayer. *J. Phys. Chem. C* **2009**, *113*, 3697–3706.

65. Ballav, N.; Weidner, T.; Zharnikov, M. UV-Promoted Exchange Reaction as a Tool for Gradual Tuning the Composition of Binary Self-Assembled Monolayers and Chemical Lithography. *J. Phys. Chem. C* **2007**, *111*, 12002–12010.

66. Ballav, N.; Shaporenko, A.; Krakert, S.; Terfort, A.; Zharnikov, M. Tuning the Exchange Reaction between a Self-Assembled Monolayer and Potential Substituents by Electron Irradiation. *J. Phys. Chem. C* **2007**, *111*, 7772–7782.

67. Ishida, T.; Mizutani, W.; Choi, N.; Ogiso, H.; Azehara, H.; Hokari, H.; Akiba, U.; Fujihira, M.; Kojima, I.; Tokumoto, H. Low Dimensional Structure Formation in Self- Assembled Monolayers on Au(111). *Colloids Surf., A* **1999**, *154*, 219–225.

68. Krafft, M. P. Fluorocarbons and Fluorinated Amphiphiles in Drug Delivery and Biomedical Research. *Adv. Drug Delivery Rev.* **2001**, *47*, 209–228.

69. Pujari, S. P.; Spruijt, E.; Cohen, S. M. A.; van, R. C. J. M.; Paulusse, J. M. J.; Zuilhof, H. Ultralow Adhesion and Friction of Fluoro-Hydro Alkyne-Derived Self-Assembled Monolayers on H-Terminated Si(111). *Langmuir* **2012**, *28*,

17690–17700.

70. Pujari, S. P.; Scheres, L.; Weidner, T.; Baio, J. E.; Cohen, S. M. A.; van, R. C. J. M.; Zuilhof, H. Covalently Attached Organic Monolayers onto Silicon Carbide from 1- Alkynes: Molecular Structure and Tribological Properties. *Langmuir* **2013**, *29*, 4019–4031.

71. Overney, R. M.; Meyer, E.; Frommer, J.; Brodbeck, D.; Luethi, R.; Howald, L.; Guentherodt, H. J.; Fujihira, M.; Takano, H.; Gotoh, Y. Friction Measurements on Phase- Separated Thin Films with a Modified Atomic Force Microscope. *Nature* **1992**, *359*, 133–135.

72. Meyer, E.; Overney, R.; Luethi, R.; Brodbeck, D.; Howald, L.; Frommer, J.; Guentherodt, H. J.; Wolter, O.; Fujihara, M.; Takano, H.; Gotoh, Y. Friction Force Microscopy of Mixed Langmuir-Blodgett Films. *Thin Solid Films* **1992**, *220*, 132–137.

73. Imae, T.; Takeshita, T.; Kato, M. Phase Separation in Hybrid Langmuir−Blodgett Films of Perfluorinated and Hydrogenated Amphiphiles. Examination by Atomic Force Microscopy. *Langmuir* **2000**, *16*, 612–621.

74. Iimura, K.-i.; Shiraku, T.; Kato, T. Micro-Phase Separation in Binary Mixed Langmuir Monolayers of N-Alkyl Fatty Acids and a Perfluoropolyether Derivative. *Langmuir* **2002**, *18*, 10183–10190.

75. Trabelsi, S.; Zhang, S.; Lee, T. R.; Schwartz, D. K. Swelling of a Cluster Phase in Langmuir Monolayers Containing Semi-Fluorinated Phosphonic Acids. *Soft Matter* **2007**, *3*, 1518–1524.

76. Schönherr, H.; Ringsdorf, H. Self-Assembled Monolayers of Symmetrical and Mixed Alkyl Fluoroalkyl Disulfides on Gold. 1. Synthesis of Disulfides and Investigation of Monolayer Properties. *Langmuir* **1996**, *12*, 3891–3897.

77. Tsao, M. W.; Hoffmann, C. L.; Rabolt, J. F.; Johnson, H. E.; Castner, D. G.; Erdelen, C.; Ringsdorf, H. Studies of Molecular Orientation and Order in Self-Assembled Semifluorinated N-Alkanethiols: Single and Dual Component Mixtures. *Langmuir* **1997**, *13*, 4317–4322.

78. Prime, K. L.; Whitesides, G. M. Adsorption of Proteins onto Surfaces Containing End- Attached Oligo(Ethylene Oxide): A Model System Using Self-Assembled Monolayers. *J. Am. Chem. Soc.* **1993**, *115*, 10714–10721.

79. Clare, T. L.; Clare, B. H.; Nichols, B. M.; Abbott, N. L.; Hamers, R. J. Functional Monolayers for Improved Resistance to Protein Adsorption: Oligo(Ethylene Glycol)- Modified Silicon and Diamond Surfaces. *Langmuir* **2005**, *21*, 6344–6355.

80. Ballav, N.;Terfort, A.; Zharnikov, M. Fabrication of Mixed Self-Assembled Monolayers Designed for Avidin Immobilization by Irradiation Promoted Exchange Reaction. *Langmuir* **2009**, *25*, 9189–9196.

81. Montague, M.; Ducker, R. E.; Chong, K. S. L.; Manning, R. J.; Rutten, F. J. M.; Davies, M. C.; Leggett, G. J. Fabrication of Biomolecular Nanostructures by Scanning near-Field Photolithography of Oligo(Ethylene Glycol)-Terminated Self-Assembled Monolayers. *Langmuir* **2007**, *23*, 7328–7337.

82. Sun, S.; Leggett, G. J. Generation of Nanostructures by Scanning near-Field Photolitography of Self-Assembled Monolayers and Wet Chemical Etching. *Nano Lett.* **2002**, *2*, 1223–1227.

83. Khan, M. N.; Zharnikov, M. Irradiation Promoted Exchange Reaction with Disulfide Substituents. *J. Phys. Chem. C* **2013**, *117*, 14534–14543.

84. Park, C. S.; Lee, H. J.; Jamison, A. C.; Lee, T. R. Robust Maleimide-Functionalized Gold Surfaces and Nanoparticles Generated Using Custom-Designed Bidentate Adsorbates. *Langmuir* **2016**, *32*, 7306–7315.

85. Acero Sánchez, J. L.; Fragoso, A.; Joda, H.; Suárez, G.; McNeil, C. J.; O'Sullivan, C. K. Site-Directed Introduction of Disulfide Groups on Antibodies for Highly Sensitive Immunosensors. *Anal. Bioanal. Chem.* **2016**, *408*, 5337–5346.

86. Pallavicini, P.; Bernhard, C.; Dacarro, G.; Denat, F.; Diaz-Fernandez, Y. A.; Goze, C.; Pasotti, L.; Taglietti, A. Optical Method for Predicting the Composition of Self-Assembled Monolayers of Mixed Thiols on Surfaces Coated with Silver

Nanoparticles. *Langmuir* **2012**, *28*, 3558–3568.

87. Campbell, C. J.; Soh, S.; Grzybowski, B. A. Blocking of Disulfide Adsorption by Coadsorbing ω-Functionalized Alkane Thiols Revealed by Wet Stamping and Fluorescence Microscopy. *Langmuir* **2008**, *24*, 11600–11604.

88. Aleveque, O.; Breton, T.; Levillain, E. Electrocatalytic Activity of Nitroxyl Mixed Self-Assembled Monolayers: Combined Effects of the Nanoscale Organization and the Composition. *Soft Matter* **2012**, *8*, 3875–3880.

89. Blanchard, P.-Y.; Alévêque, O.; Breton, T.; Levillain, E. TEMPO Mixed SAMS: Electrocatalytic Efficiency Versus Surface Coverage. *Langmuir* **2012**, 28, 13741–13745.

90. Forster, R. J.; Faulkner, L. R. Kinetic Separation of Faradaic Currents: Binary Monolayers as Model Systems. *Anal. Chem.* **1995**, *67*, 1232–1239.

91. Capitao, D.; Sahli, R.; Raouafi, N.; Limoges, B.; Fave, C.; Schöllhorn, B. Electro-Assisted Deposition of Binary Self-Assembled 1,2-Dithiolane Monolayers on Gold with Predictable Composition. *ChemElectroChem* **2016**, *3*, 1422–1428.

92. Sahli, R.; Fave, C.; Raouafi, N.; Boujlel, K.; Schöllhorn, B.; Limoges, B. Switching on/Off the Chemisorption of Thioctic-Based Self-Assembled Monolayers on Gold by Applying a Moderate Cathodic/Anodic Potential. *Langmuir* **2013**, *29*, 5360–5368.

93. Purcell, K. F.; Kotz, J. C. *Inorganic Chemistry*; London : W.B. Saunders, 1977.

94. Chang, S.-C.; Chao, I.; Tao, Y.-T. Structure of Self-Assembled Monolayers of Aromatic-Derivatized Thiols on Evaporated Gold and Silver Surfaces: Implication on Packing Mechanism. *J. Am. Chem. Soc.* **1994**, *116*, 6792–6805.

95. Chinwangso, P.; Jamison, A. C.; Lee, T. R. Multidentate Adsorbates for Self-Assembled Monolayer Films. *Acc. Chem. Res.* **2011**, *44*, 511–519.

96. Nuzzo, R. G.; Allara, D. L. Adsorption of Bifunctional Organic Disulfides on Gold Surfaces. *J. Am. Chem. Soc.* **1983**, *105*, 4481–4483.

97. Nuzzo, R. G.; Fusco, F. A.; Allara, D. L. Spontaneously Organized Molecular

Assemblies. 3. Preparation and Properties of Solution Adsorbed Monolayers of Organic Disulfides on Gold Surfaces. *J. Am. Chem. Soc.* **1987**, *109*, 2358–2368.

98. Bruening, M.; Cohen, R.; Guillemoles, J. F.; Moav, T.; Libman, J.; Shanzer, A.; Cahen, D. Simultaneous Control of Surface Potential and Wetting of Solids with Chemisorbed Multifunctional Ligands. *J. Am. Chem. Soc.* **1997**, *119*, 5720–5728.

99. Dijksma, M.; Boukamp, B. A.; Kamp, B.; van Bennekom, W. P. Effect of Hexacyanoferrate(II/III) on Self-Assembled Monolayers of Thioctic Acid and 11-Mercaptoundecanoic Acid on Gold. *Langmuir* **2002**, *18*, 3105–3112.

100. Madoz, J.; Kuznetzov, B. A.; Medrano, F. J.; Garcia, J. L.; Fernandez, V. M. Functionalization of Gold Surfaces for Specific and Reversible Attachment of a Fused β- Galactosidase and Choline-Receptor Protein. *J. Am. Chem. Soc.* **1997**, *119*, 1043–1051.

101. He, L.; Robertson, J. W. F.; Li, J.; Kärcher, I.; Schiller, S. M.; Knoll, W.; Naumann, R. Tethered Bilayer Lipid Membranes Based on Monolayers of Thiolipids Mixed with a Complementary Dilution Molecule. 1. Incorporation of Channel Peptides. *Langmuir* **2005**, *21*, 11666–11672.

102. Tokuhisa, H.; Liu, J. a.; Omori, K.; Kanesato, M.; Hiratani, K.; Baker, L. A. Efficient Biosensor Interfaces Based on Space-Controlled Self-Assembled Monolayers. *Langmuir* **2009**, *25*, 1633–1637.

103. Zhang, X.; Du, X.; Huang, X.; Lv, Z. Creating Protein-Imprinted Self-Assembled Monolayers with Multiple Binding Sites and Biocompatible Imprinted Cavities. *J. Am. Chem. Soc.* **2013**, *135*, 9248–9251.

104. Dong, Y.; Shannon, C. Heterogeneous Immunosensing Using Antigen and Antibody Monolayers on Gold Surfaces with Electrochemical and Scanning Probe Detection. *Anal. Chem.* **2000**, *72*, 2371–2376.

105. Jin, S.; Lee, J. S.; Kang, Y.; Heo, M.; Shin, J. H.; Cha, G. S.; Nam, H.; Lee, J. Y.; Helal, A.; Kim, H.-S.; Jeong, I.; Shim, J. H. Voltammetric Ion-Channel Sensing of Ammonium Ion Using Self-Assembled Monolayers Modified with Ionophoric Receptors. *Sensors and Actuators B: Chemical* **2015**, *207*, Part B, 1026–1034.

106. Casado-Montenegro, J.; Marchante, E.; Crivillers, N.; Rovira, C.; Mas-Torrent, M. Donor/Acceptor Mixed Self-Assembled Monolayers for Realising a Multi-Redox-State Surface. *ChemPhysChem* **2016**, *17*, 1810–1814.

107. Klajn, R.; Fang, L.; Coskun, A.; Olson, M. A.; Wesson, P. J.; Stoddart, J. F.; Grzybowski, B. A. Metal Nanoparticles Functionalized with Molecular and Supramolecular Switches. *J. Am. Chem. Soc.* **2009**, *131*, 4233–4235.

108. Samanta, D.; Sarkar, A. Immobilization of Bio-Macromolecules on Self-Assembled Monolayers: Methods and Sensor Applications. *Chem. Soc. Rev.* **2011**, *40*, 2567–2592.

109. Brooksby, P. A.; Anderson, K. H.; Downard, A. J.; Abell, A. D. Olefin Cross-Metathesis of a Vinyl-Terminated Self-Assembled Monolayer (SAM) on Au(111): Electrochemical Study Using a Ferrocenyl Redox Center. *Langmuir* **2006**, *22*, 9304–9312.

110. Ganesh, N. V.; Fujikawa, K.; Tan, Y. H.; Nigudkar, S. S.; Stine, K. J.; Demchenko, A. V. Surface-Tethered Iterative Carbohydrate Synthesis: A Spacer Study. *J. Org. Chem.* **2013**, *78*, 6849–6857.

111. Hassan, H. M. A.; Maltman, B. A. Mixed SAMS and MALDI–TOF MS: Preparation of N-Glycosylamine Derivative and Thioctic Acid Methyl Ester Bearing 1,2-Dithiolane Groups and Detection of Enzymatic Reaction on Au. *Bioorg. Chem.* **2012**, *40*, 6–9.

112. Lee, Y. J.; Jeon, I. C.; Paik, W.-k.; Kim, K. Self-Assembly of 1,2-Benzenedithiol on Gold and Silver: Fourier Transform Infrared Spectroscopy and Quartz Crystal Microbalance Study. *Langmuir* **1996**, *12*, 5830–5837.

113. Garg, N.; Lee, T. R. Self-Assembled Monolayers Based on Chelating Aromatic Dithiols on Gold. *Langmuir* **1998**, *14*, 3815–3819.

114. Garg, N.; Friedman, J. M.; Lee, T. R. Adsorption Profiles of Chelating Aromatic Dithiols and Disulfides: Comparison to Those of Normal Alkanethiols and Disulfides. *Langmuir* **2000**, *16*, 4266–4271.

115. Kim, C. H.; Han, S. W.; Ha, T. H.; Kim, K. *o*-Xylene-A,A‘-Dithiol Monolayer

Film on Gold: Fourier Transform Infrared Spectroscopy, Quartz Crystal Microbalance, and Atomic Force Microscopy Study. *Langmuir* **1999**, *15*, 8399–8404.

116. Lim, J. K.; Kwon, O.; Joo, S.-W. Interfacial Structure of 1,3-Benzenedithiol and 1,3- Benzenedimethanethiol on Silver Surfaces: Surface-Enhanced Raman Scattering Study and Theoretical Calculations. *J. Phys. Chem. C* **2008**, *112*, 6816–6821.

117. Lim, J. K.; Kim, Y.; Kwon, O.; Joo, S.-W. Adsorption of 1,3-Benzenedithiol and 1,3-Benzenedimethanethiol on Gold Surfaces. *ChemPhysChem* **2008**, *9*, 1781–1787.

118. Shon, Y.-S.; Lee, T. R. Chelating Self-Assembled Monolayers on Gold Generated from Spiroalkanedithiols. *Langmuir* **1999**, *15*, 1136–1140.

119. Sander, F.; Hermes, J. P.; Mayor, M.; Hamoudi, H.; Zharnikov, M. Add a Third Hook: SAcetyl Protected Oligophenylene Pyridine Dithiols as Advanced Precursors for Self- Assembled Monolayers. *PCCP* **2013**, *15*, 2836–2846.

120. Shon, Y.-S.; Lee, S.; Perry, S. S.; Lee, T. R. The Adsorption of Unsymmetrical Spiroalkanedithiols onto Gold Affords Multi-Component Interfaces That Are Homogeneously Mixed at the Molecular Level. *J. Am. Chem. Soc.* **2000**, *122*, 1278–1281.

121. Chinwangso, P.; Lee, H. J.; Lee, T. R. Self-Assembled Monolayers Generated from Unsymmetrical Partially Fluorinated Spiroalkanedithiols. *Langmuir* **2015**, *31*, 13341–13349.

122. Zenasni, O.; Jamison, A. C.; Lee, T. R. The Impact of Fluorination on the Structure and Properties of Self-Assembled Monolayer Films. *Soft Matter* **2013**, *9*, 6356–6370.

123. Colorado, R.; Villazana, R. J.; Lee, T. R. Self-Assembled Monolayers on Gold Generated from Aliphatic Dithiocarboxylic Acids. *Langmuir* **1998**, *14*, 6337–6340.

124. Lee, T.-C.; Hounihan, D. J.; Colorado, R.; Park, J.-S.; Lee, T. R. Stability of

Aliphatic Dithiocarboxylic Acid Self-Assembled Monolayers on Gold. *J. Phys. Chem. B* **2004**, *108*, 2648–2653.

125. Moore, H. J.; Colorado, R.; Lee, H. J.; Jamison, A. C.; Lee, T. R. Synthesis, Characterization, and Relative Stabilities of Self-Assembled Monolayers on Gold Generated from Bidentate N-Alkyl Xanthic Acids. *Langmuir* **2013**, *29*, 10674–10683.

126. Moore, H. J. Self-Assembled Monolayers on Gold Generated from Precisely Designed Organosulfur Adsorbates for the Preparation of Surfaces with Specific Interfacial Properties. Ph.D. Dissertation, University of Houston, 2007.

127. Eckermann, A. L.; Shaw, J. A.; Meade, T. J. Kinetic Dispersion in Redox-Active Dithiocarbamate Monolayers. *Langmuir* **2010**, *26*, 2904–2913.

128. Ford, W. E.; Gao, D.; Knorr, N.; Wirtz, R.; Scholz, F.; Karipidou, Z.; Ogasawara, K.; Rosselli, S.; Rodin, V.; Nelles, G.; von Wrochem, F. Organic Dipole Layers for Ultralow Work Function Electrodes. *ACS Nano* **2014**, *8*, 9173–9180.

129. Rittikulsittichai, S.; Park, C. S.; Jamison, A. C.; Rodriguez, D.; Zenasni, O.; Lee, T. R. Bidentate Aromatic Thiols on Gold: New Insights Regarding the Influence of Branching on the Structure, Packing, Wetting, and Stability of Self-Assembled Monolayers on Gold Surfaces. *Langmuir* **2017**, *33*, 4396–4406.

Chapter 2: Inverted Surface Dipoles in Fluorinated Self-Assembled Monolayers

2.1. Introduction

The ability of a chemist to modify the chemical functionality of partially fluorinated adsorbates at their tailgroups creates new routes for new types of fluorinated materials. In a recent report, the structure of a PEG-terminated alkanethiol was adapted by incorporating fluorocarbons in between the PEG and hydrocarbon backbone in order to create water-soluble gold nanoparticles.[1,2] Furthermore, the ability to distribute fluorinated moieties spatially within a larger network allows for an understanding of the macroscopic effect that such defined levels of fluorination have,[3] with recent examples being superhydrophobic MOFs (metal organic frameworks) that incorporate perfluorinated aromatic tetrazoles and carboxylic acids.[4] Separately, progress in organic synthesis has benefitted research on fluorinated materials; for example, Cai and co-workers have used click chemistry to create microarrays on fluorinated surfaces.[5]

In order to modify the physical and interfacial properties of monolayer films with fluorinated adsorbates, researchers continue to use self-assembled monolayers (SAMs) of thiols on gold. Studies involving the use of fluorinated self-assembled monolayer (FSAMs) have demonstrated increased inertness, oleophobicity, hydrophobicity, and thermal stability when compared to SAMs formed from normal alkanethiols.[6,7] These properties are imparted due to the highly polar C–F bond (bond strength of 105.4 kcal per mole),[8] in addition to the helical conformation of the perfluorinated chains.[9-11] Additionally, perfluorocarbon segments larger than their hydrocarbon counterparts lead to the occupation of a larger surface area.[12]

More than a decade ago, Lee and co-workers introduced a series of CF_3–terminated

alkanethiols for thin-film research.[13,14] SAMs derived from these molecules on gold have been found to be structurally similar to their hydrocarbon counterparts.[15-17] Furthermore, both types of adsorbates appear to arrange their underlying alkyl chains in the same manner despite the size difference of the terminal groups.[18] Nevertheless, the chemically dissimilar tailgroups impart different interfacial properties; the presence of a dipole at the fluorocarbon-hydrocarbon (FC–HC) junction causes the CF_3-terminated SAMs to be more wettable than the normal alkanethiol SAMs with polar liquids.[13] Further analysis involving these types of films was performed with a series of CF_3-terminated SAMs ($CF_3(CH_2)_nSH$, where n = 12–15) and their hydrocarbon analogs.[19] The same study also utilized a series of progressively fluorinated alkanethiols, while maintaining a constant carbon backbone, ($CF_3(CF_2)_n(CH_2)_mSH$, where n = 1–10 and m = 15–6; FnHmSH) in order to investigate the effect of the dipole as it was systematically buried into the SAM.[19]

The systematic investigation concluded that non-ideal dispersive interactions between the contacting liquid and the fluorinated surfaces resulted in increased oleophobicity and wettability with polar liquids for these types of films when compared to the normal alkanethiols. Furthermore, an odd-even effect is observed that is inverse of what is seen with the hydrocarbon SAMs with polar aprotic liquids. Correspondingly, the findings support the presence of the FC–HC dipole in CF_3-terminated SAMs, and the orientation of the dipole coincides with the orientation of the terminal perfluoromethyl group. The strength of the dipole in the FSAMs varies between the odd and even numbered chains, thus the observed odd-even effect depends on the total number of carbons. Furthermore, distancing the FC–HC dipole from the interface in the FnHmSH series led to a reduction in the wettability of the FSAMs with polar liquids. This latter effect was confirmed by a second series of fluorinated SAMs ($CF_3(CF_2)_n(CH_2)_{11}SH$, where n = 1–10; FnH11SH), for which the effect of the FC–HC dipole plateaued after five fluorocarbons.[20]

The chemical functionality of the tailgroup in FSAMs also influences adhesion and friction. For example, fluorinated monolayers exhibit weak adhesive properties;[21-23] however, a large coefficient of friction is found for CF_3-terminated SAMs via AFM. The latter observation is attributed to the size of the terminal group (~5.6 Å for a CF_3) in FSAMs and the locked spatial arrangement, which is dictated by the packing of the underlying hydrocarbon chain on the gold surface; the lattice spacing of the chains is ~4.8 Å.[15,18,24]

The current investigation examines the first examples of FSAMs having an inverted interfacial dipole (HC–FC). The CH_3-terminated, partially fluorinated alkanethiols featured in this study are of the form $CH_3(CF_2)_6(CH_2)_nSH$ (H1F6HnSH; where n = 10–13). *Notably, the type of interface formed from these thiols, a terminally fluorinated SAM capped with CH_3 groups, is unprecedented in interfacial science and represents a new class of organic thin film with unknown and unpredicted properties.*[25] In order to minimize the effect of the second "buried" FC–HC dipole, a six-fluorocarbon moiety was chosen for the molecules. The spacer was set at a minimum of ten methylene units to minimize the influence of the underlying gold substrate on the wetting phenomena and to allow for the generation of well-ordered films. Further, we compared the monolayers derived from the H1F6HnSH adsorbates to those derived from *n*-alkanethiol (HxSH; x = 17–20) and CF_3-terminated alkanethiol (F1HmSH; where m = 16–19) adsorbates having the same total chain lengths (see Figure 2.1). The SAMs were characterized using ellipsometry, polarization modulation infrared reflection-adsorption spectroscopy (PM-IRRAS), X–ray photoelectron spectroscopy (XPS), and contact angle goniometry.

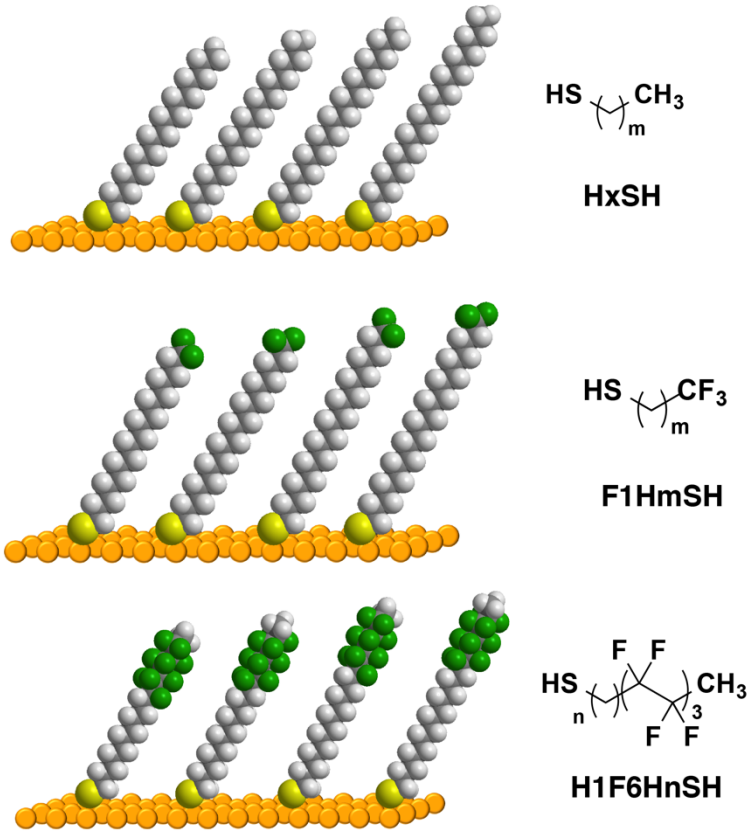

Figure 2.1. Illustrations of the chemisorbed adsorbates associated with the monolayer films formed from the deposition of (top) normal alkanethiols (HxSH), (middle) CF_3-terminated alkanethiols (F1HmSH), and (bottom) methyl-terminated partially fluorinated thiols (H1F6HnSH). All of the SAMs were prepared on gold surfaces.

2.2. Experimental Section

2.2.1. Materials and Methods

The following solvents used in this study were dried by distillation over calcium hydride (Sigma Aldrich): diethyl ether (Et_2O), dichloromethane (DCM), and tetrahydrofuran (THF) from Avantor Performance Materials (Macron Chemicals and J.T. Baker). The following solvents were used as received or degassed by purging argon: toluene, diethylene glycol (DEG), chloroform, dichloroethane (DCE), α,α,α-trifluorotoluene, dimethoxyethane (DME), ethyl acetate, and 1,3-dimethyl-3,4,5,6-tetrahydro-2(1H)-pyrimidinone (DMPU) (Sigma Aldrich); ethanol (EtOH –

Aaper Alcohol and Chemical Co.); hexanes, methanol (MeOH), and acetone (from Avantor Performance Materials).

Allyl magnesium bromide, butenyl magnesium bromide (3-butenylMgBr), allyl magnesium bromide, methanesulfonyl chloride (MsCl), vinyl magnesium bromide, lithium aluminum hydride ($LiAlH_4$), azobisisobutyronitrile (AIBN), tributyltin hydride (Bu_3SnH), *p*-toluenesulfonyl chloride (TsCl), borane tetrahydrofuran complex (BH_3·THF), *p*-toluenesulfonic acid (PTSA), triethylamine (Et_3N), 1,4,7,10,13-pentaoxacyclopentadecane (15-Crown-5), and dihydropyran (DHP) were all purchased from Sigma Aldrich and used as received.

Trifluoroethyl iodide (Cole); dimethyl perfluorosuberate (Synquest Labs); (trifluoromethyl) trimethylsilane (CF_3-TMS – Oakwood Products); cesium fluoride (CsF – Sigma Aldrich); hexadecanolide (ChemSampCo); 9-decen-1-ol and 4-nitrobenzeneulfonyl chloride (NsCl) (both from TCI America); benzyl bromide (Fluka); 1,10-decanediol, pentadecanolide, potassium thioacetate (KSAc), and 10-undecen-1-ol (Sigma Aldrich); 10% Pd/C (Alfa Aesar); were used as received. Lithium chloride (LiCl) and copper (II) chloride ($CuCl_2$) (Acros Chemicals) were used to prepare the lithium copper chloride (Li_2CuCl_4) solution.

Hydrochloric acid (HCl), potassium permanganate, sodium iodide (NaI), (Mallinckrodt Chemicals), and potassium hydroxide (KOH – Sigma Aldrich); zinc dust and hydroiodic acid (HI) (Fischer); sulfuric acid (H_2SO_4 – J.T. Baker); silver oxide (Ag_2O), sodium hydroxide (NaOH), hydrogen peroxide (30% H_2O_2), glacial acetic acid (AcOH), iodine (I_2), and ammonium chloride (NH_4Cl – all from Mallinckrodt Chemicals); potassium iodide (KI – EMD Chemicals); were all used as received.

The adsorbate octadecanethiol (**H18SH**) was purchased from Sigma-Aldrich. Heptadecanethiol (**H17SH**) was prepared by a procedure found in the literature.[26]

Nonadecanethiol (**H19SH**) and icosanehtiol (**H20SH**) were synthesized from the corresponding bromides. 11,11,12,12,13,13,14,14,15,15,16,16-dodecafluoroheptadecane-1-thiol (**H1F6H10SH)** and 12,12,13,13,14,14,15,15,16,16,17,17-dodecafluorooctadecane-1-thiol (**H1F6H11SH**) were prepared following the synthetic route outlined in the literature.[27] 17,17,17-Trifluoroheptadecane-1-thiol (**F1H16SH**) and 18,18,18-Trifluorooctadecane-1-thiol (**F1H17SH**) were synthesized following the literature.[27] Chloroform-*d* was purchased from Cambridge Isotope Laboratories and used to collect all NMR spectra. The silica gel used for column chromatography was obtained from Sorbent Technologies.

2.2.2. Synthesis of the Adsorbates

13,13,14,14,15,15,16,16,17,17,18,18-Dodecafluorononadecane-1-thiol (**H1F6H12SH**) and 14,14,15,15,16,16,17,17,18,18,19,19-dodecafluoroicosane-1-thiol (**H1F6H13SH**) were synthesized following the procedure depicted in Scheme 2.1. 19,19,19-trifluorononadecane-1-thiol (**F1H18SH**) and 20,20,20-trifluoroicosane-1-thiol (**F1H19SH**) were prepared according to Scheme 2.2.

Scheme 2.1 Synthetic Route Used to Prepare 13,13,14,14,15,15,16,16,17,17,18,18-Dodecafluorononadecane-1-thiol (**H1F6H12SH**) and 14,14,15,15,16,16,17,17,18,18,19,19-Dodecafluoroicosane-1-thiol (**H1F6H13SH**)

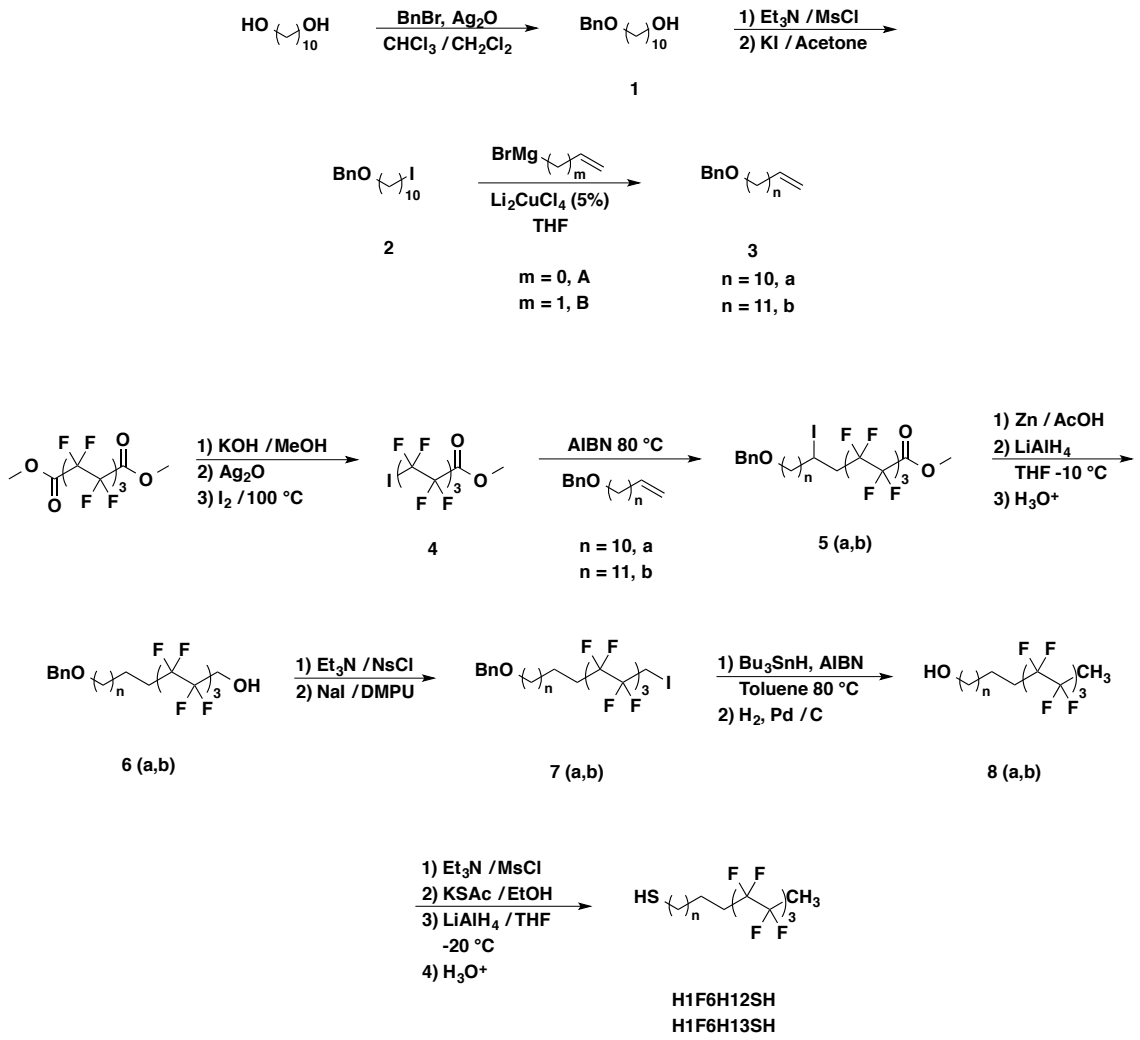

*10-(Benzyloxy)decan-1-ol (**1**)*. In a 250-mL round-bottomed flask, decane-1,10-diol (5.0349 g; 28.890 mmol) was dissolved in 150 mL of a 1:1 mixture of DCM and $CHCl_3$. Silver oxide (9.9661 g; 43.006 mmol) was then added, and the resulting mixture was stirred at 35 °C for 1 h. Benzyl bromide (3.75 mL; 31.6 mmol) was then added dropwise, followed by stirring the reaction mixture for 18 h. The solution was then filtered through a bed of Celite and washed with 200 mL of DCM. The solvent was removed by rotary evaporation, and the resulting residue was

dissolved in petroleum ether to remove the unreacted diol. After filtration, the filtrate was concentrated using rotary evaporation, and the residue was dried under high vacuum. The resulting oil was purified by column chromatography using hexanes/ethyl acetate (75/25) as the eluent to give the monoprotected diol **7** in 52% yield. ^{1}H NMR (400 MHz, $CDCl_3$): δ 7.38–7.26 (m, 5H), 4.50 (s, 2H), 3.63 (t, J = 6.73 Hz, 2H), 3.46 (t, J = 6.73 Hz, 2H), 1.64–1.52 (m, 2H), 1.35–1.24 (m, 12H).

*(((10-Iododecyl)oxy)methyl)benzene (**2**)*. The monoprotected diol (4.000 g; 15.13 mmol) was dissolved in 100 mL of dry THF at 0 ºC. Et_3N (6.3 mL; 45.39 mmol) was then added dropwise, and the reaction was stirred for 30 min before MsCl (3.5 mL; 45 mmol) was added dropwise to the solution. The reaction was stirred at rt for 6 h, followed by the addition of 50 mL of cold water. The solution was then extracted with ethyl acetate (3 × 150 mL), and then washed with water (1 × 100 mL) and brine (1 × 100 mL). The organic layer was then dried with $MgSO_4$, and the solvent removed using a rotary evaporator. The crude mesylated alcohol was then used without further purification.

The crude mesylated alcohol (6.162 g) and potassium iodide (31.3781 g; 189.022 mmol) were dissolved in 150 mL of acetone and refluxed for 24 h. The solvent was then removed by rotary evaporation. The residue was then dissolved with water (300 mL) and extracted with ethyl acetate (3 × 100 mL). The combined organic layers were then washed with 10% $NaHSO_3$ (1 × 100 mL), water (1 × 100 mL), brine (1 × 100 mL), and the organic layer dried with $MgSO_4$ followed by removal of the solvent via rotary evaporation. The crude iodide was then purified by silica gel chromatography using hexanes/ethyl acetate (98/2) as the eluent to give **2** as a colorless oil in 67% yield. ^{1}H NMR (500 MHz, $CDCl_3$): δ 7.36–7.26 (m, 5H), 4.50 (s, 2H), 3.46 (t, J =

6.53 Hz, 2H), 3.18 (t, J = 7.05 Hz, 2H), 1.84–1.78 (m, 2H), 1.63–1.58 (m, 2H), 1.37–1.28 (m, 12H).

((Tridec-12-en-1-yloxy)methyl)benzene ***(3b)***. An aliquot of **2** (4.746 g; 12.68 mmol) was dissolved in 100 mL of dried and degassed THF and then added to an oven-dried, 3-neck round-bottomed flask equipped with an addition funnel. At 0 °C, a 0.1M solution of Li_2CuCl_4 in THF (6.33 mL; 0.633 mmol) was added to the dissolved iodide. Subsequently, allyl magnesium bromide, 1M in Et_2O solution (25 mL; 25 mmol) was added dropwise. The reaction was allowed to stir at rt for 16 h under a flow of argon. The reaction was then quenched with 25 mL of saturated NH_4Cl followed by 25 mL of water. The mixture was extracted with diethyl ether (3 × 100 mL), and the combined organic layers were washed with brine (1 × 100 mL), dried over $MgSO_4$, and the solvent removed via rotary evaporation. The alkene was purified by silica gel chromatography using hexanes/dichloromethane (80/20) as the eluent to give **3b** as a colorless oil in 57% yield. ^{1}H NMR (400 MHz, $CDCl_3$): δ 7.33–7.26 (m, 5H), 5.86–5.75 (m, 1H), 5.01–4.90 (m, 2H), 4.49 (s, 2H), 3.45 (t, J = 6.59 Hz, 2H), 2.02 (q, J = 7.05 Hz, 2H), 1.64–1.56 (m, 2H), 1.36–1.25 (m, 16H).

((Dodec-11-en-1-yloxy)methyl)benzene (***9c***). 62% Yield. ^{1}H NMR (500 MHz, $CDCl_3$): δ 7.34–7.26 (m, 5H), 5.85–5.77 (m, 1H), 5.01–4.91 (m, 4H), 4.50 (s, 2H), 3.46 (t, J = 6.70 Hz, 2H), 2.05–2.01 (m, 2H), 1.63–1.58 (m, 2H), 1.36–1.25 (m, 14H).

Methyl 2,2,3,3,4,4,5,5,6,6,7,7-Dodecafluoro-7-iodoheptanoate ***(4)***. Dimethyl perfluorosuberate (10.085 g; 24.119 mmol) was dissolved in 50 mL of MeOH in a round-bottomed flask. A 10 mL solution of KOH (0.541 g; 9.64 mmol) in MeOH was added slowly, and the reaction stirred for 2.5 h at 50 °C. The reaction was quenched with 1 M HCl (12 mL) after cooling the reaction to rt, followed by 50 mL of water. The solution was extracted with Et_2O (3 × 150

mL), and the combined organic layers were washed with water (1 × 100 mL) and brine (1 × 100 mL), dried over $MgSO_4$, and evaporated to dryness by rotary evaporation.

The carboxylic acid and Ag_2O (2.46 g; 10.6 mmol) were then dispersed in 50 mL α,α,α-trifluorotoluene. The reaction ran at 75 °C for 5 h. Afterward, unreacted oxide was filtered off and then washed with hot acetone (50 mL). The solvent was then removed using rotary evaporation, and the resulting residue washed with boiling hexanes in order to recover unreacted dimethyl perfluorosuberate.

The silver salt was placed in a Schlenk flask and dried under high vacuum for 24 h. Afterwards, iodine (8.76 g; 34.3 mmol) was added under the flow of argon and the reaction heated at 100 °C for 24 h. The Schlenk flask containing the reaction mixture was then cooled to -30 °C in order to slowly release CO_2. The mixture was then dissolved in Et_2O (300 mL), and washed with 10% aqueous $NaHSO_3$ (2 × 100 mL), followed by water (1 × 100 mL) and brine (1 × 100 mL), and then dried over $MgSO_4$. The solvent was then carefully evaporated to dryness by rotary evaporation to give methyl 2,2,3,3,4,4,5,5,6,6,7,7-dodecafluoro-7-iodoheptanoate, **4**, in 33% yield from the starting diester. ^{1}H NMR (500 MHz, $CDCl_3$): δ 4.06 (s, 3H).

*Methyl 20-(Benzyloxy)-2,2,3,3,4,4,5,5,6,6,7,7-dodecafluoro-9-iodoicosanoate (**5b**).* In a 100-mL Schlenk flask with a condenser, **4** (5.170 g; 10.64 mmol), AIBN (0.1187 g; 0.7230 mmol), and **3b** (2.084 g; 7.224 mmol) were dissolved in 20 mL of DCE. After degassing the reaction using three cycles of a standard freeze-pump-thaw procedure, the reaction was stirred at 85 °C for 8 h. The progress of the reaction was monitored with ^{1}H NMR and repeated until the iodide was consumed. After completion of the reaction, the solvent was evaporated, and the crude mixture was purified by column chromatography over silica gel using hexanes/ethyl acetate (95/5) as the eluent system to give **5b** in 33% yield. ^{1}H NMR (500 MHz, $CDCl_3$): δ 7.34–7.26 (m, 5H), 4.50

(s, 2H), 4.35–4.30 (m, 1H), 3.99 (s, 3H), 3.46 (t, *J*= 6.70 Hz, 2H), 2.95–2.72 (m, 2H), 1.83–1.71 (m, 2H), 1.54–1.27 (m, 18H).

Methyl 19-(Benzyloxy)-2,2,3,3,4,4,5,5,6,6,7,7-dodecafluoro-9-iodononadecanoate (***5a***). 50% Yield. ^{1}H NMR (500 MHz, $CDCl_3$): δ 7.36–7.26 (m, 5H), 4.50 (s, 2H), 4.35–4.30 (m, 1H), 3.99 (s, 3H), 3.46 (t, *J* = 6.58 Hz, 2H), 2.96–2.70 (m, 2H), 1.85–1.71 (m, 2H), 1.43–1.28 (m, 16H).

*20-(Benzyloxy)-2,2,3,3,4,4,5,5,6,6,7,7-dodecafluoroicosan-1-ol (**6b**)*. **5b** (1.868 g; 2.412 mmol) was dissolved in 20 mL of degassed THF and 80 mL of glacial acetic acid. Zinc dust (2.365 g; 36.17 mmol) was then added under a flow of argon at rt. The reaction was stirred for 40 h. Afterwards, the mixture was diluted with 200 mL of Et_2O and filtered through Celite. The filtrate was washed with water (3 × 100 mL), saturated aqueous $NaHCO_3$ (2 × 100 mL), and brine (1 × 100 mL), and dried over $MgSO_4$. The solvent was then removed by rotary evaporation, and the resulting product carried to the next step without purification.

A solution of dissolved ester in dry THF (50 mL) was added dropwise to a stirring slurry of $LiAlH_4$ (0.1390g; 3.664 mmol) at -20 °C. The reaction was maintained under argon at -15 °C for 6 h. Afterwards, the reaction was cooled to -20 °C and quenched with 25 mL of water followed by acidification with 1M aqueous HCl solution. The product was then extracted with Et_2O (3 × 150 mL). The organic phases were then washed with water (1 × 100 mL) and brine (1 × 100 mL), dried over $MgSO_4$, and evaporated to dryness by rotary evaporation. The alcohol was purified by column chromatography on silica gel using hexanes/ethyl acetate (85/15) to give **6b** in 71% yield. ^{1}H NMR (500 MHz, $CDCl_3$): δ 7.34–7.26 (m, 5H), 4.50 (s, 2H), 4.12–4.03(m, 1H), 3.46 (t, *J*= 6.59 Hz, 2H), 2.10–1.94 (m, 2H), 1.63–1.55 (m, 2H), 1.34–1.26(m, 18H).

19-(Benzyloxy)-2,2,3,3,4,4,5,5,6,6,7,7-dodecafluorononadecan-1-ol (***6a***). 73% Yield. ^{1}H NMR (500 MHz, $CDCl_3$): δ 7.34–7.26 (m, 5H), 4.50 (m, 2H), 4.13–4.04 (m, 1H), 3.46 (t, J = 6.64 Hz, 2H), 2.08–1.93 (m, 2H), 1.64–1.55 (m, 2H), 1.34–1.26 (m, 16H).

*(((14,14,15,15,16,16,17,17,18,18,19,19-Dodecafluoro-20-iodoicosyl)oxy)methyl)benzene (**7b**)*. **6b** (1.072 g; 3.334 mmol) and NsCl (0.8267 g; 3.730 mmol) were dissolved in anhydrous DCM at 0 °C. Subsequently, Et_3N (1.4 mL; 10 mmol) was added into the solution dropwise. The reaction was then warmed to rt and stirred until consumption of the starting material (as detected by TLC). The reaction was then quenched with 1M HCl (20 mL) followed by the addition of water (100 mL). The layers were separated, and the organic layer was washed with water (1 × 100 mL), brine (1 × 100 mL), and dried over $MgSO_4$. After the evaporation of the solvent by rotary evaporation, the crude product was purified by recrystallization in ethanol to give the fluorinated nosylate in 38% yield.

The fluorinated nosylate (1.012 g; 1.281 mmol) and NaI (2.8841 g; 19.241 mmol) were dissolved in DMPU (15 mL) and heated to 100 °C for 18 h. After cooling the reaction to rt, the solution was diluted with 100 mL of water and the product extracted with ethyl acetate (3 × 150 mL). The combined organic layers were washed with water (3 x100 mL), half-saturated brine (2 × 100 mL), dried over $MgSO_4$, and the solvent was removed by rotary evaporation. The resulting residue was purified by column chromatography on silica gel using hexanes/ethyl acetate (95/5) as the eluent to give **7b** in 91% yield. ^{1}H NMR (500 MHz, $CDCl_3$): δ 7.35–7.26 (m, 5H), 4.50 (s, 2H), 3.63 (t, J = 17.18 Hz, 2H), 3.46 (t, J = 6.53 Hz, 2H), 2.10–1.99 (m, 2H), 1.64–1.51(m, 2H), 1.36–1.26 (m, 18H).

(((13,13,14,14,15,15,16,16,17,17,18,18-Dodecafluoro-19-iodononadecyl)oxy)methyl)benzene (***7a***). 98% Yield. ^{1}H NMR (500 MHz, $CDCl_3$): δ 7.36–7.26 (m, 5H), 4.50 (s, 2H), 3.63 (t, J =

17.18 Hz, 2H), 3.46 (t, *J* = 6.87 Hz, 2H), 2.09–1.98 (m, 2H), 1.63–1.54 (m, 2H), 1.35–1.26 (m, 18H).

14,14,15,15,16,16,17,17,18,18,19,19-Dodecafluoroicosan-1-ol ***(8b)***. The iodide intermediate **7b** (0.850 g; 1.16 mmol) and AIBN (10 mol %) were dissolved in anhydrous toluene followed by the addition of Bu_3SnH (0.95 mL; 3.5 mmol). The reaction was then stirred for 6 h at 85 ºC. After cooling to rt, the toluene was removed via rotary evaporation and the resulting residue suspended in Et_2O (100 mL) and filtered through a short bed of silica to remove any Bu_3SnI salt. The resulting residue was purified by flash chromatography on silica gel using hexanes/ethyl acetate (98/2) as the eluent to give the benzyl-protected alcohol in 100% yield.

To an oven dried, 2-neck round-bottomed flask was added a slurry of 10% Pd/C (0.135 g; 0.0993 mmol) in anhydrous MeOH (10 mL). The system was evacuated and filled with H_2 and allowed to stir for 10 min. Afterward, a solution of the benzyl-protected alcohol (0.764 g; 1.26 mmol) in MeOH (25 mL) was transferred into the flask and stirred for 16 h at rt. The reaction was then diluted with Et_2O (200 mL) and filtered through a pad of Celite. The solvent was then removed by rotary evaporation to give **8b** as a white solid in 100% yield. ^{1}H NMR (500 MHz, $CDCl_3$): δ 3.65 (t, *J* = 6.59 Hz, 2H), 2.11–2.00 (m, 2H), 1.88 (t, *J* = 19.18 Hz, 3H), 1.62–1.55 (m, 2H), 1.37–1.28 (20H).

13,13,14,14,15,15,16,16,17,17,18,18-Dodecafluorononadecan-1-ol ***(8a)***. 100% Yield. ^{1}H NMR (400 MHz, $CDCl_3$): δ3.64 (t, *J* = 6.64 Hz, 2H), 2.10–1.97 (m, 2H), 1.83 (t, *J* = 19.00 Hz, 3H), 1.62–1.53 (m, 2H), 1.36–1.27 (m, 18H).

14,14,15,15,16,16,17,17,18,18,19,19-Dodecafluoroicosane-1-thiol ***(H1F6H13SH)***. **8b** (0.656 g; 1.28 mmol) was dissolved in anhydrous THF under argon. The solution was cooled to 0 °C, and NEt_3 (0.55 mL; 3.9 mmol) was added slowly and allowed to stir for 30 min.

Subsequently, MsCl (0.30 mL; 3.9 mmol) was added dropwise with vigorous stirring. The reaction was allowed to warm to rt and stirred for 6 h. The reaction was then quenched with 50 mL of ice-cold water. The product was extracted with Et_2O (3 × 100 mL), and the combined organic phases were washed with 1M HCl (1 × 100 mL), water (1 × 100 mL), and brine (1 × 100 mL). The organic layer was dried over $MgSO_4$, followed by removal of the solvent via rotary evaporation. The crude product was carried to the next step without further purification.

After drying under high vacuum overnight, the crude mesylate and KSAc (0.4752 g; 4.161 mmol) were dissolved in 100 mL of degassed, absolute ethanol under argon and refluxed for 6 h. After cooling the reaction to rt, water (100 mL) was added, and the product was extracted with Et_2O (3 × 100 mL). The organic phases were combined and washed with water (1 × 100 mL) and brine (1 × 100 mL), and then dried over $MgSO_4$. The solvent was removed by rotary evaporation, and the crude thioacetate was dried and carried to the next step.

The crude thioacetate was dissolved in 50 mL of dry THF (previously degassed) and added dropwise to a stirring slurry of $LiAlH_4$ (0.0772 g; 2.03 mmol) in THF (10 mL) at -20 °C. The reaction was stirred under argon for 6 h at a temperature of -15 °C. The reaction was then quenched at -20 °C with 25 mL of water (previously degassed) and acidified with 1M H_2SO_4 (previously degassed). The resulting mixture was extracted with Et_2O (3 × 100 mL). The combined organic phases were washed with water (1 × 100 mL), brine (1 × 100 mL), dried over $MgSO_4$, and evaporated to dryness by rotary evaporation. The crude thiol was purified by flash column chromatography on silica gel using hexanes as the eluent to give 14,14,15,15,16,16,17,17,18,18,19,19-Dodecafluoroicosane-1-thiol (**H1F6H13SH**) in 76% yield. ^{1}H NMR (500 MHz, $CDCl_3$): δ 2.52 (q, J = 7.25 Hz, 2H), 2.09–1.98 (m, 2H), 1.83 (t, J = 19.18 Hz, 3H), 1.63–1.55 (m, 2H), 1.33 (t, J = 7.74 Hz, 1H), 1.43–1.26 (m, 21H). ^{13}C NMR (151 MHz,

$CDCl_3$): δ 34.2 (s), 31.1 (t, J = 21.4 Hz), 29.7–29.2 (m), 28.5 (s), 24.8 (s), 20.2 (m), 18.7(t, J = 24.4 Hz); broad peaks at δ 20.3–109.5 are characteristic of a long perfluorocarbon chain.[2] ^{19}F NMR (470 MHz, $CDCl_3$): δ -106.1 to -106.2 (m, 2F), -114.3 to -114.4 (m, 2F), -121.7 to -121.2 (m, 4F), -123.6 (m, 2F), -124.1 (m, 2F). GC-MS, *m/z*: 530 ($C_{20}H_{29}F_{12}SH^+$), 496 (M^+-SH_2), 55 ($C_4H_7^+$), 43 ($C_3H_7^+$).

*13,13,14,14,15,15,16,16,17,17,18,18-Dodecafluorononadecane-1-thiol (**H1F6H12SH**).* 100% Conversion. ^1H NMR (400 MHz, $CDCL_3$): δ 2.52 (q, J = 7.33 Hz, 2H), 2.11–1.97 (m, 2H), 1.83 (t, J = 19.00 Hz, 3H), 1.64–1.55 (m, 2H), 1.33 (t, J = 7.79 Hz, 1H), 1.36–1.25 (m, 18H). ^{13}C NMR (151 MHz, $CDCl_3$): δ 34.1 (s), 31.0 (t, J = 22.1 Hz), 29.8–29.2 (m), 28.5 (s), 24.8 (s), 20.2 (m), 18.6 (t, J = 24.4 Hz); broad peaks at δ 20.3–109.5 are characteristic of a long perfluorocarbon chain.[2] ^{19}F NMR (376 MHz, $CDCl_3$): δ -106.1 to -106.3 (m, 2F), -114.3 to -114.4 (m, 2F), -121.8 to -121.9 (m, 4F), -123.6 (m, 2F), -124.1 (m, 2F). GC-MS, *m/z*: 516 ($C_{19}H_{27}F_{12}SH^+$), 482 (M^+-SH_2), 55 ($C_4H_7^+$), 43 ($C_3H_7^+$).

Scheme 2.2. Synthetic Route Used to Prepare 19,19,19-Trifluorononadecane-1-thiol (**F1H18SH**) and 20,20,20-Trifluoroicosane-1-thiol (**F1H19SH**)

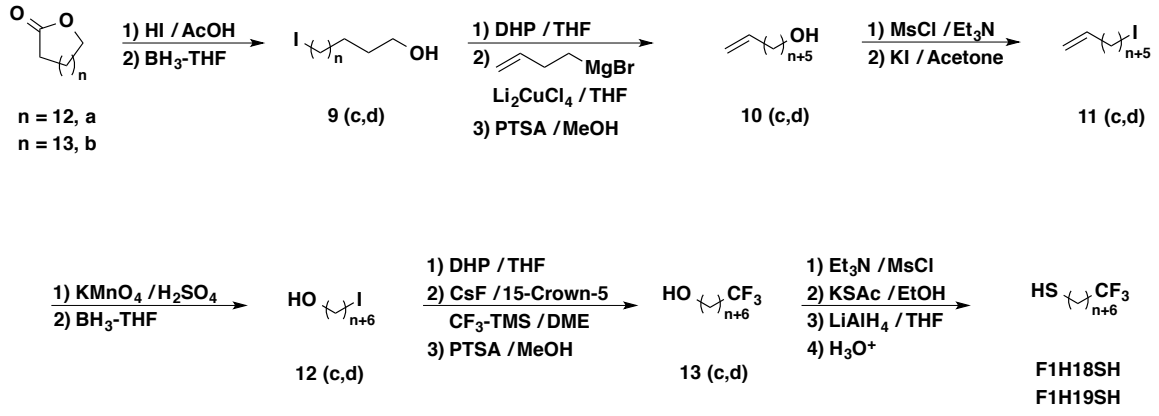

15-Iodopentadecan-1-ol (***9c***). *ω*-Pentadecalactone (15.0 g; 66.3 mmol), 57% hydroiodic acid in water (10 mL), and acetic acid (250 mL) were introduced into a 500-mL round-bottomed flask and refluxed for 24 h. Afterward, the reaction mixture was cooled to rt, and water (200 mL) was added to the flask. The heterogeneous mixture was then placed in an ice bath for 1 h and allowed to form a precipitate. The precipitate was filtered, washed extensively with water (5 × 100 mL) to remove traces of acetic acid, and recrystallized from hexanes to give 15-iodopentadecanoic acid as a white solid. Afterward, in a 500-mL round-bottomed flask, 15-iodopentadecanoic acid (22.0 g; 59.7 mmol) was dissolved in dry THF (250 mL) and cooled in an ice bath under nitrogen. Borane (1 M in THF, 90 mL) was then added to the flask through an addition funnel at 0 °C, and the mixture was stirred for 1 h at rt. After quenching with water (200 mL), the mixture was extracted with Et_2O (3 × 50 mL), and the combined organic layers were washed with brine (200 mL), dried over anhydrous Na_2SO_4, and concentrated under vacuum to afford **9c** in 90% yield. ^{1}H NMR (400 MHz, $CDCl_3$): δ 3.64 (m, 2H), 2.18 (t, J = 6.8 Hz, 2H), 1.81 (m, 2H), 1.55 (m, 2H), 1.25–1.39 (m, 22H).

16-Iodohexadecan-1-ol (***9d***). 89% Yield. ^{1}H NMR (400 MHz, $CDCl_3$): δ 3.64 (m, 2H), 2.18 (t, J = 6.8 Hz, 2H), 1.80 (m, 2H), 1.56 (m, 2H), 1.25–1.39 (m, 24H).

Nonadec-18-en-1-ol (***10c***). To a solution of 15-iodopentadecan-1-ol (10.6 g; 30.0 mmol) and dihydropyran (3.0 g; 35 mmol) in 200 mL of THF was added *p*-toluenesulfonic acid (0.57 g; 3.0 mmol). The resulting solution was stirred for 12 h at rt. The solution was then diluted with Et_2O (100 mL) and washed with brine (3 × 100 mL). The organic layer was dried over Na_2SO_4, and the solvent removed by rotary evaporation to give crude 2-(15-iodopentadecyloxy)tetrahydro-2*H*-pyran. Subsequently, to a solution of the crude iodo-pyran in 100 mL of THF were added a 0.1 M THF solution of Li_2CuCl_4 (5 mL; 0.5 mmol) at 0 °C under nitrogen. Afterward, 80 mL of

3-butenylmagnesium bromide (0.5 M in THF; 40 mmol) was added slowly over 10 min. The mixture was then warmed to rt and stirred for 12 h. The reaction was quenched by the addition of 25 mL of a saturated aqueous solution of NH_4Cl and 25 mL of water, after which the solution was extracted with Et_2O (3 × 100 mL). The combined organic layers were washed with brine (3 × 100 mL), dried with Na_2SO_4, and evaporated to dryness by rotary evaporation to give 2-(nonadec-18-enyloxy)tetrahydro-2*H*-pyran. The crude pyran was carried to the next step without purification. A mixture of the crude pyran and *p*-toluenesulfonic acid (5.7 g; 30 mmol) in 250 mL of methanol was stirred at rt for 1 h. The mixture was extracted with Et_2O (3 × 100 mL), and the combined organic layers washed with brine (3 × 100 mL) and then rotary evaporated to give 10.9 g of nonadec-18-en-1-ol in 99% yield. ^{1}H NMR (400 MHz, $CDCl_3$): δ 5.80 (m, 1H), 4.96 (m, 2H), 3.64 (m, 2H), 2.03 (m, 2H), 1.56 (m, 2H), 1.24–1.34 (m, 28H).

Icos-19-en-1-ol (***10d***). 92% Yield. ^{1}H NMR (400 MHz, CDCl3): δ 5.80 (m, 1H), 4.96 (m, 2H), 3.63 (m, 2H), 2.03 (m, 2H), 1.56 (m, 2H), 1.24–1.34 (m, 30H).

19-Iodononadec-1-ene (***11c***). In a round-bottomed flask, a mixture of nonadec-18-en-1-ol (10.9 g; 30.0 mmol) and triethylamine (8.4 mL; 60 mmol) was allowed to stir at rt for 30 min. The solution was then cooled in an ice bath, and an aliquot (4.5 mL; 60 mmol) of methanesulfonyl chloride (MsCl) was added dropwise and allowed to stir for 2 h at rt. Excess MsCl was then destroyed by adding 100 mL of water. The resulting mixture was extracted with Et_2O (3 × 50 mL), and the combined organic layers were washed with 4 M HCl (100 mL) and brine (100 mL). The organic layer was dried over Na_2SO_4, filtered, and concentrated to dryness to afford nonadec-18-enyl methanesulfonate, which was used in the next step without further purification. The crude mesylate and potassium iodide (4.00 g; 27.7 mmol) were dissolved in acetone (250 mL) and refluxed overnight. The solvent was then evaporated by rotary evaporation. Water (100 mL) and

Et_2O (50 mL) were added to dissolve the resulting residue, and the aqueous layer was extracted with Et_2O (2 × 100 mL). The combined organic layers were washed with brine (2 × 100 mL), dried over anhydrous Na_2SO_4, filtered, and rotary evaporated to dryness to afford 6.40 g (16.3 mmol) of 19-iodononadec-1-ene in 66% yield. ^{1}H NMR (400 MHz, $CDCl_3$): δ 5.81 (m, 1H), 4.95 (m, 2H), 3.18 (t, *J* = 7.3 Hz, 2H), 2.03 (m, 2H), 1.81 (m, 2H), 1.24–1.37 (m, 28H).

20-Iodoicos-1-ene (***11d***). 92% Yield. ^{1}H NMR (400 MHz, $CDCl_3$): δ 5.81 (m, 1H), 4.95 (m, 2H), 3.18 (t, *J* = 6.8 Hz, 2H), 2.03 (m, 2H), 1.81 (m, 2H), 1.24–1.37 (m, 30H).

18-Iodooctadecan-1-ol (***12c***). A mixture of 19-iodononadec-1-ene (6.40 g; 16.3 mmol), $KMnO_4$ (5.00 g; 31.6 mmol), 50% H_2SO_4 (20 mL), and glacial acetic acid (5 mL) in 200 mL of a 1:1 H_2O:DCM solution was stirred for 2 h at 40 °C. The mixture was then extracted with DCM (3 × 100 mL), and the combined organic layers washed with brine (200 mL), dried over anhydrous Na_2SO_4, and concentrated by rotary evaporation. Next, borane (1 M in THF; 90 mL) was added to the flask containing the 100 mL THF solution of 18-iodooctadecanoic acid through an addition funnel at 0 °C. After completion as monitored by TLC, the mixture was stirred for 1 h at rt. After quenching with water (200 mL), the mixture was extracted with Et_2O (3 × 50 mL). The combined organic layers were washed with brine (200 mL), dried over anhydrous Na_2SO_4, and concentrated under vacuum. The crude product was purified by column chromatography using hexanes/ethyl acetate (90/10) to give 1.80 g of 18-iodooctadecan-1-ol in 56% yield. ^{1}H NMR (400 MHz, $CDCl_3$): δ 3.63 (m, 2H), 3.18 (t, *J* = 6.9 Hz, 2H), 1.81 (m, 2H), 1.55 (m, 2H), 1.24–1.35 (m, 28H).

19-Iodononadecan-1-ol (**12d**). 35% Yield. ^{1}H NMR (400 MHz, $CDCl_3$): δ 3.63 (m, 2H), 3.18 (t, *J* = 6.9 Hz, 2H), 1.81 (m, 2H), 1.55 (m, 2H), 1.24–1.35 (m, 30H).

19,19,19-Trifluorononadecan-1-ol (***13c***). A solution of 18-iodooctadecan-1-ol (1.80 g; 4.54 mmol) and dihydropyran (0.42 g; 5.0 mmol) in 100 mL of THF containing *p*-toluenesulfonic

acid (0.10 g; 0.50 mmol) was stirred for 12 h at rt. The solution was then diluted with Et_2O (100 mL) and washed with brine (3 × 100 mL). The organic phase was subsequently dried over Na_2SO_4, and the solvent was removed by rotary evaporation to give 2-(18-iodooctadecyloxy)tetrahydro-2*H*-pyran. In the next step, CsF (1.7 g; 11 mmol) was placed in a flask and carefully dried by heating under vacuum for 2 h. After cooling to rt, 4.0 g of 15-crown-5 (18 mmol) and 20 mL of dimethoxyethane were added with vigorous stirring. The solution was then cooled to -20 °C, and a mixture of (trifluoromethyl)trimethylsilane (1.7 g; 11 mmol) and crude 2-(18-iodooctadecyloxy)tetrahydro-2*H*-pyran in 10 mL dimethoxyethane was added dropwise into the reaction flask with stirring. The mixture was then stirred overnight at rt. Upon completion as monitored by TLC, the mixture was diluted with 50 mL of Et_2O, and the mixture was then filtered to remove any precipitate. The solution was washed with brine (1 x 100 mL), dried over Na_2SO_4, and then rotary evaporated to dryness. The crude product was used in the next step without further purification. The fluorinated pyran and *p*-toluenesulfonic acid (1.1 g; 6.0 mmol) were dissolved in 100 mL methanol, and the mixture was allowed to stir for 1 h at rt. The solution was then concentrated via rotary evaporation under vacuum by removing most of the solvent. The remaining solution was diluted with Et_2O (100 mL) and washed with brine (3 x 100 mL). The solvent was then removed by rotary evaporation to give 1.1 g of 19,19,19-trifluorononadecan-1-ol in 99% yield). ^{1}H NMR (400 MHz, $CDCl_3$): δ 3.64 (t, J = 6.8 Hz, 2H), 2.05 (m, 2H), 1.52 (m, 4H), 1.24–1.34 (m, 28H).

*20,20,20-Trifluoroicosan-1-ol (**13d**)*. 99% Yield. ^{1}H NMR (400 MHz, $CDCl_3$): δ 3.64 (t, J = 6.8 Hz, 2H), 2.05 (m, 2H), 1.52 (m, 4H), 1.24–1.34 (m, 30H).

19,19,19-Trifluorononadecane-1-thiol (***F1H18SH***). In a round-bottomed flask, 19,19,19-trifluorononadecan-1-ol (1.1 g; 3.3 mmol) and Et_3N (1.4 mL; 10 mmol) were dissolved in 100 mL

of THF. To the solution, MsCl (0.80 mL; 10 mmol) was added dropwise, and the solution was allowed to stir for 2 h at rt. Excess MsCl was then destroyed by adding 100 mL of water. The mixture was extracted with Et_2O (3 × 50 mL), and the combined organic layers were washed with 4 M HCl (100 mL), $NaHCO_3$ solution (50 mL), and brine (100 mL). The organic layer was dried over Na_2SO_4, filtered, and concentrated to dryness to give 19,19,19-trifluorononadecyl methanesulfonate, which was used in the next step without further purification. Afterward, KSAc (0.53 g; 4.6 mmol) and the crude fluorinated mesylate were dissolved in ethanol (20 mL) and refluxed for 12 h. After cooling the solution to rt, the solvent was evaporated by rotary evaporation. The residue was then dissolved with Et_2O (100 mL). The resulting solution was washed with brine (3 × 100 mL), dried over anhydrous Na_2SO_4, and filtered. A rotary evaporator was used to remove the solvent to give the fluorinated thioacetate. The crude thioacetate was used in the next step without purification. The crude thioacetate was dissolved in dry THF (20 mL) and was carefully added to a suspension of $LiAlH_4$ (0.4 g, 10 mmol) in dry THF (100 mL) at 0 °C. The mixture was then refluxed for 2 h under nitrogen. The solution was cooled to 0 °C, quenched with water (20 mL), then acidified to pH ~1 using 4 M HCl. The compound was then extracted with Et_2O (3 × 50 mL). The combined organic layers were washed with brine (100 mL), dried over anhydrous Na_2SO_4, filtered, and concentrated to dryness. The residue was purified by column chromatography (hexanes) to afford 0.54 g of 19,19,19-trifluorononadecane-1-thiol in 52% yield. ^{1}H NMR (400 MHz, $CDCl_3$): δ 2.51 (m, 2H), 2.05 (m, 2H), 1.57 (m, 4H), 1.24–1.38 (m, 29H). ^{13}C NMR (151 MHz, $CDCl_3$): δ 130.1–124.6 (q, J = 275.9 Hz), 34.2 (s), 34.1–33.5 (q, J = 28.0 Hz), 29.8–29.6 (m), 29.5 (s), 29.3 (s), 29.2 (s), 28.8 (s), 28.5 (s), 24.8 (s), 21.9 (m). GC-MS, *m/z*: 354 ($C_{19}H_{36}F_3SH^+$), 320 (M^+-SH_2), 83 ($C_2H_2F_3^+$), 55 ($C_4H_7^+$), 43 ($C_3H_7^+$).

20,20,20-Trifluoroicosane-1-thiol (***F1H19SH***). 62% Yield. ^{1}H NMR (400 MHz, $CDCl_3$): δ 2.51 (m, 2H), 2.05 (m, 2H), 1.57 (m, 4H), 1.24–1.38 (m, 31H). ^{13}C NMR (151 MHz, $CDCl_3$): δ 130.1–124.6 (q, J = 276.4 Hz), 34.2 (s), 34.1–33.5 (q, J = 28.0 Hz), 29.8–29.6 (m), 29.5 (s), 29.3 (s), 29.2 (s), 28.8 (s), 28.5 (s), 24.8 (s), 21.9 (m). GC-MS, *m/z*: 368 ($C_{20}H_{38}F_3SH^+$), 334 (M^+-SH_2), 83 ($C_2H_2F_3^+$), 55 ($C_4H_7^+$), 43 ($C_3H_7^+$).

2.2.3. Preparation and Characterization of Self-Assembled Monolayers

The gold substrates were prepared by thermal evaporation. Gold shot (99.999%) was purchased from American Precious Metals. Silicon(100) wafers were purchased from Silicon Wafer Enterprises. The vacuum pressure of the system was ≤ 6×10^{-5} torr. To aid the adhesion of the Au layer, 100 Å of Cr (Chromium rods, 99.9%; R. D. Mathis Company.) was initially deposited, followed by 1000 Å of Au at rate of 0.5 Å / s. Immediately after vapor deposition, the substrates were washed with absolute ethanol and dried with ultra-pure nitrogen gas. Solutions of the thiols at 1 mM concentration in absolute ethanol (previously degassed) were prepared in 40 mL vials that had been previously cleaned with piranha solution and rinsed thoroughly with deionized water, followed by absolute ethanol. Two cut Au slides (3 cm × 1 cm) were then immersed into each of the thiol solutions and allowed to equilibrate 48 h at rt, in the dark, which was followed by a further 24 h at 40 °C for the methyl-terminated FSAMs. Prior to characterization, all films were rinsed with THF, followed by absolute ethanol, and dried with ultra-pure nitrogen gas.

Thickness measurements were collected on a Rudolph Auto EL III ellipsometer equipped with a He-Ne laser (632.8 nm) at an incident angle set of 70°. The refractive index was set to 1.45,

a typical value used in the literature for organic monolayers.[28] The reported thickness values are an average of 6 measurements (3 measurements per slide).

X-Ray photoelectron spectroscopy (XPS) measurements were taken on a PHI 5700 X-Ray photoelectron spectrometer with a monochromatic Al Kα X-ray source ($h\nu$ = 1486.7 eV) incident at 90° relative to the axis of the hemispherical energy analyzer. The takeoff angle from the surface was set at 45° with a pass energy of 23.5 eV. The Au $4f_{7/2}$ peak at 84.0 eV was used as a reference peak, with each spectrum set to align with that reference.

Surface IR spectra were collected using a Nicolet Nexus 670 Fourier transform spectrometer equipped with a mercury-cadmium-telluride (MCT) detector and a Hinds Instrument PEM-90 photoelastic modulator. The collected spectra were from surfaces mounted at an incident angle of 80° for the p-polarized light with respect to the surface normal. For each sample, we collected 512 scans at a resolution of 2 cm^{-1}.

Contact angle data were obtained using a Ramé-Hart model 100 contact angle goniometer working with a Matrix Technologies micro-Electrapette 25 dispensing liquids from a disposable pipette tip. Contacting liquids were of the highest purity available at the time of their purchase and were dispensed at a speed of 1 μL/s to obtain advancing contact angles (θ_a) and withdrawn at the same speed to obtain receding contact angles (θ_r). The specific method used to collect the contact angle data was the dynamic sessile drop procedure (where the liquid dispensing pipette remains in contact with the drop), with measurements made during the dispensing and withdrawal of the contacting liquid, maintaining the pipette tip centered on the drop. The reported contact angle data represent the average and standard deviation associated with at least 12 measurements; readings were made from each side of the dispensed droplets from 3 different locations for each SAM-coated slide.

The following polar protic, polar aprotic, and nonpolar contacting liquids were used: water (H_2O – Millipore water with a resistivity of 18.2 Ω·cm), glycerol (GL – Sigma Aldrich), formamide (FM – Sigma Aldrich), dimethyl sulfoxide (DMSO – Sigma Aldrich), nitrobenzene (NB – Acros), dimethylformamide (DMF – Sigma Aldrich), acetonitrile (ACN – Sigma Aldrich), bromonaphthalene (BNP – Sigma Aldrich), perfluorodecalin (PFD – Synquest Labs), hexadecane (HD – Aldrich), cis/trans decalin (DC – Acros Organics), 1,3-propanediol (Aldrich), 2,4-pentanediol (Acros Organics), cyclohexanol (EM Science), *iso*-propanol (Sigma Aldrich), methyl formamide (MFA – Sigma Aldrich), and *tert*-butanol (EM Science).

2.2.4. Molecular Modeling

All calculations were performed with the ORCA program package.[29] Geometry optimizations and electric properties were calculated using second order perturbation theory. In both geometry optimizations and property calculations, the def2-SVP basis set was chosen for all atoms. The RI[30] and RIJCOSX[31] approximations were applied in conjunction with the def2-SVP auxiliary basis sets. The dipole moments were calculated using the MP2 "relaxed" densities. Adsorbate orientations relative to surface normal were determined using Mathematica 10.2. Owing to complications in the calculation of the structures of the CF_3-terminated thiols, analogous normal alkanethiol chains were used for determining surface orientations for these compounds.

2.3. Results and Discussion

In this investigation, we compare the new H1F6HnSH FSAMs to SAMs derived from their normal alkanethiol analogs (HxSH). The latter SAMs have been rigorously characterized in the literature and act as a reference. Additionally, we examine SAMs derived from a series of CF_3-terminated alkanethiols (F1HmSH) bearing the same number of carbons as the H1F6HnSH adsorbates to compare the influence of the inverted dipole upon the interfacial properties of the films.

2.3.1. Ellipsometric Measurements

To generate SAMs from the H1F6HnSH series, we initially examined their development in ethanol for 48 h at rt; previous work on fluorinated alkanethiols utilize ethanol as the solvent for developing related FSAMs.[20] Initial measurements yielded thickness values for the H1F6HnSH SAMs that were thinner than anticipated, while the other films prepared for this study, monolayers formed from HxSH and F1HmSH, gave appropriate thickness values. In an effort to enhance the film thicknesses of the new thiolate adsorbates on gold, we equilibrated all of the H1F6HnSH monolayers for an additional 24 h in ethanol at 40 °C, which enhances the mobility of the thiolate species on the gold surface and, therefore, the final packing density.[32]

Table 2.1 shows the average thickness values for all of the monolayers. The HxSH series gave average thickness values that are in agreement with the literature values, 21 Å, 22 Å, 23 Å, and 25 Å for the SAMs formed from **H17SH, H18SH, H19SH**, and **H20SH**, respectively.[26,32] The average thickness measurements of the F1HmSH series were 18 Å, 20 Å, 21 Å, and 23 Å for the SAMs formed from **F1H16SH, F1H17SH, F1H18SH**, and **F1H19SH**, respectively. The obtained values are in agreement with previous research that reported an ~1.5 Å difference for the

thickness of CF_3-terminated alkanethiolate SAMs.[33] However, the thickness values for the methyl-capped fluorinated thiols were ~1 Å shorter still (but within experimental error): 17 Å, 19 Å, 20 Å, and 21 Å for the SAMs formed from **H1F6H10SH**, **H1F6H11SH**, **H1F6H12SH**, and **H1F6H13SH**, respectively. The increase in monolayer thickness within the H1F6HnSH SAM series, as well as the other two sets of SAMs, represent an increase of one methylene unit per homolog in the series (~1–2 Å per CH_2 unit).[26,34]

Table 2.1. Ellipsometric Data for SAMs Formed from the HxSH, F1HmSH, and H1F6HnSH series

Adsorbate	Thickness (Å)	Adsorbate	Thickness (Å)	Adsorbate	Thickness (Å)
H17SH	21	**F1H16SH**	18	**H1F6H10SH**	17
H18SH	23	**F1H17SH**	20	**H1F6H11SH**	19
H19SH	24	**F1H18SH**	21	**H1F6H12SH**	20
H20SH	25	**F1H19SH**	23	**H1F6H13SH**	21

Although the H1F6HnSH films are marginally thinner than the HxSH and F1HmSH films, the thickness measurements are consistent with those of more highly fluorinated alkanethiolate films (i.e., partially fluorinated FSAMs of the form FnHmSH).[34,35] Unlike the H1F6HnSH FSAMs, however, the terminally fluorinated FSAMs developed well-packed films in a shorter time and lower temperature.[20,36] For the aforementioned adsorbates, there is a difference in the tilt of the perfluorinated segment and the hydrocarbon segment, the latter of which has a greater tilt; we anticipated the H1F6HnSH SAMs to have similar thickness to their comparative offsets.[35,37] A lower packing density might be the contributing factor to the thinner H1F6HnSH SAMs as compared to the HxSH and F1HmSH SAMs. Analysis by AFM has shown that there are less fluorinated adsorbates on the gold lattice due to the larger size of the fluorinated segment (5.6 Å)

compared to a hydrocarbon chain (4.2 Å).[38,39] Moreover, previous studies on the structure of partially fluorinated alkanethiols (F10HnSH; where n = 11, 17, 33) demonstrated that the fluorinated segments exhibited an increased tilt and slight disorder in the fluorinated segment which is caused by the vdW interactions between the alkyl chains.[37,39] In addition, the reduction of the refractive index associated with fluorocarbons (1.33) versus that of hydrocarbons (1.45) might contribute to the observed reduction in the thickness values for H1F6HnSH FSAMs since we used a refractive index value of 1.45 for these films to obtain the ellipsometric thicknesses.[40] Considering these possible contributions to the marginally low thicknesses measured for the H1F6HnSH FSAMs, and that the three sets of SAMs were produced from alkanethiols with equivalent carbon counts, the analysis of the film packing characteristics provided in the following section sheds some additional light on the observed differences in film thickness.

2.3.2. XPS Analysis of the Composition and Packing of the SAMs

Analysis of SAMs by XPS bares the chemical composition of the SAM in addition to an understanding of a monolayer's structural features.[41] Survey spectra show the presence of Au, C, F, and S for both of the fluorinated SAMs, while the HxSH SAMs show Au, C, and S. Table 2.2 lists the binding energies of the elements surveyed. Confirmation of a bound thiolate is obtained through analysis of the S 2p region, shown in Figure 2.2, with the appearance of the S $2p_{3/2}$ at ~162 eV and 163.8 eV for the S $2p_{1/2}$.[42] Further confirmation is obtained by the absence of peaks corresponding to unbound thiols at ~164–166 eV. The absence of unbound thiol on the surface validates the rinse procedure used to clean the SAMs and confirms that the thickness values are those of covalently bound monolayers.

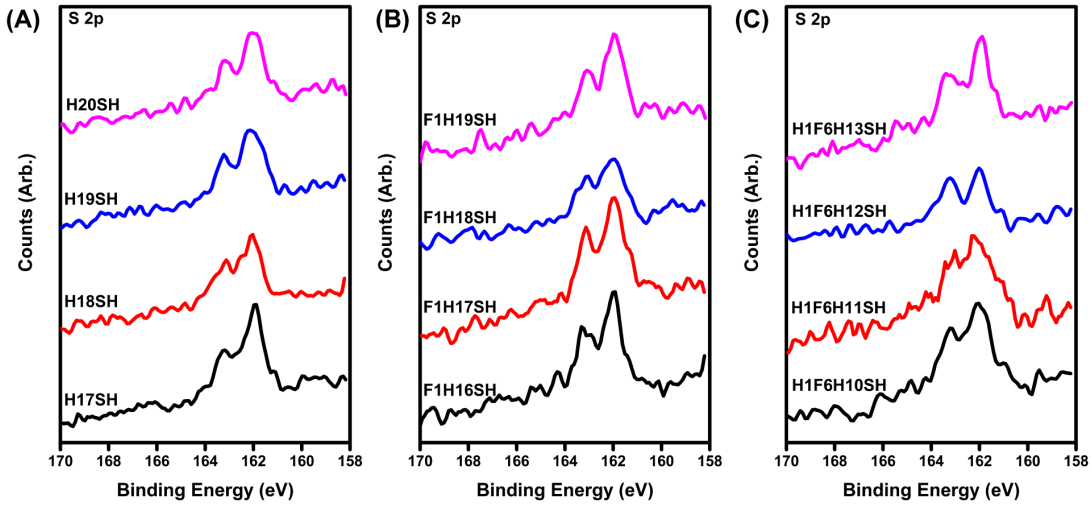

Figure 2.2. XPS spectra for the S 2p region of the investigated SAMs: (A) HxSH, (B) F1HmSH, and (C) H1F6HnSH.

Table 2.2. XPS Peak Positions for the HxSH, F1HmSH, and H1F6HnSH SAMs on Gold

Adsorbate	Peak Position (eV)				
	C 1s (CH_2)	C 1s (CF_2)	C 1s (CF_3)	S $2p_{3/2}$	F 1s
H17SH	285.0	-	-	161.9	-
H18SH	285.0	-	-	162.0	-
H19SH	285.0	-	-	162.1	-
H20SH	284.9	-	-	162.0	-
F1H16SH	284.7	-	292.7	161.9	688.3
F1H17SH	284.9	-	292.7	162.0	688.4
F1H18SH	284.9	-	292.7	162.0	688.4
F1H19SH	284.9	-	292.7	162.0	688.3
H1F6H10SH	284.6	291.2	-	162.1	688.5
H1F6H11SH	284.6	291.3	-	162.2	688.6
H1F6H12SH	284.8	291.3	-	162.0	688.6
H1F6H13SH	284.6	291.2	-	162.0	688.5

In addition to obtaining the chemical composition of a SAM, a qualitative examination of the chain density can be obtained by analyzing the films using XPS. The C 1s region of the HxSH, F1HmSH, and H1F6HnsH SAMs is presented in Figure 2.3. There are two distinct peaks in the C 1s spectra of the H1F6HnSH series associated with the CF_2 and CH_2/CH_3 units.[37,39] On the other hand, the spectra of HxSH SAMs show only one peak (i.e., that associated with the CH_2/CH_3 units), and the SAMs formed from F1HmSH show two peaks characteristic of CF_3 and CH_2 units. Comparison of the position of the C 1s peaks corresponding to the hydrocarbons (see Table 2.2), shows that the corresponding values for this peak in the H1F6HnSH FSAMs are shifted to a lower binding

energy (~284.6 eV) as compared to those of the HxSH (~285.0 eV) and F1HmSH (~284.9 eV) SAMs. Shifts in binding energy can be correlated to changes in the packing density of the alkyl chains on the gold surface.[43] The differences in the vdW diameter of the fluorinated helix and the hydrocarbon chain can explain this observation; a difference in structure can cause such adsorbates to occupy more space on the gold lattice compared to the HxSH or F1HmSH adsorbate.[15,21,39] Previous studies have concluded that well-packed films can act as good insulators, which hinders the processes of discharging positive charges generated by XPS irradiation, which will lead to the emitted electrons having a higher binding energy; on the other hand, a poorly packed film will behave as a poor insulator.[39,44,45] Additionally, the binding energy of the C 1s peak for the CH_2 units for the H1F6HnSH series falls within the same range for all the generated films. The consistency in the peak position of the C 1s peak for the CH_2 units of the H1F6HnSH FSAMs indicates the formation of a well-packed monolayer for this type of adsorbate having ten methylene (CH_2) units in the backbone.

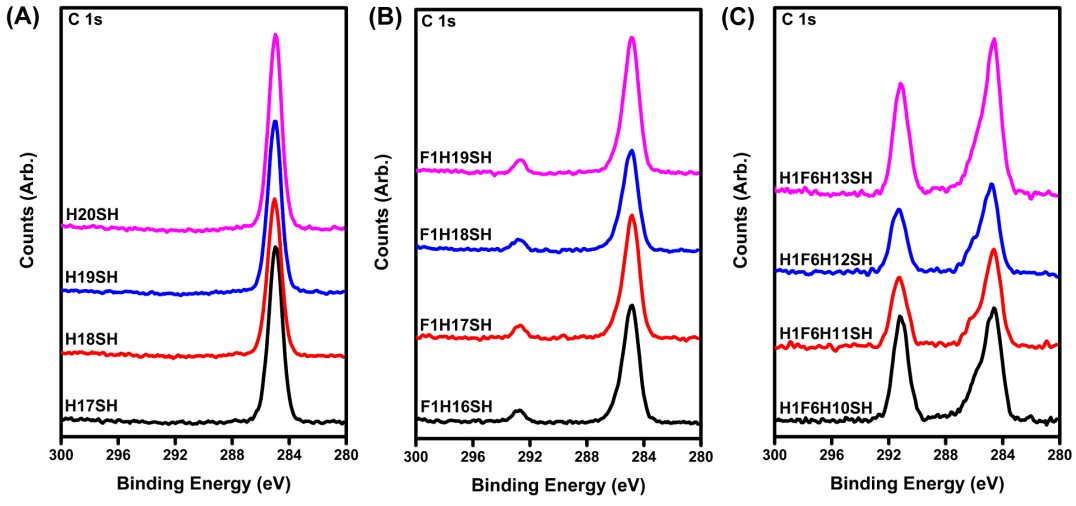

Figure 2.3. XPS spectra for the C 1s region of the investigated SAMs: (A) HxSH, (B) F1HmSH, and (C) H1F6HnSH.

Further, analysis of the F1s XPS spectra of the H1F6HnSH series in Figure 2.4 also indicate that the perfluorinated segments of these monolayers share similar packing densities – a conclusion supported by the consistency of the binding energy values for the F1s core electrons of the CF_2 units in the films. Figure 2.4 provides the F 1s spectra of the monolayers of the H1F6HnSH series and that of the F1HnSH series, which originate from the fluorine atoms on the CF_2 segment and CF_3 moiety, respectively. Note that the binding energy of the F1s electrons in CF_3 termini of the F1HnSH FSAMs (listed in Table 2.2) is lower than that of the perfluorinated segments of the H1F6HnSH. Frey *et al*. observed a change in the binding energy of the F 1s electrons in a series of terminally perfluorinated SAMs where the terminal fluorinated segment is systematically increased and attributed it to an increase in the distance between core hole and the screening electrons of the substrate, a final state effect.[37] In a separate study of SAMs derived from FnHmSH (where n + m = 16), Colorado *et al.* noted that as the amount of fluorination is increased, an attenuation of the Au 4f electrons also increased, a trend that is also seen in the FnH11SH SAMs (n = 1–10).[35] Moreover, in our data, the amount of fluorination in the H1F6HnSH FSAMs appears to have a greater role in the final state effect than the thickness of the SAMs. This effect is also observed in the broadening of the C 1s (CH_2) peak of the H1F6HnSH FSAMs. In addition, the similar peak position in the F 1s spectra for all the H1F6HnSH FSAMs might reinforce this assumption (*vide supra*).[39,44,45]

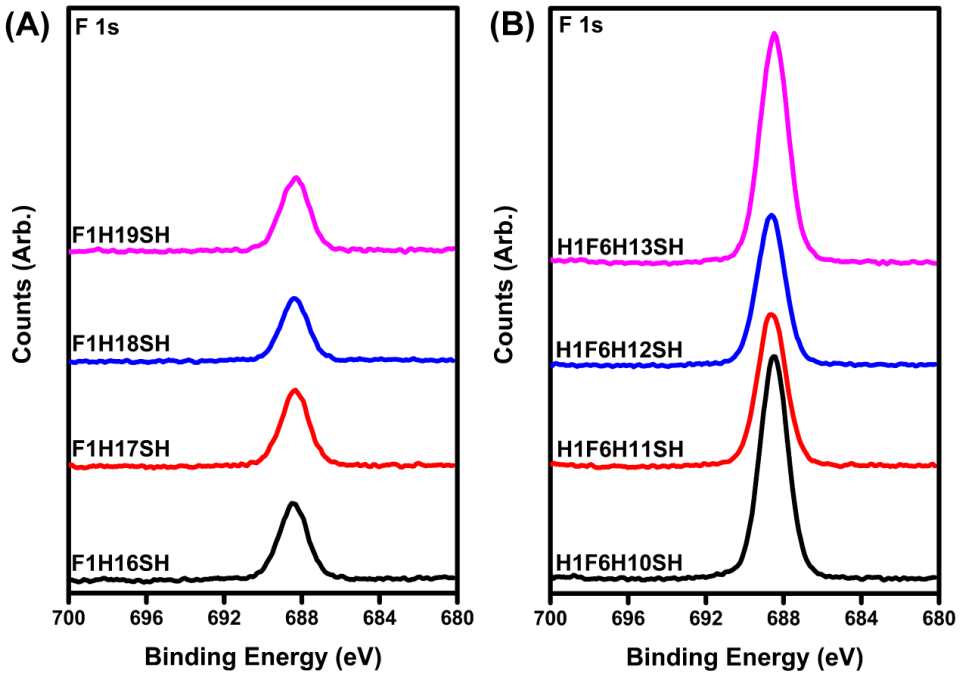

Figure 2.4. XPS spectra for the F 1s region of the investigated SAMs: (A) F1HnSH and (B) H1F6HnSH.

Taking into consideration the XPS data, the chains in the H1F6HnSH FSAMs appear to possess a lower packing density vis-à-vis those in the HxSH and the F1HmSH monolayers, and there is no clear improvement in the packing density in the H1F6HnSH FSAMs as a function of the number of methylene units for the adsorbates examined in this study.

2.3.3. PM-IRRAS Analysis of the Relative Conformational Order of the SAMs

Analysis of SAMs by surface IR can give insight into the relative conformational order, and in the case of alkenthiols, an evaluation of the chain orientation can be performed. The conformational order (or crystalline nature) of SAMs can be most easily estimated from the position of the antisymmetric methylene C–H stretching band ($\nu_{as}^{CH}{}_2$).[28,46,47] For a well-ordered (or relatively "crystalline") monolayer, $\nu_{as}^{CH}{}_2$ will appear at ~2918 cm^{-1}; in this case, the hydrocarbon chains, similar to paraffin wax, mostly adopt a *trans*-extended conformation, while a less ordered SAM possessing gauche defects will have this band at a higher wavenumber. Figure 2.5 shows the C–H stretching region for the HxSH, F1HmSH, and H1F6HnSH SAMs. Figure 2.4A shows the HxSH SAMs with a $\nu_{as}^{CH}{}_2$ at 2918 cm^{-1}, consistent with a monolayer having *trans*-extended chains.[47]

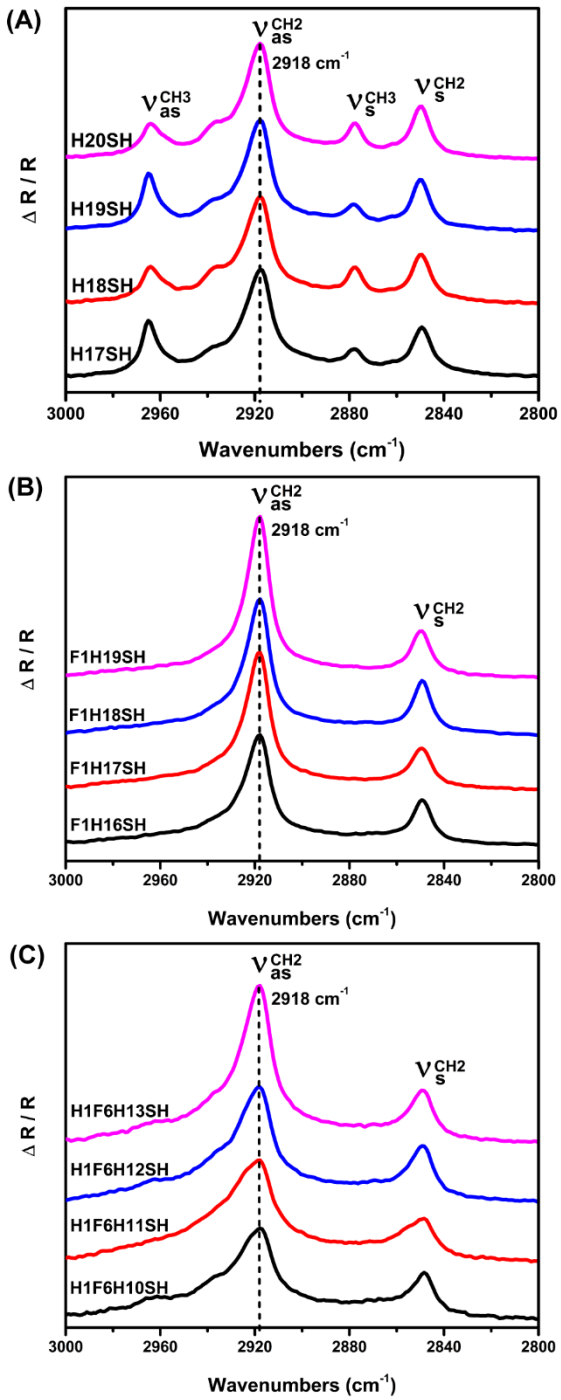

Figure 2.5. PM-IRRAS spectra for the C–H stretching region for SAMs generated from the adsorption of (A) HxSH, (B), F1HmSH and (C) H1F6HnSH on gold surfaces. SAMs of HxSH and F1HmSH serve as reference films for the H1F6HnSH SAMs for interpreting the C-H stretching vibration spectra.

The H1F6HnSH FSAMs also exhibit a $\nu_{as}^{CH}{}_2$ band at 2918 cm^{-1} (Figure 2.4C), which is consistent with the results from previous IR studies of FnH11SH FSAMs and with the SAMs formed from F1HmSH in this study, as shown in Figure 2.4B.[20,48] Based on the spectra and the values listed in Table 2.3, the hydrocarbon spacer of the H1F6HnSH FSAMs is as crystalline as the alkyl chains of the other SAMs. Note that the dynamic feature in the PM-IRRAS spectra of the H1F6HnSH SAMs is the increase in the intensity of the $\nu_{as}^{CH}{}_2$ band as the number of the underlying methylene units increases, which is an expected result.

Table 2.3. PM-IRRAS Data for SAMs Formed from the Methyl-capped Fluorinated Alkanethiols, Normal Alkanethiols, and CF_3-Terminated Alkanethiols

Adsorbate	$\nu_{as}^{CH}{}_3$ (cm^{-1})	$\nu_{as}^{CH}{}_2$ (cm^{-1})	$\nu_{s}^{CH}{}_3$ (cm^{-1})	$\nu_{s}^{CH}{}_2$ (cm^{-1})
H17SH	2965	2918	2878	2849
H18SH	2964	2918	2878	2850
H19SH	2965	2918	2878	2850
H20SH	2964	2918	2878	2850
F1H16SH	-	2918	-	2849
F1H17SH	-	2918	-	2850
F1H18SH	-	2918	-	2849
F1H19SH	-	2918	-	2850
H1F6H10SH	-	2918	-	2848
H1F6H11SH	-	2918	-	2849
H1F6H12SH	-	2918	-	2849
H1F6H13SH	-	2918	-	2849

Another aspect of the PM-IRRAS spectra worth noting is the variation in intensity of the bands associated with the methyl stretches ($\nu_s^{CH_3}$ and $\nu_{as}^{CH_3}$ at 2878 cm^{-1} and ~2965 cm^{-1}, respectively) in the spectra of the HxSH SAMs. An odd-even effect is observed in which the peak intensities of the $\nu_s^{CH_3}$ of films with an even number of carbons in their chains (**H18SH** and **H20SH**) show a greater intensity than those with an odd number of carbons (**H17SH** and **H19SH**). The opposite trend is present for the $\nu_{as}^{CH_3}$ peaks. In these films, the C-C bond that connects the methyl termini is aligned more parallel to the surface normal than in the latter films, creating variances in the observed $\nu_s^{CH_3}$ and $\nu_{as}^{CH_3}$ transition moments for the methyl termini between *odd* and *even* chains, as dictated by the metal surface selection rules associated with such surface IR techniques.[41,49-50] Interestingly, we are unable to detect these bands in the IR spectra of the H1F6HnSH SAMs, which might reflect the strong influence of the electron withdrawing fluorine atoms on the C–H bonds of a neighboring carbon atom. Such an effect can also be found in a prior report involving the spectroscopic analysis of a partially fluorinated compound.[51] A minor shoulder at ~2960 cm^{-1} is present for three of the films but is not discernible in the SAM formed from **H1F6H11SH**. We also observe intrinsic weaknesses for both the $\nu_s^{CH_3}$ and $\nu_{as}^{CH_3}$ modes in the transmission IR spectra collected for the H1F6HnSH compounds shown in Figure 2.6. The apparent diminution of these vibrations reflects the influence of the fluorocarbon chain segment on the methyl C− H bonds. Similar results can be found in the work of Durig and co-workers, who conducted research on 2,2-difluorobutane.[52] This short alkane possesses a methyl group adjacent to the fluorocarbon and one that is positioned β to the fluorinated moiety. For this compound, the authors found

that the $\nu_{as}{}^{CH}{}_3$ peak was weak for the adjacent methyl group but strong for the one that was separated from the fluorocarbon by one methylene. For our report, the poor resolution of the $\nu_s{}^{CH}{}_3$ and $\nu_{as}{}^{CH}{}_3$ bands precludes a direct odd−even comparison between the HxSH and H1F6HnSH series.

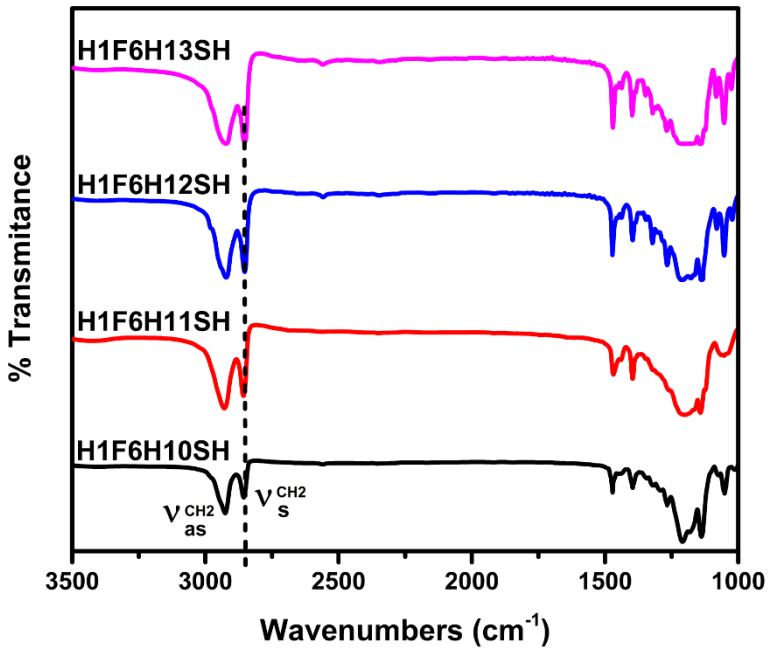

Figure 2.6. FT-IR transmission spectra for the H1F6HnSH thiols collected in KBR pellets.

Regarding the relative intensity of $\nu_s{}^{CH}{}_2$ and $\nu_{as}{}^{CH}{}_2$ in the series of SAMs formed from HxSH and H1F6HnSH, no odd-even effects are apparent. In contrast, the $\nu_s{}^{CH}{}_2$ and $\nu_{as}{}^{CH}{}_2$ bands appear to exhibit a slight odd-even trend for the series of SAMs formed from the F1HmSH adsorbates. Laibinis *et al.* have noted that the absence of such odd-even effects for the C–H stretching vibrations for the methylene moieties of a series of alkanethiolate SAMs was an indication that the chains were exhibiting a "constant chain

orientation on the surface for these films".[41] Assuming the same fundamental reasoning would apply to the methylene vibrations for the F1HmSH SAMs, that the alkyl chains are exhibiting a change in their surface orientation. Such a change would be best explained by a shift in the degree to which the chain twists around its axis from the ~53° determined by Laibinis and co-workers, likely reflecting slight realignments engendered by the termini of the chains as they align to achieve the lowest interfacial energy for the SAM.[41]

2.3.4. Contact Angle Study of the Interfacial Properties of the SAMs

2.3.4.1. Parameters Used in the Study and Wettability Trends

Surfaces that expose an abundance of fluorines are highly hydrophobic and oleophobic due to the extremely low surface energies.[6,7,53] To create surfaces with low adhesion and friction properties (surfaces with low interfacial energies), surface scientists have incorporated fluorocarbons into a variety of materials.[22,23] Consequently, terminally fluorinated FSAMs have been used to evaluate the effect that different levels of fluorination have on surface wettability, and ultimately control its impact. Research in this field has led to the detection of a dipole at the termini of the adsorbates used to make CF_3-terminated SAMs, which causes the SAMs to be less hydrophobic than those of normal alkanethiolate SAMs when that FC–HC dipole is in close proximity to the interface.[13,19,20] To expand upon current knowledge regarding the role of surface dipoles, we examine here the wettability of FSAMs formed from the H1F6HnSH molecules toward a variety of contacting liquids, including polar protic liquids (water – H_2O, γ_{LV} = 72.8 mN/m; glycerol – GL, γ_{LV} = 65.2 mN/m; formamide – FA, γ_{LV} = 57.3 mN/m),[54-56] polar aprotic liquids

(nitrobenzene – NB; γ_{LV} = 43.8 mN/m; dimethyl sulfoxide – DMSO, γ_{LV} = 43.5 mN/m; and acetonitrile – ACN; γ_{LV} = 28.7 mN/m),[55,56] and a bulky hydrocarbon liquid with a small localized dipole (bromonaphathalene – BNP; γ_{LV} = 44.6 mN/m)[57]. We also probed the FSAMs with nonpolar contacting liquids, including liquids formed from a long alkyl chain (hexadecane – HD, γ_{LV} = 27.1 mN/m),[55] a bulky bicyclic hydrocarbon (decalin – DC γ_{LV} = 29.4 mN/m (trans); 31.7 mN/m (cis)),[55] and a bulky bicyclic perfluorocarbon (perfluorodecalin – PFD, γ_{LV} = 19.2 mN/m).[56] The advancing contact angle values are presented in Tables 2.4 and 2.5, where they are compared to the advancing contact angle data for the SAMs formed from HxSH and F1HmSH. The advancing contact angle data for the HxSH SAMs are consistent with literature reports, and show that *n*-alkanethiolate SAMs with an even number of carbons in their chains (**H18SH** and **H20SH**) are less wettable than those with an odd number (**H17SH** and **H19SH**).[19] This observation is dictated by the orientation of the terminal methyl group, which in even-numbered adsorbates (*even*), is more aligned with the surface normal than those with odd-numbered adsorbates (*odd*).[41,58] For the *odd n*-alkanethiolate films, the methyl group is tilted away from the surface normal, exposing the underlying methylene unit to the SAM–liquid interface, which translates to a greater degree of molecular contact between the contacting liquid and the interface.[59] Accordingly, this attractive interaction causes the *odd* SAMs to be more wettable than the *even* SAMs, as displayed in Figure 2.7 (as well as in Figure 2.8; *vide infra*).

Table 2.4. Advancing Contact Angles (θ_a, °) for Nonpolar Contacting Liquids Measured on SAMs Formed from Normal Alkanethiols, CH_3-Terminated Partially Fluorinated Alkanethiols, and CF_3-Terminated Alkanethiols

Adsorbate	HD	DC	BNP	FDC
H17SH	41	51	64	37
H18SH	48	55	70	41
H19SH	42	50	66	36
H20SH	48	55	70	41
F1H16SH	61	67	76	25
F1H17SH	59	64	73	24
F1H18SH	63	67	77	27
F1H19SH	59	64	73	24
H1F6H10SH	56	61	69	27
H1F6H11SH	53	58	66	13
H1F6H12SH	55	60	69	21
H1F6H13SH	54	59	68	25

[a] Contact angle data are the average of at least 12 measurements reproducible within ± 1°.

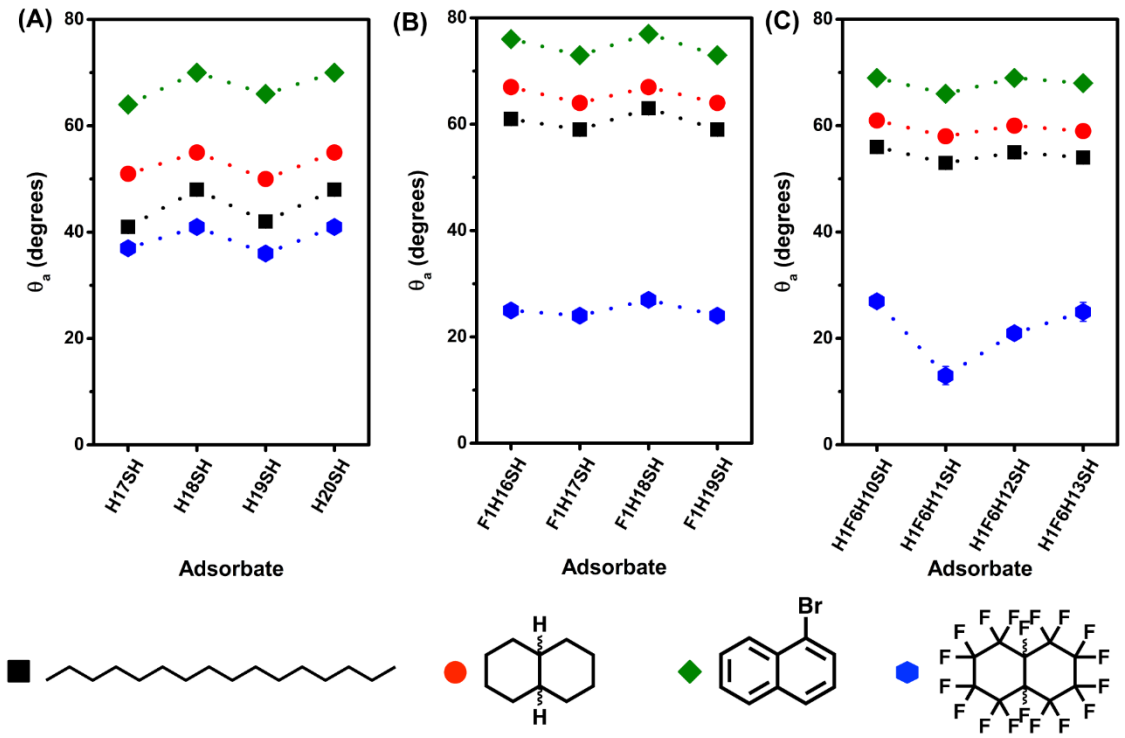

Figure 2.7. Advancing contact angle values for HD, DC, BNP, and PFD on monolayers derived from (A) HxSH, (B), F1HmSH and (C) H1F6HnSH formed on gold. *Lines connecting the data points are simply guides for the eye. Error bars that are not visible fall within the symbols.*

Prior to analyzing the contact angle data for the three series of SAMs, we had anticipated the F1HmSH SAMs to be more wettable by polar liquids, as compared to that of the HxSH SAMs, owing to the presence of the FC–HC dipole at the interface of the film -- the result of permanent dipole–dipole interactions (i.e., Keesom forces) operating at the contacting liquid–SAM interface. However, unlike our initial studies on CF_3-terminated SAMs with shorter underlying alkyl chains,[13,60] the data in Table 2.4 show that there is also a well-defined odd-even trend for our nonpolar contacting liquids when in contact with the F1HmSH SAMs that is inverse to that of the HxSH SAMs. For nonpolar contacting liquids on these films, the SAMs formed from the *even* chains are more wettable than those formed

from the *odd* chains. According to Colorado *et al*., for polar contacting liquids this phenomenon is caused by the orientation of the terminal CF_3 group (*vide supra*), which is directed upward in SAMs with *even* chains and away in SAMs with *odd* chains.[19,20] However, when using PFD as the contacting liquid, a nonpolar perfluorocarbon liquid, an odd-even effect can also be observed. This trend might be attributed to the phase-compatible interactions between fluorinated compounds and appears to be directly related to the number of fluorine atoms interacting with the liquid at the SAM-liquid interface. Thus, films with *even* chains whose terminal groups are more aligned with the surface normal are more wettable than those with *odd* ones. On the other hand, the odd-even effect observed in the wettability data for the F1HmSH films with nonpolar hydrocarbon liquids, exhibited in Figure 2.7, complicate the aforementioned interpretation of the PFD data, leading to a conclusion that the interactions of all of the nonpolar contacting liquids must be considered more carefully. In particular, the contacting liquids that interact with the SAM interface might be responding to an increase in surface tension (surface energy) associated with having an increase in electron density at the monolayer interface – a result of the CF_3 termini being oriented almost parallel to the surface normal. This orientation was determined by an analysis of the angle of the final carbon-carbon bond, which we calculated to have a tilt angle of ~17° from the surface normal using molecular modeling as shown in Figure 2.8 (i.e., the *even* chains support a permanent dipole–induced dipole interaction or "Debye force" between the SAM and the contacting liquid, respectively). On the other hand, having the CF_3 termini tilted away from the interface, as is the case with the odd-numbered chains (~58° from the surface normal, as illustrated in Figure 2.8), allows compensating head-to-tail interactions between the dipoles in the SAMs, which

reduces the magnitude of the aforementioned dipole–induced dipole interaction between the SAM and the contacting liquid, leading to a reduction in wettability.

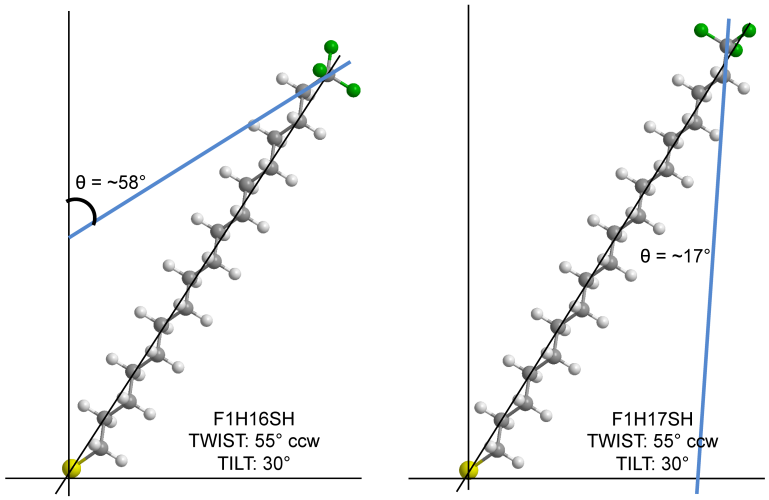

Figure 2.8. Schematic representation of the tilt angle of the final carbon-carbon bond of the F1HmSH SAMs. Both the odd and even chains are included to illustrate changes in the terminal group orientation arising from the total number of carbons in the chain. The tilt angle of the chains of the F1HmSH SAMs are assumed to align with that of typical *n*-alkanethiolate SAMs on gold.

2.3.4.2. Effects of H1F6HnSH Structure/Composition on the Interfacial Properties

To evaluate the role of structure/composition on the surface energy of the partially fluorinated monolayers generated by the introduction of the methyl termini on top of the perfluorinated segment, we first examined the contact angle data for nonpolar contacting liquids on the H1F6HnSH FSAMs. The contact angle measurements acquired for liquids that are dominated by dispersive forces (HD and DC) imply that the hydrocarbospacers of the H1F6HnSH films are well packed, as also determined by the IR analysis (*vide supra*). This hypothesis was confirmed by the contact angle values of hexadecane (see Figure 2.5), which appear to indicate that this contacting liquid fails to intercalate into the H1F6HnSH FSAMs. Furthermore, the wettability data of decalin (a bulky hydrocarbon liquid) and

hexadecane on the 18-carbon chain of the CH_3-terminated film (**H1F6H11SH**: 58° and 53°, respectively) show that this FSAM is more oleophobic than its normal alkanethiolate counterpart (**H18SH**: 55° vs. 48°, respectively). The bulky underlying perfluorocarbon segment, which is likely exposed at the interface, could be the driving force for this observation, as it possibly prevents liquid molecules from intercalating within the chains. In the H1F6HnSH series, the difference in size between the CH_3 groups and the fluorocarbon helix, for which the fluorinated helix is much larger, can also contribute to the liquids coming in contact with the underlying CF_2 units, which would lead to a higher contact angle for hydrocarbon liquids on the H1F6HnSH FSAMs. The higher contact angle is due to the non-ideal dispersive interactions between the liquid and the surface, similar to the observed wettability trends of these liquids on the F1HmSH films compared to the HxSH films. In addition, the contact angle data of perfluorodecalin on the H1F6HnSH FSAMs suggest that the underlying fluorinated chain contributes to the interfacial energy; in particular, note that H1F6HnSH films are more wettable by PFD than are the HxSH SAMs, and they exhibit similar wetting behavior toward PFD as the F1HmSH SAMs. However, complicating our interpretation is an obvious dip in the contact angle data of PFD on the **H1F6H11SH** FSAM, which might reflect a combination of influences: the low surface tension of PFD (19.2 mN/m)[56] accompanied by a reduction in chain packing for the FSAM in question. Notably, we observed a similar trend in contact angle data for the H1F6HnSH FSAMs when we tested a different low surface tension liquid (*t*-butyl alcohol, γ_{LV} = 21.1 mN/m),[55] as shown in Figure 2.9.

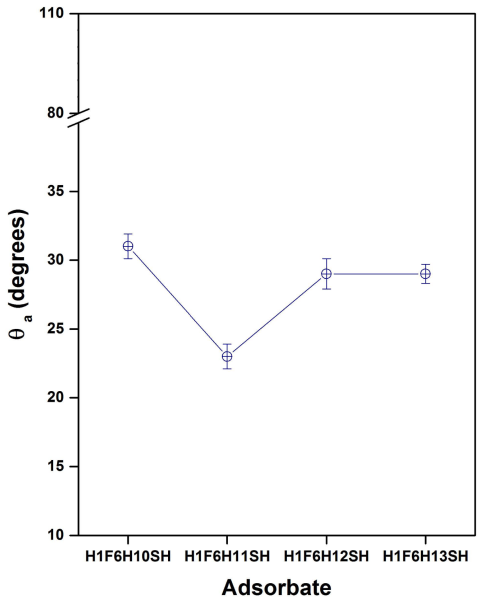

Figure 2.9. Contact angle data for *t*-butyl alcohol on the H1F6HnSH FSAMs.

To assess the role of the HC–FC dipole, we begin with a comparison of the wettability of polar contacting liquids on the newly designed H1F6HnSH FSAMs to that on the HxSH and F1HmSH SAMs (see Figure 2.10). Most apparent is that the H1F6HnSH films are uniformly more wettable than the HxSH and F1HmSH SAMs. More specifically, the H1F6HnSH FSAMs are far more wettable than the HxSH series when in contact with the polar aprotic liquids DMSO and ACN, and slightly more wettable than the F1HmSH SAMs. Further, the trends in the data for the polar liquids on the H1F6HnSH FSAMs (Figure 2.10C) appear to be more similar to that of the trends on the F1HmSH SAMs (Figure 2.10B) than those on the HxSH SAMs (Figure 2.10A). The data for the H1F6HnSH FSAMs are consistent with a model in which the CH_3-capped, partially fluorinated alkanethiolate FSAMs are more wettable than their normal alkanethiolate counterparts due to the presence of a dipole at the HC–FC termini (i.e., Keesom forces appear to be at play for the FSAMs).

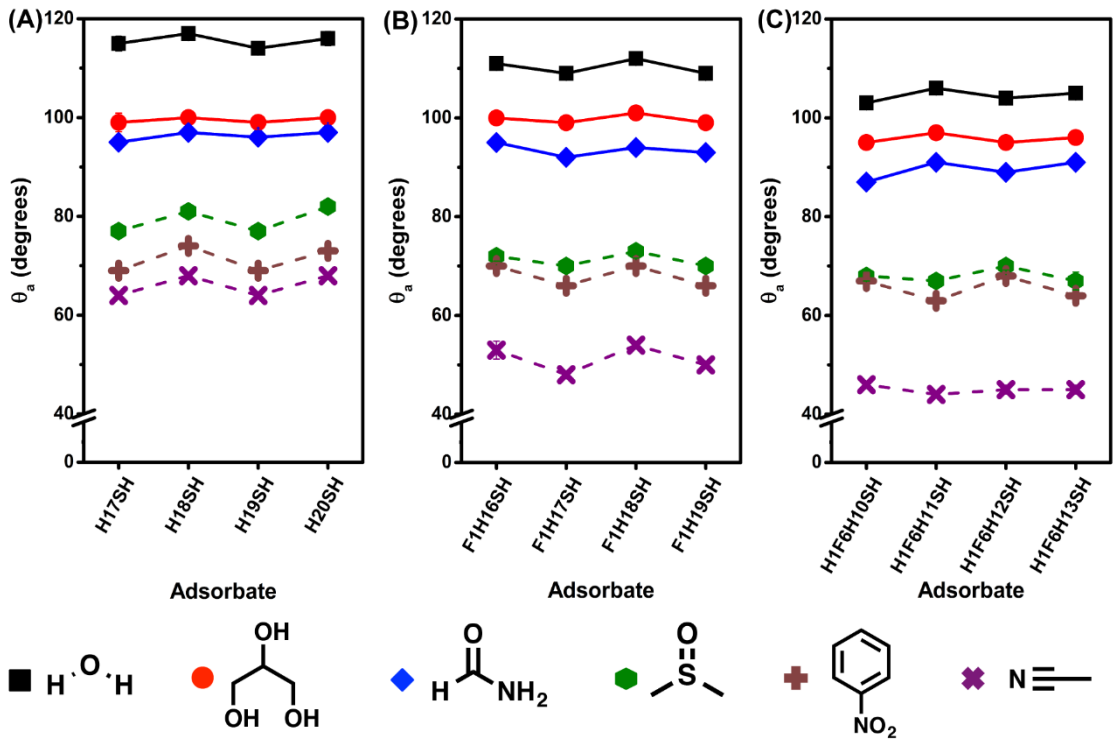

Figure 2.10. Advancing contact angle values for H_2O, GL, FA, DMSO, NB, and ACN on SAMs derived from (A) HxSH, (B), F1HmSH and (C) H1F6HnSH formed on gold. *Lines connecting the data points are simply guides for the eye. Error bars that are not visible fall within the symbols.*

Other effects, however, appear to be in play as well. More specifically, the chemical composition of the terminal groups of the FSAMs as well as their spatial arrangement with the contacting liquids are reflected in the dissimilar trends in the wettability of the polar contact. Additionally, the different underlying segments will affect the wettability of these SAMs; the CF_3 termini have well-packed hydrocarbon spacers whereas the CH_3 termini of the H1F6HnSH FSAMs have the larger perfluorinated helix which likely causes the termini to be loosely packed (*vide supra*).[15,21,39] Therefore, smaller probe liquids can readily surround the terminal methyl group, the outermost layer of the monolayer, leading to an increase in wetting for small polar molecules on H1F6HnSH films

(e.g., 103° for H_2O and 46° for ACN on the **H1F6H10SH** SAM) as compared to F1HnSH films (e.g., 111° for H_2O and 53° for ACN on the **F1H17SH** SAM). Examining the wettability data for BNP and NB (bulky liquids with a localized dipole) appears to support this "intercalation" model. The inability of either BNP or NB to intercalate past the fluorinated helix causes a reduced interaction between the surface dipoles and those of the liquid, thus giving both liquids similar contact angle values on these FSAMs (i.e., 66° for BNP and 63° for NB on the **H1F6H11SH** SAM). In contrast, the contact angle values of these liquids differ significantly on F1HmSH FSAMs, where NB, a liquid with a stronger dipole (4.22 D),[61] wets these monolayers more than BNP (1.55 D)[62] (i.e., 73° for BNP and 66° for NB on the **F1H17SH** SAM). Nonetheless, the H1F6HnSH films are still more wettable toward BNP and NB than are the F1HnSH films. This difference is likely due to non-deal dispersive interactions between the liquid and the fluorinated surface of the F1HmSH SAMs.

Table 2.5. Advancing Contact Angles (θ_a, °) for Polar Contacting Liquids Measured on SAMs Formed from Normal Alkanethiols, CH_3-Terminated Partially Fluorinated Alkanethiols, and CF_3-Terminated Alkanethiols

Adsorbate	H_2O	GL	FA	DMF	DMSO	ACN	NB
H17SH	115	99	95	69	77	64	69
H18SH	117	100	97	74	81	68	74
H19SH	114	99	96	69	77	64	69
H20SH	116	100	97	74	82	68	73
F1H16SH	111	100	95	63	72	53	70
F1H17SH	109	99	92	60	70	48	66
F1H18SH	112	101	94	63	73	54	70
F1H19SH	109	99	93	61	70	50	66
H1F6H10SH	103	95	87	57	68	46	67
H1F6H11SH	106	97	91	56	67	44	63
H1F6H12SH	104	95	89	59	70	45	68
H1F6H13SH	105	96	91	56	67	45	64

[a] Contact angle data are the average of at least 12 measurements reproducible within ± 1°.

2.3.4.3. Odd-Even Effects of Polar Aprotic and Nonpolar Liquids on the H1F6HnSH FSAMs

The inclusion of a systematic series of H1F6HnSH adsorbates to the library of SAMs evaluated herein provides insight into the unique interfacial wettabilities of these newly derived SAMs due either to the number of methylenes in the alkyl spacer, the total number of carbons, or the structural variation at the interface. In earlier sections,

evaluations of the underlying methylene units have shown that the hydrocarbon moieties in all H1F6HnSH FSAMs possess similar packing densities and crystalline structure. Further, the wettability data in Tables 2.4 and 2.5 indicate that for these new organic films, the *even* monolayers (**H1F6H11SH** and **H1F6H13SH**) are more wettable than the *odd* films (**H1F6H10SH** and **H1F6H12SH)** for all nonpolar hydrocarbon liquids and polar aprotic liquids examined in this study. The XPS and IR data discussed earlier inform us that the alkyl chains in the H1F6HnSH FSAMs exhibit similar packing densities, and that the alkyl segments are well ordered for all of these monolayers. Yet there is a clear effect related to the total number of carbons on the structural arrangement of the methyl termini at the monolayer interface—a consequence of the underlying alkyl chain length (*odd* or *even*) on the orientation of the terminal group. While the effect is not as straightforward as that found with the *trans*-extended thiolate SAMs observed in earlier studies,[13,19] the positioning of the methyl terminus of the perfluorinated chain should follow the helicity of the perfluorocarbon chain, and the orientation of this segment should reflect the alignment of the underlying alkyl chain. Thus, the fluorinated segment, with a half-turn helix at six fluorocarbons, will likely give rise to a terminal CH_3 unit being oriented at the interface differently from that of the terminal CF_3 unit at the interface of a *trans*-extended alkanethiolate chain, as illustrated in Figure 2.11. Therefore, the observed odd-even effect will have contributions from several factors: changes in the orientation of the terminal CH_3 group at the interface of the H1F6HnSH FSAMs due to the change in the number of underlying CH_2 units, as well as the nature of the exposure of the underlying fluorocarbons at the interface, and the orientation of the final CH_3-CF_2 bond as dictated by the small helical twist associated with the six perfluorocarbon moieties.

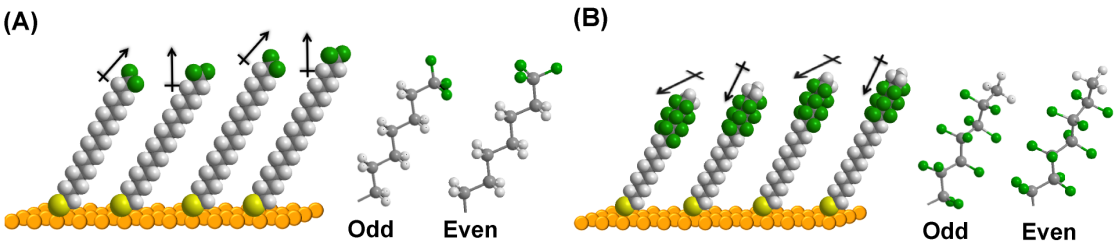

Figure 2.11. Illustration of the orientation of the methyl and trifluoromethyl termini in SAMs derived from the adsorption of (A) F1HnSH and (B) H1F6HnSH on gold. Molecular modeling was performed using the ORCA program package, as described in the Experimental Section.

In the case of the nonpolar liquids HD and DC in Figure 2.7 and Table 2.4, the odd-even effect portrayed by the wettability data on the H1F6HnSH FSAMs follows the trend observed in earlier wettability studies on CF_3–terminated monolayers.[13,60] The exposure of the underlying perfluorinated segment toward the interface for the H1F6HnSH films varies systematically with the number of the underlying methylene units in the spacer. Therefore, in the case of the *odd* chains, the increased exposure of the perfluorinated unit at the liquid-SAM interface, as compared to the *even* chains, leads to a slightly lower value in the contact angle of the respective liquid on the even films compared to the odd ones (for **H1F6H11SH** and **H1F6H13SH**; HD: 53° and 54°, and DC: 58° and 59°, versus for **H1F6H10SH** and **H1F6H12SH**; HD: 56° and 55°, and DC: 61° and 60°). Notably for DC, the possibility of wetting anomalies due to liquid intercalation are minimal due to the bulkiness of the liquid molecules; therefore, the observed odd-even effect most likely arises from differences in the attractive dispersive forces between the hydrocarbon liquid and the methyl termini and the non-ideal dispersive forces between the hydrocarbon liquid and the underlying perfluorinated segment.

Regarding the data in Figure 2.10 and Table 2.5 for the H1F6HnSH SAMs, we focus first on the trends observed for the polar *aprotic* liquids (i.e., DMSO, NB, and ACN).

Notably, the validity of the hypothesis described above is reinforced by the odd-even effect in the wettability data observed for these liquids. As with the CF_3-terminated films, we use the orientation of the final carbon-carbon bond (the HC-FC transition) as a means of estimating the orientation of the interfacial dipole. In this case, the liquids wet *even* films more than *odd* ones. According to our models in Figure 2.12, the terminal methyl group is aligned more toward the interface in the case of films with *even* chains (~19° tilt angle from surface normal for the terminal carbon-carbon bond), which corresponds to the HC–FC surface dipole being aligned more toward the interface (and thus largely uncompensated); for the *odd* chains, the HC–FC surface dipole is aligned more parallel with the interface with a calculated tilt angle of ~79°, as shown in Figure 2.12 (and thus largely head-to-tail compensated). We note that an analogous effect is revealed by the wetting behavior of polar aprotic liquids on the F1HmSH SAMs where the tilt angles for the terminal carbon-carbon bonds are predicted to be ~17° and ~58° for the even and odd chains, respectively, as shown in Figure 2.8. However, the two series differ in that the odd-even effect in the case of small liquids (e.g., ACN) is less pronounced on the H1F6HnSH films as compared to the F1HmSH films. A possible rationalization for the difference might be that small liquid molecules are able to intercalate into the H1F6HnSH films beyond the methyl termini; this model is supported by the observation that NB (a bulky liquid with a strong dipole) shows a similar trend in the contact angle values for *odd* and *even* surfaces on both types of films.

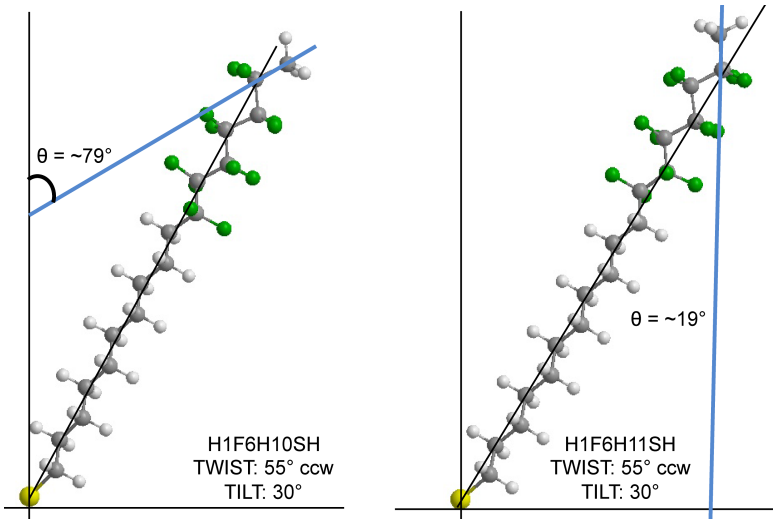

Figure 2.12. Schematic representation of the tilt of the final carbon-carbon bond of the H1F6HnSH FSAMs. Both the odd and even chains are included to illustrate changes in the terminal group orientation arising from the total number of carbons in the chain and the influence of the helical structure of the perfluorinated segment. The tilt angle of the chains in the H1F6HnSH FSAMs follow the model described by Lu et al.[63]

2.3.4.4. The HC–FC Dipole vs. the Intermolecular H-Bonding of Polar Protic Contacting Liquids

Next, we focus on the wettability trends in Figure 2.10 and Table 2.5 derived from the polar *protic* liquids (i.e., H_2O, GL, and FA) in contact with the H1F6HnSH SAMs. To our surprise, the wettability data for these liquids show an odd-even effect that is opposite of that observed in the wettability data of the polar *aprotic* liquids on these SAMs. Specifically, H_2O, GL, and FA show a higher value on *even* films (**H1F6H11SH** and **H1F6H13SH**) than on *odd* ones (**H1F6H10SH** and **H1F6H12SH**). This effect is also the opposite of that observed in the wettability data of these liquids on the F1HmSH SAMs. Since both types of SAMs (F1HmSH and H1F6HnSH) show similar trends with polar aprotic liquids, we attribute these changes, at least in part, to the orientation of the SAM interfacial dipole (FC–HC for F1HmSH and HC–FC for H1F6HnSH). Notably, earlier

studies on CF_3-terminated systems have shown that the negative charge density of the interfacial dipole of the CF_3–CH_2 moiety is associated with the fluorinated end of the molecule.[64] Therefore, the HC–FC dipole at the CH_3–CF_2 junction should also be oriented so that the more electronegative aspect (the perfluorinated segment) of the molecule is associated with the negative end of the dipole. To verify these assumptions, we constructed models to depict the chain termini of the F1HmSH and H1F6HnSH adsorbates derived from molecular modeling described in the Experimental Section; the differing dipole orientations are illustrated in Figure 2.11 (see also Figure 2.13). Such a difference in the intramolecular direction of the dipole gives rise to a partial positive charge at the interface of the H1F6HnSH films and a partial negative charge at the interface of the F1HmSH SAMs.

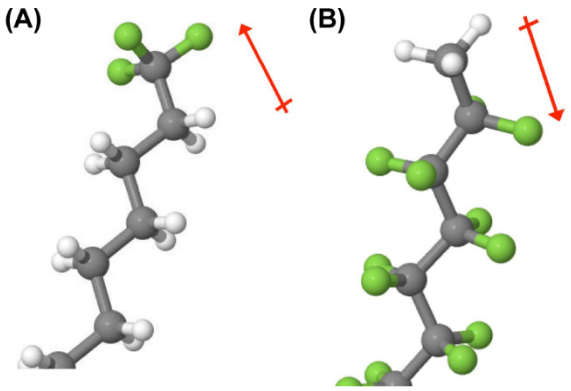

Figure 2.13. Molecular model corresponding to the chain termini of the (A) F1HmSH and (B) H1F6HnSH adsorbates.

These efforts notwithstanding, the structure of the chain termini at the SAM interface alone cannot rationalize the contrasting trends for the polar protic and polar aprotic liquids. We propose an analysis of the interfacial organization of polar protic liquids with extensive hydrogen bonding (H-bonding) networks, an example being that of

water. Prior research that intended to elucidate the nature of the intermolecular interactions of interfacial water molecules provides an understanding of how hydrogen bonds dictate the orientation of the water molecules at the liquid-vapor interface and create an outer layer of molecules that are predominantly oriented with a free –OH group pointed toward the vapor phase.[65,66] A review by Shen *et al.* provides perspective and detailed discussions regarding the orientation of water molecules at interfaces.[67] In a study focused on the interfacial region between water and carbon tetrachloride (CCl_4), Scatena *et al.* also found that water molecules arrange with –OH groups oriented toward the outer shell of the H-bonding network at the H_2O–CCl_4 interface.[68] This orientation has been interpreted to indicate the presence of weak hydrogen bonds with the chlorine atoms of CCl_4, but it could also be an indication that the positive ends of the water molecular dipoles were locally orienting with the negative ends of the Cl–C dipoles. However, such a molecular orientation for water on the H1F6HnSH films would lead to an arrangement that gives rise to an unfavorable interfacial interaction between the dipoles of the protic liquid (δ^+) and that of the HC–FC dipoles (δ^+) of the chain termini of the H1F6HnSH FSAMs. If the strength of the underlying H-bonding network maintains this geometrical arrangement for the surface molecules of the contacting liquid, with the free –OH groups or the positive end of their molecular dipole oriented outward with respect to the drop, this unfavorable interaction would provide impetus for rearrangement of the interfacial water molecules of the liquid drop when in contact with a surface exposing an array of HC-FC dipoles. When rearrangement fails to occur because of H-bonding, then repulsive polar interactions exist at the interface. Such circumstances might lead to a reduction in the wettability by water on monolayers where the surface dipoles are oriented more toward the liquid interface and

more closely aligned with the surface normal. This interpretation is supported by the data in Figure 2.10, which show higher contact angle values for water on the *even* H1F6HnSH films as compared to the *odd* ones.

On the other hand, working with this current model for water in contact with our FSAMs, such strains upon the H-bonding network are unlikely for water in contact with the CF_3-terminated films since the latter interfaces expose an array of interfacial dipoles oriented with their negative ends toward the contacting liquid -- an array of FC-HC dipoles. Neither is there a sufficient barrier for the interfacial molecules of polar aprotic contacting liquids to reorient on the surfaces of the H1F6HnSH films, owing to the absence of an extensive H-bonding network that would deter such interfacial reordering. This interpretation is also supported by the data in Figure 2.10, which show lower contact angle values for DMSO on the *even* H1F6HnSH films as compared to the *odd* ones.

To provide further insight into the wettability of the H1F6HnSH FSAMs, we pursued a series of tests to determine the influence of the H-bonding network within the three polar protic contacting liquids that exhibited inverse trends in Figure 2.10C: (1) water; by adding ions to interrupt the hydrogen bonding network of water through a comparison of wettability by water versus brine, (2) glycerol; by systematically varying the molecular structure of glycerol by decreasing the number of –OH groups and increasing the steric bulk to interfere with hydrogen bonding within the liquid (i.e., comparing the wettability by glycerol to that by 1,3-propanediol, isopropanol, 2,4-pentanediol, and cyclohexanol), and (3) formamide; by systematically decreasing the hydrogen bonding capacity of formamide through a comparison of wettability by formamide (FA) to that by methylformamide (MFA) and dimethylformamide (DMF). The pursuit of these tests starts

with the assumption that if the highly hydrogen-bonded liquids that we first tested each preferentially orient with their more electronegative element(s) toward the center of the liquid drop (via the negative end of their molecular dipoles), then it is likely that most liquids that form extensive H-bonding networks will also orient in a similar manner.

2.3.4.4.1. Water vs Brine

Figure 2.14 shows the contact angles of water and brine on the F1HmSH and H1F6HnSH films; notably, brine fails to show the odd-even trend exhibited by water on these films. Previous studies of aqueous salt solutions and the structural interactions within the associated liquid drops have shown that the interfacial region of the liquid has a higher concentration of anions compared to the bulk, which weakens the H-bonding networks.[69] Further, the concentration of anions in the interfacial region of brine can plausibly lead to an enhanced interaction between the liquid and the HC–FC dipoles in the even H1F6HnSH SAMs, for which the dipoles are oriented roughly normal to the surface. We propose that this interaction is responsible for negating the odd-even trend seen for water. Importantly, the wettability of brine on the F1HmSH SAMs (which expose an FC–HC dipole that is repulsive to the anions in brine) exhibits the same trend as water. Furthermore, the H1F6HnSH series is more wettable than the F1HmSH series toward both water and brine, and brine exhibits higher contact angles than water on both sets of SAMs. The former observation is likely due to the structure/composition of the interface of the H1F6HnSH FSAMs, as discussed earlier. On the other hand, the latter observation likely arises from an increase in interfacial surface tension within the liquid (water vs. brine) associated with the fact that the charged ions produce stronger intermolecular attractions than that

associated with H-bonding.

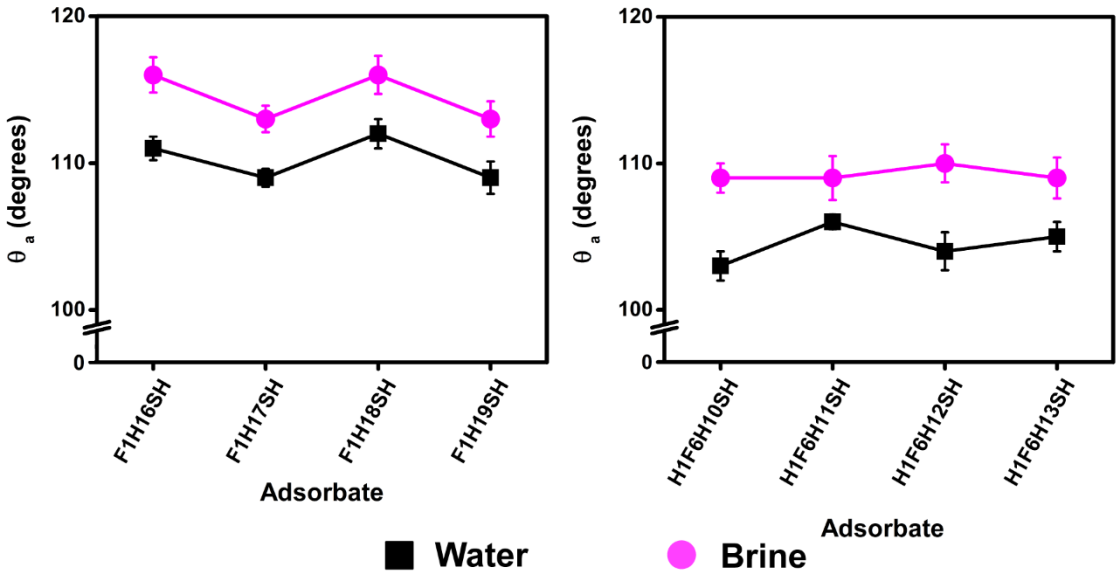

Figure 2.14. Wettability data of brine and water on the F1HnSH (left plot) and H1F6HnSH (right plot) FSAMs on gold. *Lines connecting the data points are simply guides for the eye. Error bars that are not visible fall within the symbols.*

2.3.4.4.2. Glycerol and Its Analogs

Figure 2.15 shows the contact angles of glycerol and systematically chosen analogs having either increasing steric bulk -- 2,4-pentanediol and cyclohexanol (γ_{LV} = 33.4 mN/m)[55] -- or decreasing numbers of hydroxyl groups relative to the alkyl component -- 1,3-propanediol (γ_{LV} = 47.4 mN/m) and *iso*-propanol (γ_{LV} = 21.7 mN/m). On the H1F6HnSH FSAMs, both of the liquids with two –OH groups, 1,3-propanediol and 2,4-pentanediol, failed to produce any odd-even trend. We interpret these results to indicate that the H-bonding networks within the interfacial region of these liquids are disrupted sufficiently to allow minor interfacial molecular rearrangements when in contact with the H1F6HnSH surfaces, but the H-bonding network is still strong enough to interrupt a full reorientation of the interfacial molecules when in contact with HC-FC dipoles of the

H1F6HnSH FSAMs. However, in the case of cyclohexanol, which possesses a bulky cyclohexane ring and only one OH group, the H-bonding network within the liquid appears to be too weak to overcome the dipole-dipole interactions between the liquid and the surface of the H1F6HnSH FSAMs, leading to an inversion of the odd-even trend exhibited by glycerol. Unfortunately, the last of the test contacting liquids chosen for this series, *iso*-propanol, is a relatively small molecule with a low surface tension; consequently, the advancing contact angles measured on our FSAMs using this probe liquid were quite low (on the order of perfluorodecalin), hindering our ability to fully interpret the results obtained.

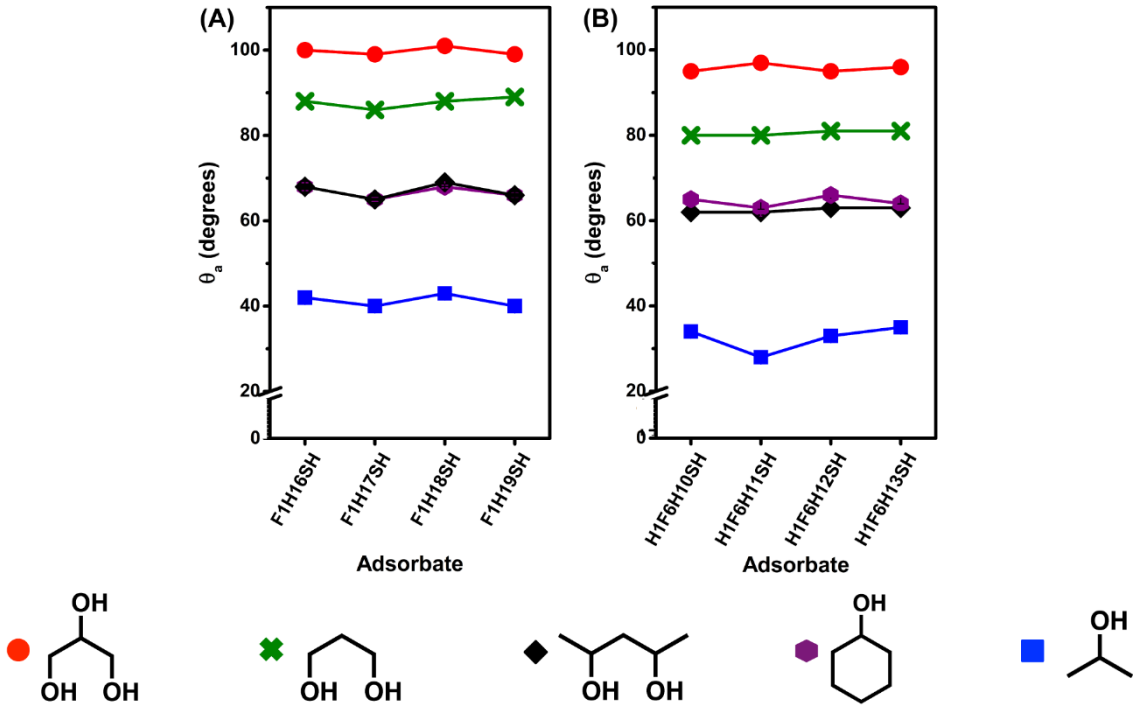

Figure 2.15. Wettability data of glycerol, 1,3-propanediol, 2,4-pentanediol, cyclohexanol, and isopropanol on SAMs derived from the adsorption of (A) F1HmSH and (B) H1F6HnSH on gold. *Lines connecting the data points are simply guides for the eye. Error bars that are not visible fall within the symbols.*

2.3.4.4.3. Formamide and Its Analogs

Figure 2.16 shows the contact angles of FA, MFA, and DMF -- a series of probe liquids with decreasing H-bonding sites via the progressive substitution of a proton with a methyl substituent on the amide nitrogen. These contacting liquids provide a straightforward comparison of the effect that the availability of H-bonding sites has on the contact angle trends for the SAMs derived from F1HmSH and H1F6HnSH. Formamide, in contact with the H1F6HnSH films, exhibits an odd-even trend opposite to that observed for this contacting liquid on the F1HmSH films. As with the other protic liquids discussed above, we attribute this inverse odd-even effect to the existence of a strong hydrogen bonding network in the contacting liquid, which gives rise to unfavorable interfacial interactions between the dipoles of the protic liquid (δ^+) and that of the HC–FC dipoles (δ^+) of the chain termini of the H1F6HnSH FSAMs. However, with the substitution of one methyl group for an amide proton to give methylformamide (MFA, γ_{LV} = 37.96 mN/m), the resulting contact angle data reveal that the H-bonding network within the interfacial region of this contacting liquid is sufficiently disrupted to reduce this interaction and consequently eliminate the odd-even trend on the H1F6HnSH films. Furthermore, with the substitution of the second methyl group for the remaining amide proton to give dimethylformamide (DMF, γ_{LV} = 34.4 mN/m), the resulting contact angle data show an odd-even trend on the H1F6HnSH FSAMs opposite to that observed for formamide. In contrast, we note that all three of these contacting liquids (in fact, all of the polar liquids examined here) give rise to a consistent odd-even trend on the F1HmSH or "CF_3-terminated" films.

As a whole, the studies involving water, brine, glycerol, formamide, and the analogs

of the latter two contacting liquids support a model in which highly hydrogen-bonded liquid molecules at the liquid–FSAM interface adopt a more favorable orientation (on the basis of polarity) when in the presence of the inverted HC–FC dipole. Given that strongly hydrogen-bonded liquids possess high surface tension, it is interesting to note that the effect of the HC–FC dipoles on the polar contacting liquids appears to correlate with the magnitude of their surface tension; that is, polar liquids with relatively high surface tension follow an odd-even trend opposite to that observed for polar liquids with relatively low surface tension (see Figures 2.14 – 2.16). More broadly, the collective results presented demonstrate that the unusual and rich wettability behavior observed on the new H1F6HnSH films arises from its unique structure and the orientation of its molecular dipole.

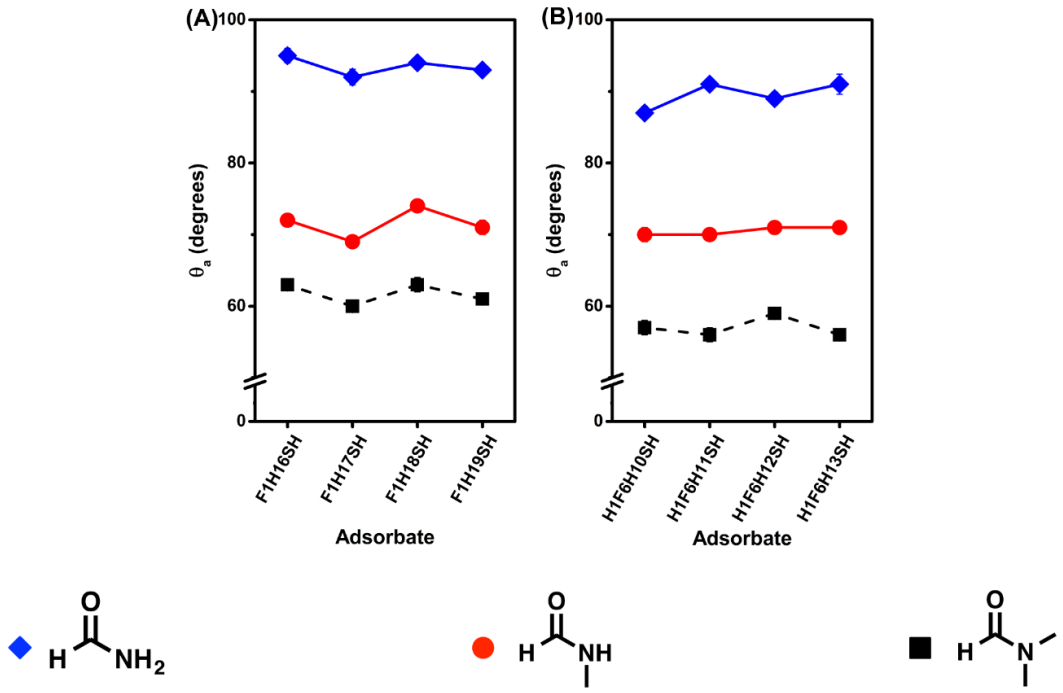

Figure 2.16. Wettability data of FA, MFA, and DMF on SAMs derived from the adsorption of (A) F1HmSH and (B) H1F6HnSH on gold. *Lines connecting the data points are simply guides for the eye. Error bars that are not visible fall within the symbols.*

2.4. Conclusions

We prepared a series of new CH_3-capped, partially fluorinated alkanethiols (H1F6HnSH) and used them to generate FSAMs that expose an array of inverted surface dipoles on gold surfaces. Upon developing the SAMs in ethanol for 48 h, followed by further equilibration at 40 °C for 24 h, formation of monolayer films was confirmed by both ellipsometry and XPS. Analysis of the C 1s binding energies of the H1F6HnSH FSAMs by XPS indicate they have lower packing densities than the normal alkanethiolate SAMs (HxSH). Nonetheless, the PM-IRRAS spectra of the antisymmetric C–H stretching vibrations of the methylene units reveal highly ordered, *trans*-extended conformations adopted for the alkyl spacers of the H1F6HnSH FSAMs. Therefore, we concluded that the observed shift in the C 1s binding energies in the XPS spectra probably arise from the increased vdW diameter of the fluorinated helix, leading to an increased inter-chain distance.

Wettability studies allowed us to examine systematically the effect of the inverted dipoles (HC–FC) on the interfacial energies. Contact angle values of nonpolar (dispersive) contacting liquids showed that the H1F6HnSH FSAMs have an oleophobic character greater than or equal to that of the HxSH SAMs, suggesting that the underlying fluorocarbon units might be partially exposed at the interface. Further, wettability studies using polar contacting liquids revealed that the H1F6HnSH FSAMs are more wettable than their hydrocarbon and CF_3-terminated counterparts. We attribute the enhanced wettability to the presence of the interfacial HC–FC dipole at the termini of the new adsorbates. In addition, the larger fluorinated layer below the terminal methyl unit permits the polar molecules to intercalate into the interfacial region of the H1F6HnSH films more than the

F1HmSH films. We also observed odd-even wettability effects for both nonpolar and polar liquids on the H1F6HnSH films, allowing us to draw several conclusions regarding the effect of the HC–FC surface dipoles on the interfacial properties versus that of the influence of the underlying perfluorinated segment: (1) for nonpolar liquids on the H1F6HnSH films, the systematic variation in exposure of the underlying perfluorinated segment to the liquid-SAM interface renders the *even* monolayers more wettable than the *odd* ones; (2) for polar aprotic liquids, systematic variation in the orientation of the surface dipole generated from the HC–FC junction in the H1F6HnSH films leads the surface dipole to be largely uncompensated in the *even* H1F6HnSH monolayers as compared to the *odd* ones, yielding an increase in the dipole–dipole interactions between the contacting liquid and the *even* FSAMs (more wettable) as compared to the *odd* FSAMs (less wettable); (3) for polar protic liquids, the observed odd-even effects on the H1F6HnSH films were sometimes analogous and sometimes opposite to the that of corresponding CF_3-terminated films due to a combination of dipole-dipole interactions and H-bonding within the contacting liquids that restricted the molecular organization/reorientation of the liquid molecules within the interfacial region of the liquid drop in response to the dipoles at the liquid-SAM interface, thus separating the effect of the polarity of the surface dipole (i.e., HC–FC vs. FC–HC) from its interfacial orientation. Nevertheless, the compelling story from the wetting behavior of contacting liquids on the FSAMs derived from both F1HmSH and H1F6HnSH is that interactions at the liquid-SAM interface are governed by a variety of factors that arise from the surface-confined dipoles interacting with the interfacial molecules of a contacting liquid, giving rise to both dipole-dipole interactions (i.e., Keesom forces for polar contacting liquids) and dipole-induced dipole interactions (i.e., Debye forces for

nonpolar contacting liquids).

As a whole, these studies on fluorocarbon films open new avenues for controlling the properties of 2D macro-systems similar to what has been observed on other dipole-bearing SAM systems, such as work function and friction as outlined in recent review articles.[6,62,63] Therefore, subsequent work will include analysis of the orientation of the methyl terminal group on the surface of the H1F6HnSH FSAMs using a more interface-sensitive spectroscopic technique (i.e., sum frequency generation spectroscopy, SFG) along with investigations utilizing isotopic labeling. In addition, the magnitude and the direction of the molecular dipole need to be determined experimentally, possibly by UV-photoelectron spectroscopy (UPS), and compared to the results described herein. Finally, the effect of this new type of surface dipole (HC–FC) on the frictional properties of these films will also be explored; recognizing that having a small alkyl tailgroup placed on a wider rigid perfluorinated segment might reduce the interfacial friction of these model boundary lubricants.

2.5. Acknowledgments

We are grateful for generous financial support from the National Sciene Foundation (CHE-1411265), the Robert A. welch Foundation (E-1320), and the Texas Center for Superconductivity at the University of Houston.

2.6. References

1. Gentilini, C.; Boccalon, M.; Pasquato, L. Straightforward Synthesis of Fluorinated Amphiphilic Thiols. *Eur. J. Org. Chem.* **2008**, *2008*, 3308–3313.
2. Gentilini, C.; Evangelista, F.; Rudolf, P.; Franchi, P.; Lucarini, M.; Pasquato, L. Water-Soluble Gold Nanoparticles Protected by Fluorinated Amphiphilic Thiolates. *J. Am. Chem. Soc.* **2008**, *130*, 15678–15682.

3. Lee, S.; Park, J.-S.; Lee, T. R. The Wettability of Fluoropolymer Surfaces: Influence of Surface Dipoles. *Langmuir* **2008**, *24*, 4817–4826.

4. Chen, T.-H.; Popov, I.; Zenasni, O.; Daugulis, O.; Miljanic, O. S. Superhydrophobic Perfluorinated Metal-Organic Frameworks. *Chem. Commun.* **2013**, *49*, 6846–6848.

5. Santos, C. M.; Kumar, A.; Zhang, W.; Cai, C. Functionalization of Fluorous Thin Films *Via* "Click" Chemistry. *Chem. Commun.* **2009**, 2854–2856.

6. Zenasni, O.; Jamison, A. C.; Lee, T. R. The Impact of Fluorination on the Structure and Properties of Self-Assembled Monolayer Films. *Soft Matter* **2013**, *9*, 6356–6370.

7. Barriet, D.; Lee, T. R. Fluorinated Self-Assembled Monolayers: Composition, Structure and Interfacial Properties. *Current Opinion in Colloid & Interface Science* **2003**, *8*, 236–242.

8. O'Hagan, D. Understanding Organofluorine Chemistry. An Introduction to the C-F Bond. *Chem. Soc. Rev.* **2008**, *37*, 308–319.

9. Bunn, C. W.; Howells, E. R. Structures of Molecules and Crystals of Fluoro-Carbons. *Nature* **1954**, *174*, 549–551.

10. Clark, E. S. The Molecular Conformations of Polytetrafluoroethylene: Forms II and IV. *Polymer* **1999**, *40*, 4659–4665.

11. Golden, W. G.; Brown, E. M.; Solem, S. E.; Zoellner, R. W. Complete Conformational Analyses of Perfluoro-n-Pentane, Perfluoro-n-Hexane, and Perfluoro-n-Heptane. *J. Mol. Struc-THEOCHEM* **2008**, *867*, 22–27.

12. Krafft, M. P.; Riess, J. G. Chemistry, Physical Chemistry, and Uses of Molecular Fluorocarbon−Hydrocarbon Diblocks, Triblocks, and Related Compounds—Unique "Apolar" Components for Self-Assembled Colloid and Interface Engineering. *Chem. Rev.* **2009**, *109*, 1714–1792.

13. Graupe, M.; Takenaga, M.; Koini, T.; Colorado, R., Jr.; Lee, T. R. Oriented Surface Dipoles Strongly Influence Interfacial Wettabilities. *J. Am. Chem. Soc.* **1999**, *121*, 3222–3223.

14. Graupe, M.; Koini, T.; Wang, V. Y.; Nassif, G. M.; Colorado, R., Jr.; Villazana, R. J.; Dong, H.; Miura, Y. F.; Shmakova, O. E.; Lee, T. R. Terminally Perfluorinated Long-Chain Alkanethiols. *Journal of Fluorine Chemistry* **1999**, *93*, 107–115.

15. Kim, H. I.; Koini, T.; Lee, T. R.; Perry, S. S. Systematic Studies of the Frictional Properties of Fluorinated Monolayers with Atomic Force Microscopy: Comparison of CF_3- and CH_3-Terminated Films. *Langmuir* **1997**, *13*, 7192–7196.

16. Kim, H. I.; Graupe, M.; Oloba, O.; Koini, T.; Imaduddin, S.; Lee, T. R.; Perry, S. S. Molecularly Specific Studies of the Frictional Properties of Monolayer Films: A Systematic Comparison of CF_3-, $(CH_3)_2CH$-, and CH_3-Terminated Films. *Langmuir* **1999**, *15*, 3179–3185.

17. Pflaum, J.; Bracco, G.; Schreiber, F.; Colorado Jr, R.; Shmakova, O. E.; Lee, T. R.; Scoles, G.; Kahn, A. Structure and Electronic Properties of Ch3- and Cf3-Terminated Alkanethiol Monolayers on Au(111): A Scanning Tunneling Microscopy, Surface X-Ray and Helium Scattering Study. *Surf. Sci.* **2002**, *498*, 89–104.

18. Colorado, R. J.; Graupe, M.; Kim, H. I.; Takenaga, M.; Oloba, O.; Lee, S.; Perry, S. S.; Lee, T. R. Interfacial Properties of Specifically Fluorinated Self-Assembled Monolayer Films. *ACS Symp. Ser.* **2001**, *781*, 58–75.

19. Colorado, R., Jr.; Lee, T. R. Physical Organic Probes of Interfacial Wettability Reveal the Importance of Surface Dipole Effects. *J. Phys. Org. Chem.* **2000**, *13*, 796–807.

20. Colorado, R., Jr.; Lee, T. R. Wettabilities of Self-Assembled Monolayers on Gold Generated from Progressively Fluorinated Alkanethiols. *Langmuir* **2003**, *19*, 3288–3296.

21. Holger, S.; Vancso, G. J. Afm Study on Lattice Orientation and Tribology of Sams of Fluorinated Thiols and Disulfides on Au(111): The Influence of the Molecular Structure. *ACS Symp. Ser.* **2001**, *787*, 15–30.

22. Pujari, S. P.; Scheres, L.; Weidner, T.; Baio, J. E.; Cohen, S. M. A.; van, R. C. J. M.; Zuilhof, H. Covalently Attached Organic Monolayers onto Silicon Carbide

from 1-Alkynes: Molecular Structure and Tribological Properties. *Langmuir* **2013**, *29*, 4019–4031.

23. Pujari, S. P.; Spruijt, E.; Cohen, S. M. A.; van, R. C. J. M.; Paulusse, J. M. J.; Zuilhof, H. Ultralow Adhesion and Friction of Fluoro-Hydro Alkyne-Derived Self-Assembled Monolayers on H-Terminated Si(111). *Langmuir* **2012**, *28*, 17690–17700.

24. Li, S.; Cao, P.; Colorado, R.; Yan, X.; Wenzl, I.; Shmakova, O. E.; Graupe, M.; Lee, T. R.; Perry, S. S. Local Packing Environment Strongly Influences the Frictional Properties of Mixed CH_3- and CF_3-Terminated Alkanethiol SAMs on Au(111). *Langmuir* **2005**, *21*, 933–936.

25. Johnson, R., Jr.; Dettre, R. H. *Surf. Sci. Series* **1993**, *49*, 1.

26. Bain, C. D.; Troughton, E. B.; Tao, Y. T.; Evall, J.; Whitesides, G. M.; Nuzzo, R. G. Formation of Monolayer Films by the Spontaneous Assembly of Organic Thiols from Solution onto Gold. *J. Am. Chem. Soc.* **1989**, *111*, 321–335.

27. Zenasni, O.; Marquez, M. D.; Jamison, A. C.; Lee, H. J.; Czader, A.; Lee, T. R. Inverted Surface Dipoles in Fluorinated Self-Assembled Monolayers. *Chem. Mater.* **2015**, *27*, 7433-7446.

28. Porter, M. D.; Bright, T. B.; Allara, D. L.; Chidsey, C. E. D. Spontaneously Organized Molecular Assemblies. 4. Structural Characterization of *n*-Alkyl Thiol Monolayers on Gold by Optical Ellipsometry, Infrared Spectroscopy, and Electrochemistry. *J. Am. Chem. Soc.* **1987**, *109*, 3559–3568.

29. Neese, F. *Orca*, Version 3.0.3; University of Bonn, 2015.

30. Eichkorn, K.; Weigend, F.; Treutler, O.; Ahlrichs, R. Auxiliary Basis Sets for Main Row Atoms and Transition Metals and Their Use to Approximate Coulomb Potentials. *Theor. Chem. Acc.* **1997**, *97*, 119–124.

31. Neese, F.; Wennmohs, F.; Hansen, A.; Becker, U. Efficient, Approximate and Parallel Hartree–Fock and Hybrid DFT Calculations. A "Chain-of-Spheres" Algorithm for the Hartree–Fock Exchange. *Chem. Phys.* **2009**, *356*, 98–109.

32. Chinwangso, P. Self-Assembled Monolayers Generated from Custom-Tailored Spiroalkanedithiols Offer Unprecedented Multi-Component Interfaces. Ph.D., University of Houston, 2009.

33. Barriet, D. Synthesis and Characterization of Specifically Fluorinated and Structurally Tailored Self-Assembled Monolayers on Gold. Ph.D., University of Houston, 2005.

34. Colorado, R., Jr.; Lee, T. R. Attenuation Lengths of Photoelectrons in Fluorocarbon Films. *J. Phys. Chem. B* **2003**, *107*, 10216–10220.

35. Colorado, R., Jr.; Graupe, M.; Shmakova, O. E.; Ramon, J. V.; Lee, T. R. Structural Properties of Self-Assembled Monolayers on Gold Generated from Terminally Fluorinated Alkanethiols. *ACS Symp. Ser.* **2001**, *781*, 276–292.

36. Yuan, Y.; Yam, C. M.; Shmakova, O. E.; Colorado, R., Jr.; Graupe, M.; Fukushima, H.; Moore, H. J.; Lee, T. R. Solution-Phase Desorption of Self-Assembled Monolayers on Gold Derived from Terminally Perfluorinated Alkanethiols. *J. Phys. Chem. C* **2011**, *115*, 19749–19760.

37. Frey, S.; Heister, K.; Zharnikov, M.; Grunze, M.; Tamada, K.; Colorado, R., Jr.; Graupe, M.; Shmakova, O. E.; Lee, T. R. Structure of Self-Assembled Monolayers of Semifluorinated Alkanethiols on Gold and Silver Substrates. *Isr. J.Chem.* **2000**, *40*, 81–97.

38. Alves, C. A.; Porter, M. D. Atomic Force Microscopic Characterization of a Fluorinated Alkanethiolate Monolayer at Gold and Correlations to Electrochemical and Infrared Reflection Spectroscopic Structural Descriptions. *Langmuir* **1993**, *9*, 3507–3512.

39. Tamada, K.; Ishida, T.; Knoll, W.; Fukushima, H.; Colorado, R., Jr.; Graupe, M.; Shmakova, O. E.; Lee, T. R. Molecular Packing of Semifluorinated Alkanethiol Self-Assembled Monolayers on Gold: Influence of Alkyl Spacer Length. *Langmuir* **2001**, *17*, 1913–1921.

40. Zenasni, O.; Jamison, A. C.; Marquez, M. D.; Lee, T. R. Self-Assembled Monolayers on Gold Generated from Terminally Perfluorinated Alkanethiols

Bearing Propyl Vs. Ethyl Hydrocarbon Spacers. *J. Fluorine Chem.* **2014**, *168*, 128–136.

41. Laibinis, P. E.; Whitesides, G. M.; Allara, D. L.; Tao, Y. T.; Parikh, A. N.; Nuzzo, R. G. Comparison of the Structures and Wetting Properties of Self-Assembled Monolayers of *n*-Alkanethiols on the Coinage Metal Surfaces, Copper, Silver, and Gold. *J. Am. Chem. Soc.* **1991**, *113*, 7152–7167.

42. Castner, D. G.; Hinds, K.; Grainger, D. W. X-Ray Photoelectron Spectroscopy Sulfur 2p Study of Organic Thiol and Disulfide Binding Interactions with Gold Surfaces. *Langmuir* **1996**, *12*, 5083–5086.

43. Rittikulsittichai, S.; Jamison, A. C.; Lee, T. R. Self-Assembled Monolayers Derived from Alkoxyphenylethanethiols Having One, Two, and Three Pendant Chains. *Langmuir* **2011**, *27*, 9920–9927.

44. Ishida, T.; Hara, M.; Kojima, I.; Tsuneda, S.; Nishida, N.; Sasabe, H.; Knoll, W. High Resolution X-Ray Photoelectron Spectroscopy Measurements of Octadecanethiol Self-Assembled Monolayers on Au(111). *Langmuir* **1998**, *14*, 2092–2096.

45. Ishida, T.; Nishida, N.; Tsuneda, S.; Hara, M.; Sasabe, H.; Knoll, W. Alkyl Chain Length Effect on Growth Kinetics of N-Alkanethiol Self-Assembled Monolayers on Gold Studied by X-Ray Photoelectron Spectroscopy. *Jpn. J. Appl. Phys.* **1996**, *35*, L1710.

46. Snyder, R. G.; Strauss, H. L.; Elliger, C. A. Carbon-Hydrogen Stretching Modes and the Structure of N-Alkyl Chains. 1. Long, Disordered Chains. *J. Phys. Chem.* **1982**, *86*, 5145–5150.

47. MacPhail, R. A.; Strauss, H. L.; Snyder, R. G.; Elliger, C. A. Carbon-Hydrogen Stretching Modes and the Structure of n-Alkyl Chains. 2. Long, All-Trans Chains. *J. Phys. Chem.* **1984**, *88*, 334–341.

48. Fukushima, H.; Seki, S.; Nishikawa, T.; Takiguchi, H.; Tamada, K.; Abe, K.; Colorado, R.; Graupe, M.; Shmakova, O. E.; Lee, T. R. Microstructure,

Wettability, and Thermal Stability of Semifluorinated Self-Assembled Monolayers (Sams) on Gold. *J. Phys. Chem. B* **2000**, *104*, 7417–7423.

49. Nuzzo, R. G.; Dubois, L. H.; Allara, D. L. Fundamental Studies of Microscopic Wetting on Organic Surfaces. 1. Formation and Structural Characterization of a Self-Consistent Series of Polyfunctional Organic Monolayers. *J. Am. Chem. Soc.* **1990**, *112*, 558–569.

50. Greenler, R. G. Infrared Study of Adsorbed Molecules on Metal Surfaces by Reflection Techniques. *J. Chem. Phys.* **1966**, *44*, 310–315.

51. Li, Y. S.; Cox, F. O.; Durig, J. R. Low-Resolution Microwave, Infrared, and Raman Spectra, Conformational Stability, and Vibrational Assignment of 2,2,2-Trifluoroethyl Methyl Ether. *J. Phys. Chem.* **1987**, *91*, 1334–1344.

52. Durig, J. R.; Yu, Z.; Guirgis, G. A. Conformational Stability, Barriers to Internal Rotation, Vibrational Assignment, and Ab Initio Calculations of 2,2-Difluorobutane. *Journal of Molecular Structure* **1999**, *509*, 115–135.

53. Dalvi, V. H.; Rossky, P. J. Molecular Origins of Fluorocarbon Hydrophobicity. *Proc. Natl. Acad. Sci.* **2010**, *107*, 13603–13607.

54. Smallwood, I. M. *Handbook of Organic Solvent Properties*; John Wiley & Sons: New York, 1996.

55. Yaws, C. L. *Chemical Properties Handbook Physical, Thermodynamic, Environmental, Transport, Safety, and Health Related Properties for Organic and Inorganic Chemicals*; McGraw-Hill: New York, 1999.

56. Fowkes, F. M.; Riddle Jr, F. L.; Pastore, W. E.; Weber, A. A. Interfacial Interactions between Self-Associated Polar Liquids and Squalane Used to Test Equations for Solid—Liquid Interfacial Interactions. *Colloid Surface* **1990**, *43*, 367–387.

57. Jańczuk, B.; Białłopiotrowicz, T. Surface Free-Energy Components of Liquids and Low Energy Solids and Contact Angles. *J. Colloid Inter. Sci.* **1989**, *127*, 189–204.

58. Baghbanzadeh, M.; Simeone, F. C.; Bowers, C. M.; Liao, K.-C.; Thuo, M.; Baghbanzadeh, M.; Miller, M. S.; Carmichael, T. B.; Whitesides, G. M. Odd–Even

Effects in Charge Transport across N-Alkanethiolate-Based Sams. *J. Am. Chem. Soc.* **2014**, *136*, 16919–16925.

59. Barriet, D.; Chinwangso, P.; Lee, T. R. Can Cyclopropyl-Terminated Self-Assembled Monolayers on Gold Be Used to Mimic the Surface of Polyethylene? *ACS Appl. Mater. Interfaces* **2010**, *2*, 1254–1265.

60. Graupe, M.; Koini, T.; Kim, H. I.; Garg, N.; Miura, Y. F.; Takenaga, M.; Perry, S. S.; Lee, T. R. Wettability and Friction of CF_3-Terminated Monolayer Films on Gold. *Mater. Res. Bull.* **1999**, *34*, 447–453.

61. Nelson, R. D.; Lide, D. R.; Maryott, A. A. Selected Values of Electric Dipole Moments for Molecules in the Gas Phase. Natl. Stnds. Ref. Data Ser.: Natl. Bur. Stnds. 10, 1967.

62. Riddick, J. A.; Bunger, W. B.; Sakano, T. K. *Organic Solvents*; Fourth ed.; John Wiley & Sons: New York, 1986.

63. Neese, F.; Schwabe, T.; Kossmann, S.; Schirmer, B.; Grimme, S. Assessment of Orbital-Optimized, Spin-Component Scaled Second-Order Many-Body Perturbation Theory for Thermochemistry and Kinetics. *J. Chem. Theory Comput.* **2009**, *5*, 3060–3073.

64. Petrov, J. G.; Andreeva, T. D.; Möhwald, H. Fluorination of the Hydrophilic Head Accelerates the Collapse of the Monolayer but Stabilizes the Bilayer of a Long-Chain Trifluoroethyl Ether on Water. *Langmuir* **2006**, *22*, 4136–4143.

65. Du, Q.; Freysz, E.; Shen, Y. R. Surface Vibrational Spectroscopic Studies of Hydrogen Bonding and Hydrophobicity. *Science* **1994**, *264*, 826.

66. Du, Q.; Superfine, R.; Freysz, E.; Shen, Y. R. Vibrational Spectroscopy of Water at the Vapor/Water Interface. *Phys. Rev. Lett.* **1993**, *70*, 2313–2316.

67. Shen, Y. R.; Ostroverkhov, V. Sum-Frequency Vibrational Spectroscopy on Water Interfaces: Polar Orientation of Water Molecules at Interfaces. *Chem. Rev.* **2006**, *106*, 1140–1154.

68. Scatena, L. F.; Brown, M. G.; Richmond, G. L. Water at Hydrophobic Surfaces: Weak Hydrogen Bonding and Strong Orientation Effects. *Science* **2001**, *292*, 908–912.

69. Raymond, E. A.; Richmond, G. L. Probing the Molecular Structure and Bonding of the Surface of Aqueous Salt Solutions. *J. Phys. Chem. B* **2004**, *108*, 5051–5059.

Chapter 3: Alkyl-Terminated Partially-Fluorinated Alkanethiols: Burying the Inverted Surface Dipole

3.1. Introduction

Recent advancements in nanotechnology have benefitted from the use of fluorinated organic thin films. Properties inherent to fluorocarbons allow them to be a leading candidate for nanoscale applications that include their use as lubricants for nanoelectromechanical systems (NEMS) and microelectromechanical systems (MEMS).[1-3] The lubricant of choice for these types of systems has generally been partially fluorinated alkyl silanes in the form of fluorinated self-assembled monolayers (FSAMs). A better understanding of these robust films, with properties such as low adhesion and thermal stability, has been gained from studies regarding the structural/compositional features of these monolayers at the interface.[4-6] For example, recent reports have described greater frictional properties for perfluorinated silane films on silica when compared to those of Teflon.[3,7] Moreover, perfluorinated coatings can alter the work function of electrodes, leading to a reduction in the charge-transfer barrier between the electrode and an overlying conjugated polymer.[8-10] Nevertheless, fluorinated thin films enjoy widespread use in applications beyond those of mechanical and electronic devices. For example, fluorinated adsorbates have been used to generate anti-fouling coatings that inhibit the adsorption of biomaterials.[11,12]

Self-assembled monolayers (SAMs) derived from the adsorption of alkanethiols on gold continue to be widely used as model systems to investigate how the molecular features of an adsorbate alter the physical properties of the investigated films.[13-16] Several synthetic routes have

evolved from research involving partially fluorinated alkanethiols in efforts to impart specifically desired properties into thin films.[4,17] Notably, the physical properties of SAMs formed from a series of fluorinated alkanethiols of the form $CF_3(CF_2)_n(CH_2)_2SH$ are dictated by the large perfluorinated segment rather than the short hydrocarbon spacer.[18-21] Insights into the role that limited levels of fluorination play on the interfacial properties of such films have been gained by the use of uniquely structured fluorinated adsorbates.[22-25] Lee and co-workers, for example, have shown the dependence of physical properties on the degree of fluorination by forming SAMs from partially fluorinated molecules of the form $CF_3(CF_2)_n(CH_2)_{11}SH$ where n = 1-10 (FnH11SH).[22-25] Moreover, the alkyl spacers of the SAMs largely dictate the structural features of the minimally fluorinated films, such as the relative crystallinity and packing density.[26,27] Additionally, the improved thermal stability of fluorinated SAMs appears to depend on the enhanced van der Waals (vdW) interactions between the alkyl spacers that increases with increasing chain length, giving the films their high degree of conformational order.[25]

In a recent article,[28] we introduced methyl-terminated partially fluorinated SAMs of the form $CH_3(CF_2)_6(CH_2)_nSH$, where n = 10–13 (H1F6HnSH), as the first examples of fluorinated thin films with an inverted oriented surface dipole (i.e., HC–FC dipole) at the terminal interface. These films, which represent a clear example on manipulating the interfacial energies of monolayers using polarized dipoles, are more wettable by polar liquids than CF_3-terminated SAMs;[28,29] in addition, the CH_3-terminated FSAMs are less wettable than their hydrocarbon counterparts. However, the impact of the work lies in the ability of the films to exhibit an odd-even effect that is inverted to the one observed in CF_3-terminated films when in contact with polar protic liquids. In such liquids, the intermolecular H-bonds restrain the molecules from adopting a

more favorable interfacial orientation (based on polarity) in the presence of the inverted surface dipole, as shown in Figure 3.1.

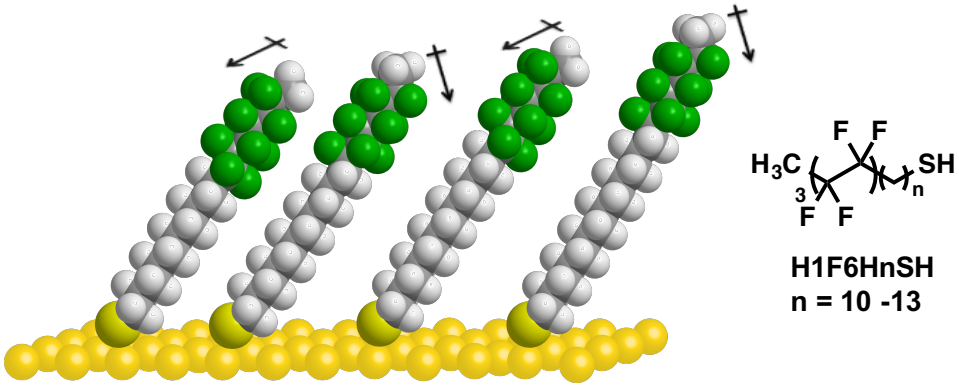

Figure 3.1. Illustration of SAMs generated from **H1F6HnSH** on gold.

In addition to the inverted odd-even effect observed for the H1F6HnSH FSAMs, the underlying perfluorinated segment in these adsorbates renders the films more oleophobic than their all-hydrocarbon counterparts. Additionally, the wetting behavior of various nonpolar liquids indicates that the orientation of the HC–FC dipole dictates the oleophobic character of the films through changes in the degree by which the underlying CF_2 units are exposed at the interface.

Building on our earlier work, the current study aims to draw a clearer conceptualization of the extent of the influence of the HC–FC dipole. To this end, we designed, synthesized, and generated monolayer thin films from a series of alkyl-capped partially fluorinated alkanethiols of the structures $CH_3(CH_2)_n(CF_2)_6(CH_2)_{11}SH$ (**HnF6H11SH**, where n = 1–7). This study sought to determine the length of the top hydrocarbon segment beyond which the HC–FC dipole ceases to influence the interfacial energetics of the system. We also wished to evaluate the effect of the extended alkyl moiety on the structural features of the fluorinated thin-films. Along with the new adsorbates, we also describe studies of a series of normal alkanethiol SAMs $H(CH_2)_mSH$ (**HmSH**,

where m = 18–24) to serve as reference films in our efforts to evaluate the structural and interfacial properties of the FSAMs generated from **HnF6H11SH**. Depictions of the partially fluorinated films examined in this study are shown in Figure 3.2. SAMs formed from **HnF6H11SH** and the reference **HmSH** adsorbates were analyzed using optical ellipsometry, contact angle goniometry, polarization modulation infrared reflection-adsorption spectroscopy (PM-IRRAS), and X–ray photoelectron spectroscopy (XPS).

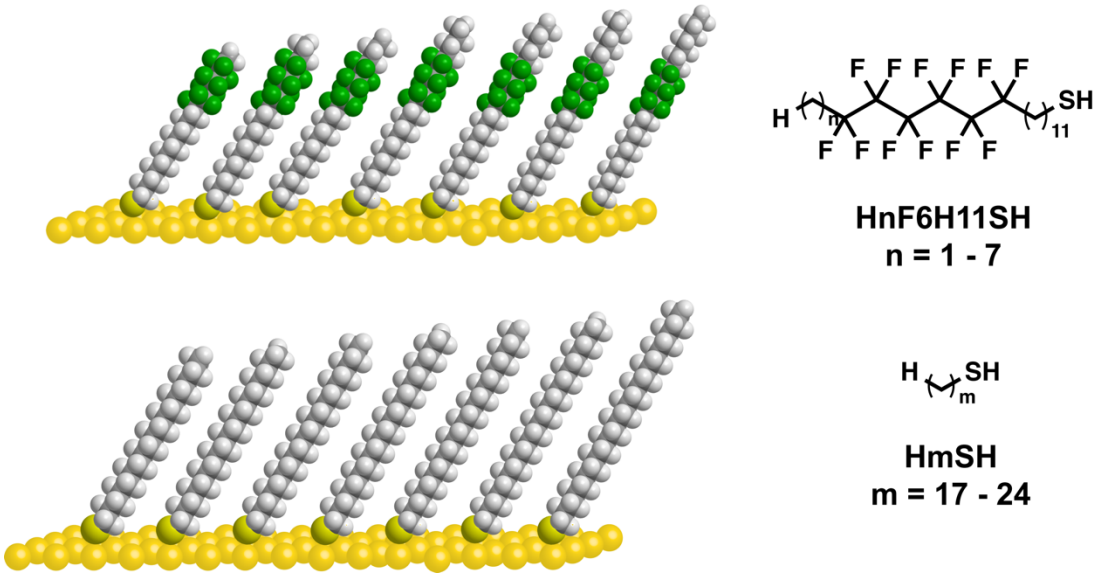

Figure 3.2. Schematic representation of SAMs generated from the **HnF6H11SH** and **HmSH** series.

3.2. Experimental Section

3.2.1. Materials and Methods

Gold shot (99.999%) was purchased from Americana Precious Metals. Chromium rods (99.9%) were purchased from R. D. Mathis Company. Polished single-crystal silicon (100) wafers were purchased from Silicon Wafer Enterprises. Diethyl ether (Et_2O) and Tetrahydrofuran (THF) were purchased from Avantor Performance Materials (Macron Chemicals and J.T. Baker), and were dried by distilling over calcium hydride (Sigma-Aldrich). Methanol (MeOH), acetone, and

hexanes (from Avantor Performance Materials); ethyl acetate and dichloroethane (DCE) (from Sigma Aldrich) were either used as received or degassed by purging with argon gas.

Azobisisobutyronitrile (AIBN), methanesulfonyl chloride (MsCl), lithium aluminum hydride ($LiAlH_4$), allyl alcohol, triethylamine (Et_3N), palladium on carbon (Pd/C), potassium thioacetate (KSAc), Tetrabutylammonium fluoride solution, and methyl 10-undecenoate were all purchased from Sigma Aldrich and used as received. 1,6-Diiodoperfluorohexane (Synquest Labs), 4-bromo-1-butene and 5-bromo-1-pentene (TCI America), 7-bromohept-1-ene (Oakwood), and 6-bromohex-1-ene (Matrix Sxientific) were used as received. Sulfuric acid (H_2SO_4 – from J.T. Baker) and Hydrochloric acid (HCl); potassium iodide (KI - EMD Chemicals); zinc dust (Fischer); glacial acetic acid (AcOH - Mallinckrodt Chemicals) were all used as received.

The adsorbate 1-octadecanethiol (**H18SH**) was purchased from Sigma Aldrich and used as received. The adsorbates 1-nonadecanethiol (**H19SH**), 1-icosanethiol (**H20SH**), 1-henicosanethiol (**H21SH**), 1-docosanethiol (**H22SH**), 1-tricosanethiol (**H23SH**), 1-tetracosanethiol (**H24SH**), and 12,12,13,13,14,14,15,15,16,16,17,17-dodecafluorooctadecane-1-thiol (**H1F6H11SH**) were synthesized according to literature procedures.[27-31]

3.2.2. Synthesis of Terminally-Alkylated Partially-Fluorinated Alkanethiols.

The adsorbate 12,12,13,13,14,14,15,15,16,16,17,17-dodecafluorononadecane-1-thiol (**H2F6H11SH**) was synthesized according to Scheme 1, while the adsorbate 12,12,13,13,14,14,15,15,16,16,17,17-dodecafluoroicosane-1-thiol (**H3F6H11SH**) was synthesized according to Scheme 2. Similarly, the adsorbates 12,12,13,13,14,14,15,15,16,16,17,17-dodecafluorohenicosane-1-thiol (**H4F6H11SH**), 12,12,13,13,14,14,15,15,16,16,17,17-dodecafluorodocosane-1-thiol (**H5F6H11SH**),

12,12,13,13,14,14,15,15,16,16,17,17-dodecafluorotricosane-1-thiol (**H6F6H11SH**), and 12,12,13,13,14,14,15,15,16,16,17,17-dodecafluorotetracosane-1-thiol (**H7F6H11SH**) were synthesized according to Scheme 3 as detailed below.

Scheme 3.1. Synthesis of 12,12,13,13,14,14,15,15,16,16,17,17-Dodecafluorononadecane-1-thiol **(H2F6H11SH)**.

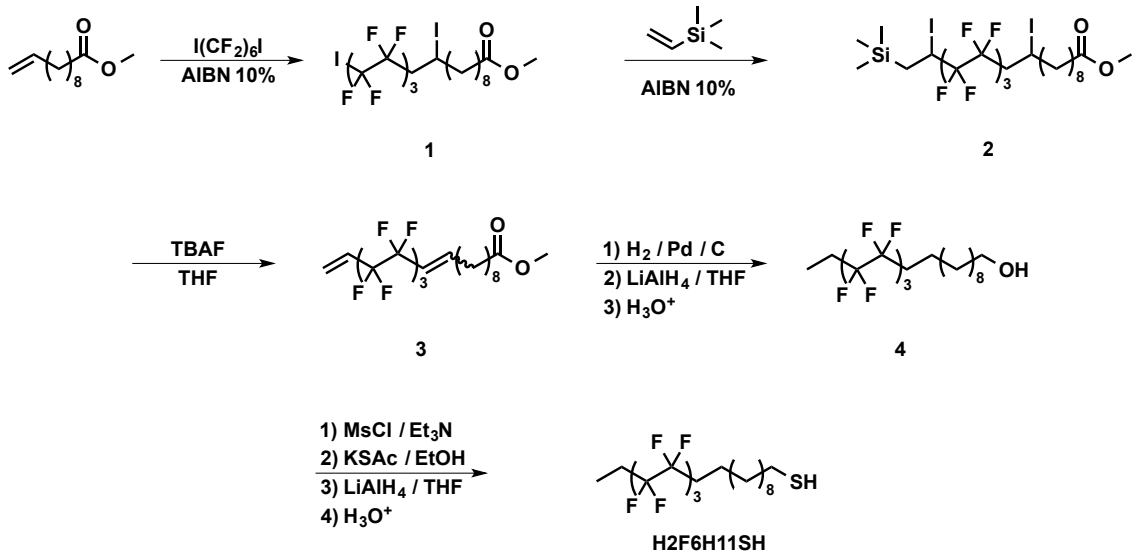

Methyl 12,12,13,13,14,14,15,15,16,16,17,17-dodecafluoro-10,17-diiodoheptadecanoate (1). In a 100-mL Schlenk flask, the starting materials 1,6-diiodoperfluorohexane (6.00 g; 10.8 mmol), AIBN (10 mol %) and methyl 10-undecenoate (1.83 g; 9.21 mmol) were dissolved in 20 mL of DCE. The system was degassed with three cycles of a standard freeze-pump-thaw procedure, and the mixture was heated to 85 °C for 5 h. After cooling to rt, the solvent was removed by rotary evaporation, and the product was purified by silica gel chromatography using hexanes / ethyl acetate (95:5) as the eluent to give methyl 12,12,13,13,14,14,15,15,16,16,17,17-dodecafluoro-10,17-diiodoheptadecanoate (**1**) in 56% yield. ^{1}H NMR (600 MHz, $CDCl_3$): δ 4.32

(m, 1 H), 3.66 (s, 3 H), 2.70–2.95 (m, $2H_2$), 2.30 (t, J = 7.56 Hz, 2 H), 1.71–1.85 (m, 2 H), 1.51–1.63 (m, 4 H), 1.24–1.42 (m, 8 H). ^{19}F NMR (565 MHz, $CDCl_3$): δ -58.8 (m, 2 F), -111.8 – -115.2 (m, 4 F), -120.91 (m, 2 F), -121.45 (m, 2 F), -123.50 (m, 2 F).

*Methyl 12,12,13,13,14,14,15,15,16,16,17,17-dodecafluoro-10,19-diiodo-19-(trimethylsilyl)nonadecanoate (**2**).* In a 100-mL Schlenk flask, *F*-iodoester **1** (2.75 g; 3.6 mmol), trimethyl(vinyl)silane (0.80 mL; 5.4 mmol), and AIBN (10 %) were dissolved in 20 mL of DCE. The mixture was degassed with three cycles of a standard freeze-pump-thaw procedure then heated to 85 °C until consumption of the starting alkene. Afterward, the solvent was removed by rotary evaporation, and the product was purified by silica gel chromatography using hexanes / ethyl acetate (95:5) as the eluent to give the intermediate silane in 99% yield. ^{1}H NMR (400 MHz, $CDCl_3$): δ 4.29–4.36 (m, 1H), 3.66 (s, 3H), 3.19–3.22 (m, 1H), 2.50–2.99 (m, 4H), 2.30 (t, J = 7.66 Hz, 2H), 1.71–1.86 (m, 2H), 1.58–1.63 (m, 2H), 1.21–1.43 (m ,10H), 0.19 (s, 9H). ^{19}F NMR (376 MHz, $CDCl_3$): δ -115.7 – -111.2 (m, 4F, broad), -121.6 (m, 4F), -123.61 (m, 4F).

*Methyl 12,12,13,13,14,14,15,15,16,16,17,17-dodecafluorononadeca-10,18-dienoate (**3**).* In a 100-mL round bottom flask, compound **2** (3.03 g; 3.55 mmol) was dissolved in 50 mL of distilled THF and cooled to 0 °C. Once cooled, 1 M TBAF solution (14.2 mL; 14.2 mmol) was added dropwise to the flask. The mixture was allowed to stir at rt for 16 h. Afterward, the reaction was quenched with 50 mL of 1 M HCl. The product was extracted with Et_2O (3 × 100 mL), and the organic layer washed with water (2 × 100 mL) and brine (1 × 100 mL), and dried with $MgSO_4$. After the solid was filtered off, the solution was passed through a short bed of silica gel, and then the solvent was removed by rotary evaporation to give **3**, which was carried on to the next step without further purification. ^{1}H NMR (600 MHz, $CDCl_3$): δ 6.36–6.40 (m, 1H), 5.93–6.03 (m,

2H), 5.77–5.84 (m, 1H), 5.59 (q, J = 13.06 Hz, 1H), 3.66 (s, 3H), 2.30 (t, J = 7.21 Hz, 2H), 2.18 (m, 2H), 1.60–1.62 (m, 2H), 1.42–1.47 (m, 2H), 1.19–1.29 (m, 7H). ^{19}F NMR (565 MHz, $CDCl_3$): δ -111.1 (m, 2F), -113.7 (m, 2F), -121.5 (m, 4F), -123.6 (m, 4F).

*12,12,13,13,14,14,15,15,16,16,17,17-Dodecafluorononadecan-1-ol (**4**).* A slurry of Pd/C (10 mol %) in anhydrous MeOH (15 mL) was prepared in an oven dried 2-neck round bottom flask. The slurry was evacuated, refilled with H_2, and stirred for 20 min. Afterward, a solution of dissolved diene **3** (1.93 g; 3.69 mmol) in MeOH (20 mL) was transferred into the slurry. The mixture was stirred at rt for 48 h, refilling the flask with H_2 as necessary. Afterward, the mixture was diluted with Et_2O (200 mL) and filtered through a Celite pad. The solvent was then removed to give the ethyl-terminated partially fluorinated ester, which was carried on to the next step without purification. The crude ester (1.95 g; 3.69 mmol) was dissolved in dry THF (50 mL) and added dropwise to a stirring slurry of $LiAlH_4$ (0.218 g; 5.75 mmol) at 0 °C. The mixture was then warmed to rt and stirred for 6 h. The reaction was quenched at 0 °C with H_2O (10 mL) and acidified with 2 M HCl (20 mL). The compound was extracted with Et_2O (3 × 100 mL), and the organic layer washed with water (1 × 100 mL) and brine (1 × 100 mL), dried with $MgSO_4$, and the solvent removed by rotary evaporation. The crude alcohol was purified using silica gel chromatography with hexanes / ethyl acetate (80:20) as the eluent to give alcohol **4** in 82% yield from the iodo-silane. ^{1}H NMR (600 MHz, $CDCl_3$): δ 3.64 (q, J = 6.19 Hz, 2H), 1.99–2.17 (m, 4H), 1.54–1.61 (m, 4H), 1.25–1.36 (m, 14H), 1.19 (t, J = 5.5 Hz, 1H), 1.14 (t, J = 7.56 Hz, 3H). ^{19}F NMR (565 MHz, $CDCl_3$): δ -114.4 – -114.3 (m, 2F), -116.3 – -116.2 (m, 2F), -121.8 (m, 4F), -123.6 (m, 4F).

*12,12,13,13,14,14,15,15,16,16,17,17-Dodecafluorononadecane-1-thiol (**H2F6H11SH**).* The alcohol (1.47 g; 2.95 mmol) was dissolved in anhydrous THF (75 mL), and at 0 °C Et_3N (1.3

mL; 9.3 mmol) was added. After stirring for 30 min, an aliquot of MsCl (0.7 mL; 1.5 mmol) was added to the flask, and the mixture was allowed to stir at rt for 6 h. Afterward, the reaction was quenched with cold H_2O (50 mL), and the product was extracted with Et_2O (3 × 100 mL). The organic layer was then washed with 1 M HCl (1 × 100 mL), water (1 × 100 mL), brine (1 × 100 mL), and dried with $MgSO_4$. The solvent was then removed by rotary evaporation, and the crude mesylate carried to the next step without purification. The crude mesylated alcohol (1.98 g; 3.42 mmol) and KSAc (1.180 g; 10.3 mmol) were dissolved in anhydrous EtOH (75 mL, previously degassed) and refluxed for 4 h. After cooling to rt, the reaction was quenched with H_2O (50 mL) and the product extracted with Et_2O (3 × 100 mL). The organic layers were combined and washed with H_2O (1 × 100 mL) and brine (1 × 100 mL), and dried with $MgSO_4$. After removal of the solvent by rotary evaporation, the crude thioacetate was carried to the next step without further purification. The crude thioacetate (1.6 g; 2.9 mmol) was dissolved in anhydrous THF (50 mL, previous degassed). Once dissolved, the solution was added to a slurry of $LiAlH_4$ (0.17 g; 4.5 mmol) in 10 mL of THF (previously degassed) at 0 °C. The mixture was stirred at rt for 6 h. Afterward, the reaction was quenched with H_2O (20 mL, previously degassed) at 0 °C and immediately acidified with 1 M H_2SO_4 (50 mL, previously degassed) until the pH of the solution was ~1. The product was then extracted with Et_2O (3 × 100 mL), and the combined organic layers were washed with H_2O (1 × 100 mL) and brine (1 × 100 mL), and dried with $MgSO_4$. After removal of the solvent by rotary evaporation, the crude thiol was purified using silica gel chromatography with hexanes / ethyl acetate (99:1) as the eluent to give 12,12,13,13,14,14,15,15,16,16,17,17-dodecafluorononadecane-1-thiol (**H2F6H11SH**) in 88% yield. ^{1}H NMR (600 MHz, $CDCl_3$): δ 2.52 (q, J = 7.33 Hz, 2H), 2.15 (m, 4H), 1.56–1.63 (m, 4H),

1.27–1.43 (m, 14H), 1.33 (t, J = 7.90 Hz, 1H), 1.13 (t, J = 7.21 Hz, 3H). ^{19}F NMR (565 MHz, $CDCl_3$): δ -114.4 (m, 2F), -116.4 (m, 2F), -121.8 (m, 4F), - 123.6 (m, 4F). ^{13}C NMR (125 MHz, $CDCl_3$): δ 34.1 (s), 31.0 (t, J = 22.18 Hz), 29.2–29.6 (m), 28.5 (s), 24.7 (t, J = 11.09 Hz), 24.5 (s), 20.2 (m), 4.6 (t, J = 4.44 Hz). Broad peaks at δ 109.4–120.6 are characteristic of a long perflurocarbon chain.[24] HR-CI-MS, *m/z*: 515.1644 $[M-H]^+$.

Scheme 3.2. Synthesis of 12,12,13,13,14,14,15,15,16,16,17,17-Dodecafluoroicosane-1-thiol (**H3F6H11SH**).

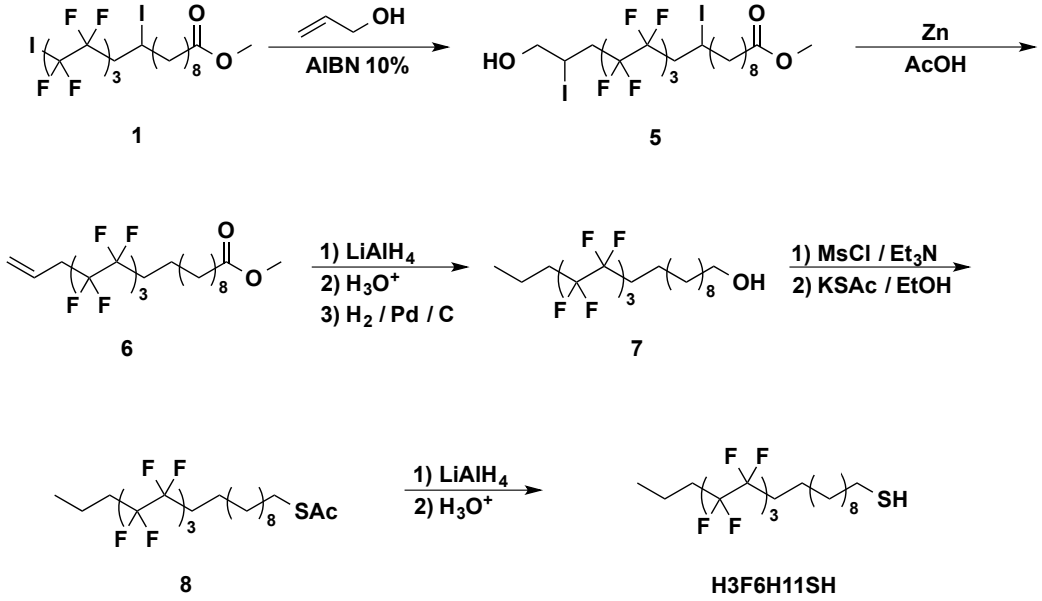

*Methyl 12,12,13,13,14,14,15,15,16,16,17,17-Dodecafluoro-20-hydroxy-10,19-diiodoicosanoate (**5**)*. In a 100-mL Schlenk flask, *F*-iodoester **1** (0.85 g; 1.1 mmol), AIBN (10 mol %), and allyl alcohol (0.13 g; 2.2 mmol) were dissolved in 20 mL of DCE. The mixture was degassed with three cycles of a standard freeze-pump-thaw procedure, and the reaction heated to 85 ºC for 12 h. The solvent was then removed by rotary evaporation, and the product was purified by silica gel chromatography using hexanes / ethyl acetate (70:30) as the eluent system to give methyl 12,12,13,13,14,14,15,15,16,16,17,17-dodecafluoro-20-hydroxy-10,19-diiodoicosanoate (**5**) in 93% yield. ^{1}H NMR (500 MHz, $CDCl_3$): δ 4.43 (m, 1 H), 4.32 (m, 1 H), 3.79 (m, 2 H), 3.66 (s, 3 H), 2.70–3.06 (m, 4 H), 2.30 (t, J = 7.56 Hz, 2 H), 2.06 (t, J = 6.87 Hz, 1 H), 1.71–1.85 (m, 2 H), 1.51–1.63 (m, 2 H), 1.24–1.42 (m, 10 H). ^{19}F NMR (470 MHz, $CDCl_3$): δ -111.2 – 114.9 (m, 4 F), -121.6 (m, 4 F), -123.6 (m, 4 F).

*Methyl 12,12,13,13,14,14,15,15,16,16,17,17-dodecafluoroicos-19-enoate (**6**).* Compound **5** (0.85 g; 1.0 mmol) was dissolved in a solution of THF (20 mL) and glacial acetic acid (50 mL). Zinc dust (2.06 g; 31.4 mmol) was then added under a flow of argon, and the mixture was stirred at rt for 48 h. The mixture was then diluted with 200 mL of Et_2O and filtered through Celite. The filtrate was then washed with water (3 × 100 mL), saturated aqueous $NaHCO_3$ (1 × 100 mL), and brine (1 × 50 mL), and dried over $MgSO_4$. The solvent was removed by rotary evaporation to give *methyl* 12,12,13,13,14,14,15,15,16,16,17,17-dodecafluoroicos-19-enoate (**6**) in 90% yield. ^{1}H NMR (500 MHz, $CDCl_3$): δ 5.79 (m, 1 H), 5.32 (m, 2 H), 3.66 (s, 3 H), 2.84 (m, 2 H), 2.29 (t, J = 7.56 Hz, 2 H), 1.98–2.10 (m, 2 H), 1.55–1.63 (m, 2 H), 1.21–1.37 (m, 14 H). ^{19}F NMR (470 MHz, $CDCl_3$): δ -113.2 (m, 2 F), -114.3 (m, 2 F), -121.8 (m, 4 F), -123.2 (m, 2 F), -123.6 (m, 2 F).

*12,12,13,13,14,14,15,15,16,16,17,17-Dodecafluoroicosan-1-ol (**7**).* Olefin **6** (0.51 g; 0.94 mmol) was dissolved in anhydrous THF (50 mL) and added dropwise to a stirring slurry of $LiAlH_4$ (0.107 g; 2.82 mmol) in THF (10 mL) at 0 °C. The mixture was then warmed to rt and stirred for 6 h under argon. Afterward, at 0 °C, the reaction was quenched with 20 mL of water, followed by the addition of 1 M aqueous HCl solution (20 mL). The mixture was then extracted with Et_2O (3 × 100 mL). The combined organic layers were washed with water (1 × 100 mL) and brine (1 × 100 mL), dried over $MgSO_4$, and evaporated to dryness by rotary evaporation. The crude alcohol was carried to the next step without further purification.

The crude compound was dissolved in 30 mL of MeOH and added to a slurry of Pd/C (10%). The mixture was placed under 1 atm of hydrogen and stirred at rt for 12 h. The mixture was filtered through a bed of Celite and then washed with Et_2O (100 mL). After removal of solvent, the product was purified by silica gel chromatography using hexanes / ethyl acetate

(70:30) as the eluent system to give 12,12,13,13,14,14,15,15,16,16,17,17-dodecafluoroicosan-1-ol (**7**) in 66% yield. ^{1}H NMR (500 MHz, $CDCl_3$): δ 3.64 (t, *J* = 6.70 Hz, 2 H), 1.98–2.08 (m, 4 H), 1.55–1.65 (m, 6 H), 1.14–1.41 (m, 14 H), 1.01 (t, *J* = 7.22 Hz, 3 H). ^{19}F NMR (470 MHz, $CDCl_3$): δ -114.4 (m, 4 F), -121.8 (m., 4 F), -123.7 (m, 4 F).

*S-(12,12,13,13,14,14,15,15,16,16,17,17-Dodecafluoroicosyl) ethanethioate (**8**).* Alcohol **7** (0.32 g; 0.62 mmol) was dissolved in anhydrous THF (20 mL), and at 0 °C NEt_3 (0.26 mL; 1.9 mmol) was added to the flask. After stirring for 30 min, MsCl (0.24 mL; 3.1 mmol) was added dropwise, and the mixture was allowed to stir at rt for 12 h. The reaction was then quenched with 50 mL of cold water, and the product was extracted with Et_2O (3 × 100 mL). The combined organic phases were washed with 1 M aqueous HCl (1 × 100 mL), water (1 × 100 mL), brine (1 × 100 mL), and dried with $MgSO_4$. The solvent was then removed by rotary evaporation, and the crude mesylate carried to the next step without purification.

The crude product and KSAc (0.345 g; 3.02 mmol) were dissolved in anhydrous ethanol (50 mL, previously degassed) and refluxed for 6 h. After cooling to rt, the reaction was quenched with H_2O (50 mL) and the product extracted with Et_2O (3 × 100 mL). The organic layers were combined and washed with H_2O (1 × 100 mL) and brine (1 × 100 mL), and dried with $MgSO_4$. After removal of the solvent by rotary evaporation, the crude thioacetate was purified by column chromatography on silica gel (hexanes / ethyl acetate; 95:5) to give S-(12,12,13,13,14,14,15,15,16,16,17,17-dodecafluoroicosyl) ethanethioate (**8**) in 98% yield. ^{1}H NMR (500 MHz, $CDCl_3$): δ 2.85 (t, *J* = 7.39 Hz, 2 H), 2.32 (s, 3 H), 1.98–2.08 (m, 6 H), 1.52–1.66 (m, 4 H), 1.26–1.36 (m, 14 H), 1.02 (t, *J* = 7.39 Hz, 3 H). ^{19}F NMR (470 MHz, $CDCl_3$): δ -114.3 (m, 4 F), -121.8 (m, 4 F), -123.7 (m, 4 F).

12,12,13,13,14,14,15,15,16,16,17,17-Dodecafluoroicosane-1-thiol ***(H3F6H11SH)***.

Thioacetate **8** (0.30 g; 0.52 mmol) was dissolved in anhydrous THF (30 mL). Once dissolved, the solution was added to a slurry of $LiAlH_4$ (0.059 g; 1.6 mmol) in THF (5 mL) at -10 °C. The mixture was stirred at ~ -10 °C for 6 h under argon. Afterward, the reaction was quenched with H_2O (20 mL, previously degassed) at 0 °C and immediately acidified with 1 M H_2SO_4 (50 mL, previously degassed) until the pH of the solution was ~1. The product was then extracted with Et_2O (3 × 100 mL) and the combined organic layers washed with H_2O (1 × 100 mL) and brine (1 × 100 mL), and dried with $MgSO_4$. After removal of the solvent by rotary evaporation. The resulting thiol was purified by column chromatography on silica gel (hexanes / ethyl acetate; 99:1) to give 12,12,13,13,14,14,15,15,16,16,17,17-dodecafluoroicosane-1-thiol (**H3F6H11SH**) in 50% yield. ^{1}H NMR (600 MHz, $CDCl_3$): δ 2.51 (q, J = 7.45 Hz, 2 H), 1.96–2.09 (m, 4 H), 1.55–1.68 (m, 6 H), 1.25–1.36 (m, 15 H), 1.02 (t, J = 7.45 Hz, 3 H). ^{19}F NMR (565 MHz, $CDCl_3$): δ -114.3 (m, 4F), -121.8 (m, 4F), -123.7 (m, 4F). ^{13}C NMR (150 MHz, $CDCl_3$): δ 34.2 (s), 33.0 (t, J = 22.18 Hz), 31.1 (t, J = 22.18 Hz), 29.2–29.6 (m), 28.5 (s), 24.8 (s), 20.3 (s), 13.9 (m), 13.8 (s). Broad peaks at δ 109.4–120.5 are characteristic of a long perfluorocarbon chain.[24] HR-CI-MS, *m/z*: 529.1797 $[M\text{-}H]^+$.

Scheme 3.3. Synthesis of 12,12,13,13,14,14,15,15,16,16,17,17-Dodecafluorohenicosane-1-thiol (**H4F6H11SH**), 12,12,13,13,14,14,15,15,16,16,17,17-Dodecafluorodocosane-1-thiol (**H5F6H11SH**), 12,12,13,13,14,14,15,15,16,16,17,17-Dodecafluorotricosane-1-thiol (**H6F6H11SH**), and 12,12,13,13,14,14,15,15,16,16,17,17-Dodecafluorotetracosane-1-thiol (**H7F6H11SH**).

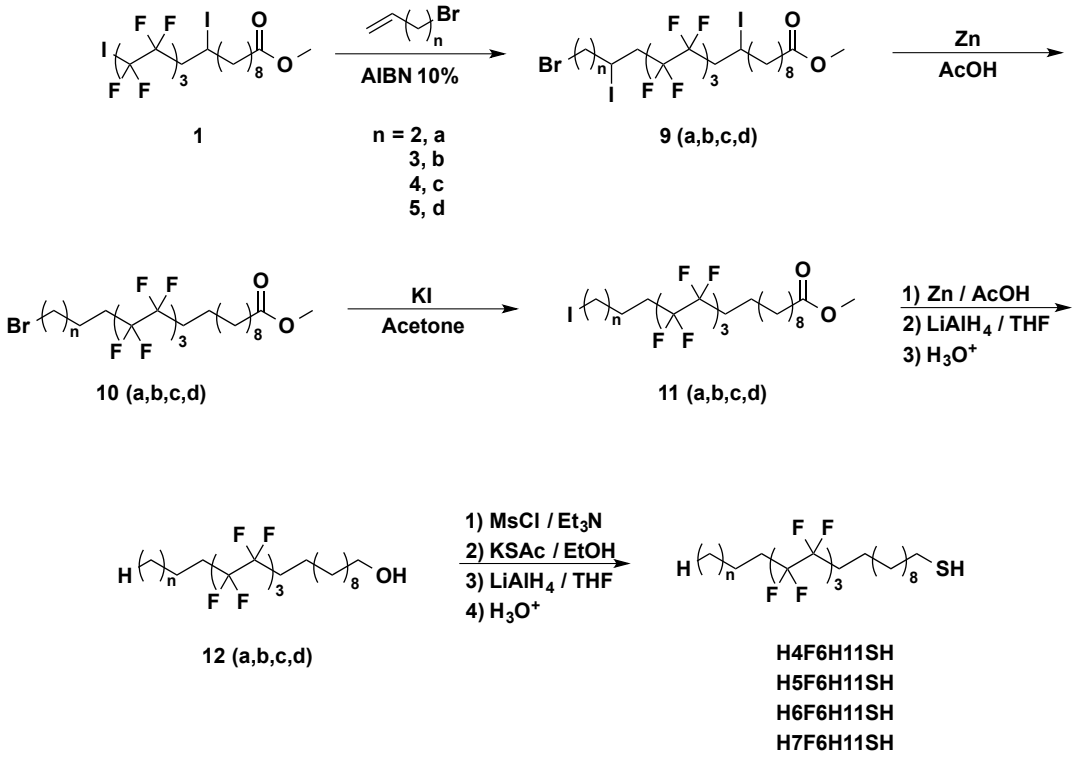

*Methyl 21-bromo-12,12,13,13,14,14,15,15,16,16,17,17-dodecafluoro-10,19-diiodohenico-sanoate (**9a**).* In a 100-mL Schlenk flask, *F*-iodoester **1** (1.64 g; 2.18 mmol), AIBN (10 mol %), and 4-bromo-heptene (0.60 g; 4.4 mmol) were dissolved in 20 mL of DCE and degassed using three cycles of a standard freeze-pump-thaw procedure. After degassing, the reaction was run at 85 °C for 12 h. Afterward, the solvent was removed by rotary evaporation, and the crude product purified by silica gel chromatography using hexanes / ethyl acetate (90:10) as the eluent to give **9a** in 88 % yield. ^{1}H NMR (500 MHz, $CDCl_3$): δ 4.49–4.51 (m, 1 H), 4.30–

4.35 (m, 1 H), 3.66 (s, 3 H), 3.59–3.61 (m, 1 H), 3.46–3.51 (m, 1 H), 2.75–3.04 (m, 4 H), 2.30 (t, *J* = 7.56 Hz, 2 H), 2.22–2.34 (m, 2 H), 1.72–1.83 (m, 2 H), 1.51–1.63 (m, 4 H), 1.18–1.42 (m, 8 H). ^{19}F NMR (476 MHz, $CDCl_3$): δ -110.5 – -114.8 (m, 4 F), -121.5 (m, 4 F), -123.5 (m, 4 F). Compounds **9b**, **9c**, and **9d** were prepared using analogous methodology (vide infra).

Methyl 22-bromo-12,12,13,13,14,14,15,15,16,16,17,17-dodecafluoro-10,19-diiododocosanoate (**9b**) in 86% yield. ^{1}H NMR (500 MHz, $CDCl_3$): δ 4.30–4.34 (m, 2 H), 3.66 (s, 3 H), 3.43–3.45 (m, 2 H), 2.73–2.92 (m, 4 H), 2.30 (t, *J* = 7.56 Hz, 2 H), 2.11–2.19 (m, 1 H), 1.92–2.04 (m, 3 H), 1.72–1.84 (m, 2 H), 1.60–1.63 (m, 2 H), 1.51–1.56 (m, 1 H), 1.23–1.42 (m, 9 H). ^{19}F NMR (476 MHz, $CDCl_3$): δ -111.2 – -114.8 (m, 4F), -121.6 (m, 4F), -123.6 (m, 4F).

Methyl 23-bromo-12,12,13,13,14,14,15,15,16,16,17,17-dodecafluoro-10,19-diiodotricosanoate (**9c**) in 88 % yield. ^{1}H NMR (500 MHz, $CDCl_3$): δ 4.30–4.35 (m, 2H), 3.66 (s, 3H), 3.42 (t, *J* = 6.7 Hz, 2H), 2.71–2.99 (m, 4H), 2.30 (t, *J* = 7.56 Hz, 2H), 1.68–1.98 (m, 6H), 1.51–1.63 (m, 4H), 1.24–1.42 (m, 10H). ^{19}F NMR (476 MHz, $CDCl_3$): δ -111.9 – -111.1 (m, 2F), -114.8 – -114.2 (m, 2F), -121.6 (m, 4F), -123.6 (m, 4F).

Methyl 24-bromo-12,12,13,13,14,14,15,15,16,16,17,17-dodecafluoro-10,19-diiodotetracosanoate (**9d**) in 90 % yield. ^{1}H NMR (400 MHz, $CDCl_3$): δ 4.29–4.36 (m, 2H), 3.67 (s, 3H), 3.42 (t, *J* = 6.6 Hz, 2H), 2.69–2.99 (m, 4H), 2.31 (t, *J* = 7.56 Hz, 2H), 1.71–1.93 (m, 6H), 1.21–1.64 (m, 16H). ^{19}F NMR (376 MHz, $CDCl_3$): δ -111.2 (m, 1F), -111.9 – -111.8 (m, 2F), -114.2 (m, 2F), -114.9 (m, 1F), -121.6 (m, 4F), -123.6 (m, 4F).

*Methyl 21-bromo-12,12,13,13,14,14,15,15,16,16,17,17-dodecafluorohenicosanoate (**10a**)* Intermediate **9a** (1.7 g; 1.9 mmol) was dissolved in a 500-mL round bottom flask in glacial acetic acid (100 mL); 20 mL of distilled THF were added in order to help the compound dissolve. Zn

powder (3.77 g; 57.5 mmol) was added under the flow of argon with vigorous stirring. The mixture was allowed to stir at rt in the dark for 48 h. Afterward, the accumulated pressure was carefully released before opening the flask. The mixture was diluted with Et_2O and filtered through a bed of Celite. The filtrate was then washed with a copious amount of water (10 × 100 mL), saturated $NaHCO_3$ solution (2 × 50 mL), brine (1 × 100 mL), and dried with $MgSO_4$. The solvent was then removed by rotary evaporation giving intermediate **10a** in 94% yield. ^{1}H NMR (500 MHz, $CDCl_3$): δ 3.66 (s, 3 H), 3.43 (t, J = 6.70, 2 H), 2.30 (t, J = 7.56, 2 H), 2.13–1.91 (m, 6 H), 1.78 (m, 2 H), 1.62–1.54 (m, 4H), 1.35 (m, 12 H). ^{19}F NMR (476 MHz, $CDCl_3$): δ -114.3 (m, 4 F), -121.8 (m, 4 F), -123.6 (m, 4 F). Compounds **10b**, **10c**, and **10d** were prepared using analogous methodology (vide infra).

Methyl 22-bromo-12,12,13,13,14,14,15,15,16,16,17,17-dodecafluorodocosanoate (**10b**) in 96% yield. ^{1}H NMR (500 MHz, $CDCl_3$): δ 3.66 (s, 3 H), 3.42 (t, *J* = 6.70 Hz, 2 H), 2.30 (t, *J* = 7.56 Hz, 2 H), 1.98–2.13 (m, 4 H), 1.87–1.93 (m, 2 H), 1.54–1.64 (m, 8 H), 1.24–1.37 (m, 12 H). ^{19}F NMR (476 MHz, $CDCl_3$): δ -114.3 (m, 4F), -121.8 (m, 4F), -123.6

Methyl 23-bromo-12,12,13,13,14,14,15,15,16,16,17,17-dodecafluorotricosanoate (**10c**) in 92% yield. ^{1}H NMR (500 MHz, $CDCl_3$): δ 3.65 (s, 3H), 3.40 (t, *J* = 6.70 Hz, 2H), 2.29 (t, *J* = 7.56 Hz, 2H), 1.97–2.10 (m, 4H), 1.84–1.89 (m, 2H), 1.54–1.65 (m, 6H), 1.20–1.51 (m, 16H). ^{19}F NMR (476 MHz, $CDCl_3$): δ -114.3 (m, 4F), -121.6 (m, 4F), -123.1

Methyl 24-bromo-12,12,13,13,14,14,15,15,16,16,17,17-dodecafluorotetracosanoate (**10d**) in 93% yield. ^{1}H NMR (500 MHz, $CDCl_3$): δ 3.67 (s, 3H), 3.41 (t, *J* = 6.87 Hz, 2H), 2.30 (t, *J* = 7.73 Hz, 2H), 2.03–2.05 (m, 4H), 1.83–1.89 (m, 2H), 1.55–1.62 (m, 6H), 1.25–1.47 (m, 18H). ^{19}F NMR (476 MHz, $CDCl_3$): δ -114.3 (m, 4F), -121.8 (m, 4F), -123.6.

*Methyl 12,12,13,13,14,14,15,15,16,16,17,17-dodecafluoro-21-iodohenicosanoate (**11a**).* The bromo-ester (1.33 g; 2.09 mmol) and potassium iodide (1.74 g; 10.5 mmol) were dissolved in 50 mL of acetone in a 100-mL round bottom flask. The mixture was then refluxed for 24 h. After cooling to rt, the solvent was removed by rotary evaporation, and the resulting residue was dissolved in Et_2O (200 mL). The organic layer was then washed with water (1 × 100 mL) and brine (1 × 100 mL), and dried with $MgSO_4$. The solvent was removed by rotary evaporation to give **11a** in 95% yield. ^{1}H NMR (500 MHz, $CDCl_3$): δ 3.66 (s, 3 H), 3.20 (t, *J* = 6.87 Hz, 2 H), 2.30 (t, *J* = 7.56 Hz, 2 H), 1.98–2.10 (m, 4 H), 1.91 (m, 2H), 1.71–1.78 (m, 2 H), 1.54–1.63 (m, 4 H), 1.20–1.43 (m, 12 H). ^{19}F NMR (476 MHz, $CDCl_3$): δ -114.3 (m, 4 F), -121.8 (m, 4 F), -123.6 (m, 4 F). Compounds **11b**, **11c**, and **11d** were prepared using analogous methodology.

Methyl 12,12,13,13,14,14,15,15,16,16,17,17-dodecafluoro-22-iododocosanoate (**11b**) in 97% yield. ^{1}H NMR (500 MHz, $CDCl_3$): δ 3.66 (s, 3 H), 3.20 (t, *J* = 6.87 Hz, 2 H), 2.30 (t, *J* = 7.56 Hz, 2 H), 2.01–2.11 (m, 4 H), 1.83–1.89 (m, 2 H), 1.43–1.65 (m, 8 H), 1.25–1.36 (m, 12 H). ^{19}F NMR (476 MHz, $CDCl_3$): δ -114.3 (m, 4 F), -121.8 (m, 4 F), -123.6 (m, 4 F).

Methyl 12,12,13,13,14,14,15,15,16,16,17,17-dodecafluoro-23-iodotricosanoate (**11c**) in 100 % yield. ^{1}H NMR (500 MHz, $CDCl_3$): δ 3.66 (s, 3H), 3.18 (t, *J* = 7.04 Hz, 2H), 2.29 (t, *J* = 7.56 Hz, 2H), 1.97–2.10 (m, 4H), 1.80–1.86 (m, 2H), 1.54–1.64 (m, 6H), 1.27–1.47 (m, 16H). ^{19}F NMR (476 MHz, $CDCl_3$): δ -114.3 (m, 4F), -121.6 (m, 4F), -123.6 (m, 4F).

Methyl 12,12,13,13,14,14,15,15,16,16,17,17-dodecafluoro-24-iodotetracosanoate (**11d**) in 99% yield. ^{1}H NMR (500 MHz, $CDCl_3$): δ 3.67 (s, 3H), 3.19 (t, *J* = 6.87 Hz, 2H), 2.30 (t, *J* = 7.73 Hz, 2H), 1.99–2.09 (m, 4H), 1.80–1.85 (m, 2H), 1.57–1.63 (m, 6H), 1.25–1.44 (m, 18H). ^{19}F NMR (470 MHz, $CDCl_3$): δ -114.3 (m, 4F), -121.8 (m, 4F), -123.6 (m, 4F).

*12,12,13,13,14,14,15,15,16,16,17,17-Dodecafluorohenicosan-1-ol (**12a**).* Intermediate **11a**

(1.37 g; 2.00 mmol) was dissolved in a mixture of glacial acetic acid (100 mL) and THF (20 mL). The addition of zinc dust (1.98 g; 30.1 mmol) was performed under a flow of argon with vigorous stirring. The mixture was allowed to stir at rt for 48 h, at which point the mixture was diluted with Et_2O (200 mL) and filtered through a bed of Celite. The filtrate was then washed with H_2O (10 × 100 mL), saturated $NaHCO_3$ (2 × 50 mL), brine (1 × 100 mL), and dried with $MgSO_4$. The solvent was removed by rotary evaporation, and the crude product carried into the next step without further purification.

The resulting crude ester (0.916 g; 1.65 mmol) was dissolved in dry THF (50 mL) and added to a stirring slurry of $LiAlH_4$ (0.188 g; 4.94 mmol) at 0 °C. The mixture was allowed to stir at rt for 4 h under argon. The mixture was cooled to 0 °C, quenched with H_2O (20 mL), and acidified with 1 M HCl (50 mL). The solution was then extracted with Et_2O (3 × 100 mL). The combined Et_2O layers were washed with water (1 × 100 mL) and brine (1 × 100 mL), and dried with $MgSO_4$. Afterward, the solvent was removed by rotary evaporation, and the compound purified with silica gel chromatography using hexanes / ethyl acetate (80:20) as the eluent to give 12,12,13,13,14,14,15,15,16,16,17,17-dodecafluorotetracosan-1-ol (**12a**) in 76% yield. ^{1}H NMR (500 MHz, $CDCl_3$): δ 3.64 (t, J = 6.70 Hz, 2 H), 1.98–2.10 (m, 4 H), 1.55–1.58 (m, 6 H), 1.28–1.41 (m, 16 H), 0.95 (t, J = 7.22 Hz, 3 H). ^{19}F NMR (476 MHz, $CDCl_3$): δ -114.3 (m, 4 F), -121.8 (m, 4 F), -123.6 (m, 4 F). Compounds **12b**, **12c**, and **12d** were prepared using analogous methodology.

12,12,13,13,14,14,15,15,16,16,17,17-Dodecafluorodocosan-1-ol (**12b**) in 95% yield. ^{1}H NMR (500 MHz, $CDCl_3$): δ 3.63 (q, J = 6.30 Hz, 2 H), 1.98–2.09 (m, 4 H), 1.54–1.61 (m, 6 H), 1.25–1.37 (m, 18 H), 0.91 (t, J = 7.05 Hz, 3 H). ^{19}F NMR (476 MHz, $CDCl_3$): δ -114.3 (m, 4 F), -121.8 (m, 4 F), -123.6 (m, 4 F).

12,12,13,13,14,14,15,15,16,16,17,17-Dodecafluorotricosan-1-ol (**12c**) in 40% yield. ^{1}H

NMR (500 MHz, $CDCl_3$): δ 3.62–3.67 (m, 2H), 1.98–2.10 (m, 4H), 1.54–1.62 (m, 6H), 1.21–1.40 (m, 20H), 0.90 (t, J = 7.04 Hz, 3H). ^{19}F NMR (476 MHz, $CDCl_3$): δ -114.3 (m ,4F), -121.8 (m, 4F), - 123.6 (m, 4F).

12,12,13,13,14,14,15,15,16,16,17,17-Dodecafluorotetracosan-1-ol (**12d**) in 76% yield. ^1H NMR (400 MHz, $CDCl_3$): δ 3.62–3.67 (q, J = 6.11 Hz, 2H), 1.97–2.11 (m, 4H), 1.53–1.63 (m, 6H), 1.28–1.36 (m, 22H), 1.19 (t, J = 5.27 Hz, 1H), 0.89 (t, J = 6.87 Hz, 3H). ^{19}F NMR (376 MHz, $CDCl_3$): δ -114.3 (m, 4F), -121.8 (m, 4F), -123. 7– -123.6 (m, 4F).

12,12,13,13,14,14,15,15,16,16,17,17-Dodecafluorohenicosane-1-thiol (***H4F6H11SH***). Alcohol **12a** (0.66 g; 1.2 mmol) was dissolved in 50 mL of anhydrous THF followed by cooling to 0 °C. Afterward, Et_3N (0.52 mL; 3.7 mmol) was added dropwise, and the solution was allowed to stir at 0 °C for 30 min. Subsequently, an aliquot of MsCl (0.48 mL; 6.2 mmol) was slowly added to the mixture. The mixture was warmed to rt and stirred for 6 h. The reaction was then quenched with ice-cold water (50 mL) followed by 1 M HCl (50 mL). The solution was then extracted with Et_2O (3 × 100 mL). The combined organic layers were then washed with 1 M HCl (1 × 100 mL), H_2O (1 × 100 mL), brine (1 × 100 mL), and dried with $MgSO_4$. The solvent was removed by rotary evaporation, and the resulting mesylated alcohol was carried to the next step without further purification.

The crude mesylated-alcohol (0.87 g; 1.4 mmol) and KSAc (0.819 g; 7.17 mmol) were dissolved in anhydrous ethanol (100 mL, previously degassed). The mixture was then refluxed for 4 h. Afterward, the solvent was removed by rotary evaporation, and the resulting residue was dissolved in Et_2O (200 mL). The organic layer was washed with water (1 × 100 mL) and brine (1 × 100 mL), dried with $MgSO_4$, and the solvent removed by rotary evaporation. The crude

thioacetate was dried under high vacuum overnight and carried to the next step without further purification.

The resulting crude thioacetate (0.61 g; 2.11 mmol) was dissolved in anhydrous THF (20 mL; previously degassed) and added dropwise to a stirring slurry of $LiAlH_4$ (0.119 g: 3.12 mmol) at 0 °C. The mixture was allowed to stir at rt for 3 h. The reaction was quenched at 0 °C with H_2O (20 mL; previously degassed) and immediately acidified with 1 M H_2SO_4 (50 mL; previously degassed). The aqueous layer was then extracted with Et_2O (3 × 100 mL), and the organic layer was washed with H_2O (1 × 100 mL) and brine (1 × 100 mL), and dried with $MgSO_4$. The solvent was removed by rotary evaporation, and the crude thiol was purified using silica gel chromatography with hexanes as the eluent to give 12,12,13,13,14,14,15,15,16,16,17,17-Dodecafluorohenicosane-1-thiol (**H4F6H11SH**) in 91% yield. ^{1}H NMR (500 MHz, $CDCl_3$): δ 2.53 (q, J = 7.45 Hz, 2 H), 1.98–2.09 (m, 4 H), 1.55–1.63 (m, 6 H), 1.28–1.44 (m, 16 H), 0.95 (t, J = 7.39 Hz, 3 H). ^{19}F NMR (476 MHz, $CDCl_3$): δ -114.3 (m, 4 F), -121.8 (m, 4 F), -123.6 (m, 4 F). ^{13}C NMR (125 MHz, $CDCl_3$): δ 39.2 (s), 34.1 (s), 30.6–31.2 (m), 29.0–29.5 (m), 28.4–28.6 (d), 24.7 (s), 22.2–22.3 (d), 20.2 (s), 13.8 (s), 4.0 (s). Broad peaks at δ 108.9–120.6 are characteristic of a long perfluorocarbon chain.[24] HR-CI-MS, *m/z*: 543.1969 $[M-H]^+$. Compounds **H5F6H11SH**, **H6F6H11SH**, and **H7F6H11SH** were prepared using analogous methodology.

12,12,13,13,14,14,15,15,16,16,17,17-Dodecafluorodocosane-1-thiol (**H5F6H11SH**) in 85% yield. ^{1}H NMR (600 MHz, $CDCl_3$): δ 2.52 (q, J = 7.33 Hz, 2 H), 1.99–2.08 (m, 4 H), 1.56–1.62 (m, 6 H), 1.28–1.43 (m, 19 H), 0.91 (t, J = 7.05 Hz, 3 H). ^{19}F NMR (565 MHz, $CDCl_3$): δ -114.5 (m, 4F), -121.9 (m, 4F), -123.7 (m, 4F). ^{13} C NMR (500 MHz, $CDCl_3$): δ 76.8–77.4 (m), 34.1 (s), 31.3 (s), 31.2 (m), 31.0 (m), 30.9 (m), 29.1–29.5 (m), 28.4 (s), 24.7 (s), 22.4 (s), 19.9–20.2 (d),

13.9 (s). Broad peaks at δ 108.7–120.6 are characteristic of a long perfluorocarbon chain.[24] HR-CI-MS, *m/z*: 557.2106 $[M-H]^+$.

12,12,13,13,14,14,15,15,16,16,17,17-Dodecafluorotricosane-1-thiol (**H6F6H11SH**) in 83% yield. ^{1}H NMR (500 MHz, $CDCl_3$): δ 2.53 (q, *J* = 7.45 Hz, 2H), 1.99–2.09 (m, 4H), 1.56–1.63 (m, 4H), 1.28–1.39 (m, 22H), 1.33 (t, J = 7.73 Hz, 1H), 0.90 (t, *J* = 6.87 Hz, 3H). ^{19}F NMR (476 MHz, $CDCl_3$): δ -114.3 (m, 4F), -121.8 (m, 4F), -123.6 (m, 4F). ^{13}C NMR (150 MHz, $CDCl_3$): δ 31.5 (s), 31.0 (t, *J* = 22.8 Hz), 29.1–29.5 (m), 28.9 (s), 28.4 (s), 22.5 (s), 20.2 (s), 14.1 (s). Broad peaks at δ 109.2–120.6 are characteristic of a long perfluorocarbon chain.[24] HR-CI-MS, *m/z*: 571.2254 $[M-H]^+$.

12,12,13,13,14,14,15,15,16,16,17,17-dodecafluorotetracosane-1-thiol (**H7F6H11SH**) in 76% yield. ^{1}H NMR (600 MHz, $CDCl_3$): δ 2.53 (q, *J* = 7.33 Hz, 2H), 1.99–2.08 (m, 4H), 1.55–1.63 (m, 4H), 1.28–1.37 (m, 25H), 0.89 (t, *J* = 6.87 Hz, 3H). ^{19}F NMR (565 MHz, $CDCL_3$): δ -114.4 (m, 4F), -121.9 (m, 4F), -123.7 (m, 4F). ^{13}C NMR (150 MHz, $CDCl_3$): δ 34.2 (s), 31.7 (s), 31.1 (t, *J* = 22.2 Hz), 29.1–29.6 (m), 28.5 (s), 24.8 (s), 22.7 (s), 20.3 (s), 14.2 (s). Broad peaks at δ 109.4–120.5 are characteristic of a long perfluorocarbon chain.[24] HR-CI-MS, *m/z*: 585.2423 $[M-H]^+$.

3.2.3. Substrate Preparation and Monolayer Formation

Gold slides were prepared by the thermal evaporation of 1000 Å of gold atop 100 Å of chromium on Si(100) wafers under vacuum (pressure ≤ 6 x 10^{-5} torr) at a rate of 0.5 Å/s. Prior to SAM formation, gold wafers were cut into 3 cm × 1 cm slides, rinsed with absolute ethanol, and dried with ultra-pure nitrogen gas. After collecting the ellipsometric constants, two gold slides

were immersed per 1 mM thiol solutions (5% THF in EtOH) for 48 h; all solvents were degassed with argon prior to SAM formation. The glass vials were cleaned with piranha solution and rinsed thoroughly with deionized water, followed by absolute ethanol. [*Caution: Piranha solution is highly corrosive, should never be stored, and should be handled with extreme care.*]. SAMs were rinsed with THF followed by ethanol and dried with ultra-pure nitrogen gas before characterization.

3.2.4. Characterization of Monolayers

A Rudolph Research Auto EL III ellipsometer equipped with a He-Ne laser (632.8 nm) was used to obtain the thickness values. The incident angle was set at 70°, and a refractive index of 1.45, typical for an organic film, was used.[31] An average of 6 measurements (3 per slide) was used to obtain the reported thickness.

XPS spectra of the SAMs were obtained on a PHI 5700 X-ray photoelectron spectrometer with monochromatic Al Kα X-ray source (1486.7 eV) incident at 90° relative to the axis of the hemispherical energy analyzer with a take-off angle of 45° from the surface and a pass energy of 23.5 eV. The Au $4f_{7/2}$ peak was referenced at a binding energy of 84.0 eV in all of the spectra.

Polarization-modulation infrared reflection-absorption spectroscopy (PM-IRRAS) was performed using a Nicolet Nexus 670 Fourier transform spectrometer equipped with a mercury-cadmium-telluride (MCT) detector and a Hinds Instrument PEM-90 photoelastic modulator. The incident angle of the p-polarized light reflected from the sample was set to 80° with respect to the surface normal. The spectra were collected using 512 scans at a spectral resolution of 2 cm^{-1}.

A Ramé-Hart model 100 contact angle goniometer was used to collect the contact angles of the various liquids on the SAM surfaces. A Matrix Technologies micro-Electrapette 25 was

used to dispense the liquids at a speed of 1 μL/s. The reported data is an average of 12 measurements, 3 drops per slide from both edges of the drop.

3.3. Results and Discussion

3.3.1. Measurements of Monolayer Thickness by Ellipsometry

Development of the **HnF6H11SH** series in EtOH yielded SAMs that were thinner than the expected values in addition to displaying poor binding and disorder in the alkyl chains. Equilibration of the FSAMs at 40 °C, as in a previous report on similarly structured alkanethiols, led to even more disorder and reduced thicknesses.[28] Consequently, we chose to develop the SAMs in a series of EtOH / THF mixtures in efforts to obtain densely packed and conformationally ordered monolayer films. The thickness measurements obtained for the adsorption of **H2F6H11SH** (chosen as a representative adsorbate) onto gold from various mixtures of solvents are shown in Table 3.1. It is apparent from the data that high concentrations of THF are detrimental to the thickness of the SAMs, and further equilibration at 40 °C failed to yield any significant difference in the thickness values. Additional trials revealed that the FSAMs developed in a mixture of 5% THF and 95% EtOH gave the best results; characterization of these FSAMs by XPS and surface infrared spectroscopy are discussed in the following sections.

Table 3.1. Ellipsometric Thicknesses of SAMs Derived from **H2F6H11SH** Via Equilibration in Systematically Varied Mixtures of EtOH and THF

Volume % THF	rt Thickness (Å)	40 °C Thickness (Å)
0 %	18 ± 1	17 ± 1
5 %	16 ± 1	17 ± 0
10 %	17 ± 2	17 ± 0
25 %	18 ± 1	17 ± 1
50 %	17 ± 1	16 ± 1
75 %	17 ± 1	16 ± 1
100 %	14 ± 1	13 ± 1

Given the preceding studies, we generated monolayers from **HnF6H11SH** in a mixture of 5% THF and 95% EtOH with equilibration for 48 h at rt. The average thickness values obtained for these FSAMs and the HmSH SAMs (developed in EtOH) are displayed in Table 3.2. Further, the thickness values for the hydrocarbon SAMs gave results that are in accordance to what has been observed in the literature.[33] On the other hand, the SAMs derived from **HnF6H11SH** exhibit average thickness values that are thinner than their hydrocarbon analogs. In our previous investigation of the first member of this series, **H1F6HnSH**,[28] we attributed the reduction in thickness to the larger vdW diameter of the fluorinated segment (~ 5.6 Å) compared to the smaller hydrocarbon spacer (~4.2 Å).[4,28] Moreover, the data in Table 3.2 show that the **HnF6H11SH** FSAMs with the adsorbates with the shortest terminal alkyl chains (n = 1–4) all exhibit roughly the same ellipsometic thickness (~18 Å); in contrast, the adsorbates with the longest terminal alkyl chains (n = 5-7) show an initial increase in thickness, which then remains roughly constant (~ 22 Å). Accordingly, based on the thickness measurements, it appears that the orientation and packing of the molecules in the SAMs depend, at least in part, on the length of the terminal alkyl chain.

Table 3.2. Ellipsometric Thicknesses of SAMs Derived from **HmSH** and **HnF6H11SH**

Adsorbate	Thickness (Å)	Adsorbate	Thickness (Å)
H18SH	23 ± 1	**H1F6H11SH**	17 ± 1
H19SH	25 ± 1	**H2F6H11SH**	18 ± 1
H20SH	26 ± 1	**H3F6H11SH**	19 ± 2
H21SH	27 ± 0	**H4F6H11SH**	18 ± 1
H22SH	28 ± 1	**H5F6H11SH**	21 ± 2
H23SH	31 ± 1	**H6F6H11SH**	22 ± 2
H24SH	32 ± 2	**H7F6H11SH**	22 ± 1

3.3.2. Analysis of the Monolayer Films by XPS

The XPS spectra of the C 1s and S 2p photoelectrons for the hydrocarbon SAMs are presented in Figure 3.3, and their binding energies are listed in Table 3.3. Additionally, the C 1s, F 1s, and S 2p regions for the FSAMs are presented in Figure 3.2, and their corresponding binding energies are listed in Table 3.4. All of the SAMs in this study have a characteristic doublet in the S 2p region in a 1:2 ratio, which can be assigned to the S $2p_{3/2}$ and S $2p_{1/2}$ electrons. For a bound thiolate, the S $2p_{3/2}$ peak is characterized by a binding energy of ~162 eV;[32,34] Furthermore, the absence of peaks at ~164 eV and ~168 eV indicates that there are no unbound or oxidized sulfur species, respectively, in the samples.[32,34] These data can therefore be taken to indicate that the sulfur atoms in all of these monolayers are fully bond to gold as surface thiolates.[32,34] We note also that the absence of any peaks consistent with the presence of fluorine is consistent with the chemical makeup of the all-hydrocarbon adsorabtes used.

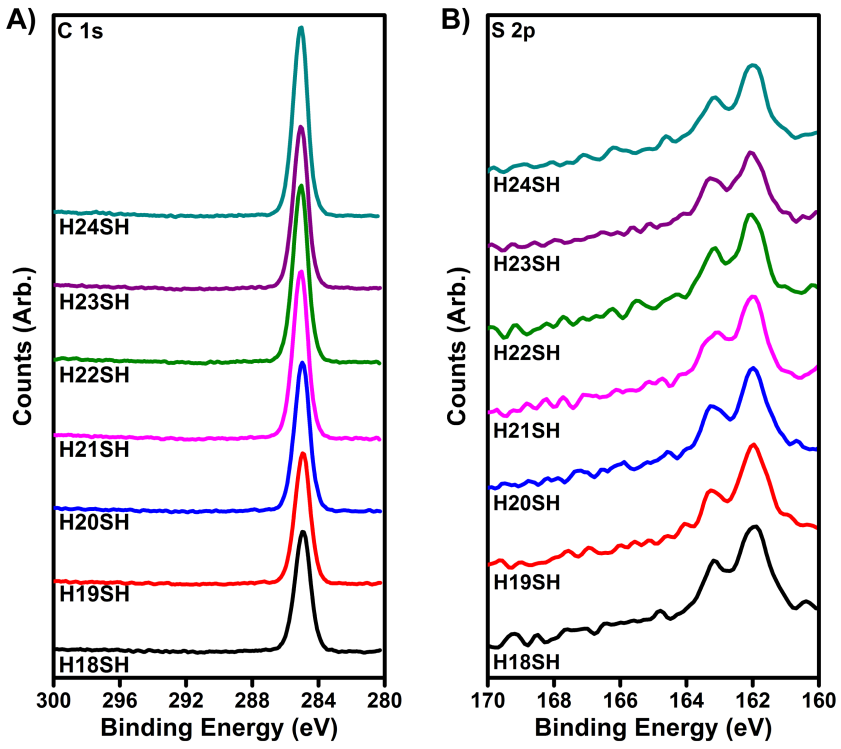

Figure 3.3. XPS spectra of the (A) C 1s and (B) S 2p regions collected from the HmSH SAMs.

Table 3.3. XPS Peak Positions for the SAMs Derived from HmSH

Adsorbate	Peak Position (eV)			
	C 1s (CH_2/ CH_3)	C 1s (CF_2)	F 1s	S 2p
H18SH	285.0	--	--	161.9
H19SH	285.0	--	--	162.0
H20SH	285.0	--	--	162.0
H21SH	285.0	--	--	162.0
H22SH	285.0	--	--	162.0
H23SH	285.1	--	--	162.1
H24SH	285.0	--	--	162.0

The "--" indicate that no peak intensities were observed at these binding energies.

The C 1s region of the FSAMs derived from **HnF6H11SH** in Figure 3.4A shows two peaks at ~284 eV and ~291 eV that are associated with the CH_2 and CF_2 carbons, respectively.[28] The peak position of the C 1s photoelectrons arising from the CH_2 carbons can give insight into the relative packing density of the film; typically, an increase in the binding energy of the peak indicates an increase in the packing density of the alkyl spacer in the SAMs.[35-37] Examination of the peak position of the C 1s (CH_3/CH_2) for the **HnF6H11SH** FSAMs reveals a shift to higher binding energies as the top alkyl chain is extended. For the SAMs with the longer alkyl chains (i.e., **H5F6H11SH** and longer), the FSAMs appear to pack similarly to the hydrocarbon SAMs, with a binding energy ~285.0 eV. Additionally, examination of the peak position of the F 1s electrons shows that as the length of the terminal alkyl chain is increased, the binding energy decreases; notably, an analogous shift is observed in the binding energy of the C 1s electrons of the CF_2 moieties. Previous reports have observed a similar shift for the binding energy of the fluorinated segments for FSAMs in which the underlying spacer is systematically increased.[26] Such an effect has been attributed to the greater distance between the gold substrate and the excited atoms.[26,37,38] Since, however, the distance between the gold substrate and the fluorinated segments in the **HnF6H11SH** SAMs is constant, a different phenomenon must be causing the shifts observed here.

It is apparent from the data that for the FSAMs derived from adsorbates having shorter terminal alkyl chains, the vdW interactions between the fluorinated segments dictate the structural features of the SAMs, whereas for the FSAMs derived from the adsorbates having longer terminal alkyl chains, the terminal alkyl chains are influencing the structure of the SAMs. Furthermore, since the vdW diameter of the alkyl chains is much smaller than that of the fluorinated segment

(4.2 Å v 5.6 Å),[4,14,15] it is plausible that the underlying fluorocarbon moieties in the FSAMs pack poorly. Given that the observed shifts in the F 1s and CF_2 C 1s peaks behave analogously to the observed shifts in the CH_2 C 1s peaks in hydrocarbon films that become disordered (i.e., loosely packed), we interpret the shifts observed here to indicate that disorder (i.e., loose packing) is induced in the fluorinated segment as the length of the terminal alkyl chains is increased.

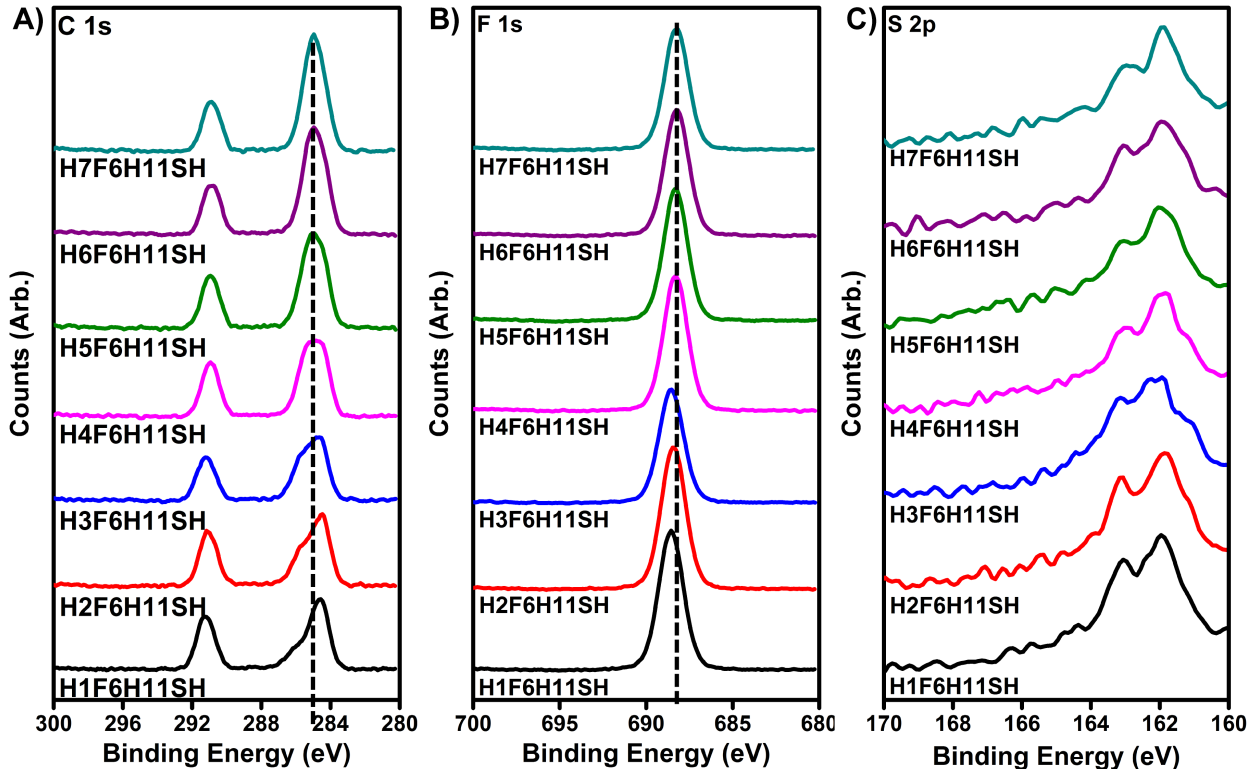

Figure 3.4. XPS spectra of the (A) C 1s and (B) F 1s and (C) S 2p regions collected from the HnF6H11SH SAMs.

In addition to the shifts in the binding energies of the electrons of the FSAMs, the shape of the peak associated with the C 1s (CH_2/CH_3) provides additional information. There appears to be an asymmetry associated with the **HnF6H11SH** FSAMs for n = 1-3, which is possibly arising from the impact of the perfluorocarbons on the binding energies of the adjacent CH_2 species. For

the films with the longer terminal alkyl chains, however, it is plausible that the signal intensities from those photoelectrons are being attenuated.

Table 3.4. XPS Peak Positions for the SAMs Derived from **HnF6H11SH**

Adsorbate	Peak Position (eV)			
	C 1s (CH_2 / CH_3)	C 1s (CF_2)	F 1s	S 2p
H1F6H11SH	284.6	291.3	688.6	162.0
H2F6H11SH	284.5	291.2	688.5	161.9
H3F6H11SH	284.8	291.2	688.5	161.8
H4F6H11SH	284.8	290.9	688.3	161.8
H5F6H11SH	284.9	290.9	688.3	161.9
H6F6H11SH	285.0	290.8	688.3	162.0
H7F6H11SH	285.0	290.9	688.2	161.9

3.3.3. PM-IRRAS Analysis of the Conformational Order of the Monolayers

We utilized PM-IRRAS to obtain insight into the packing/orientation of the terminal group in the FSAMs as well as the relative conformation of the alkyl chains. Figure 3.5 shows the PM-IRRAS spectra for the C–H stretching vibration region for the hydrocarbon SAMs and FSAMs examined in this study. Previous research has utilized the position of the methylene C–H antisymmetric stretching vibration as an indicator of the relative conformational order of the films; specifically, for a well-ordered highly crystalline film, the antisymmetric vibration ($\nu_{as}^{CH_2}$) appears at ~2918 cm^{-1}.[32] Conversely, a shift to a higher wavenumber is an indication of a disordered film. All of the SAMs examined in this study exhibit a $\nu_{as}^{CH_2}$ of 2918 ± 2 cm^{-1}, indicating well-ordered SAMs with the hydrocarbon chains in mostly trans-extended conformations.

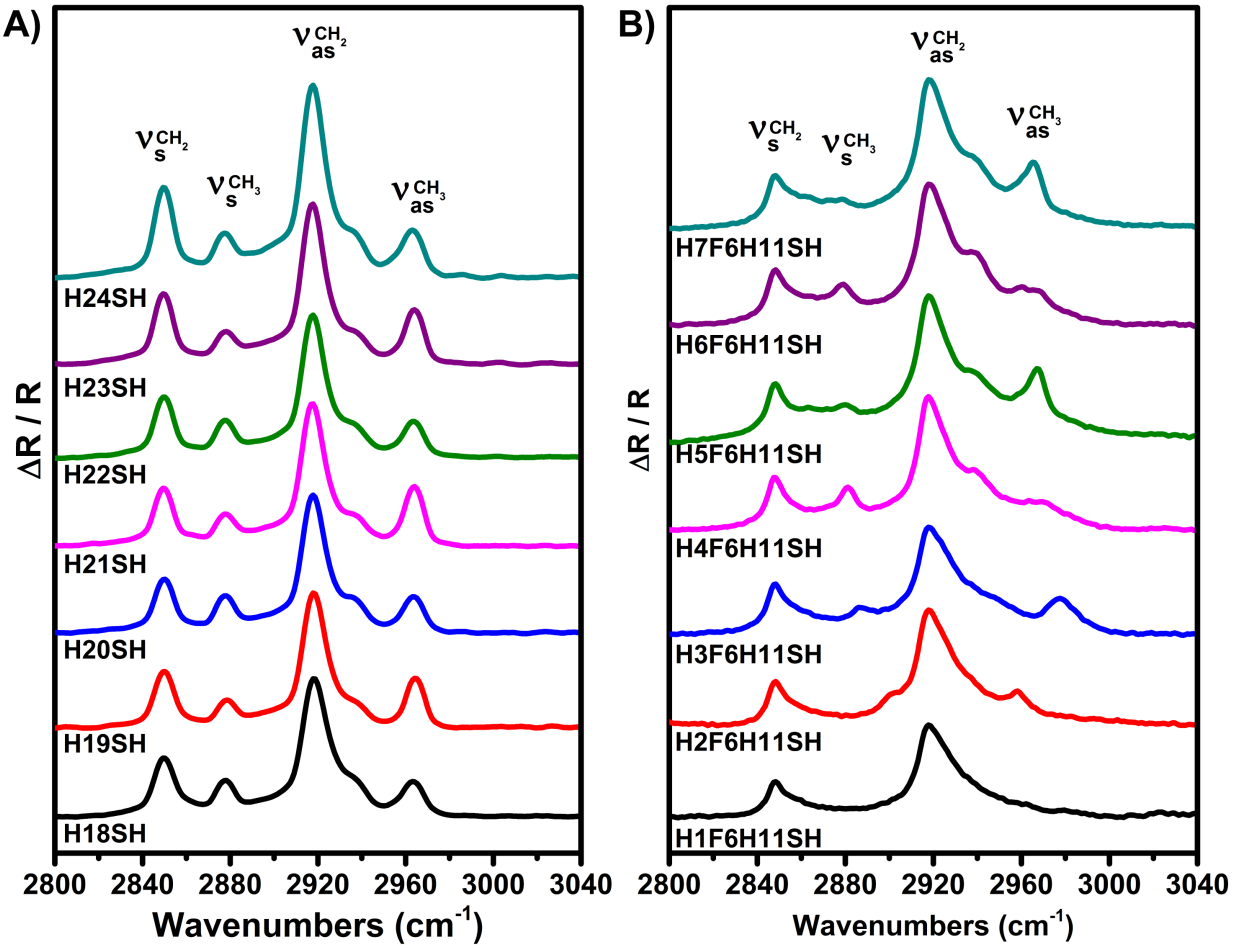

Figure 3.5. PM-IRRAS spectra for the C–H stretching region collected from (A) **HmSH** SAMs and (B) **HnF6H11SH** FSAMs.

The position of the antisymmetric C-H stretching vibrations associated with the methyl, $\nu_{as}^{CH_3}$ provides additional insight into the nature of these SAMs. For the SAM derived from **H1F6H11SH**, the peaks associated with $\nu_{as}^{CH_3}$ are not visible.[28] For the SAM derived from **H2F6H11SH**, the peak appears at 2958 cm^{-1}. Interestingly, the peak for the SAM derived from **H3F6H11SH** shifts to a higher wavenumber (2977 cm^{-1}), while the peak shifts to lower wavenumber as the terminal alkyl chain is extended until it reaches a value similar to that observed for SAMs derived from alkanethiols (2964 cm^{-1}). A similar trend is observed for the peaks of the

Table 3.5. Peak Positions of the C-H Stretching Vibrations for the Indicated SAMs

Adsorbate	$\nu_{as}^{CH_3}$ (cm^{-1})	$\nu_{as}^{CH_2}$ (cm^{-1})	$\nu_{as}^{CH_3}$ (cm^{-1})	$\nu_{as}^{CH_2}$ (cm^{-1})
H18SH	2963	2918	2878	2850
H19SH	2964	2918	2879	2850
H20SH	2964	2918	2878	2850
H21SH	2964	2917	2878	2850
H22SH	2964	2918	2878	2850
H23SH	2964	2918	2878	2850
H24SH	2963	2918	2877	2850
H1F6H11SH	-	2920	-	2852
H2F6H11SH	2958	2919	2902	2851
H3F6H11SH	2977	2920	2887	2852
H4F6H11SH	2967	2929	2881	2850
H5F6H11SH	2965	2919	2880	2850
H6F6H11SH	2962	2919	2879	2850
H7F6H11SH	2965	2920	2878	2851

symmetric CH_3 stretches ($\nu_s^{CH_3}$). The observed shifts for these vibrations correspond to the distance between the terminal methyl groups and the strongly electron withdrawing fluorocarbon species. Notably, this trend mirrors that found in the peak positions of the methyl carbon in the carbon NMR data of the corresponding adsorbates (see Figure 3.6). We are currently undertaking additional studies to determine the origin of the shifts highlighted here.

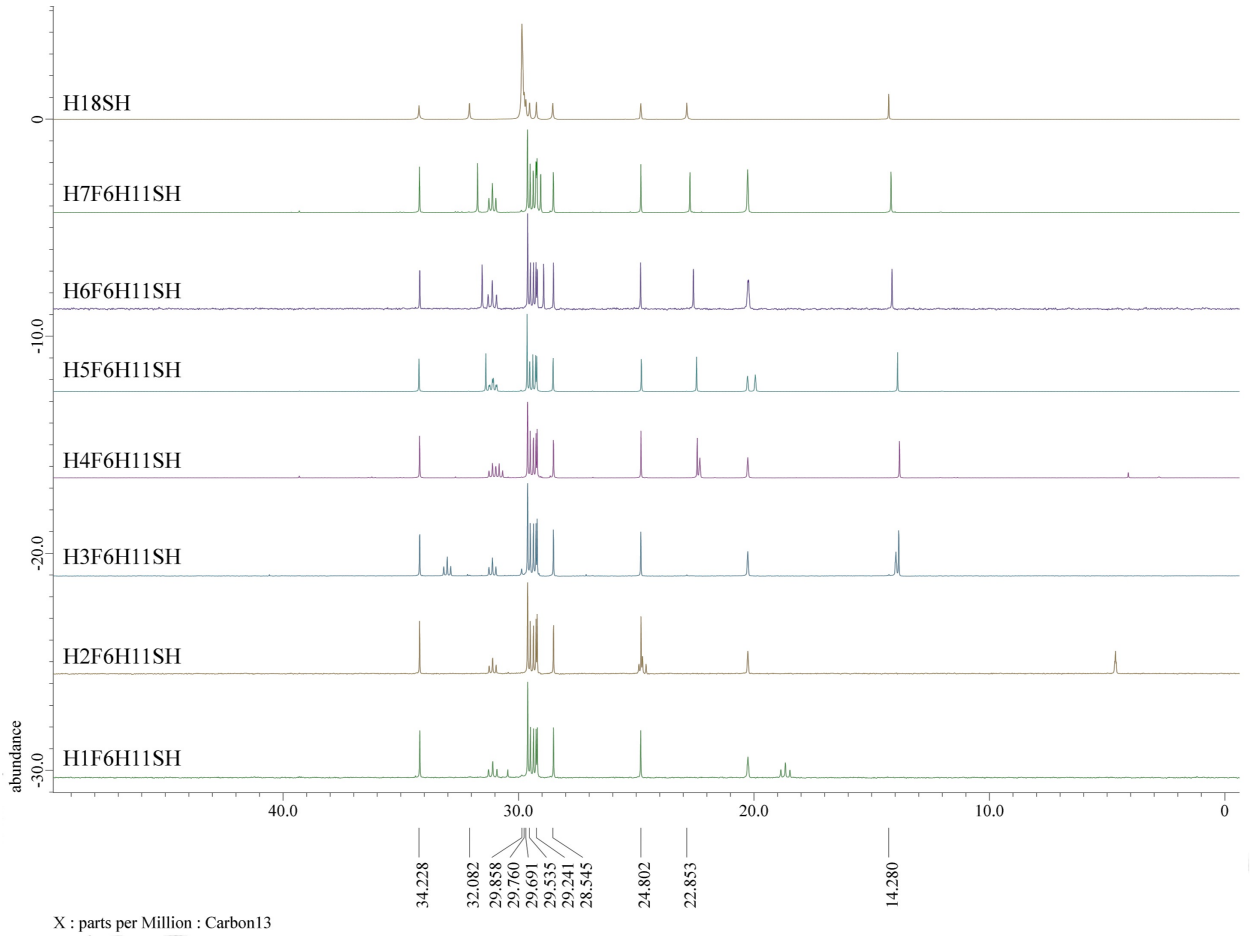

Figure 3.6. ^{13}C NMR spectra for the **H18SH** and **HnF6H11SH** adsorbates. For all adsorbates, the CH_3 carbon appears at the lowest chemical shift. $CDCl_3$ was referenced at 77.16 ppm for these spectra.

In addition to the conformational order of the SAMs and the shifts observed for the methyl vibrations, the relative intensity of the $\nu_{as}^{CH_3}$ and $\nu_s^{CH_3}$ peaks for the SAMs can crudely yield some insight into the orientation of the terminal methyl group. In the surface IR spectra of the hydrocarbon SAMs, there is a variation in the relative intensity of the vibrations associated with the methyl group that depends on the total number of carbons in the chain. For the chains having an even number of carbon atoms (**HmSH**, where m = 18, 20, 22, and 24), the ratio of the intensity of $\nu_s^{CH_3}$ to $\nu_{as}^{CH_3}$ is ~ 1:1, whereas for the chains having an odd number of carbon atoms, (**HmSH**, where m = 19, 21, and 23), the ratio is ~1:2. Odd-even effects have been observed in the surface

IR spectra of hydrocarbon SAMs derived from *n*-alkanethiols on gold and has been attributed to the direction of the transition dipole moment (TDM) of the vibration and the metal surface selection rules that govern the IR technique.[35,39]

The spectra of the FSAMs having terminal alkyl chains longer than one carbon atom (**HnF6H11SH**, where n = 2-7), also show a variation in the intensity of the C-H stretches of the methyl groups. In the FSAM series, the odd-even effect is opposite to that observed in the hydrocarbon SAMs and dependent on the number of carbons in the terminal alkyl chain rather than the total carbon count. In this case, the films with **odd-**numbered chains have a $\nu_s^{CH_3}$ to $\nu_{as}^{CH_3}$ ratio of ~**1:1**, and the films with **even**-numbered chains have a ratio of **1:2** (see Figure 3.5). Taking into account the reversal of the odd-even effect in the FSAMs and the surface selection rules, we can conclude that the terminal methyl groups are oriented differently in the SAMs derived from **HnF6H11SH** compared to those derived from *n*-alkanethiols (i.e., **HmSH**).

Based on the surface selection rules, transition dipole moments that are perpendicular to the surface can be detected by surface infrared spectroscopy, while those parallel to the surface cannot be detected due to the interference between the molecular dipoles and the image charges on the surface.[35,39] Given these established rules, we can conclude that the methyl group in FSAMs with **even**-numbered chain lengths (**HnF6H11SH** where n = 3, 5, and 7) must be tilted away from the surface normal. In this scenario, the transition dipole moment of the stretches are pointed somewhat parallel to the gold surface, causing both stretches ($\nu_s^{CH_3}$ and $\nu_{as}^{CH_3}$) to have similar intensity. On the other hand, in the FSAMs with **odd**-numbered chain lengths, the transition dipole moment for the symmetric stretch is aligned with the surface normal while for the antisymmetric stretch it is tilted from the surface normal, causing $\nu_s^{CH_3}$ to be more intense than $\nu_{as}^{CH_3}$.

3.3.4. Contact Angles of the Monolayers

An understanding of the interfacial energy and heterogeneity of a film can be determined by examining the wetting behavior of the film when exposed to a systematically chosen set of contacting probe liquids. We used several polar and nonpolar liquids to probe the effect of the HC–FC dipole as it was buried in the FSAMs. The polar liquids used included a series of protic and aprotic liquids of varying polarity: water (H_2O), glycerol (GL), formamide (FA), dimethylsulfoxide (DMSO), dimethylformamide (DMF), and acetonitrile (ACN). In addition, the nonpolar liquids decalin (DC) and hexadecane (HD) were used along with the perfluorinated liquid perfluorodecalin (FDC). Additionally, two liquids having a strong localized dipole were used, bromonaphthalene (BNP) and nitrobenzene (NB). For the sake of comparison, we also examined the wettability of the SAMs derived from the corresponding *n*-alkanethiols.

The advancing contact angles obtained for the polar liquids on the SAMs are shown in Figure 3.7 and Table 3.6. The wettability of the polar protic liquids (H_2O, GL, and FA), on the FSAMs show an increase in the contact angle as the terminal alkyl chain is increased until it reaches a value similar to the hydrocarbon SAMs for n = 5-7. A similar trend is observed with the wettability of the polar aprotic liquids (DMSO, DMF, and ACN), except for NB, where the contact angles on the FSAMs remain relatively constant with increasing terminal alkyl chain length, save for the odd-even effect observed across the series (vide infra). The systematic increase in the contact angles of the polar liquids could be indicative of a diminishing effect the dipole has on the wetting properties of the films. As the alkyl chain is extended, the dipole-dipole interactions (Keesom forces) between the HC-FC dipole and those of the contacting liquid diminish, which

then lead to dipole-induced dipole (Debye forces) interactions between the dipole of the liquid and the hydrocarbon surface.

Interestingly, the odd-even effect for the NB, vide supra, varies systematically with the length of the terminal alkyl chain. It is also interesting that the FSAMs where n is an odd (**H1F6H11SH**, **H3F6H11SH**, **H5F6H11SH**, and **H7F6H11SH**) are more wettable by NB than are the FSAMs where n is even (**H2F6H11SH**, **H4F6H11SH**, **H6F6H11SH**). Furthermore, it is important to note that the odd-even effect is opposite to that observed with the polar aprotic liquids on the hydrocarbon SAMs, reinforcing the analysis made in the IR section regarding the orientation of the terminal methyl group. The data suggest that the orientation of the terminal methyl group in the FSAMs is opposite to that on the hydrocarbon SAMs, suggesting that the fluorinated segment behaves as a surrogate surface. Although the orientation of the terminal methyl moiety plays a role in the wettability of the NB, the effect of the HC-FC dipole for the shorter alkyl chains also contributes to the wetting properties of the films. The difference in the contact angle for the **H1F6H11SH** (67 °) and the **H2F6H11SH** (71°) is much greater than the contact angles of the **H4F6H11SH** (71°) and the **H5F6H11SH** (70 °) suggesting a greater dipole-dipole interaction between the HC-FC dipole and the dipole of the contacting liquid for the shorter alkyl chains.

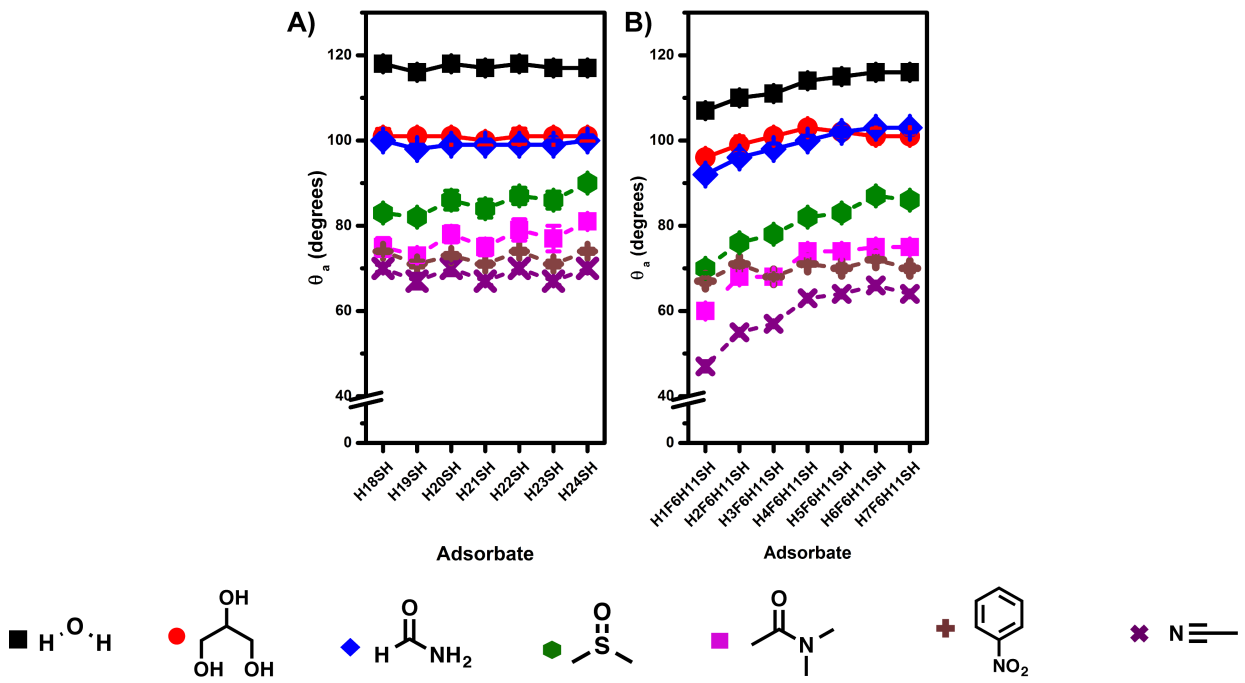

Figure 3.7. Advancing contact angle values of the polar liquids on (A) the **HmSH** SAMs and (B) the **HnF6HnSH** FSAMs.

Figure 3.8 and Table 3.7 show the advancing contact angles obtained for the nonpolar and weakly polar liquids on the SAMs. There is a clear odd-even effect in the wettability data of the hydrocarbon SAMs in which the odd SAMs are more wettable than the even SAMs, an observation that is in agreement with literature studies of alkanethiols on Au.[28,40,41] For the FSAMs, the contact angles of the nonpolar liquids DC and HD systematically decrease as the length of the terminal alkyl chain is increased until the values reach those of the hydrocarbon SAMs. For the FSAMs having n = 1-3, there appears to be unfavorable dispersive interactions between the contacting liquids and the underlying fluorinated segment (and possibly the dipole), leading to an increase in the contact angles compared to the hydrocarbon SAMs. For the FSAMs having n = 4-7, no unfavorable interactions between the contacting liquid and the fluorinated segment can be detected, further corroborating the diminished effect of the HC-FC dipole with the polar liquids

(vide supra). We expected the wettability of BNP, a liquid with a localized dipole, to give further insight into the effect of the HC-FC dipole. Unfortunately, for the FSAMs the contact angles of BNP are surprisingly the same across the series. The planar geometry of the liquid coupled with the exposed fluorinated segment at the interface (vide supra) could be a reason for this observation.

Additionally, an odd-even effect can be seen for the FSAMs with n = 4-7 in which the SAMs with an alkyl chain length having an odd number of carbon atoms are more wettable than those with length having an even number of carbon atoms. In the former SAMs, the terminal methyl group appears to be tilted away from the surface normal, exposing the underlying CH_2 groups and increasing molecular contact between the surface and the liquid,[28,40,41] depicted in **Figure 3.9.**

The wettability of FDC on the FSAMs allows us to understand the effect of the underlying fluorocarbon segment on the wettability of these SAMs. The contact angles of the FDC on the FSAMs where n = 1-3 imply that the CF_2 is exposed at the interface of these SAMs. The contact angle for the **H2F6H11SH** is dramatically higher than for the **H1F6H11SH** due to the unfavorable interaction between the fluorinated liquid and the hydrocarbon interface. However, there is a slight decrease in the contact angle of the **H3F6H11SH**. This could be due to the ethyl group being pointed more upward while the propyl group is more tilted away exposing the CF_2, and the dipole, at the interface. Another dramatic increase in the contact angle is seen in going from the propyl to butyl terminated FSAM; an odd-even effect greatly affected by the underlying CF_2. For the FSAMs with n = 4-7, the odd-even effect continues to be observed, but it is not dramatic as for the shorter alkyl groups.

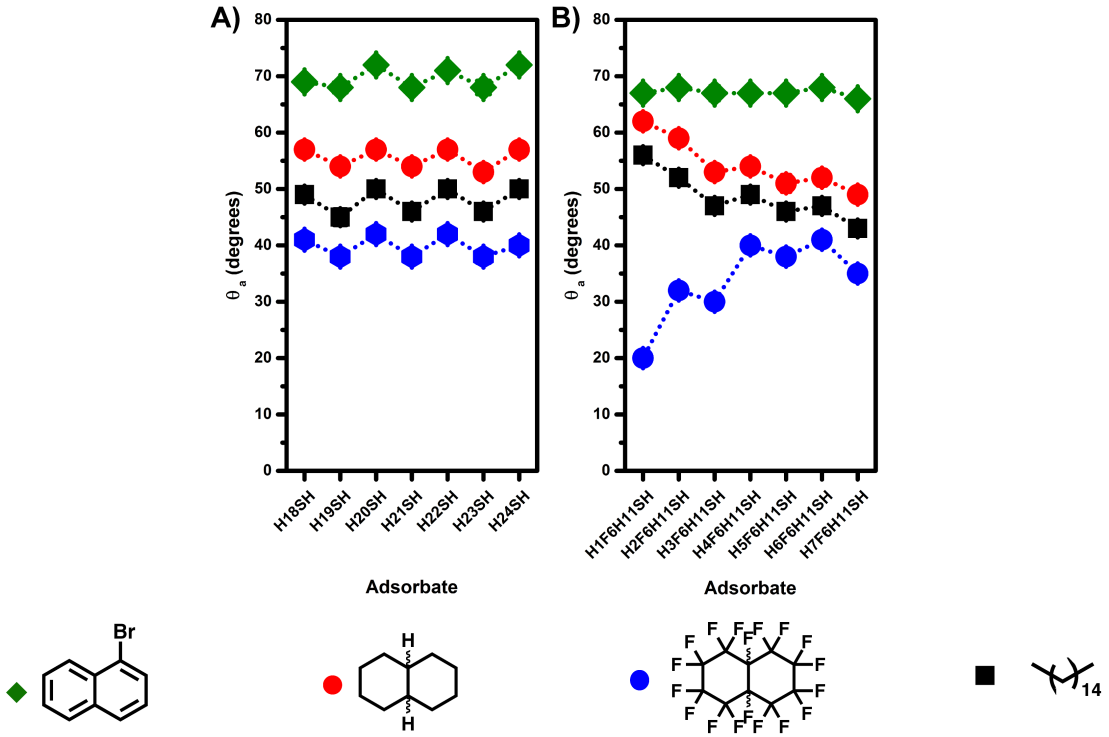

Figure 3.8. Advancing contact angle values of the nonpolar liquids on (A) **HmSH** SAMs and (B) **HnF6H11SH** FSAMs.

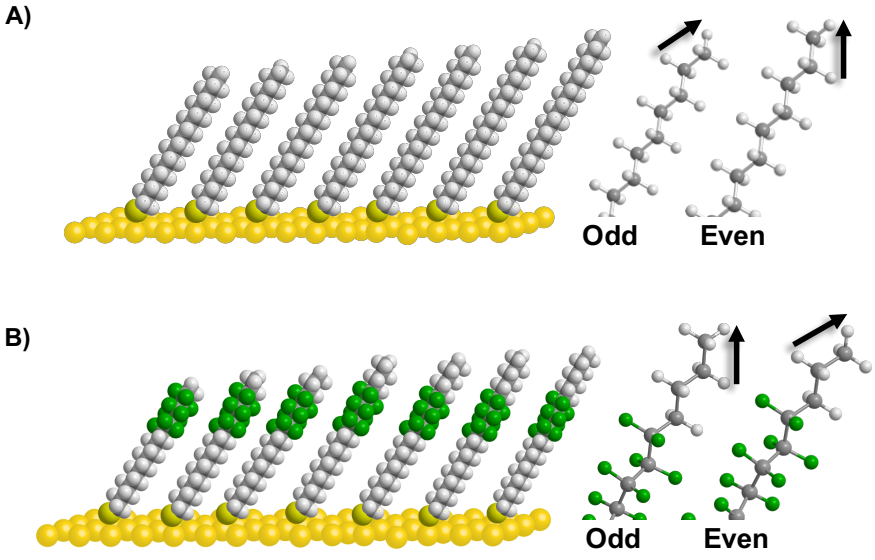

Figure 3.9. Illustration of the orientation of the methyl termini in SAMS derived from the adsorption of (A) HmSH and (B) HnF6H11SH SAMs on gold.

Table 3.6. Advancing contact angles (°) of the polar liquids on the SAMS Derived from **HmSH** and **HnF6H11SH**

Adsorbate	H_2O	GL	FA	DMSO	DMF	ACN	NB
H18SH	118	102	100	83	75	70	74
H19SH	116	101	98	82	73	67	71
H20SH	118	101	99	86	78	70	73
H21SH	117	100	99	84	75	67	71
H22SH	118	101	99	87	79	70	74
H23SH	117	101	99	86	77	67	71
H24SH	117	101	100	90	81	70	74
H1F6H11SH	107	96	92	70	60	47	67
H2F6H11SH	110	99	96	76	68	55	71
H3F6H11SH	111	101	98	78	68	57	68
H4F6H11SH	114	103	100	82	74	63	71
H5F6H11SH	115	102	102	83	74	64	70
H6F6H11SH	116	101	103	87	75	66	72
H7F6H11SH	116	101	103	86	75	64	70

Table 3.7. Advancing contact angles (°) of the nonpolar and weakly polar liquids on the SAMS Derived from **HmSH** and **HnF6H11SH**

Adsorbate	BNP	DC	HD	FDC
H18SH	69	57	49	41
H19SH	68	54	45	38
H20SH	72	57	50	42
H21SH	68	54	46	38
H22SH	71	57	50	42
H23SH	68	53	46	38
H24SH	72	57	50	40
H1F6H11SH	67	62	56	20
H2F6H11SH	68	59	52	32
H3F6H11SH	67	53	47	30
H4F6H11SH	67	54	49	40

H5F6H11SH	67	51	46	38
H6F6H11SH	68	52	47	41
H7F6H11SH	66	49	43	35

3.4. Conclusions

A series of novel alkyl-terminated alkanethiols were synthesized and used to generate FSAMs on Au. Initial studies revealed that a mixed THF / EtOH solvent system was the medium of choice for the formation of these monolayers. Analysis by ellipsometry found that there was no significant differences in the thicknesses of the FSAMS with n = 1-4 (~18 Å) and similarly for those with n = 5-7 (~21 Å). Moreover, analysis by XPS of the C 1s and F 1s regions indicated an increase in the packing density of the hydrocarbon segments with increasing terminal alkyl chain length with a concomitantly reduced packing density in the fluorocarbon segments. This observation can be attributed to the differences in the vdW diameter of the hydrocarbon and fluorocarbon segments. Analysis using surface IR found that all of the FSAMs were well-ordered. Furthermore, an odd-even effect was observed for the methyl C-H stretching bands of the FSAMs that corresponded to the number of carbons in the terminal alkyl chain rather than the total number of carbons, consistent with a model in which the methyl groups in the FSAMs where n = 3, 5, and 7 were oriented more parallel to the surface, whereas the methyl groups in the FSAMs where n = 2, 4, and 6 were oriented more perpendicular to the surface. The wettability data further corroborate the proposed orientations of the terminal methyl groups in these types of SAMs. Additionally, the wettability data showed that the underlying HC-FC dipoles and the structure of the FSAM have a strong effect on the wettability of the FSAMs. For the FSAMs where n = 1-3, the HC-FC dipole appears to have a stronger effect on the wettability, apparent in the wettability with the polar liquids, but for the FSAMs with longer chains the effect of the HC-FC dipole began

to dissipate as the length of the terminal alkyl group was increased. The wettability of the nonpolar liquids on FSAMs suggest that the structural features of the films also play a role in the wettability of the films.

3.5. References

1. Srinivasan, U.; Houston, M. R.; Howe, R. T.; Maboudian, R. Alkyltrichlorosilane-Based Self-Assembled Monolayer Films for Stiction Reduction in Silicon Micromachines. *J. Microelectrochem. Syst.* **1998**, *7*, 252–260.
2. Palacio, M.; Bhushan, B. Ultrathin Wear-Resistant Ionic Liquid Films for Novel Mems/Nems Applications. *Adv. Mater.* **2008**, *20*, 1194–1198.
3. Pujari, S. P.; Spruijt, E.; Cohen Stuart, M. A.; van Rijn, C. J. M.; Paulusse, J. M. J.; Zuilhof, H. Ultralow Adhesion and Friction of Fluoro-Hydro Alkyne-Derived Self-Assembled Monolayers on H-Terminated Si(111). *Langmuir* **2012**, *28*, 17690–17700.
4. Zenasni, O.; Jamison, A. C.; Lee, T. R. The Impact of Fluorination on the Structure and Properties of Self-Assembled Monolayer Films. *Soft Matter* **2013**, *9*, 6356–6370.
5. Fréchette, J.; Maboudian, R.; Carraro, C. Thermal Behavior of Perfluoroalkylsiloxane Monolayers on the Oxidized Si(100) Surface. *Langmuir* **2006**, *22*, 2726–2730.
6. Hoque, E.; DeRose, J. A.; Hoffmann, P.; Mathieu, H. J. Robust Perfluorosilanized Copper Surfaces. *Surf. Interface Anal.* **2006**, *38*, 62–68.
7. Ma, H.; Yip, H.-L.; Huang, F.; Jen, A. K. Y. Interface Engineering for Organic Electronics. *Adv. Funct. Mater.* **2010**, *20*, 1371–1388.
8. de Boer, B.; Hadipour, A.; Mandoc, M. M.; van Woudenbergh, T.; Blom, P. W. M. Tuning of Metal Work Functions with Self-Assembled Monolayers. *Adv. Mater.* **2005**, *17*, 621–625.
9. Feng, S.; Huang, Y.; Wang, Q.; Qing, F.-L. Nonbiofouling Surface Based on Amphiphilic Alkanethiol Self-Assembled Monolayers. *Surf. Interface Anal.* **2011**, *43*, 770–776.

10. Klein, E.; Kerth, P.; Lebeau, L. Enhanced Selective Immobilization of Biomolecules onto Solid Supports Coated with Semifluorinated Self-Assembled Monolayers. *Biomaterials* **2008**, *29*, 204–214.

11. Ulman, A. Formation and Structure of Self-Assembled Monolayers. *Chem. Rev.* **1996**, *96*, 1533–1554.

12. Love, J. C.; Estroff, L. A.; Kriebel, J. K.; Nuzzo, R. G.; Whitesides, G. M. Self-Assembled Monolayers of Thiolates on Metals as a Form of Nanotechnology. *Chem. Rev.* **2005**, *105*, 1103–1170.

13. Vericat, C.; Vela, M. E.; Benitez, G.; Carro, P.; Salvarezza, R. C. Self-Assembled Monolayers of Thiols and Dithiols on Gold: New Challenges for a Well-Known System. *Chem. Soc. Rev.* **2010**, *39*, 1805–1834.

14. Jamison, A. C.; Chinwangso, P.; Lee, T. R. Self–Assembled Monolayers: The Development of Functional Nanoscale Films. In *Functional Polymer Films*, Knoll, W.; Advincula, R. C., Eds.; Wiley–VCH: Weinheim, 2011; Vol. 1, pp 151– 217.

15. Barriet, D.; Lee, T. R. Fluorinated Self-Assembled Monolayers: Composition, Structure and Interfacial Properties. *Curr. Opin. Colloid Interface Sci.* **2003**, *8*, 236–242.

16. Patole, S. N.; Baddeley, C. J.; O'Hagan, D.; Richardson, N. V.; Zerbetto, F.; Zotti, L. A.; Teobaldi, G.; Hofer, W. A. Self-Assembly of Semifluorinated N-Alkanethiols on {111}-Oriented Au Investigated with Scanning Tunneling Microscopy Experiment and Theory. *J. Chem. Phys.* **2007**, *127*, 024702.

17. Alves, C. A.; Porter, M. D. Atomic Force Microscopic Characterization of a Fluorinated Alkanethiolate Monolayer at Gold and Correlations to Electrochemical and Infrared Reflection Spectroscopic Structural Descriptions. *Langmuir* **1993**, *9*, 3507–3512.

18. Liu, G. y.; Fenter, P.; Chidsey, C. E. D.; Ogletree, D. F.; Eisenberger, P.; Salmeron, M. An Unexpected Packing of Fluorinated N-Alkane Thiols on Au(111): A Combined Atomic Force Microscopy and X-Ray Diffraction Study. *J. Chem. Phys.* **1994**, *101*, 4301–4306.

19. Chidsey, C. E. D.; Loiacono, D. N. Chemical Functionality in Self-Assembled Monolayers: Structural and Electrochemical Properties. *Langmuir* **1990**, *6*, 682–691.

20. Colorado, R., Jr.; Graupe, M.; Shmakova, O. E.; Ramon, J. V.; Lee, T. R. Structural Properties of Self-Assembled Monolayers on Gold Generated from Terminally Fluorinated Alkanethiols. *ACS Symp. Ser.* **2001**, *781*, 276–292.

21. Weinstein, R. D.; Moriarty, J.; Cushnie, E.; Colorado, R.; Lee, T. R.; Patel, M.; Alesi, W. R.; Jennings, G. K. Structure, Wettability, and Electrochemical Barrier Properties of Self-Assembled Monolayers Prepared from Partially Fluorinated Hexadecanethiols. *J. Phys. Chem. B* **2003**, *107*, 11626–11632.

22. Yuan, Y.; Yam, C. M.; Shmakova, O. E.; Colorado, R.; Graupe, M.; Fukushima, H.; Moore, H. J.; Lee, T. R. Solution-Phase Desorption of Self-Assembled Monolayers on Gold Derived from Terminally Perfluorinated Alkanethiols. *J. Phys. Chem. C* **2011**, *115*, 19749–19760.

23. Alloway, D. M.; Hofmann, M.; Smith, D. L.; Gruhn, N. E.; Graham, A. L.; Colorado, R.; Wysocki, V. H.; Lee, T. R.; Lee, P. A.; Armstrong, N. R. Interface Dipoles Arising from Self-Assembled Monolayers on Gold: Uv−Photoemission Studies of Alkanethiols and Partially Fluorinated Alkanethiols. *J. Phys. Chem. B* **2003**, *107*, 11690–11699.

24. Frey, S.; Heister, K.; Zharnikov, M.; Grunze, M.; Tamada, K.; Colorado, R., Jr.; Graupe, M.; Shmakova, O. E.; Lee, T. R. Structure of Self-Assembled Monolayers of Semifluorinated Alkanethiols on Gold and Silver Substrates. *Isr. J. Chem.* **2000**, *40*, 81–97.

25. Fukushima, H.; Seki, S.; Nishikawa, T.; Takiguchi, H.; Tamada, K.; Abe, K.; Colorado, R.; Graupe, M.; Shmakova, O. E.; Lee, T. R. Microstructure, Wettability, and Thermal Stability of Semifluorinated Self-Assembled Monolayers (Sams) on Gold. *J. Phys. Chem. B* **2000**, *104*, 7417–7423.

26. Tamada, K.; Ishida, T.; Knoll, W.; Fukushima, H.; Colorado, R., Jr.; Graupe, M.; Shmakova, O. E.; Lee, T. R. Molecular Packing of Semifluorinated Alkanethiol Self-Assembled Monolayers on Gold: Influence of Alkyl Spacer Length. *Langmuir* **2001**, *17*, 1913–1921.

27. Bain, C. D.; Troughton, E. B.; Tao, Y. T.; Evall, J.; Whitesides, G. M.; Nuzzo, R. G. Formation of Monolayer Films by the Spontaneous Assembly of Organic Thiols from Solution onto Gold. *J. Am. Chem. Soc.* **1989**, *111*, 321–335.

28. Zenasni, O.; Marquez, M. D.; Jamison, A. C.; Lee, H. J.; Czader, A.; Lee, T. R. Inverted Surface Dipoles in Fluorinated Self-Assembled Monolayers. *Chem. Mater.* **2015**, *27*, 7433–7446.

29. Lee, H. J.; Jamison, A. C.; Lee, T. R. Surface Dipoles: A Growing Body of Evidence Supports Their Impact and Importance. *Acc. Chem. Res.* **2015**, *48*, 3007–3015.

30. Leatherman, G.; Durantini, E. N.; Gust, D.; Moore, T. A.; Moore, A. L.; Stone, S.; Zhou, Z.; Rez, P.; Liu, Y. Z.; Lindsay, S. M. Carotene as a Molecular Wire: Conducting Atomic Force Microscopy. *J. Phys. Chem. B* **1999**, *103*, 4006–4010.

31. Nozaki, K.; Munekane, M.; Yamamoto, T.; Ogawa, Y. X-Ray and Thermal Studies on the Crystalline Phases of Normal Alkanethiols N-Cnh2n+1sh (N = 18, 19, 22, 23, 24). *J. Mater. Sci.* **2006**, *41*, 3935–3946.

32. Castner, D. G.; Hinds, K.; Grainger, D. W. X-Ray Photoelectron Spectroscopy Sulfur 2p Study of Organic Thiol and Disulfide Binding Interactions with Gold Surfaces. *Langmuir* **1996**, *12*, 5083–5086.

33. Biebuyck, H. A.; Bain, C. D.; Whitesides, G. M. Comparison of Organic Monolayers on Polycrystalline Gold Spontaneously Assembled from Solutions Containing Dialkyl Disulfides or Alkanethiols. *Langmuir* **1994**, *10*, 1825–1831.

34. Ishida, T.; Hara, M.; Kojima, I.; Tsuneda, S.; Nishida, N.; Sasabe, H.; Knoll, W. High Resolution X-Ray Photoelectron Spectroscopy Measurements of Octadecanethiol Self-Assembled Monolayers on Au(111). *Langmuir* **1998**, *14*, 2092–2096.

35. *Surface Analysis: The Principal Techniques*; 2nd ed.; John Wiley & Sons: Chichester, 2009.

36. Lummerstorfer, T.; Hoffmann, H. Ir Reflection Spectra of Monolayer Films Sandwiched between Two High Refractive Index Materials. *Langmuir* **2004**, *20*, 6542–6545.

37. Porter, M. D.; Bright, T. B.; Allara, D. L.; Chidsey, C. E. D. Spontaneously Organized Molecular Assemblies. 4. Structural Characterization of *N*-Alkyl Thiol Monolayers on Gold by Optical Ellipsometry, Infrared Spectroscopy, and Electrochemistry. *J. Am. Chem. Soc.* **1987**, *109*, 3559–3568.

38. Barriet, D.; Chinwangso, P.; Lee, T. R. Can Cyclopropyl-Terminated Self-Assembled Monolayers on Gold Be Used to Mimic the Surface of Polyethylene? *ACS Appl. Mater. Interfaces* **2010**, *2*, 1254–1265.

39. Wenzl, I.; Yam, C. M.; Barriet, D.; Lee, T. R. Structure and Wettability of Methoxy-Terminated Self-Assembled Monolayers on Gold. *Langmuir* **2003**, *19*, 10217–10224.

40. Laibinis, P. E.; Whitesides, G. M.; Allara, D. L.; Tao, Y. T.; Parikh, A. N.; Nuzzo, R. G. Comparison of the Structure and Wetting Properties of Self-Assembled Monolayers of *n*-Alakenthiols on the Coinage Metal Surfaces, Cu, Ag, Au. *J. Am. Chem. Soc.* **1991**, *113*, 7152–7167.

41. Nuzzo, R. G.; Dubois, L. H.; Allara, D. L. Fundamental Studies of Microscopic Wetting on Organic Surface. 1. Formation and Structural Characterization of a Self-Consistent Series of Polyfunctional Organic Monolayers. *J. Am. Chem. Soc.* **1990**, *112*, 558–569.

Chapter 4: Reversing the Odd-Even Effects in Self-Assembled Monolayers Using UPD Silver

4.1. Introduction

The ability to generate an array of oriented dipoles is of paramount interest to material engineers and surface scientists.[1-6] Such surfaces are used in aligning energy levels in organic field transistors,[7-9] generating reactive surfaces for biolabeling applications,[10-12] and patterning for photoresponsive surfaces.[13-14] These applications rely heavily on self-assembled monolayers (SAMs) technique to generate well designed nanocoatings. SAMs have vast usage in a variety of applications ranging from surfaces pertinent to biological applications,[15-19] lubricants for microelectromechanical systems (MEMs),[20-21] corrosion inhibitors,[22] nanoparticle protectants / stabilizers,[23-27] and catalyst modifiers in the form of alkanethiols in hydrogenation reactions.[28-29] Among SAMs is the thiol on gold system, which includes the spontaneous adsorption of organothiols onto gold surfaces. This system continues to be widely studied due to ease of preparation of the films, inertness of the Au substrate, strong Au–S bond of ~50 kcal/mole, well defined structural features, and the ability to manipulate the interfacial properties of the films via synthetic tailoring of the organic adsorbates.[30] The plethora of SAM-related literature points toward the fact that most properties of the generated SAMs are dictated by the structural properties of the organic molecules adsorbed on the surface.

The incorporation of highly electronegative fluorine atoms into an adsorbate is an example of altering the structural and interfacial properties of the resulting films by modifying the organic constituent. Further, targeting different degrees of fluorination in the terminus of the adsorbate allows for tuning the interfacial properties (i.e., wettability, friction, and adhesion).[31] For instance,

the increase in the number of terminal fluorocarbons in an alkanethiol brought about nanoscale thin films with interfacial properties resembling those of polytetrafluoroethylene (PTFE). Such highly fluorinated surfaces exhibit extremely low surface energies, with highly hydrophobic and oleophobic character.[32-33] Previous research involving partially fluorinated SAMs (FSAMs) with minimal fluorination, CF_3-terminated, determined that the presence of an oriented dipole, FC-HC, yields films that are less hydrophobic than their hydrocarbon analogs.[6] The effect of the dipole on the interfacial properties of the FSAMs dissipates by further extending the amount of fluorination in the chain.[32] Further research lead to the development of FSAMs with an inverted dipole which further explored the effect of such a dipole, HC-FC, on the properties of the films.[5] Chapter 3 further explores the effect of the HC-FC dipole as it is buried in the film.

SAMs of adsorbates with various headgroups (i.e., alkanethiols, carboxylic acids, and phosphonic acids) have also been generated on silver surfaces.[34-38] However, the rapid oxidation of silver substrates in air make it difficult to work with such a SAM system.[30] Yet, the underpotential deposition (UPD) of metals is a means for mitigating his problem and can be used to generate a unique metal surface. The UPD method, which is achieved electrochemically, can deposit a single monolayer of a metal element atop a metal surface comprised if a different element. The process is dictated by a stronger adatom-substrate interaction than an adatom-adatom interaction, which occurs during bulk material deposition.[39] The combination of UPD and SAMs has been explored for a variety of reason such as: the enhancement of thermal stability of SAMs on Au,[40-42] the use of non-sulfur adsorbates on Au,[43-44] and the post modification of SAM surfaces.[45] The structural and interfacial properties of the SAMs on UPD Ag or Cu differ sometimes dramatically from those of SAMs on bare Au substrate. SAMs of alkanethiols on Au

(111) have a ($\sqrt{3}$ x $\sqrt{3}$)*R*30° adlayer structure;[31] however, for SAMs on Ag, the alkanethiols adopt a ($\sqrt{7}$ x $\sqrt{7}$)*R*19° adlayer.[35,46-48]

Herein, we aim to modify evaporated Au substrates by the electrochemical deposition of Ag metal in efforts to evaluate the structural and interfacial properties of FSAMs derived from a series of CF_3-terminated alkanethiols, Figure 4.1, along with their hydrocarbon analogs.

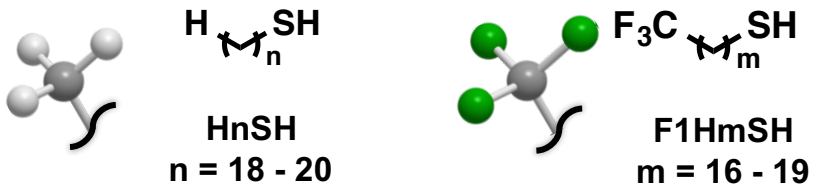

Figure 4.1. Molecules used in this study along with an illustration of their terminal groups.

All SAMs, illustrated in Figure 4.2, were characterized by ellipsometry to determine the thickness of the films and X-ray photoelectron spectroscopy (XPS) to determine the chemical composition of the films. Polarization-modulation infrared reflection-absorption spectroscopy (PM-IRRAS) was used to determine the conformational order of the films, and contact angle goniometry was used to probe the wetting properties.

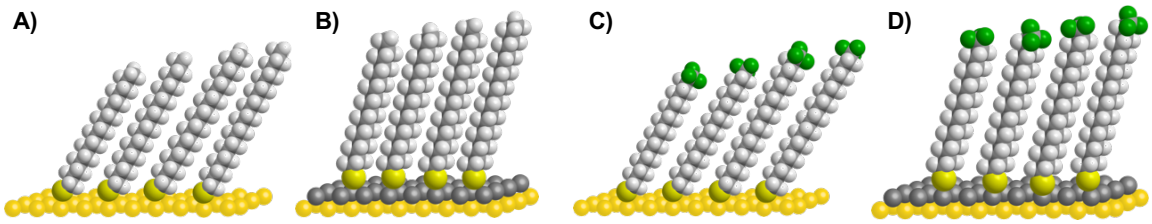

Figure 4.2. Illustration showing the SAMs on Au (A and C) and UPD Ag (B and D). Hydrogen atoms are denoted as white spheres while fluorine atoms in green.

4.2. Experimental Section

4.2.1. Materials and Methods

Gold Shot (99.999%) bought from Kamis Inc. Chromium rods (99.9%) were purchased from R. D. Mathis Company. Silicon(100) wafers (polished, single crystal) were bought from University Wafer and used as received. Tetrahydrofuran (Sigma-Aldrich) and ethanol (Aaper Alcohol and Chemical Co) used on the SAMs was used as received. The adsorbate 1-octadecanethiol (**H18SH**) was purchased from Sigma-Aldrich. 1-heptadecanethiol (**H17SH**), 1-nonadecanethiol (**H19SH**), 1-eicosanethiol (**H20SH**), 17,17,17-trifluoroheptadecane-1-thiol (**F1H16SH**), 18,18,18-trifluorooctadecane-1-thiol (**F1H17SH**), 19,19,19-Trifluorononadecane-1-thiol (**F1H18SH**), and 20,20,20-trifluoroicosane-1-thiol (**F1H19SH**) were synthesized according to procedures found in the literature.[5,49]

4.2.2. Substrate Preparation

Gold slides were prepared by the thermal evaporation of 1000 Å of gold atop 100 Å of chromium on Si (100) wafers under vacuum (pressure $\leq 6 \times 10^{-5}$ torr) at a rate of 0.5 Å/s. The wafers were then cut into slides and stored in milliQ water until use for electrochemical measurements.

4.2.3. Underpotential Deposition of Silver (UPD Ag)

For cyclic voltammetry (CV), a Princeton Applied Research potentiostat/galvanostat model 263A was used to modulate the potential applied to and to measure the current of the electrochemical systems. A homemade glass cell was used to hold the three-electrodes used for electrochemical measurements using the gold slide as the working electrode, a platinum wire as the counter electrode, and mercury/mercurous sulfate as the reference electrode. The electrolyte for all CVs used was 0.1M sulfuric acid (Ultrex II Ultrapure Reagent from J. T. Baker) with 0.6 mM Ag_2SO_4 (99.999% trace metals basis from Aldrich) added for the silver voltammetry. Gold slides were cycled ten times in sulfuric acid, rinsed with plenty of milliQ water and stored in milliQ

water until measurement of their optical properties with ellipsometry. For the deposition of silver, the cycled gold slides were cycled in silver solution ten times, then held at a potential of 0.15 V vs MSE for the underpotential deposition of silver, pulled out of the cell while held at potential, and rinsed with copious amounts of milliQ water, and stored in milliQ water until analysis with ellipsometry.

4.2.4. Monolayer Formation and Characterization

Immediately after ellipsometry measurements, the slides were immersed in a 1 mM ethanol solution of the corresponding thiol in a 40mL vial, previously cleaned with piranha. The self-assembled monolayers were allowed to equilibrate for 48 h in the dark at ambient temperature. Prior to characterization of the SAMs, the slides were rinsed with THF followed by ethanol and dried with ultra-pure nitrogen.

A Rudolph Auto El III ellipsometer equipped with a He-Ne laser (632.8 nm) set at an incidence angle of 70° and a refractive index of 1.45, a value typical for organic thin films,[50] was used to obtain thickness measurements for the monolayer films. An average of three measurements per slide was used as the reported thickness.

X-Ray photoelectron spectroscopy (XPS) was performed on a PHI 5700 x-ray photoelectron spectrometer with a monochromatic Al Kα X-ray source (1486.7 eV) incident at 90° relative to the axis of the hemispherical analyzer with a takeoff angle of 45° from the surface and a pass energy of 23.5 eV. The Au $4f_{7/2}$ peak was referenced to 84.0 eV in all the spectra.

Polarization-modulation infrared reflectance-absorption spectroscopy (PM-IRRAS) was performed using a Nicolet Nexus 670 Fourier transform equipped with a mercury-cadmium-telluride (MCT) detector and a Hinds Instrument PEM-90 photoelastic modulator. The surfaces

were mounted at an incident angle of 80° for the p-polarized light with respect to the surface normal. The spectra were collected using 512 scans at a resolution of 2 cm^{-1}.

Contact angle data were obtained using a ramé-hart model 100 contact angle goniometer set up with a Matrix Technologies micro-Electrapette 25 to dispense liquids. The advancing contact angles (θ_a) and receding contact angles (θ_r) were obtained at a speed of 1μL/s. The reported data are an average of six measurements with readings being made from each side of three droplets on different locations along the slides.

The contacting liquids used in the study include a variety of nonpolar, polar protic, and polar aprotic liquids: bromonaphthalene (BNP – Sigma Aldrich); decalin (DC – Acros Organics); hexadecane (HD – Aldrich); perfluorodecalin (FDC – Synquest Labs); acetonitrile (MeCN – Sigma Aldrich); nitro-benzene (NB - Acros); dimethylformamide (DMF – Sigma Aldrich); dimethyl sulfoxide (DMSO – Sigma Aldrich); formamide (FA – Sigma Aldrich); glycerol (GY – Sigma Aldrich); and water (H_2O – Millipore water with resistivity of 18.2 Ω).

4.3. Results and Discussion

4.3.1. Ellipsometric Thickness Assessment

In this study, the series of CF_3-terminated SAMs were compared to their hydrocarbon analogs formed on the same batch of vapor-deposited gold that was treated electrochemically prior to formation of the SAMs. Accounts in the literature have fully characterized these hydrocarbon SAMs, which serve as a point of reference in the analysis of the SAMs on UPD Ag and the FSAMs on both substrates.[5,41] Figure 4.2. and Table 4.1 below depict the average thickness measurements for the SAMs used in the study. The thickness values of the **H17SH**, **H18SH**, **H19SH**, and **H20SH**

SAMs on gold exhibit thicknesses of 21, 22, 23, and 25 Å, respectively, and are in accordance with literature values.[5] Additionally, the observed increase in the thickness values with increasing chain length, ~ 1Å, is consistent with the increase in the methylene units of the hydrocarbon backbone.[49,51]. Notably, the hydrocarbon SAMs on UPD Ag are much thicker than the corresponding SAMs on Au by ~3 Å, which is in accordance to the difference in thickness for a hydrocarbon on Au and Ag in the literature.[41]

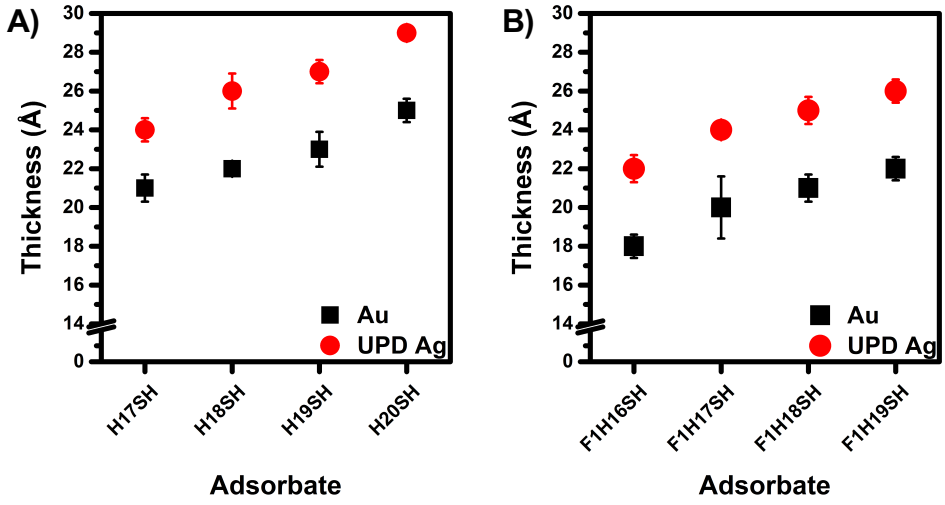

Figure 4.3. Average thickness measurements obtained for the (A) HnSH SAMs and the (B) F1HmSH SAMs.

The conformation of alkanethiols of SAMs on bulk Ag have been described in the literature as having an orientation different from that of alkanethiols on Au.[30] For our study, we anticipate that the molecules on UPD Ag might behave similarly to adsorbates on bulk Ag. Alkanethiols on an Au surface adopt a twist angle of ~55° and an overall tilt of ~33°, with respect to the surface normal.[5,52] While on Ag surfaces, the same molecule will have a twist of ~45° and a tilt of ~10°.[52] The underlying difference for the way the adsorbates are oriented on the Au and Ag substrates originates from the different binding geometries the sulfur atom has on the respective metals; the Au-S-C bond angle is ~104°, while the Ag-S-C bond angle is ~180°.[53] The difference in the

binding geometries dictates the orientation of the carbon backbone on the metals. Consequently, a more densely packed monolayer is formed on the UPD Ag surface as compared to the Au surfaces, a scenario that might lead to a thicker film. Comparing between the alkanethiols and the CF_3-terminated alkanethiols, the thickness measurements on both gold and UPD Ag surfaces of films of the latter adsorbates are slightly lower than those for the alkanethiol analogs. Previous research on CF_3-terminated alkanethiol SAMs determined the thicknesses for these types of SAMs are ~1 Å shorter than the hydrocarbon analogs, which corroborates our results.

Table 4.1. Ellipsometric Thickness Values of the Investigated SAMs.

Adsorbate	Au Thickness (Å)	UPD Ag Thickness (Å)	Adsorbate	Au Thickness (Å)	UPD Ag Thickness (Å)
H17SH	21	24	**F1H16SH**	18	22
H18SH	22	26	**F1H17SH**	20	24
H19SH	23	27	**F1H18SH**	21	25
H20SH	25	29	**F1H19SH**	22	26

4.3.2. Conformational Order Using PM-IRRAS

Surface IR analysis gives insight into the relative crystallinity and conformational order of an organic monolayer thin film. The conformational order of the SAMs is determined by the position of the C-H antisymmetric stretch of the methylene units ($\nu_{as}^{CH}{}_2$) at 2918 cm-^{1}.[50,54-55] Appearance of this band at 2918 cm^{-1} indicates that the hydrocarbon chains have a trans-extended conformation. A disordered, or liquid like film, is obtained when the band shifts to a higher wavenumber. For the hydrocarbon SAMs on Au, all of the SAMs in the series are well ordered, Figure 4.3, displaying their $\nu_{as}^{CH}{}_2$ at 2918 cm^{-1}. A similar observation is observed with the hydrocarbon SAMs on UPD Ag with the $\nu_{as}^{CH}{}_2$ at 2918 / 2917 cm^{-1}.

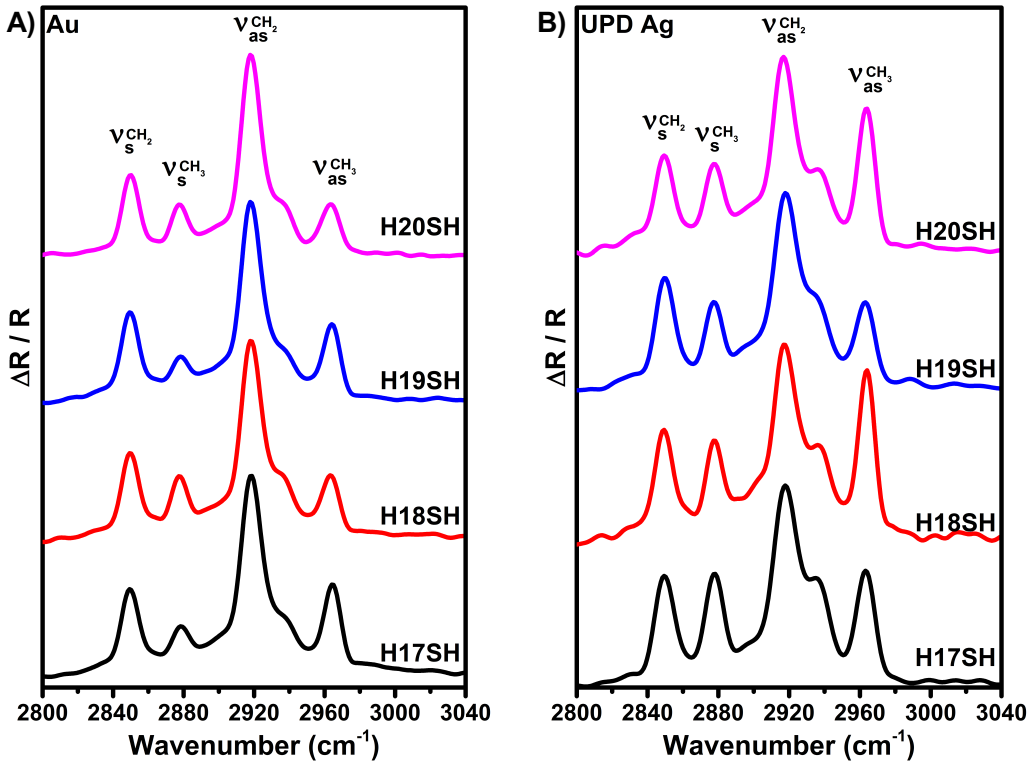

Figure 4.4. PM-IRRAS of the HnSH SAMs on (A) Au and (B) UPD Ag.

Another aspect to note from the analysis of the SAMs on both substrates from the PM-IRRAS involves the difference in intensity of the methyl C-H stretches, $\nu_{as}^{CH_3}$ at ~2964 cm^{-1} and $\nu_{s}^{CH_3}$ at ~2878 cm^{-1}. A discernable "odd-even" effect is observed with the ratio intensities of the C-H stretches associated with the methyl moiety. For the SAMs on Au, the intensity of the symmetric and antisymmetric stretches on the even SAMs, **H18SH** and **H20SH**, is roughly the same. For the odd SAMs, **H17SH** and **H19SH**, the intensity of the symmetric C-H stretch is weaker than the intensity of the antisymmetric stretch. For these hydrocarbon SAMs on UPD Ag, the trends are the opposite. For the even-numbered chains, **H18SH** and **H20SH**, the intensity of the symmetric stretching bands is weaker than that of the antisymmetric stretching, while for the odd-numbered chains, **H17SH** and **H19SH**, the intensity of the two stretching bands is roughly the same. The reason for the change in the intensities can be attributed to the different orientation

of the methyl termini in the films on the two metal surfaces as shown in Figure 4.5. The intensity is enhanced for vibrations that give rise to a transition dipole moment parallel to the surface normal, while it diminishes for vibrations with a transition dipole moment perpendicular to the surface normal.

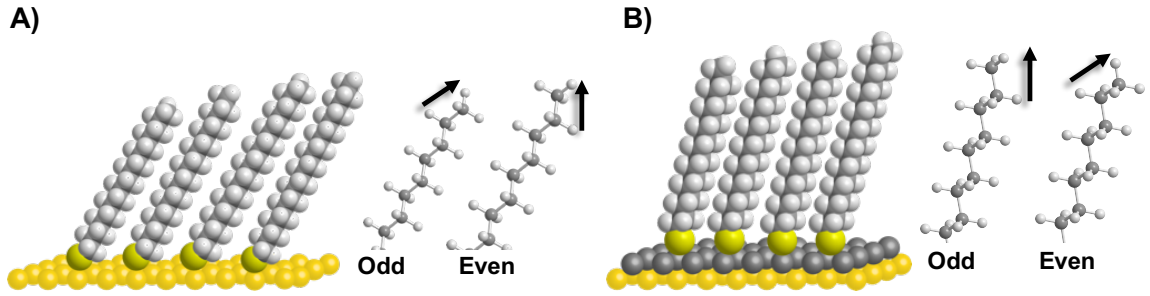

Figure 4.5. Illustration of the HnSH SAMs on (A) Au and (B) UPD Ag surfaces with the orientation of the terminal methyl group for odd and even numbered chains.

For the hydrocarbon SAMs on Au, the terminal methyl group in the odd-numbered chains is tilted away from the surface normal, giving a transition dipole moment for the symmetric stretch that is slightly perpendicular to the surface normal; whereas in the even-numbered chains, the transition dipole moment is parallel to the surface normal. However, the direction of the terminal methyl group is opposite in hydrocarbon SAMs on UPD Ag; the odd-numbered chains have a more upward orientation, while the even numbered chains have a tilted direction.

The surface IR spectra for the CF_3-terminated FSAMs, Figure 4.6, shows that the FSAMs on Au and UPD Ag surfaces are well-ordered with the alkyl chains having a trans-extended configuration. Previous studies on these types of FSAMs have shown that the carbon backbones have similar structural features as the hydrocarbon analogs.[56] A stark difference that is observable in the spectra of the FSAMs on the Au and UPD Ag surfaces is the relative ratio of the intensities of the symmetric and antisymmetric stretches. For the FSAMs on UPD Ag, the relative ratio of the symmetric to antisymmetric stretch appears to be higher than for the FSAMs on Au. This

phenomenon might be due to either an increase in the intensity of the symmetric stretch or a decrease of the intensity of the antisymmetric stretch; both likely arise from a decrease in chain tilt on the UPD Ag surface.[57]

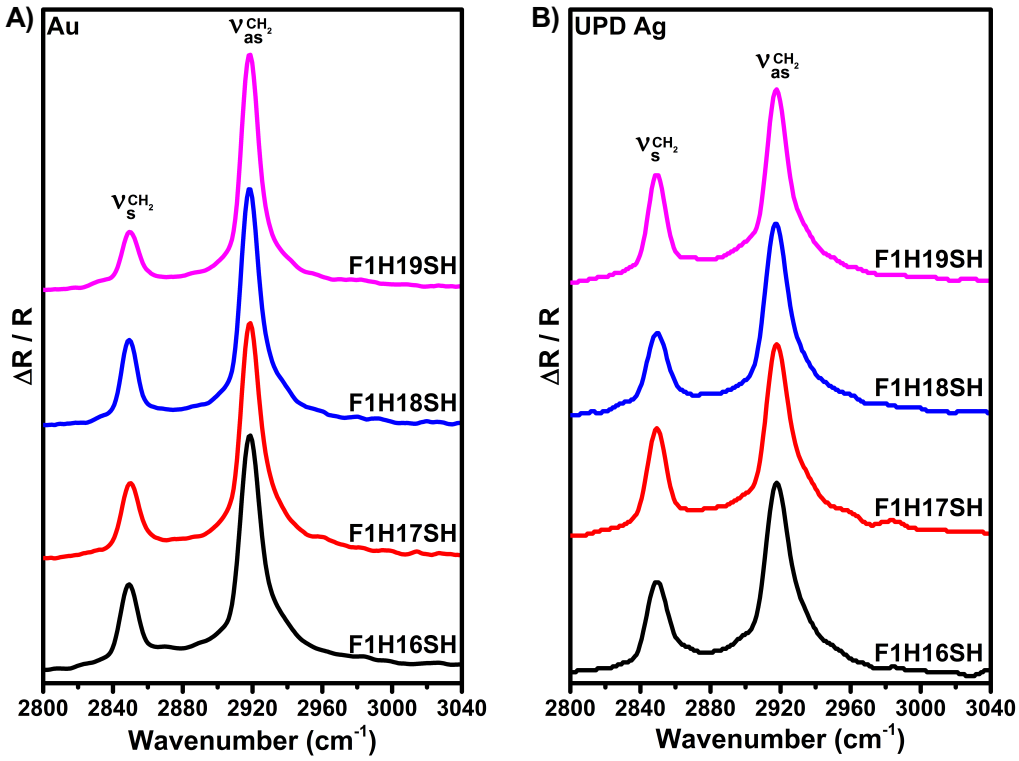

Figure 4.6. PM-IRRAS of the F1HmSH SAMs on (A) Au and (B) UPD Ag.

4.3.3. Analysis of The Monolayer Films by XPS

XPS is a surface-sensitive technique that yields qualitative and quantitative information on most elements present on a sample. In the analysis of SAMs, XPS can also give insight into the structural features of the films.[58] For the hydrocarbon SAMs, a survey scan detected the presence of Au, C and S, and Ag for the SAMs on UPD Ag. Figure 4.7 depicts high resolution spectra of the C 1s and S 2p for the hydrocarbon SAMs on Au, and Table 4.2 shows the peak positions for the photoelectrons. All of the SAMs in the study, on Au and UPD Ag, exhibit a doublet with a

ratio of 2:1 in the S 2p region, Figures 4.7.B, 4.8.D, 4.9.C, and 4.10.E, with a binding energy of ~162.0 eV for the S $2p_{3/2}$, which is indicative of a bound thiolate.[59] The lack of a peak at higher binding energies, ~168 eV, or a peak at ~164 indicates the absence of highly oxidized sulfur or unbound thiol on the surface.

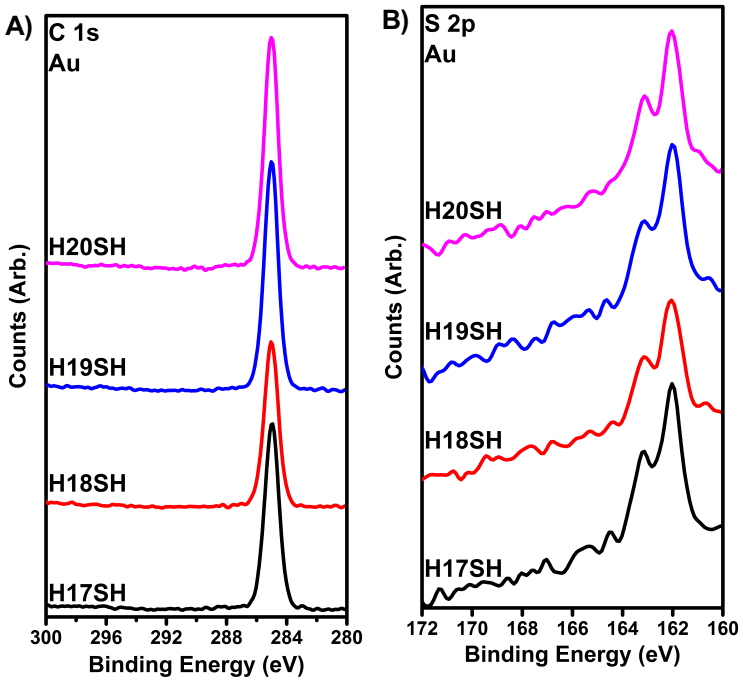

Figure 4.7. XPS spectra for the (A) C 1s and (B) S 2p region for the HnSH SAMs on Au.

Figures 4.8. and 4.10 show the XPS spectra for the Ag 3d, O 1s, C 1s, S 2p, and F 1s (for the FSAMs) regions for the SAMs on UPD Ag. All of the samples analyzed indicate the presence of Ag atoms and the absence of oxygen. In addition to obtaining the oxidation state of elements present in a SAM, a qualitative examination of the packing density of the chains can be obtained from the binding energy of the C 1s peak. For the hydrocarbon SAMs on UPD Ag, the C 1s is at ~285.2 ±1 eV, an increase from the hydrocarbon SAMs on Au. The increase in the binding energy arises from a more densely packed film for the hydrocarbon SAMs on UPD Ag. In the present study, the observed increase in binding energy can be attributed to the chains being more upright

on the UPD Ag surface.[60] On the other hand, the binding energy of C 1s for the FSAMs on Au, (Figure 4.9.A) shows a slight decrease in comparison to the hydrocarbon SAMs on Au, which suggests a lower chain packing in the former films due plausibly to the larger chain termini. A similar decrease in the binding energy is seen when comparing the FSAMs on UPD Ag to the hydrocarbon SAMs on UPD Ag. For the FSAMs on UPD Ag, there is a shift to higher binding energy for the C 1s electrons, which is in accordance with the trend observed in the hydrocarbon SAMs; the methylene chains on Ag are more upright and therefore allow for a more densely packed film. A previous friction-force microscopy study of SAMs on Au and Ag concluded increased stability in SAMs on Ag due to their greater packing density than on Au.[36]

Table 4.2. XPS Peak Positions for the HnSH SAMs on Au and UPD Ag.

Adsorbate/ Metal	Peak Postion (eV)					
	Ag $3d_{5/2}$	Ag $3d_{3/2}$	C 1s (CH_2/ CH_3)	C 1s (CF_2)	F 1s	S 2p
H17SH/Au	-	-	284.9	-	-	162.0
H18SH/Au	-	-	285.0	-	-	162.0
H19SH/Au	-	-	285.0	-	-	162.0
H20SH/Au	-	-	285.0	-	-	162.
H17SH/UPD Ag	368.0	374.0	285.1	-	-	161.9
H18SH/UPD Ag	367.9	374.0	285.2	-	-	161.8
H19SH/UPD Ag	367.9	373.9	285.3	-	-	161.9
H20SH/UPD Ag	367.9	374.0	285.3	-	-	161.8

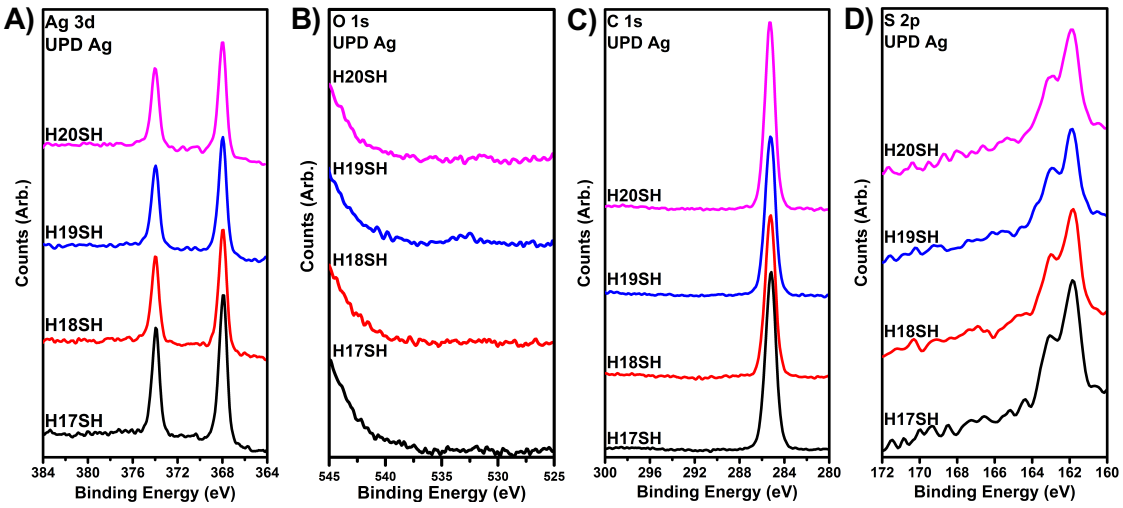

Figure 4.8. XPS spectra for the (A) Ag 3d, (B) O 1s, (C) C 1s, and (D) S 2p region for the HnSH SAMs on UPD Ag.

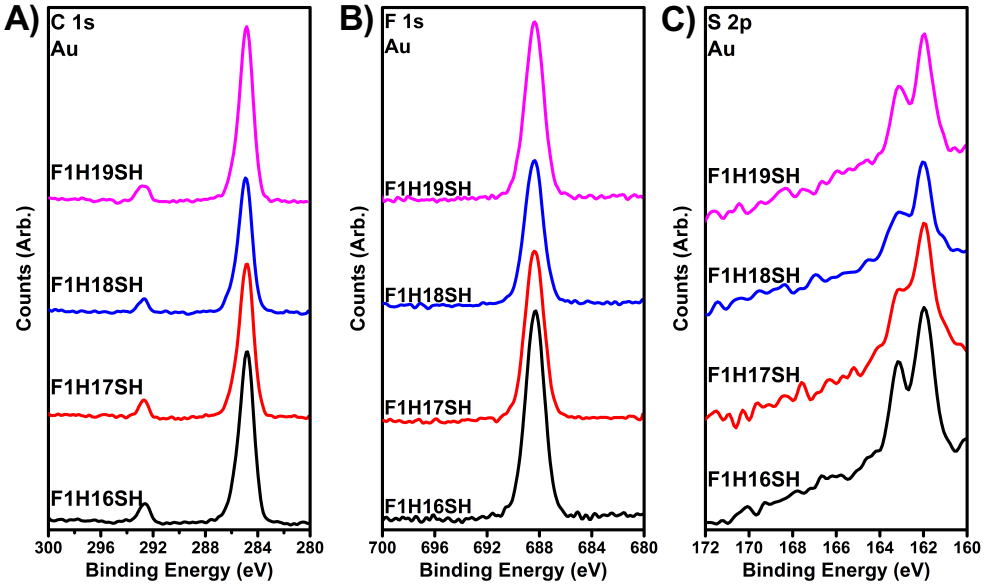

Figure 4.9. XPS spectra for the (A) C 1s, (B) F 1s, and (C) S 2p region for the F1HmSH SAMs on Au.

Table 4.3. XPS Peak Positions for the F1HmSH SAMs on Au and UPD Ag.

Adsorbate/ Metal	Peak Postion (eV)					
	Ag $3d_{5/2}$	Ag $3d_{3/2}$	C 1s (CH_2/ CH_3)	C 1s (CF_2)	F 1s	S 2p
F1H16SH/Au	-	-	284.8	292.6	688.3	162.0
FH17SH/Au	-	-	284.8	292.7	688.4	162.0
FH18SH/Au	-	-	248.9	292.6	688.3	162.0
FH19SH/Au	-	-	284.8	292.8	688.3	161.9
F1H16SH/UPD Ag	367.9	373.9	285.1	292.9	688.6	161.8
F1H17SH/UPD Ag	367.9	373.9	285.1	292.9	688.5	161.8
F1H18SH/UPD Ag	368.0	374.0	285.1	293.0	688.6	161.9
F1H19SH/UPD Ag	367.9	374.0	285.1	293.0	688.5	161.8

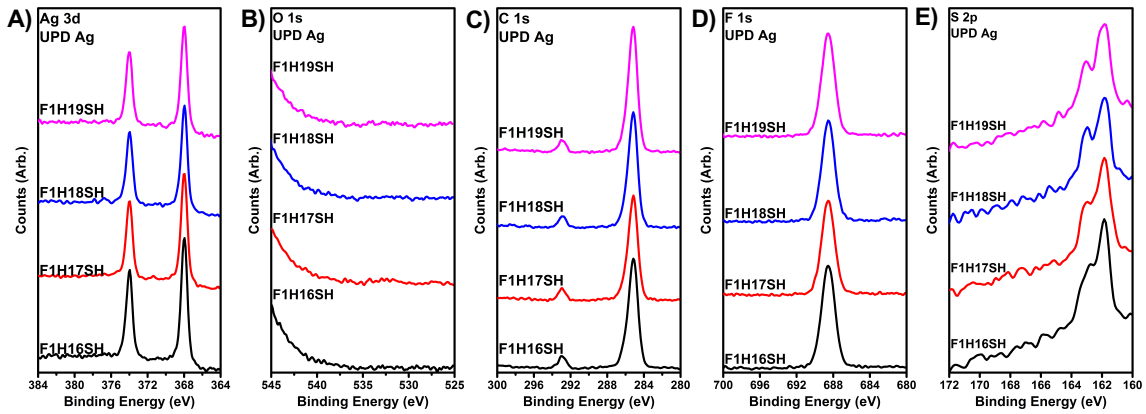

Figure 4.10. XPS spectra for the (A) Ag 3d, (B) O 1s, (C) C 1s, (D) F 1s, and (E) S 2p region for the F1HmSH SAMs on Au.

4.3.4. Wettability

The SAMs on Au and UPD Ag were probed with a variety of liquids ranging in polarity to evaluate the wettability of the SAMs on the different metals. The liquids used were: water – H_2O; glycerol – GL; formamide – FA; dimethylsulfoxide – DMSO; dimethylformamide – DMF;

nitrobenzene – NB; acetonitrile – ACN; bromonaphthalene – BNP; decalin – DC; hexadecane – HD; and perfluorodecalin – FDC. Table 4.4 contains their surface tension values.[61-64]

Table 4.4. Contacting Liquids Used in the Study and their Surface Tensions.

Liquid	γ_{LV} (mN/m)	Liquid	γ_{LV} (mN/m)
H_2O	72.8	**NB**	43.8
GL	65.2	**BNP**	44.6
FA	57.3	**DC (cis)**	31.7
DMSO	43.5	**DC (trans)**	29.4
DMF	34.4	**HD**	27.1
ACN	28.7	**FDC**	19.2

Figure 4.11 shows the advancing contact angle values for the hydrocarbon SAMs on Au and UPD Ag for the nonpolar liquids: BNP, DC, HD, and FDC. Separately, Figure 4.12 shows the contact angles for the polar contacting liquids: H_2O, GL, FA, DMSO, DMF, ACN, and NB. For the hydrocarbon SAMs on Au, there is an odd-even effect in which the odd chains (total number of carbon atoms in the chain) are more wettable than the even chains. This phenomenon can be attributed to the orientation of the terminal methyl group: in the even SAMs, the methyl group is oriented more perpendicular to the surface, while in the odd SAMs, it is tilted away (Figure 4.5) allowing for an increase in molecular contact with the underlying CH_2 unit.[65] For the hydrocarbon SAMs on UPD Ag, the odd-even effect is the opposite; the even SAMs are more wettable than the odd ones. The inversion of the odd even effect for the UPD Ag surfaces can also be attributed to the orientation of the terminal methyl group: in the odd SAMs, the methyl group is more perpendicular to the surface, while in the even SAMs, it is tilted as illustrated in Figure 4.5. Moreover, the odd-even effect observed in the wettability of the hydrocarbon SAMs on both

substrates is in accordance with the interpretation made above in the PM-IRRAS section for these SAMs (*vide supra*).

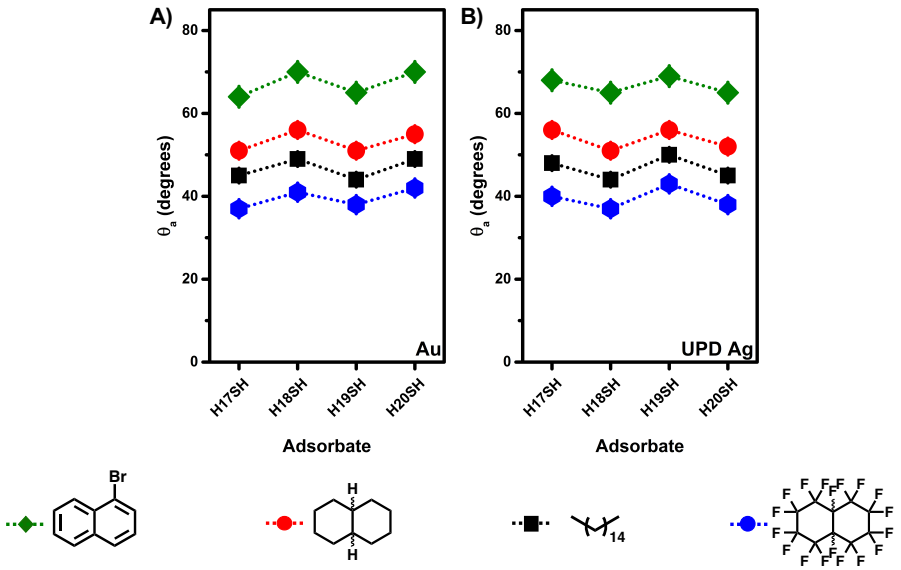

Figure 4.11. Advancing contact angles for BNP, DC, HD, and FDC on HnSH SAMs on (A) Au and (B) UPD surfaces. *Error bars fall within the symbol.*

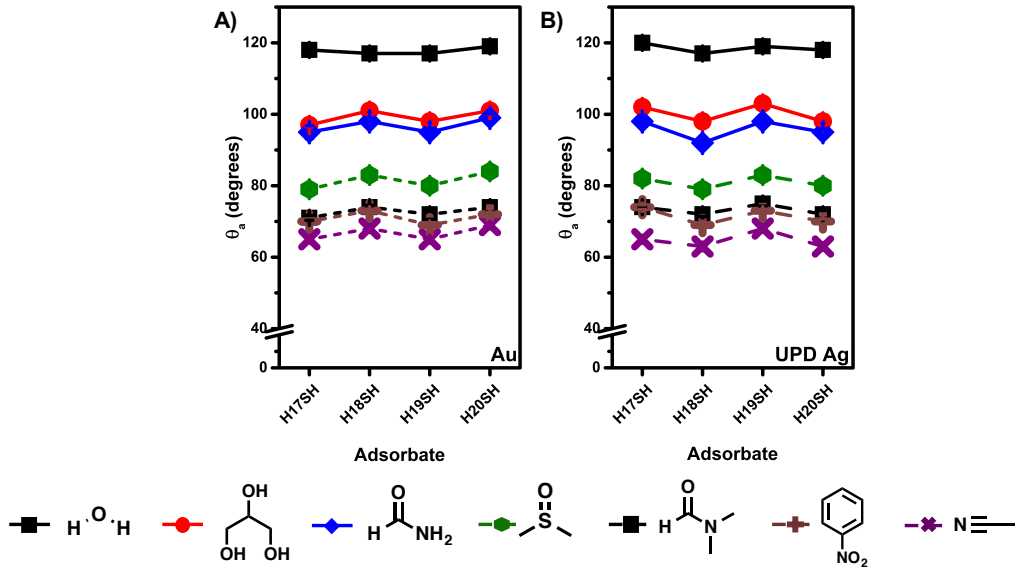

Figure 4.12. Advancing contact angles for H_2O, GL, FA, DMSO, DMF, NB, and ACN on HnSH SAMs on (A) Au and (B) UPD surfaces. *Error bars fall within the symbol.*

The advancing contact angles for nonpolar liquids on the FSAMs are presented in Figure 4.13 and those of polar liquids in Figure 4.14. With the nonpolar liquids, the contact angle values

for the FSAMs are higher than those on the hydrocarbon SAMs. On the hydrocarbon SAMs, there are favorable dispersive interactions between the nonpolar liquids and the hydrocarbon surfaces. On the FSAMS, there are unfavorable non-ideal interactions between the fluorinated surface and the hydrocarbon liquids. These observations follow the phenomena of "like dissolves like". Moreover, the contact angles of the polar liquids are lower on the FSAMs when compared to the hydrocarbon SAMs. This observation has been attributed to the presence of an interfacial dipole in the FSAMs.[6]

The FSAMs on Au show an odd-even effect in which the even chains are more wettable than the odd ones for both sets of liquids tested. Important to note is the inversion of the odd-even effect observed for the FSAMs from what is observed with the hydrocarbon SAMs. The trends in the wettability of the hydrocarbon SAMs can be explained in terms of atomic contact between the surface and the contacting liquid.[5] However, the same argument cannot be made with the FSAMs. Previous research with CF_3-termianted alkanethiols has demonstrated that the presence of a permanent dipole at the interface of these types of SAMs has a profound effect on the wettability of the films.[6,32,66] For the FSAMs on Au, the dipole is oriented more along the surface normal in even chains (~17° with respect to the surface normal) while for the odd chains it is tilted away (~58° with respect to the surface normal).[5] When the dipoles are aligned along the surface (i.e. the even chains) there are greater dipole-dipole interactions when in contact with the polar liquids, but only dipole-induced dipole interactions when in contact with the nonpolar liquids. On the other hand, when the dipoles are canted (i.e. the odd chains) there is a compensation between the dipoles which leads to a reduced favorable interaction between the surface and the liquid.

In the case of FDC, the odd-even effect that is observed cannot be attributed to a dipole effect, but is more likely due to van der Waals (induced dipole-induced dipole) interactions. In

the even-numbered chains, the CF_3 group is pointed more along the surface normal, exclusively exposing fluorine atoms; whereas in the odd chains, the CF_3 group is canted, exposing the underlying CH_2. Exposure of the CH_2 in the odd chains causes an unfavorable dispersive interaction with the fluorinated liquid and a higher contact angle.

For the FSAMs on UPD Ag, the odd-even effect is opposite to that observed on Au. Previous research has shown that the CF_3-terminated SAMs have similar structural properties as their hydrocarbon analogs.[56] Correspondingly, it is reasonable to assume that the CF_3-terminated alkanethiols on the UPD Ag surfaces will have similar structural properties as the alkanethiols on UPD Ag. Taking the twist and tilt angle, ~45° and ~11° respectively, that an alkanethiol adopts on a silver surface[30,52] gives the model featured in Figure 4.15.B. It is apparent from the wettability data and the model in Figure 4.15, that the CF_3 termini on the films have the opposite orientation on the silver surface.

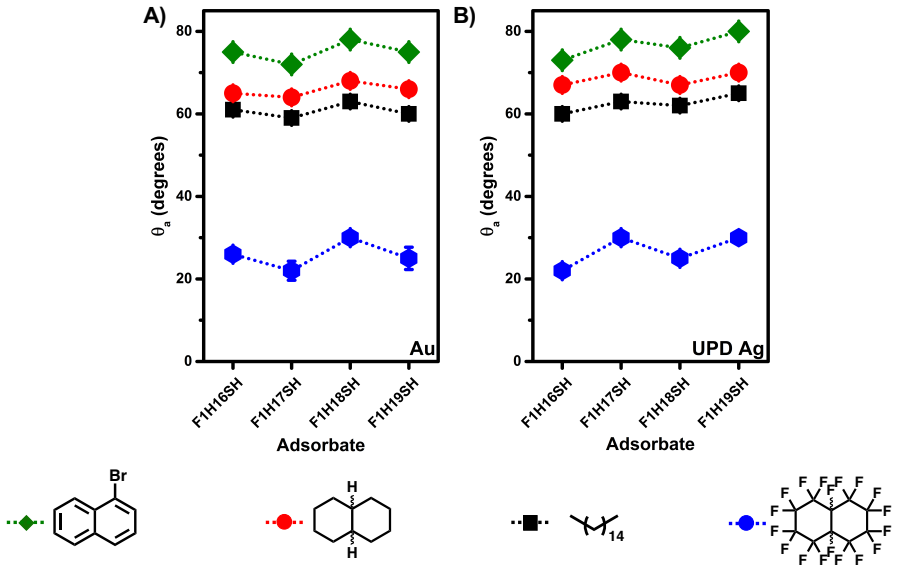

Figure 4.13. Advancing contact angles for BNP, DC, HD, and FDC on F1HmSH SAMs on (A) Au and (B) UPD Ag surfaces. *Error bars fall within the symbols.*

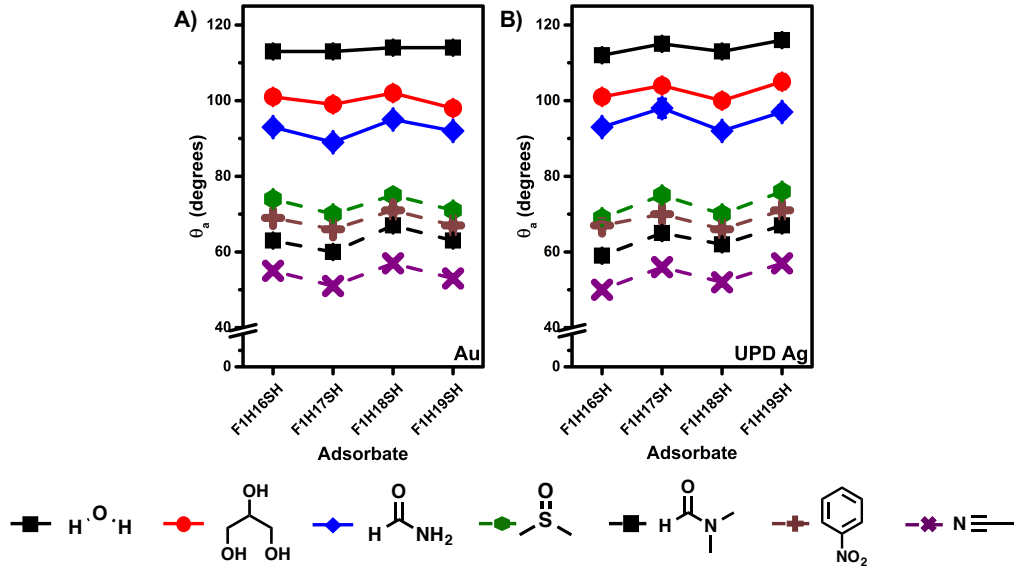

Figure 4.14. Advancing contact angles for H_2O, GL, FA, DMSO, DMF, NB, and ACN on F1HmSH SAMs on (A) Au and (B) UPD surfaces. *Error bars fall within the symbols.*

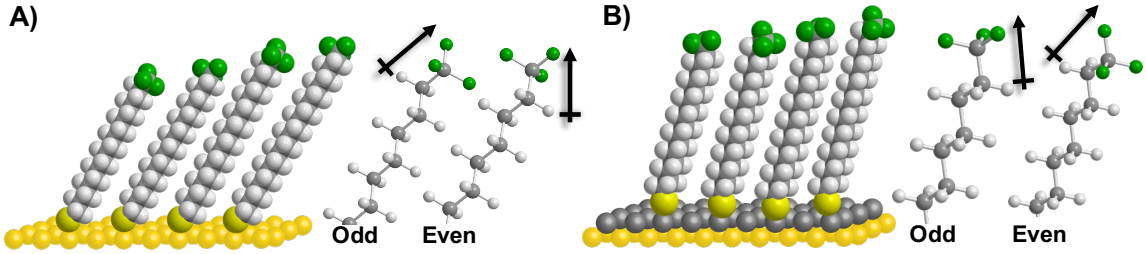

Figure 4.15. Illustration of the F1HmSH SAMs on (A) Au and (B) UPD Ag surfaces with the orientation of the dipole for odd and even numbered chains.

Table 4.5. Advancing Contact Angles (°) of the Polar Liquids on HnSH and F1HmSH SAMs on Au and UPD Ag Surfaces.

Adsorbate	H_2O	GL	FA	DMSO	DMF	ACN	NB	BNP
H17SH/Au	118	97	95	79	71	65	70	64
H18SH/Au	117	101	98	83	74	68	73	70
H19SH/Au	117	98	95	80	72	65	69	65
H20SH/Au	119	101	99	84	74	69	72	70
H17SH/UPD Ag	120	102	98	82	74	65	74	68
H18SH/UPD Ag	117	98	92	79	72	63	69	65
H19SH/UPD Ag	119	103	98	83	75	68	73	69
H20SH/UPD Ag	118	98	95	80	72	63	70	65
F1H16SH/Au	113	101	93	74	63	55	69	75
F1H17SH/Au	113	99	89	70	60	51	66	72
F1H18SH/Au	114	102	95	75	67	57	71	78
F1H19SH/Au	114	98	92	71	63	53	67	75
F1H16SH/UPD Ag	112	101	93	69	59	50	67	73
F1H17SH/UPD Ag	115	104	98	75	65	56	70	78
F1H18SH/UPD Ag	113	100	92	70	62	52	66	76
F1H19SH/UPD Ag	116	105	97	76	67	57	71	80

Table 4.6. Advancing Contact Angles (°) of the Nonpolar and Weakly Polar Liquids on HnSH SAMs and F1HmSH SAMs on Au and UPD Ag Surfaces.

Adsorbate	BNP	DC	HD	FDC
H17SH/Au	64	51	45	37
H18SH/Au	70	56	49	41
H19SH/Au	65	51	44	38
H20SH/Au	70	55	49	42
H17SH/UPD Ag	68	56	48	40
H18SH/UPD Ag	65	51	44	37
H19SH/UPD Ag	69	56	50	43
H20SH/UPD Ag	65	52	45	38
F1H16SH/Au	75	65	61	26
F1H17SH/Au	72	64	59	22
F1H18SH/Au	78	68	63	30
F1H19SH/Au	75	66	60	25
F1H16SH/UPD Ag	73	67	60	22
F1H17SH/UPD Ag	78	70	63	30
F1H18SH/UPD Ag	76	67	62	25
F1H19SH/UPD Ag	80	70	65	30

4.4. Conclusions

The alkanethiols and CF_3-termianted alkanethiols in this study were used to form SAMs on Au and UPD Ag with distinct properties. The thickness of the SAMs on UPD Ag were thicker by ~3 Å than the corresponding SAMS on Au. The alkane chains for the SAMS on UPD Ag are likely more aligned with the surface normal, leading to the thicker film values. Analysis of the films by PM-IRRAS revealed well-ordered films with the chains adopting a trans-extended conformation. There was no major difference observed in the ordering of the SAMs between the Au and UPD Ag substrates. Further, analysis by XPS confirmed the composition of the film, and

determined that the SAMs on UPD Ag were more densely packed than those on Au. The increase in packing density of the SAMs on UPD Ag likely arises from the molecules being more upright, which will allow them to pack more densely. The wettability data obtained from the SAMs allowed us to probe the direction of the dipole and gave us an idea of how the chains orient in the SAMs on the surface of UPD Ag.

4.5. References

1. Lee, H. J.; Jamison, A. C.; Lee, T. R. Surface Dipoles: A Growing Body of Evidence Supports Their Impact and Importance. *Acc. Chem. Res.* **2015**, *48*, 3007–3015.
2. Schwartz, J. J.; Mendoza, A. M.; Wattanatorn, N.; Zhao, Y.; Nguyen, V. T.; Spokoyny, A. M.; Mirkin, C. A.; Baše, T.; Weiss, P. S. Surface Dipole Control of Liquid Crystal Alignment. *J. Am. Chem. Soc.* **2016**, *138*, 5957–5967.
3. Cabarcos, O. M.; Schuster, S.; Hehn, I.; Zhang, P. P.; Maitani, M. M.; Sullivan, N.; Giguère, J.-B.; Morin, J.-F.; Weiss, P. S.; Zojer, E.; Zharnikov, M.; Allara, D. L. Effects of Embedded Dipole Layers on Electrostatic Properties of Alkanethiolate Self-Assembled Monolayers. *J. Phys. Chem. C* **2017**, *121*, 15815–15830.
4. Vilan, A.; Cahen, D. Chemical Modification of Semiconductor Surfaces for Molecular Electronics. *Chem. Rev.* **2017**, *117*, 4624–4666.
5. Zenasni, O.; Marquez, M. D.; Jamison, A. C.; Lee, H. J.; Czader, A.; Lee, T. R. Inverted Surface Dipoles in Fluorinated Self-Assembled Monolayers. *Chem. Mater.* **2015**, *27*, 7433–7446.
6. Graupe, M.; Takenaga, M.; Koini, T.; Colorado, R., Jr.; Lee, T. R. Oriented Surface Dipoles Strongly Influence Interfacial Wettabilities. *J. Am. Chem. Soc.* **1999**, *121*, 3222–3223.

7. Liu, D.; He, Z.; Su, Y.; Diao, Y.; Mannsfeld, S. C. B.; Bao, Z.; Xu, J.; Miao, Q. Self-Assembled Monolayers of Cyclohexyl-Terminated Phosphonic Acids as a General Dielectric Surface for High-Performance Organic Thin-Film Transistors. *Adv. Mater.* **2014**, *26*, 7190–7196.

8. Schmaltz, T.; Gothe, B.; Krause, A.; Leitherer, S.; Steinrück, H.-G.; Thoss, M.; Clark, T.; Halik, M. Effect of Structure and Disorder on the Charge Transport in Defined Self-Assembled Monolayers of Organic Semiconductors. *ACS Nano* **2017**, *11*, 8747–8757.

9. Kimura, T.; Kobayashi, K.; Yamada, H. Direct Investigations of the Interface Impedance of Organic Field-Effect Transistors with Self-Assembled-Monolayer-Modified Electrodes. *Org. Electron.* **2016**, *38*, 74–78.

10. Lísalová, H.; Brynda, E.; Houska, M.; Víšová, I.; Mrkvová, K.; Song, X. C.; Gedeonová, E.; Surman, F.; Riedel, T.; Pop-Georgievski, O.; Homola, J. Ultralow-Fouling Behavior of Biorecognition Coatings Based on Carboxy-Functional Brushes of Zwitterionic Homo- and Copolymers in Blood Plasma: Functionalization Matters. *Anal. Chem.* **2017**, *89*, 3524–3531.

11. Lee, H. J.; Lee, S. S. Label-Free Quantitative Detection of Nucleic Acids Based on Surface-Immobilized DNA Intercalators. *Sens. Actuators, B* **2017**, *241*, 1310–1315.

12. Jang, H.; Kim, D.-E.; Min, D.-H. Self-Assembled Monolayer Mediated Surface Environment Modification of Poly(Vinylpyrrolidone)-Coated Hollow Au–Ag Nanoshells for Enhanced Loading of Hydrophobic Drug and Efficient Multimodal Therapy. *ACS Appl. Mater. Interfaces* **2015**, *7*, 12789–12796.

13. Valley, D. T.; Onstott, M.; Malyk, S.; Benderskii, A. V. Steric Hindrance of Photoswitching in Self-Assembled Monolayers of Azobenzene and Alkane Thiols. *Langmuir* **2013**, *29*, 11623–11631.

14. Moldt, T.; Brete, D.; Przyrembel, D.; Das, S.; Goldman, J. R.; Kundu, P. K.; Gahl, C.; Klajn, R.; Weinelt, M. Tailoring the Properties of Surface-Immobilized Azobenzenes by Monolayer Dilution and Surface Curvature. *Langmuir* **2015**, *31*, 1048–1057.

15. Bethencourt, M. I.; Barriet, D.; Frangi, N. M.; Lee, T. R. Model Glycol-Terminated Surfaces for Adhesion Resistance. *J. Adhes.* **2005**, *81*, 1031–1048.

16. Im, H.; Shao, H.; Park, Y. I.; Peterson, V. M.; Castro, C. M.; Weissleder, R.; Lee, H. Label-Free Detection and Molecular Profiling of Exosomes with a Nano-Plasmonic Sensor. *Nat. Biotechnol.* **2014**, *32*, 490–495.

17. Miller, J. S.; Bethencourt, M. I.; Hahn, M.; Lee, T. R.; West, J. L. Laser-Scanning Lithography (LSL) for the Soft Lithographic Patterning of Cell-Adhesive Self-Assembled Monolayers. *Biotechnol. and Bioeng.* **2006**, *93*, 1060–1068.

18. Jeyachandran, Y. L.; Weber, T.; Terfort, A.; Zharnikov, M. Application of Long Wavelength Ultraviolet Radiation for Modification and Patterning of Protein-Repelling Monolayers. *J. Phys. Chem. C* **2013**, *117*, 5824–5830.

19. Jeyachandran, Y. L.; Terfort, A.; Zharnikov, M. Controlled Modification of Protein-Repelling Self-Assembled Monolayers by Ultraviolet Light: The Effect of the Wavelength. *J. Phys. Chem. C* **2012**, *116*, 9019–9028.

20. Lee, T. R.; Barriet, D.; Moore, H. J. Structure and Properties of Fluorinated Organic Thin Films: Implications for Mems Devices. *NDSI Digest* **2005**, *2*, 93.

21. Bhushan, B.; Kasai, T.; Kulik, G.; Barbieri, L.; Hoffmann, P. AFM Study of Perfluoroalkylsilane and Alkylsilane Self-Assembled Monolayers for Anti-Stiction in MEMS/NEMS. *Ultramicroscopy* **2005**, *105*, 176–188.

22. Patois, T.; Et Taouil, A.; Lallemand, F.; Carpentier, L.; Roizard, X.; Hihn, J.-Y.; Bondeau-Patissier, V.; Mekhalif, Z. Microtribological and Corrosion Behaviors of 1H,1H,2H,2H-Perfluorodecanethiol Self-Assembled Films on Copper Surfaces. *Surf. Coat. Technol.* **2010**, *205*, 2511–2517.

23. Lee, H. J.; Jamison, A. C.; Yuan, Y.; Li, C.-H.; Rittikulsittichai, S.; Rusakova, I.; Lee, T. R. Robust Carboxylic Acid-Terminated Organic Thin Films and Nanoparticle Protectants Generated from Bidentate Alkanethiols. *Langmuir* **2013**, *29*, 10432–10439.

24. Srisombat, L.-o.; Park, J.-S.; Zhang, S.; Lee, T. R. Preparation, Characterization, and Chemical Stability of Gold Nanoparticles Coated with Mono-, Bis-, and Tris-Chelating Alkanethiols. *Langmuir* **2008**, *24*, 7750–7754.

25. Park, C. S.; Lee, H. J.; Jamison, A. C.; Lee, T. R. Robust Maleimide-Functionalized Gold Surfaces and Nanoparticles Generated Using Custom-Designed Bidentate Adsorbates. *Langmuir* **2016**, *32*, 7306–7315.

26. Huang, C.-J.; Chu, S.-H.; Wang, L.-C.; Li, C.-H.; Lee, T. R. Bioinspired Zwitterionic Surface Coatings with Robust Photostability and Fouling Resistance. *ACS Appl. Mater. Interfaces* **2015**, *7*, 23776–23786.

27. Zhang, S.; Leem, G.; Srisombat, L.-o.; Lee, T. R. Rationally Designed Ligands That Inhibit the Aggregation of Large Gold Nanoparticles in Solution. *J. Am. Chem. Soc.* **2008**, *130*, 113–120.

28. Kahsar, K. R.; Schwartz, D. K.; Medlin, J. W. Control of Metal Catalyst Selectivity through Specific Noncovalent Molecular Interactions. *J. Am. Chem. Soc.* **2014**, *136*, 520–526.

29. Pang, S. H.; Schoenbaum, C. A.; Schwartz, D. K.; Medlin, J. W. Effects of Thiol Modifiers on the Kinetics of Furfural Hydrogenation over Pd Catalysts. *ACS Catalysis* **2014**, *4*, 3123–3131.

30. Love, J. C.; Estroff, L. A.; Kriebel, J. K.; Nuzzo, R. G.; Whitesides, G. M. Self-Assembled Monolayers of Thiolates on Metals as a Form of Nanotechnology. *Chem. Rev.* **2005**, *105*, 1103–1170.

31. Zenasni, O.; Jamison, A. C.; Lee, T. R. The Impact of Fluorination on the Structure and Properties of Self-Assembled Monolayer Films. *Soft Matter* **2013**, *9*, 6356–6370.

32. Colorado, R., Jr.; Lee, T. R. Physical Organic Probes of Interfacial Wettability Reveal the Importance of Surface Dipole Effects. *J. Phys. Org. Chem.* **2000**, *13*, 796–807.

33. Colorado, R., Jr.; Lee, T. R. Wettabilities of Self-Assembled Monolayers on Gold Generated from Progressively Fluorinated Alkanethiols. *Langmuir* **2003**, *19*, 3288–3296.

34. Tiani, D. J.; Yoo, H.; Mudalige, A.; Pemberton, J. E. Interfacial Structure in Thin Water Layers Formed by Forced Dewetting on Self-Assembled Monolayers of Ω-Terminated Alkanethiols on Ag. *Langmuir* **2008**, *24*, 13483–13489.

35. Yu, M.; Woodruff, D. P.; Satterley, C. J.; Jones, R. G.; Dhanak, V. R. Structure of the Pentylthiolate Self-Assembled Monolayer on Ag(111). *J. Phys. Chem. C* **2007**, *111*, 10040–10048.

36. Brewer, N. J.; Foster, T. T.; Leggett, G. J.; Alexander, M. R.; McAlpine, E. Comparative Investigations of the Packing and Ambient Stability of Self-Assembled Monolayers of

Alkanethiols on Gold and Silver by Friction Force Microscopy. *J. Phys. Chem. B* **2004**, *108*, 4723–4728.

37. Park, C. S.; Lee, H. J.; Lee, D.; Jamison, A. C.; Galstyan, E.; Zagozdzon-Wosik, W.; Freyhardt, H. C.; Jacobson, A. J.; Lee, T. R. Semifluorinated Alkylphosphonic Acids Form High-Quality Self-Assembled Monolayers on Ag-Coated Yttrium Barium Copper Oxide Tapes and Enable Filamentization of the Tapes by Microcontact Printing. *Langmuir* **2016**, *32*, 8623–8630.

38. Aitchison, H.; Lu, H.; Hogan, S. W. L.; Früchtl, H.; Cebula, I.; Zharnikov, M.; Buck, M. Self-Assembled Monolayers of Oligophenylenecarboxylic Acids on Silver Formed at the Liquid–Solid Interface. *Langmuir* **2016**, *32*, 9397–9409.

39. Herrero, E.; Buller, L. J.; Abruña, H. D. Underpotential Deposition at Single Crystal Surfaces of Au, Pt, Ag and Other Materials. *Chem. Rev.* **2001**, *101*, 1897–1930.

40. Jennings, G. K.; Laibinis, P. E. Underpotentially Deposited Metal Layers of Silver Provide Enhanced Stability to Self-Assembled Alkanethiol Monolayers on Gold. *Langmuir* **1996**, *12*, 6173–6175.

41. Jennings, G. K.; Laibinis, P. E. Self-Assembled N-Alkanethiolate Monolayers on Underpotentially Deposited Adlayers of Silver and Copper on Gold. *J. Am. Chem. Soc.* **1997**, *119*, 5208–5214.

42. Hsieh, M.-H.; Chen, C.-H. Scanning Tunneling Microscopy Observations of Butanethiol Self-Assembled Monolayers on Ag Underpotential Deposition Modified Au(111). *Langmuir* **2000**, *16*, 1729–1733.

43. Lin, S.-Y.; Chen, C.-h.; Chan, Y.-C.; Lin, C.-M.; Chen, H.-W. Self-Assembly of Alkanoic Acids on Gold Surfaces Modified by Underpotential Deposition. *J. Phys. Chem. B* **2001**, *105*, 4951–4955.

44. Lin, S.-Y.; Tsai, T.-K.; Lin, C.-M.; Chen, C.-h.; Chan, Y.-C.; Chen, H.-W. Structures of Self-Assembled Monolayers of N-Alkanoic Acids on Gold Surfaces Modified by Underpotential Deposition of Silver and Copper: Odd−Even Effect. *Langmuir* **2002**, *18*, 5473–5478.

45. Oyamatsu, D.; Kanemoto, H.; Kuwabata, S.; Yoneyama, H. Nanopore Preparation in Self-Assembled Monolayers of Alkanethiols with Use of the Selective Desorption Technique Assisted by Underpotential Deposition of Silver and Copper. *J. Electroanal.* **2001**, *497*, 97–105.

46. Hutt, D. A.; Cooper, E.; Leggett, G. J. A SEXAFS Investigation of Self-Assembled Monolayers on Silver. *Surf. Sci.* **1998**, *397*, 154–163.

47. Rieley, H.; Kendall, G. K.; Jones, R. G.; Woodruff, D. P. X-Ray Studies of Self-Assembled Monolayers on Coinage Metals. 2. Surface Adsorption Structures in 1-Octanethiol on Cu(111) and Ag(111) and Their Determination by the Normal Incidence X-Ray Standing Wave Technique. *Langmuir* **1999**, *15*, 8856–8866.

48. Floriano, P. N.; Schlieben, O.; Doomes, E. E.; Klein, I.; Janssen, J.; Hormes, J.; Poliakoff, E. D.; McCarley, R. L. A Grazing Incidence Surface X-Ray Absorption Fine Structure (GIXAFS) Study of Alkanethiols Adsorbed on Au, Ag, and Cu. *Chem. Phys. Lett.* **2000**, *321*, 175–181.

49. Bain, C. D.; Troughton, E. B.; Tao, Y. T.; Evall, J.; Whitesides, G. M.; Nuzzo, R. G. Formation of Monolayer Films by the Spontaneous Assembly of Organic Thiols from Solution onto Gold. *J. Am. Chem. Soc.* **1989**, *111*, 321–335.

50. Porter, M. D.; Bright, T. B.; Allara, D. L.; Chidsey, C. E. D. Spontaneously Organized Molecular Assemblies. 4. Structural Characterization of *n*-Alkyl Thiol Monolayers on Gold by Optical Ellipsometry, Infrared Spectroscopy, and Electrochemistry. *J. Am. Chem. Soc.* **1987**, *109*, 3559–3568.

51. Colorado, R., Jr.; Lee, T. R. Attenuation Lengths of Photoelectrons in Fluorocarbon Films. *J. Phys. Chem. B* **2003**, *107*, 10216–10220.

52. Tao, F.; Bernasek, S. L. Understanding Odd−Even Effects in Organic Self-Assembled Monolayers. *Chem. Rev.* **2007**, *107*, 1408–1453.

53. Chen, I. W. P.; Chen, C.-C.; Lin, S.-Y.; Chen, C.-H. Effect of Underpotentially Deposited Adlayers on Sulfur Bonding Schemes of Organothiols Self-Assembled on Polycrystalline Gold: Sp or Sp3 Hybridization. *J. Phys. Chem. B* **2004**, *108*, 17497–17504.

54. Snyder, R. G.; Strauss, H. L.; Elliger, C. A. Carbon-Hydrogen Stretching Modes and the Structure of *n*-Alkyl Chains. 1. Long, Disordered Chains. *J. Phys. Chem.* **1982**, *86*, 5145–5150.

55. MacPhail, R. A.; Strauss, H. L.; Snyder, R. G.; Elliger, C. A. Carbon-Hydrogen Stretching Modes and the Structure of *n*-Alkyl Chains. 2. Long, All-Trans Chains. *J. Phys. Chem.* **1984**, *88*, 334–341.

56. Pflaum, J.; Bracco, G.; Schreiber, F.; Colorado Jr, R.; Shmakova, O. E.; Lee, T. R.; Scoles, G.; Kahn, A. Structure and Electronic Properties of CH_3- and CF_3-Terminated Alkanethiol

Monolayers on Au(111): A Scanning Tunneling Microscopy, Surface X-Ray and Helium Scattering Study. *Surf. Sci.* **2002**, *498*, 89–104.

57. Frey, S.; Heister, K.; Zharnikov, M.; Grunze, M.; Tamada, K.; Colorado, R.; Graupe, M.; Shmakova, O. E.; Lee, T. R. Structure of Self-Assembled Monolayers of Semifluorinated Alkanethiols on Gold and Silver Substrates. *Isr. J. Chem.* **2000**, *40*, 81–97.

58. Laibinis, P. E.; Whitesides, G. M.; Allara, D. L.; Tao, Y. T.; Parikh, A. N.; Nuzzo, R. G. Comparison of the Structures and Wetting Properties of Self-Assembled Monolayers of *n*-Alkanethiols on the Coinage Metal Surfaces, Copper, Silver, and Gold. *J. Am. Chem. Soc.* **1991**, *113*, 7152–7167.

59. Castner, D. G.; Hinds, K.; Grainger, D. W. X-Ray Photoelectron Spectroscopy Sulfur 2p Study of Organic Thiol and Disulfide Binding Interactions with Gold Surfaces. *Langmuir* **1996**, *12*, 5083–5086.

60. Heister, K.; Johansson, L. S. O.; Grunze, M.; Zharnikov, M. A Detailed Analysis of the C 1s Photoemission of *n*-Alkanethiolate Films on Noble Metal Substrates. *Surf. Sci.* **2003**, *529*, 36–46.

61. Smallwood, I. M. *Handbook of Organic Solvent Properties*; John Wiley & Sons: New York, 1996.

62. Yaws, C. L. *Chemical Properties Handbook Physical, Thermodynamic, Environmental, Transport, Safety, and Health Related Properties for Organic and Inorganic Chemicals*; McGraw-Hill: New York, 1999.

63. Fowkes, F. M.; Riddle Jr, F. L.; Pastore, W. E.; Weber, A. A. Interfacial Interactions between Self-Associated Polar Liquids and Squalane Used to Test Equations for Solid—Liquid Interfacial Interactions. *Colloid Surface* **1990**, *43*, 367–387.

64. Jańczuk, B.; Białłopiotrowicz, T. Surface Free-Energy Components of Liquids and Low Energy Solids and Contact Angles. *J. Colloid Inter. Sci.* **1989**, *127*, 189–204.

65. Barriet, D.; Chinwangso, P.; Lee, T. R. Can Cyclopropyl-Terminated Self-Assembled Monolayers on Gold Be Used to Mimic the Surface of Polyethylene? *ACS Appl. Mater. Interfaces* **2010**, *2*, 1254–1265.

66. Graupe, M.; Koini, T.; Kim, H. I.; Garg, N.; Miura, Y. F.; Takenaga, M.; Perry, S. S.; Lee, T. R. Wettability and Friction of CF_3-Terminated Monolayer Films on Gold. *Mater. Res. Bull.* **1999**, *34*, 447–453.

Chapter 5: Substrate Effects on Inverted Interfacial Dipoles in Fluorinated Self-Assembled Monolayers

5.1. Introduction

The modulation of the interfacial properties of self-assembled monolayers (SAMs) can be controlled via tuning the structure and chemical functionality of the adsorbate broadens the use this technology in various applications such as organic semiconductors,[1-3] sensors,[4-6] antifouling, [7-10] and as lubricants.[11-12] The most widely used SAM model is that formed from alkanethiols on coinage metals. The adsorbate can be tailored through synthetic methods to give specific macroscopic properties. For example, the incorporation of fluorine atoms into the carbon backbone of an adsorbate will introduce rigidity, thermal stability, oleophobicity, and hydrophobicity.[13-16] The properties an adsorbate imparts on a monolayer thin film can also be modified by changing the substrate. The electrochemical underpotential deposition (UPD) of one metal onto another to form a single monolayer is an example of such modification. This process is dictated by a stronger adatom-substrate interaction than an adatom-adatom interaction which occurs when depositing bulk material.[17]

As seen in chapter 4, the incorporation of a monolayer of silver atop a gold substrate changes the structural and interfacial properties of a series of CF_3-terminated SAMs (FSAMs). The SAMs formed on the underpotentially deposited silver (UPD Ag) have a different binding geometry than on the bare gold substrates which give the same molecules different structural properties. The structural changes in the FSAMs on Au and UPD Ag gave rise to an inversion in the odd-even effect of the wettability of the

SAMs by changing the direction of the interfacial dipole present in these types of SAMs.[18-20]

In this study, a series of partially fluorinated alkanethiols containing an inverted dipole at the chain termini, illustrated in Figure 5.1, were used to make SAMs on Au and UPD Ag in order to analyze the effect of the UPD Ag on the interfacial properties of the resulting FSAMs. The FSAMs were also compared to SAMs formed from normal alkanethiols (HSAMs) of comparative carbon chain lengths on both Au and UPD Ag substrates. The SAMs were characterized using ellipsometry, X-ray photoelectron spectroscopy (XPS), polarization-modulation infrared reflection-absorption spectroscopy (PM-IRRAS), and contact angle goniometry using a variety of contacting liquids.

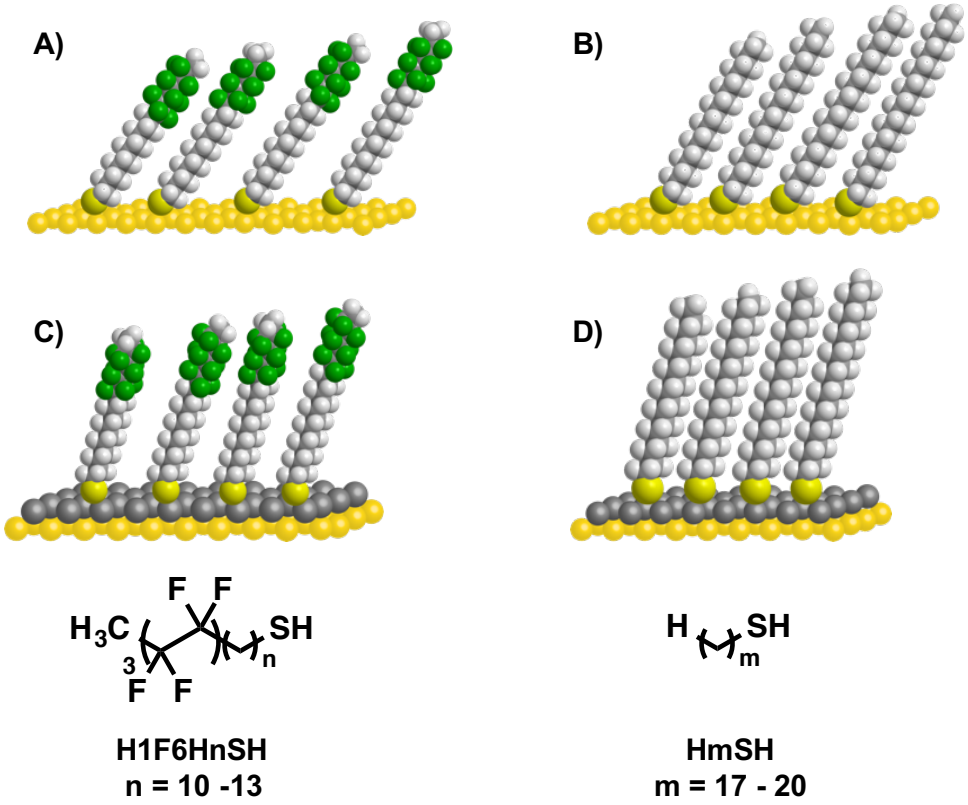

Figure 5.1. Illustrations of the SAMs formed from the H1F6HnSH on (A) Au and (C) UPD Ag along with the hydrocarbon analogs, HmSH, on (B) Au and (D) UPD Ag.

5.2. Experimental Section

5.2.1. Materials and Methods

Gold Shot (99.999%) bought from Kamis Inc. Chromium rods (99.9%) were purchased from R. D. Mathis Company. Silicon (100) wafers (polished, single crystal) were bought from University Wafer and used as received. Tetrahydrofuran (Sigma-Aldrich) and ethanol (Aaper Alcohol and Chemical Co) used to make the SAMs were used as received. The adsorbate 1-octadecanethiol (**H18SH**) was purchased from Sigma-Aldrich. 1-heptadecanethiol (**H17SH**), 1-nonadecanethiol (**H19SH**), 1-eicosanethiol (**H20SH**), 11,11,12,12,13,13,14,14,15,15,16,16-Dodecafluoroheptadecane-1-thiol (**H1F6H10SH),** 12,12,13,13,14,14,15,15,16,16,17,17-dodecafluorooctadecane-1-thiol (**H1F6H11SH**), 13,13,14,14,15,15,16,16,17,17,18,18-Dodecafluorononadecane-1-thiol (**H1F6H12SH**), and 14,14,15,15,16,16,17,17,18,18,19,19-dodecafluoroicosane-1-thiol (**H1F6H13SH**) were synthesized according to a procedure in the literature.[20]

5.2.2. Substrate Preparation

Gold wafers were prepared by the thermal evaporation of 100 Å of chromium followed by 1000 Å of gold under vacuum (pressure ≤ 6 x 10^{-5} torr). The evaporation of the metals was performed at a rate of 0.5 Å/s. After evaporation, the wafers were cut into slides and stored in milliQ water until use for electrochemical measurements.

5.2.3. Underpotential Deposition of Silver (UPD Ag)

For cyclic voltammetry (CV), a Princeton Applied Research potentiostat/galvanostat model 263A controlled by PowerSuite software was used to modulate the potential applied to and measure the current of the electrochemical systems.

A homemade glass cell was used to hold the three-electrodes used for electrochemical measurements with the gold slide as the working electrode, a platinum wire as the counter electrode, and mercury/mercurous sulfate in saturated K_2SO_4 as the reference electrode. The electrolyte for all CVs used was 0.1M sulfuric acid (Ultrex II Ultrapure Reagent from J. T. Baker) with 0.6mM Ag_2SO_4 (99.999% trace metals basis from Aldrich) added for the silver voltammetry. Gold slides were cycled ten times at a scan rate of 15 mV/s in degassed sulfuric acid, rinsed with plenty of Millipore water and stored in Millipore water until measurement of their optical properties with ellipsometry. For the deposition of silver, the cycled gold slides were cycled in deaerated silver solution ten times at a scan rate of 15 mV/s, then held at a potential of 0.15 V vs MSE for the underpotential deposition of a monolayer of silver, pulled out of the cell while held at potential, and rinsed with copious amounts of Millipore water, and stored in Millipore water until analysis with ellipsometry.

5.2.4. SAMs Characterization

A Rudolph Auto El III ellipsometer equipped with a He-Ne laser (632.8 nm) set at an incidence angle of 70° and a refractive index of 1.45, a value typical for organic thin films,[21] was used to obtain thickness measurements for the monolayer films. An average of three measurements per slide was used as the reported thickness.

X-Ray photoelectron spectroscopy (XPS) was performed on a PHI 5700 x-ray photoelectron spectrometer with a monochromatic Al Kα X-ray source (1486.7 eV) incident at 90° relative to the axis of the hemispherical analyzer with a takeoff angle of 45° from the surface and a pass energy of 23.5 eV. The Au $4f_{7/2}$ peak was referenced to 84.0 eV in all the spectra.

Polarization-modulation infrared reflection-absorption spectroscopy (PM-IRRAS) was performed using a Nicolet Nexus 670 Fourier transform equipped with a mercury-cadmium-telluride (MCT) detector and a Hinds Instrument PEM-90 photoelastic modulator. The surfaces were mounted at an incident angle of 80° with respect to the surface normal for p-polarized light. The spectra were collected using 1024 scans at a resolution of 2 cm^{-1}.

Contact angle data was obtained using a Ramé-Hart model 100 contact angle goniometer set up with a Matrix Technologies micro-Electrapette 25 to dispense liquids. The advancing contact angles (θ_a) and receding contact angles (θ_r) were obtained at a speed of 1μL/s. The reported data is an average of six measurements with readings being made from each side of three droplets on different locations along the slides.

The contacting liquids used in the study include a variety of nonpolar, polar protic, and polar aprotic liquids: bromonaphthalene (BNP – Sigma Aldrich); decalin (DC – Acros Organics); hexadecane (HD – Aldrich); perfluorodecalin (FDC – Synquest Labs); acetonitrile (ACN – Sigma Aldrich); nitro-benzene (NB – Acros); dimethylformamide (DMF – Sigma Aldrich); dimethyl sulfoxide (DMSO – Sigma Aldrich); formamide (FA – Sigma Aldrich); glycerol (GY – Sigma Aldrich); and water (H_2O – Millipore water with resistivity of 18.2 Ω).

5.3. Results and Discussion

5.3.1. Monolayer Thickness Analysis

In this chapter, the FSAMs formed were compared to their hydrocarbon analogs that were prepared on the same batch of substrates. The thickness of the hydrocarbon

SAMs, shown in Figure 5.2 and Table 5.1, were 20 Å, 22 Å, 24 Å, and 25 Å for the **H17SH**, **H18SH**, **H19SH**, and **H20SH**, respectively, which are in accordance with what has been observed in the literature.[20,22]

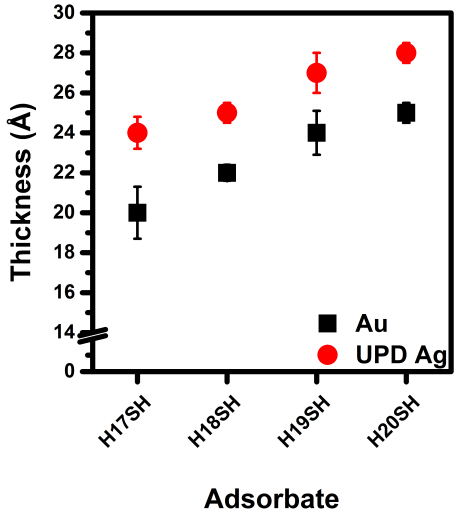

Figure 5.2. Average thickness measurements obtained for the HmSH SAMs.

Table 5.1. Ellipsometric Thickness Values of the HmSH SAMs.

Adsorbate	Au Thickness (Å)	UPD Ag Thickness (Å)
H17SH	20	21
H18SH	22	23
H19SH	24	24
H20SH	25	25

For the FSAMs, two temperatures were used during SAM formation, room temperature (rt) and 50°C. After 48 h at rt, the FSAMs resulted in thickness values shown in Figure 5.3 and Table 5.2 that are ~ 2Å thinner than what has been observed on Au that is not treated electrochemically.[20] As a result, the FSAMs were further

equilibrated at elevated temperatures. First, the FSAMs were heated at 40°C for 24 h, then an additional 16h at 50°C; there was no significant change between the thickness of the FSAMs equilibrated at 40° and 50°C. The additional equilibration at elevated temperatures resulted in film thicknesses that were 2-3 Å thicker than what was originally observed, which could be attributed to the ability of the thiolates to move and pack better with the increase in kinetic energy of the system.[20]

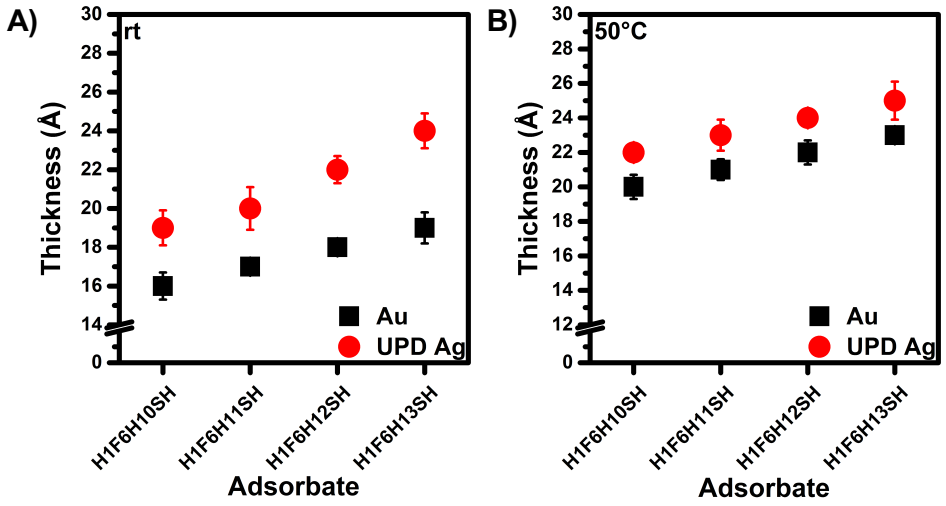

Figure 5.3. Average thickness measurements obtained for the FSAMs developed at (A) room temperature and (B) 50°C.

Table 5.2. Ellipsometric Thickness Values of the Investigated SAMs.

Adsorbate	Au-rt Thickness (Å)	Au-50°C Thickness (Å)	UPD Ag-rt Thickness (Å)	UPD Ag-50°C Thickness (Å)
H1F6H10SH	16	20	19	22
H1F6H11SH	17	21	20	23
H1F6H12SH	18	22	22	24
H1F6H13SH	19	23	24	25

5.3.2. XPS Analysis

In order to gain insight into the chemical composition of an organic film, X-ray photoelectron spectroscopy (XPS) is employed. In addition to obtaining the chemical composition of a SAM, XPS can also yield information on the ordering of the film.[23] A survey scan revealed the presence of Au, C, and S for the hydrocarbon SAMs on Au and the presence of Ag, in addition to the other elements, for the hydrocarbon SAMs on UPD Ag. All of the SAMs analyzed in this study exhibit a doublet in the S 2p region at ~162 eV with the characteristic 1:2 ratio for the S $2p_{3/2}$ photoelectrons of a bound thiolate.[24] High resolution spectra of the Ag 3d, O 1s, C 1s, and S 2p regions for the hydrocarbon SAMs are shown in Figure 5.4 while Table 5.3 lists their binding energies. The hydrocarbon SAMs on both substrates display bound thiolate on the surface and lack oxidized sulfur species. In addition, the binding energy of the C 1s, which can be used to gain insight into the relative packing density of a film, shifts to a higher value for the hydrocarbon SAMs on UPD Ag. The shift to a higher binding energy has been attributed to an increase in the packing density.[25] Further, the increase in the packing density for the SAMs on silver substrates has been attributed to the chains being more upright on the surface.[26]

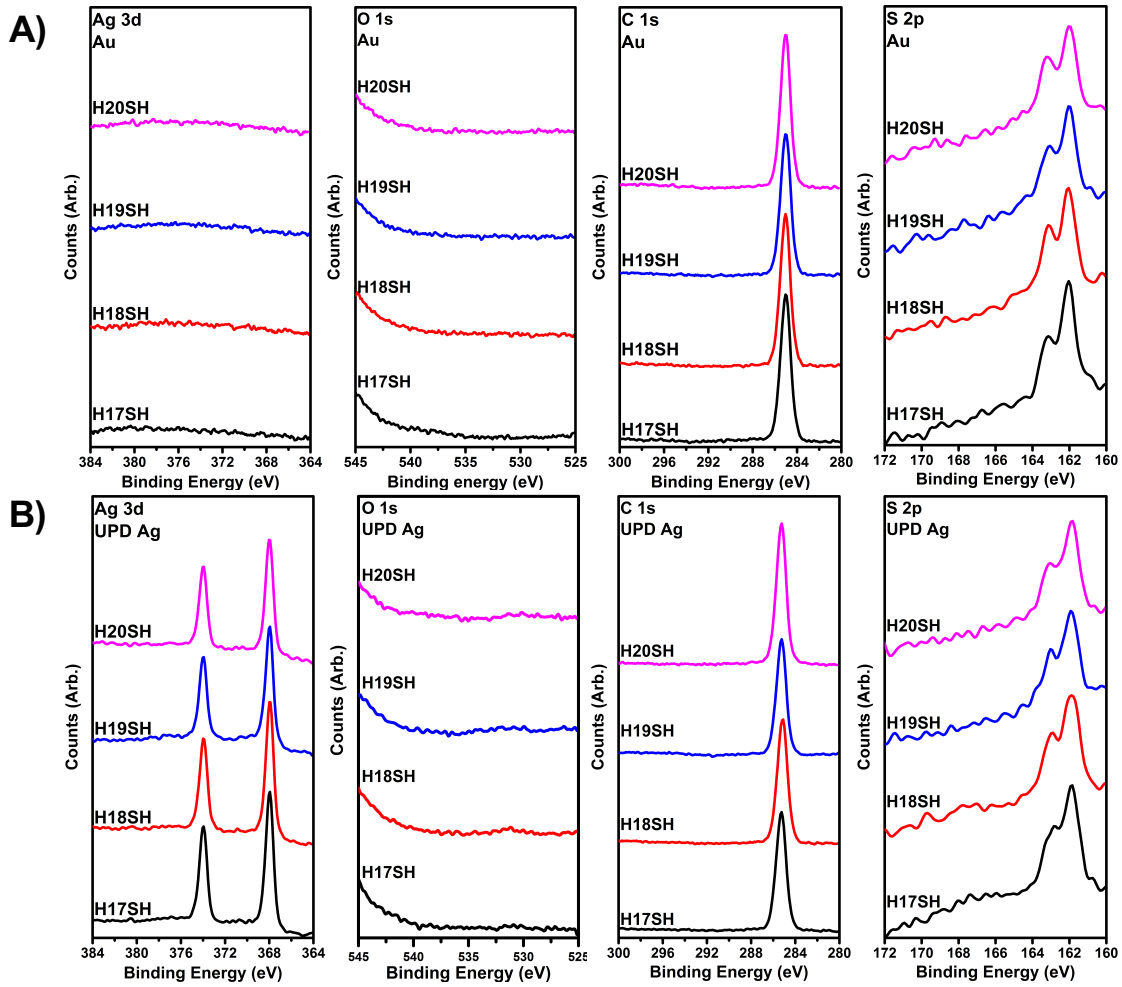

Figure 5.4. XPS spectra for the Ag 3d, O 1s, C 1s, and S 2p regions for the HmSH SAMs on (A) Au and (B) UPD Ag.

Table 5.3. XPS Peak Positions for the HmSH SAMs on Au and UPD Ag.

Adsorbate/ Metal	Peak Postion (eV)					
	Ag $3d_{5/2}$	Ag $3d_{3/2}$	C 1s (CH_2/ CH_3)	C 1s (CF_2)	F 1s	S 2p
H17SH/Au	-	-	285.0	-	-	162.0
H18SH/Au	-	-	285.0	-	-	162.0
H19SH/Au	-	-	285.1	-	-	162.1
H20SH/Au	-	-	285.0	-	-	162.0
H17SH/UPD Ag	367.9	373.9	285.2	-	-	161.8
H18SH/UPD Ag	368.0	374.0	285.1	-	-	161.9
H19SH/UPD Ag	367.9	373.9	285.2	-	-	161.9
H20SH/UPD Ag	368.0	373.9	285.2	-	-	161.8

Initial XPS analysis of the FSAMs formed at rt, for both substrates, inconsistently showed the presence of oxidized sulfur species in S 2p region at ~168 eV, Figure 5.5. After heating the monolayers at elevated temperatures, the presence of oxidized sulfur peaks disappeared, Figure 5.6. The inconsistence and the disappearance of the oxidized sulfur species suggests that the oxidized species present in the samples could be residual SO_4^{-2} used in the electrochemical treatment of the substrates rather than oxidized thiol species. Previous studies have suggested that the higher temperature increases the mobility of the thiolates on the surface.[20,27] The increased mobility of the thiolates in this case will lead to increased ability of the thiolates to remove the residual sulfate, which, apparent from our results, is difficult to do for equilibration at room temperature.

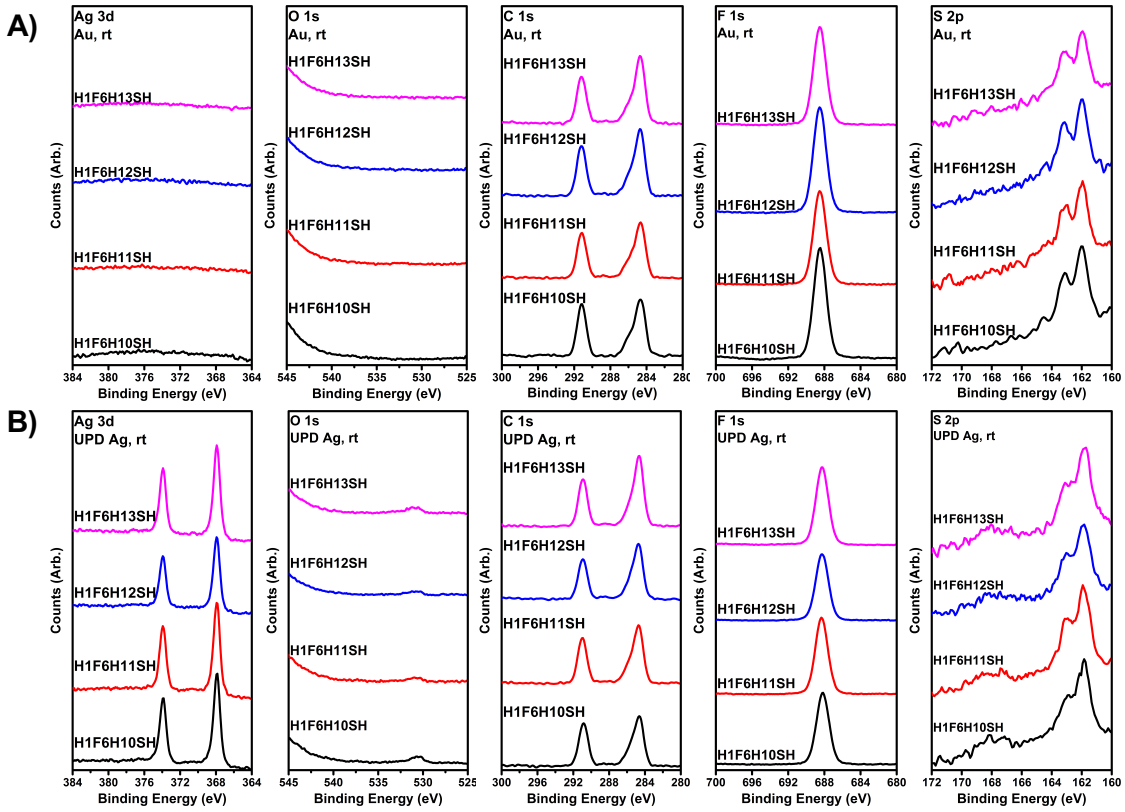

Figure 5.5. XPS spectra for the Ag 3d, O 1s, C 1s, F 1s, and S 2p regions for the H1F6HnSH SAMs equilibrated at room temperature on (A) Au and (B) UPD Ag.

Figure 5.6 shows the high resolution spectra of the Ag 3d, O 1s, C 1s, F 1s, and S 2p regions for the FSAMs, while Table 5.4 details their peak positions. For insight into the relative packing characteristics of the FSAMs on Au, the C 1s binding energies for the methylene chains are analyzed. The peaks for the FSAMs on Au and UPD Ag shift to a lower the binding energy when compared to the corresponding hydrocarbon SAMs. The structural differences between a fluorinated adsorbate and non-fluorinated adsorbate will dictate the packing densities of the resulting films. Structurally, the vdW diameter of the fluorinated helix in the FSAMs is much larger than that of a hydrocarbon chain for the hydrocarbon SAMs, at 5.6 Å versus 4.2 Å respectively.[16,28-30] As a result, the fluorinated adsorbate will occupy a larger volume on the metal surface when compared to the hydrocarbon adsorbate.[31-33] A densely packed film will act as an insulator by not allowing the complete discharge of the positive charges generated during photoelectron emission, while a loosely packed SAM will be better at discharging, acting as a poor insulator.[25,33-34] Therefore, the relatively lower binding energy of the FSAMs on Au and UPD Ag can be attributed to lower packing density of the films.

For all of the SAMs on UPD Ag, there is a slight increase in the binding energy of the C 1s photoelectron when compared to the SAMs on Au, as shown in Tables 5.3 and 5.4. The partially fluorinated alkanethiols are expected to adopt similar binding geometries to the normal alkanethiols on UPD Ag. For an alkanethiol on UPD Ag-modified Au substrates, the sulfur will bind with a Ag-S-C bond angle of ~180°, compared to ~104° for an Au-S-C bond.[35] The higher bond angle will also result in a smaller tilt angle, ~10 ° on Ag versus ~33° on Au, which leads to a more densely packed

monolayer. Additionally, a similar increase is observed for the binding energies of the F 1s photoelectrons.

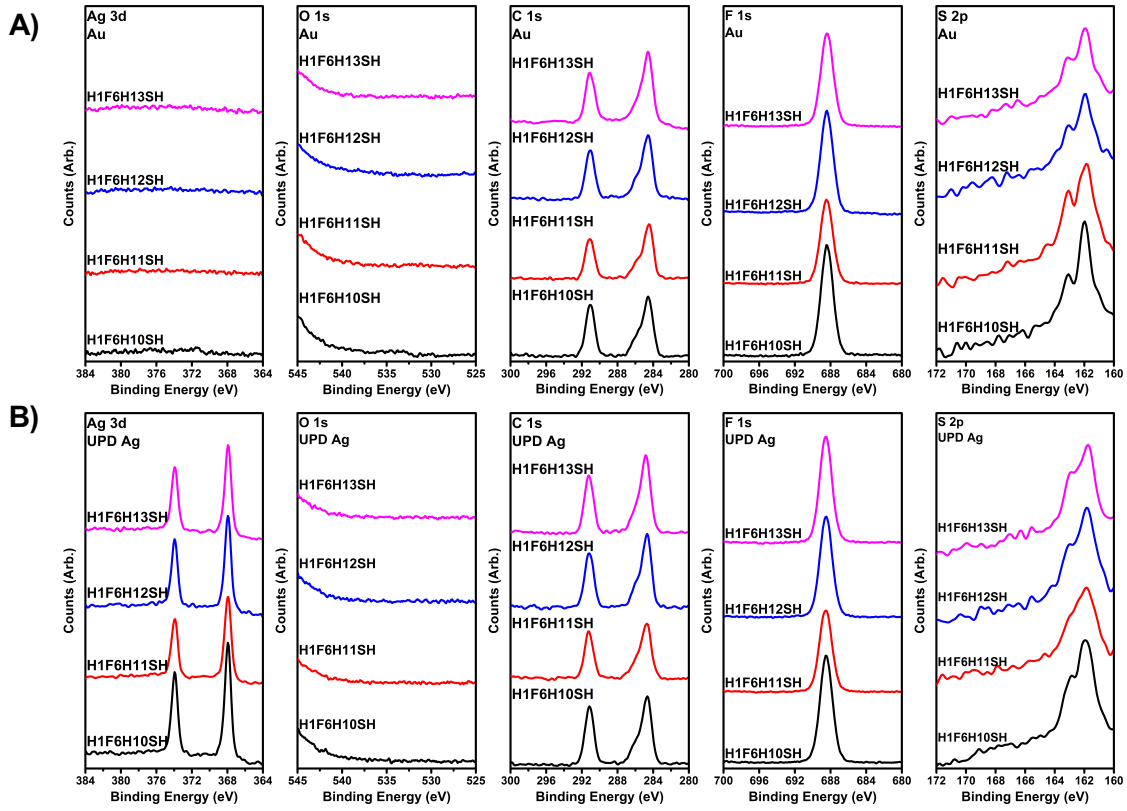

Figure 5.6. XPS spectra for the Ag 3d, O 1s, C 1s, F 1s, and S 2p regions for the H1F6HnSH SAMs equilibrated at 50°C on (A) Au and (B) UPD Ag.

Table 5.4. XPS Peak Positions for the H1F6HnSH SAMs on Au and UPD Ag.

Adsorbate/ Metal	Peak Postion (eV)					
	Ag $3d_{5/2}$	Ag $3d_{3/2}$	C 1s (CH_2/ CH_3)	C 1s (CF_2)	F 1s	S 2p
H1F6H10SH/Au	-	-	284.6	291.1	688.5	162.0
H1F6H11SH/Au	-	-	284.5	291.1	688.5	161.9
H1F6H12SH/Au	-	-	284.6	291.0	688.4	161.9
H1F6H13SH/Au	-	-	284.6	291.1	688.4	161.9
H1F6H10SH/UPD Ag	368.0	374.0	284.7	291.2	688.6	162.0
H1F6H11SH/UPD Ag	367.9	373.9	284.7	291.3	688.5	162.0
H1F6H12SH/UPD Ag	368.0	374.0	284.7	291.2	688.5	161.9
H1F6H13SH/UPD Ag	368.0	374.0	284.9	291.3	688.6	161.8

5.3.3. PM-IRRAS Analysis of SAMs

The PM-IRRAS spectra for the hydrocarbon SAMs is presented in Figure 5.7. To determine the relative crystallinity of the films, the position of the C-H antisymmetric vibration ($\nu_{as}{}^{CH}{}_2$) of the methylene units is analyzed. The appearance of this band at 2918 cm^{-1} is indicative of a well-ordered film with trans-extended chains.[21,36-37] The hydrocarbon SAMs display the $\nu_{as}{}^{CH}{}_2$ at 2918 and 2917 cm^{-1} on Au and UPD Ag, respectively. Additionally, there is an odd-even effect observed in the intensities of the stretches associated with the methyl terminal group of the hydrocarbon SAMs Au that is inverse for the SAMs on UPD Ag. The reason for the odd-even effect on the Au substrates and their inversion on the UPD Ag is due to the orientation of the terminal methyl group and is covered extensively in chapter 4 and the literature.[20,38-40]

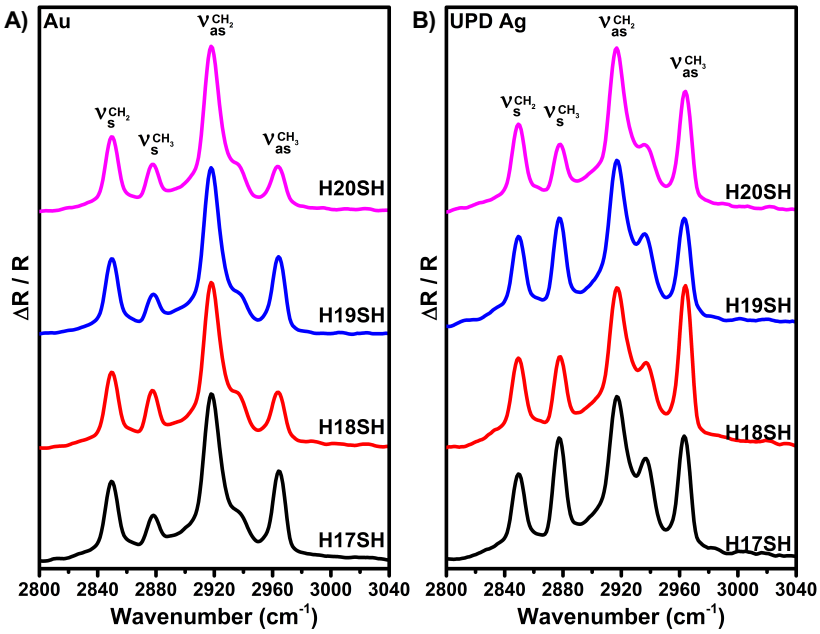

Figure 5.7. PM-IRRAS of the HmSH SAMs on (A) Au and (B) UPD Ag.

The PM-IRRAS spectra of the FSAMs are presented in Figure 5.8. Similarly, the FSAMs also display the $\nu_{as}^{CH_2}$ at 2918 ± 2cm^{-1} indicating well-ordered films. For the FSAMs on UPD Ag, there is a significant change in the intensities of the vibrations of the methylene units. The ratio of the symmetric to antisymmetric peaks for the FSAMs on UPD Ag is close to 1:1, whereas in the FSAMs on Au it is smaller. Similar observations have been made by Frey et al. on similarly structured partially fluorinated alkanethiols, F10HnSH where n = 11 and 17.[41] Frey et al. concluded that the hydrocarbon chains in the FSAMs on Ag have a smaller tilt angle than the FSAMs on Au. They attributed the decrease in intensity of the peaks on more parallel transition dipole moments of the C-H vibrations to the surface. According to the metal surface selection rule that dictates IRRAS techniques, the intensity of vibrations with vector components of the transition dipole moment more perpendicular to the surface will be enhanced, while those with vector components more parallel to the surface will not.

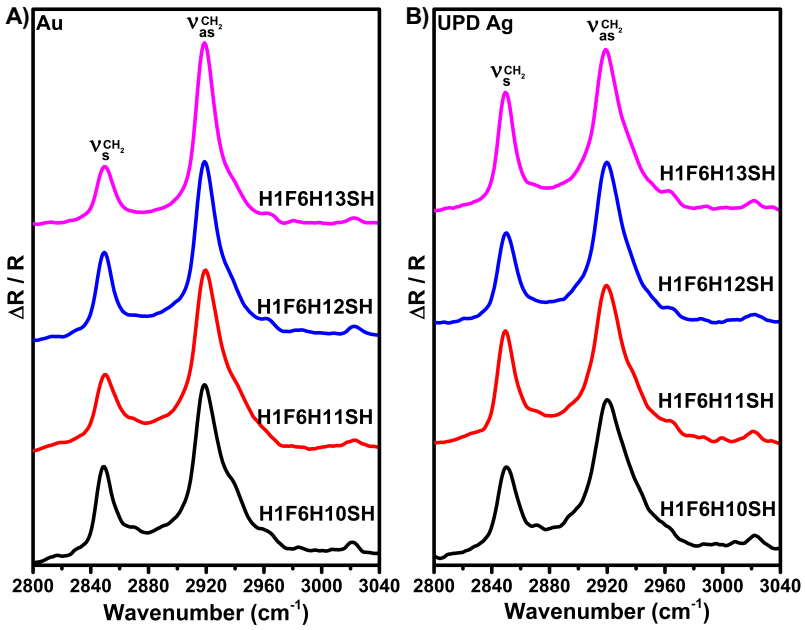

Figure 5.8. PM-IRRAS of the H1F6HnSH SAMs on (A) Au and (B) UPD Ag.

There is no apparent odd-even effect for the C-H symmetric or antisymmetric stretches, ~2963 and ~3022 cm^{-1}, associated with the terminal methyl group.[42] Conversely, there is an apparent odd-even effect in the intensity of the vibrations associated with the methylene units. For the FSAMs on Au, the relative ratio of the $\nu_s^{CH_2}$:$\nu_{as}^{CH_2}$ in the even chains is ~1:3 while in the odd chains it is ~1:2 (even and odd are with respect to the total number of carbons in the molecule); it appears that the symmetric vibrations are more intense in the odd chains than in the even chain. For the FSAMs on UPD Ag, the effect is inverted. The relative ratio of $\nu_s^{CH_2}$:$\nu_{as}^{CH_2}$ in the even chains is ~1:2 while in the odd chains it is closer to 1:1; it appears as if the intensity of the symmetric stretch is larger in the even chains than in the odd chains, opposite of the trend observed on Au. A reason for the observed odd-even effect might arise from differences in the orientation of the odd chains vis-à-vis the even ones on the same substrate. Previous spectroscopic research on normal alkanethiols has attributed the absence of an odd-even effect for the C-H stretches of the methylene units to the chains having a constant orientation on the surface.[23] For CF_3-terminated SAMs on Au, a slight odd-even effect in the C-H vibrations of the methylene units can be due to a possible change in their surface orientation in order to achieve the lowest possible interfacial energy.[20] Similarly, in phenyl-terminated SAMs the observed odd-even effect for the C-H vibrations of the CH_2 units was attributed to a twist or tilt that was likely caused by the terminal phenyl group interactions.[43] Taking these studies and the metal surface selection rule into account, it is reasonable to assume that the odd-even effect observed in the IR spectra is attributed to the differences in how the chains are twisted or tilted on the surface.

5.3.3. Wettability Studies

In order to probe the effect of the inverted dipole on contacting liquids, we choose several polar protic and aprotic liquids. The polar protic liquids were water (H_2O), glycerol (GL), and formamide (FA). The polar aprotic liquids used were dimethylsulfoxide (DMSO), dimethylformamide (DMF), and acetonitrile (ACN). Further, we used two liquids with a localized dipole, bromonaphtalene (BNP) and nitrobenzene (NB) and two nonpolar liquids, decalin (DC) and hexadecane (HD). Finally, in order to further test the surfaces, a fluorinated liquid, perfluorodecalin (FDC), was also included. Table 5.5 below lists the surface tensions of the liquids tested as well as the dipole moments of the polar liquids.[44-50]

Table 5.5. Surface Tension and Dipole Moments for Contacting Liquids Used in the Study.

Liquid	γ_{LV} (mN/m)	Dipole Moment (D)	Liquid	γ_{LV} (mN/m)	Dipole Moment (D)
H_2O	72.8	1.85	**NB**	43.8	4.22
GL	65.2	2.68	**BNP**	44.6	1.55
FA	57.3	3.73	**DC (cis)**	31.7	-
DMSO	43.5	3.96	**DC (trans)**	29.4	-
DMF	34.4	3.82	**HD**	27.1	-
ACN	28.7	3.92	**FDC**	19.2	-

The advancing contact angles for all the SAMs in this study are listed in Tables 5.6 and 5.7 below. The wetting properties of the hydrocarbon SAMs on Au and UPD Ag, plotted in Figures 5.9 and 5.10, show, in accordance with previous research, that the odd SAMs (**H17SH** and **H19SH**) are more wettable than the even SAMs (**H18SH** and **H20SH**) for Au substrates.[20] Additionally, the observed odd-even effect in the hydrocarbon SAMs on Au is inverted for the hydrocarbon SAMs on UPD Ag for all

liquids tested, which is consistent with the results presented in chapter 4 and the literature.[23,35]

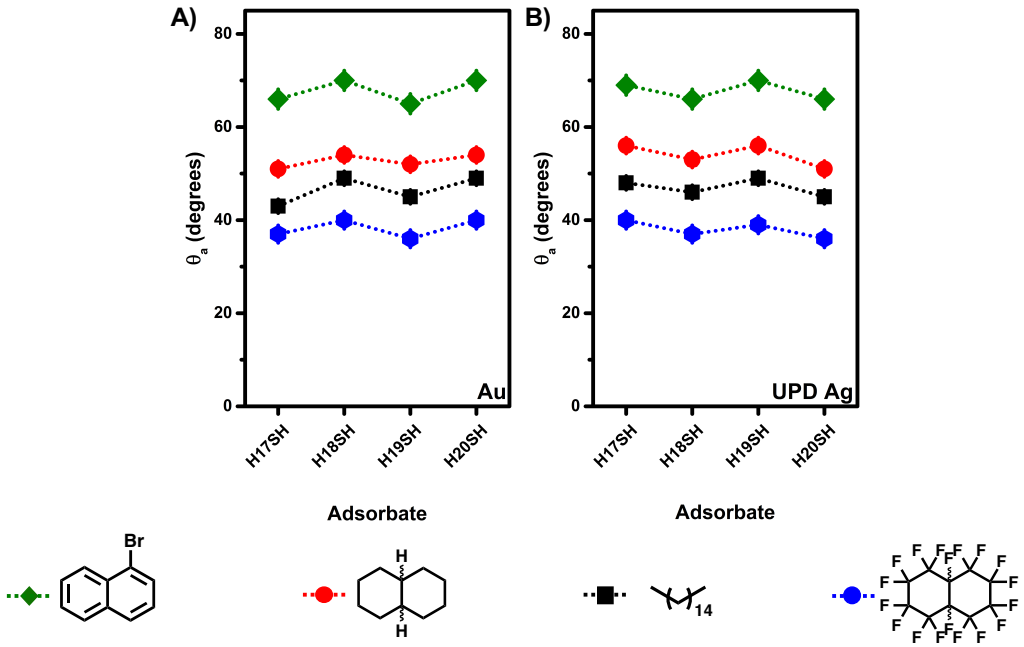

Figure 5.9. Advancing contact angles for BNP, DC, HD, and FDC on HmSH SAMs on (A) Au and (B) UPD surfaces. *Error bars fall within the symbol.*

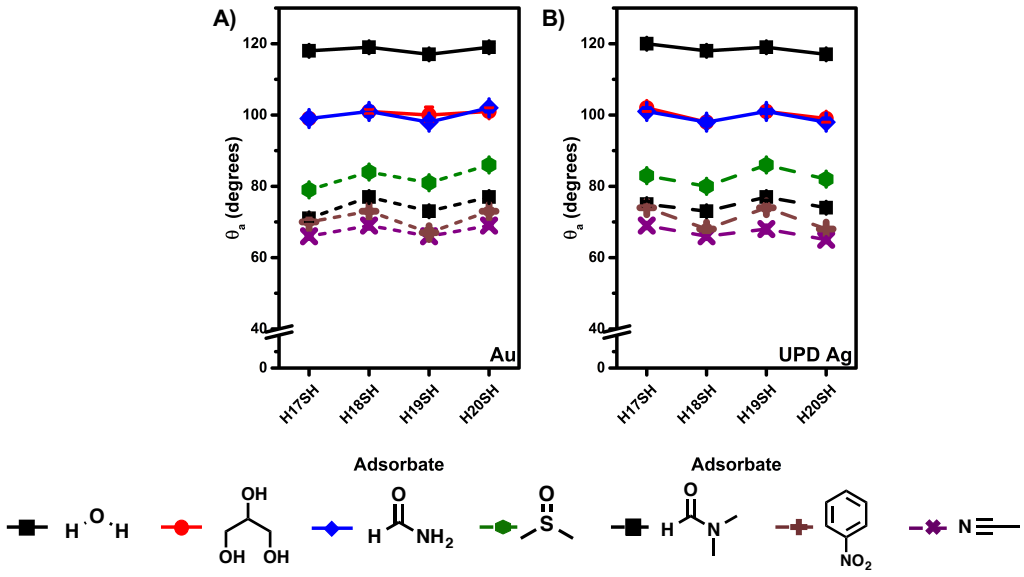

Figure 5.10. Advancing contact angles for H_2O, GL, FA, DMSO, DMF, NB, and ACN on HmSH SAMs on (A) Au and (B) UPD surfaces. *Error bars fall within the symbol.*

5.3.3.1. Wettability of Nonpolar and Weakly Polar Liquids on the FSAMs

The contact angles for the FSAMs using nonpolar and weakly polar liquids are presented in Figure 5.11 and Table 5.6. Overall, the contact angle values are similar between the two substrates. For the FSAMs on Au, there is no apparent odd-even effect in the wettability. However, previous research on these types of FSAMs on Au showed that the even SAMs (**H1F6H11SH** and **H1F6H13SH**) were more wettable than the odd SAMs (**H1F6H10SH** and **H1F6H12SH**).[20] A potential reason for the discrepancy could be due to the chains orienting themselves in such a way that the terminal group is pointed in the same direction, regardless of chain length. The electrochemical treatment of the Au substrates prior to SAM preparation, in addition to the elevated temperature during SAM formation, might alter the overall structure of the film.

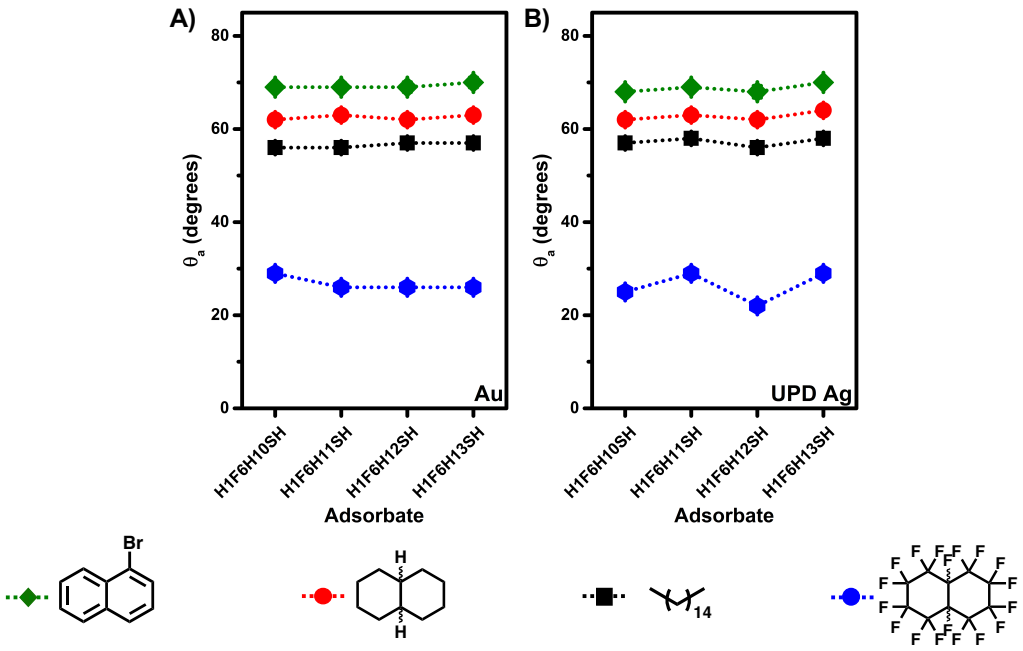

Figure 5.11. Advancing contact angles for BNP, DC, HD, and FDC on H1F6HnSH SAMs on (A) Au and (B) UPD surfaces. *Error bars fall within the symbol.*

For the FSAMs on UPD Ag, a distinct odd-even effect is only observed for the FDC, in which the odd SAMs (**H1F6H10SH** and **H1F6H12SH**) are more wettable than the even SAMs (**H1F6H11SH** and **H1F6H13SH**). From the contact angle data of the non-fluorinated liquids, the effect the dipole on the wettability of the SAMs is not apparent. However, from the wettability of the FDC it is probable that the CF_2 unit underneath the methyl is more exposed at the interface for the odd SAMs (**H1F6H10SH** and **H1F6H12SH**), leading to more sites for favorable interaction between the contacting liquid and the molecules in the film.

Table 5.6. Advancing Contact Angles (°) of the Nonpolar and Weakly Polar Liquids on HmSH SAMs and H1F6HnSH SAMs on Au and UPD Ag Surfaces.

Adsorbate	BNP	DC	HD	FDC
H17SH/Au	66	51	43	37
H18SH/Au	70	54	49	40
H19SH/Au	65	52	45	36
H20SH/Au	70	54	49	40
H17SH/UPD Ag	69	56	48	40
H18SH/UPD Ag	66	53	46	37
H19SH/UPD Ag	70	56	49	39
H20SH/UPD Ag	66	51	45	36
H1F6H10SH/Au	69	62	56	29
H1F6H11SH/Au	69	63	56	26
H1F6H12SH/Au	69	62	57	26
H1F6H13SH/Au	70	63	57	26
H1F6H10SH/UPD Ag	68	62	57	25
H1F6H11SH/UPD Ag	69	63	58	29
H1F6H12SH/UPD Ag	68	62	56	22
H1F6H13SH/UPD Ag	70	64	58	29

5.3.3.2. Wettability of Polar Liquids on the FSAMs

The contact angles of polar liquids on the FSAMs are shown in Figure 5.12 and Table 5.7. The contact angle values between the two substrates are similar. For the FSAMs on Au, there is an odd-even effect with GL and FA, in which the odd SAMs (**H1F6H10SH** and **H1F6H12SH**) are more wettable than the even SAMs (**H1F6H11SH** and **H1F6H13SH**), in accordance with what was observed in the literature.[20] However, the contact angle values of water do not show an odd-even effect on the Au surfaces. The values for the aprotic liquids DMSO and DMF on the Au surfaces in this study also do not show any odd-even effects, but do slightly increase as the hydrocarbon chain is extended. Following the reasoning mentioned in the analysis of the IR, if the molecules are orienting themselves in order to minimize their surface energy, this might result in the terminal CH_3-CF_2 bonds having similar tilts rather than the ~79° and ~19° previously observed for the odd and even chains, respectively. For the NB there is a very slight odd-even effect in the wettability data, in contrast to the strong effect seen in previous research for these FSAMs on evaporated Au.[20] In this case, if the chains are reorienting themselves to give similar tilt angles for the terminal group of both odd and even SAMs there might be a diminished effect from the dipole on the contact angle. Since NB has a much stronger dipole moment (4.22 D) than the other aprotic liquids DMF (3.82 D) and DMSO (3.96 D), it may have a stronger interaction with the surface dipole. The other polar liquid, ACN (3.92 D) does not show an odd-even effect on the FSAMs on Au. ACN is a small molecule with a low surface tension which facilitates its intercalation into the top portion of the film. Additionally, the larger vdW diameter of the fluorinated segment compared to the CH_3 group, ~5.6Å and ~4.2Å respectively, allows for a tightly

packed fluorinated segment and loosely packed methyl termini which allows smaller liquids to intercalate into the top portion of the film. [20,32-33]

For the FSAMs on UPD Ag, there is no odd-even effect in the wettability of water, DMSO, and NB. Moreover, there is a slight reversal, compared to the FSAMS on Au, of the odd-even effect for the wettability of FA and GL, in which the even SAMs (**H1F6H11SH** and **H1F6H13SH**) are more wettable than the odd SAMs (**H1F6H10SH** and **H1F6H12SH**). The reason for the reversal of the wettability trend for SAMs on UPD Ag versus Au has been attributed to the different binding geometry of the sulfur on the respective surfaces, which causes a change in the orientation of the terminal group. Assuming the same reasoning for the FSAMs in this study, the inversion of the odd-even effect will also be due to a change in the orientation of the terminal group.

Interestingly, the contact angles of DMF and ACN on the FSAMs on UPD Ag show a distinct odd-even effect that is opposite to the polar protic liquids on the same substrate; the odd SAMs (**H1F6H10SH** and **H1F6H12SH**) are more wettable than the even SAMs (**H1F6H11SH** and **H1F6H13SH**). Following the FDC data, it is likely that the CF_2 unit may be exposed at the interface for the odd SAMs, leading to the conclusion that the adsorbate must be reorienting in such a way to tilt the terminal CH_3 group and the interfacial dipole. A reversal in the odd-even effect between polar protic and polar aprotic liquids on a gold substrate has been attributed to the polarity of the surface and the ability of the interfacial dipoles of the liquid to reorient.[20] Our FSAMs have the electropositive portion of the dipole at the interface while the electronegative aspect is inside the film. When on the surface, the hydrogen bond networks present in the protic liquids lock the position of the interfacial molecules of the liquid. Studies on the liquid-

vapor interface of water have revealed the presence of a free OH at the interface.[51-52] As a result, for the protic liquids, the positive aspect of the dipole is exposed at the interface and is in contact with the SAM surface. Since the liquids are held together by hydrogen bonding networks, there is an unfavorable electrostatic interaction when the direction of the dipoles on the SAMs are oriented more upwards, resulting in a higher contact angle, i.e. GL on **H1F6H10SH** and **H1F6H12SH**. For the aprotic liquids, since there are no hydrogen bond networks restricting the mobility of the interfacial liquid molecules they will reorient themselves to interact favorably with the dipoles of the SAM surface. Consequently, when the direction of the dipoles on the SAM are more upward, a greater dipole-dipole interaction will occur between the surface and the contacting liquid, which will lead to a lower contact angle, i.e. DMF on **H1F6H10SH** and **H1F6H12SH**.

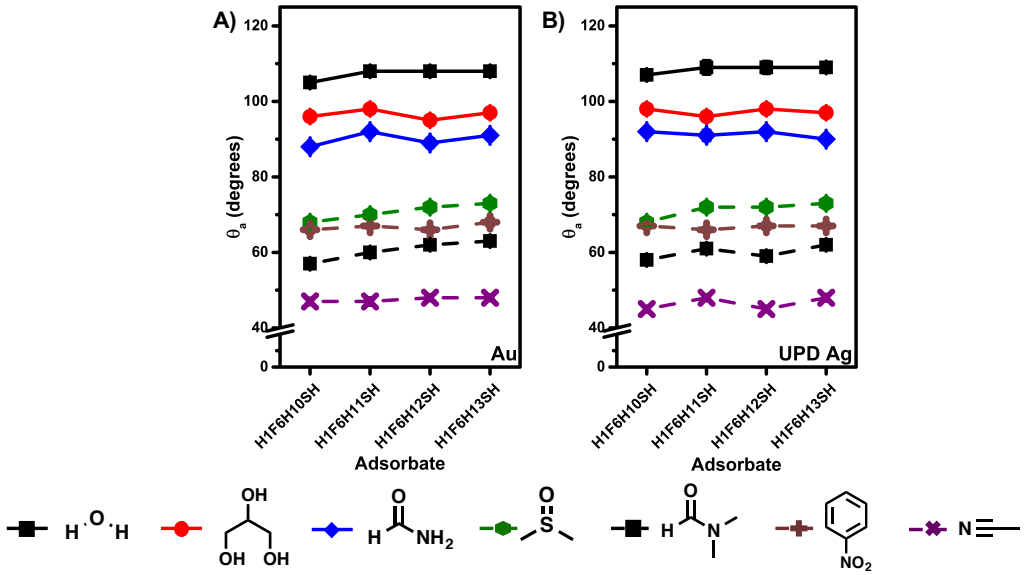

Figure 5.12. Advancing contact angles for H_2O, GL, FA, DMSO, DMF, NB, and ACN on H1F6HnSH SAMs on (A) Au and (B) UPD surfaces. *Error bars fall within the symbol.*

Table 5.7. Advancing Contact Angles (°) of the Polar Liquids on HmSH SAMs and H1F6HnSH SAMs on Au and UPD Ag Surfaces.

Adsorbate	H_2O	GL	FA	DMSO	DMF	ACN	NB
H17SH/Au	118	99	99	79	71	66	70
H18SH/Au	119	101	101	84	77	69	73
H19SH/Au	117	100	98	81	73	66	67
H20SH/Au	119	101	102	86	77	69	73
H17SH/UPD Ag	120	102	101	83	75	69	74
H18SH/UPD Ag	118	98	98	80	73	66	68
H19SH/UPD Ag	119	101	101	86	77	68	74
H20SH/UPD Ag	117	99	98	82	74	65	68
H1F6H10SH/Au	105	96	88	68	57	47	66
H1F6H11SH/Au	108	98	92	70	60	47	67
H1F6H12SH/Au	108	95	89	72	62	48	66
H1F6H13SH/Au	108	97	91	73	63	48	68
H1F6H10SH/UPD Ag	107	98	92	68	58	45	67
H1F6H11SH/UPD Ag	109	96	91	72	61	48	66
H1F6H12SH/UPD Ag	109	98	92	72	59	45	67
H1F6H13SH/UPD Ag	109	97	90	73	62	48	67

5.4. Conclusions

The CH_3-terminated partially fluorinated alkanethiols were used to form SAMs on Au and UPD Ag along with their hydrocarbon analogs. Ellipsometry and XPS analysis confirmed that the SAMs are best formed at room temperature with further equilibration at 50°C resulting in thicker films for the SAMs on UPD Ag. Analysis of the C 1s photoelectrons determined the SAMs on UPD Ag have higher packing densities than the SAMs on Au, which likely arises from the molecules being more upright on the silver

surfaces. PM-IRRAS analysis showed that the FSAMs on both substrates are well-ordered, with the hydrocarbon chains adopting a trans-extended conformation. Additionally, the IR spectra showed an odd-even effect in the relative ratio of $\nu_s^{CH}{}_2$:$\nu_{as}^{CH}{}_2$ that likely arises from a reorientation of the molecules on the surface in order to achieve lower surface energies.

The wettability of the nonpolar liquids for the FSAMs on Au give the impression that the terminal methyl groups in the chains are all pointed in a similar direction. For the FSAMs on UPD Ag, the wettability of the nonpolar liquids, FDC in particular, reveal that the underlying CF_2 is potentially exposed at the interface of the odd FSAMs (**H1F6H10SH** and **H1F6H12SH**) which tilts the terminal CH_3 group and the dipole for these SAMs, leading to a more wettable surface. However, in the even FSAMs (**H1F6H11SH** and **H1F6H13SH**) the dipole may be more upright. The contact angles of the polar liquids for the FSAMs on Au mostly agree with the assessment of the nonpolar liquids, with the exception of the protic liquids GL and FA. Interestingly, for the FSAMs on UPD Ag, a slight odd-even effect with GL and FA was observed that is inverted from the one on Au; the odd SAMs (**H1F6H10SH** and **H1F6H12SH**) are more wettable than the even SAMs (**H1F6H11SH** and **H1F6H13SH**).

It is apparent from the wettability data that the electrochemical treatment is affecting the structure of the resulting FSAMs making it difficult to construct an image of the effect of the substrate on the orientation of the dipole. In order to obtain a better understanding of the phenomena presented in this study, further analysis, such as orientation analysis of the terminal group of the current SAMs, in addition to further

studies on evaporated Au and Ag surfaces without the electrochemical treatment, is needed.

5.5. References

1. Schmaltz, T.; Gothe, B.; Krause, A.; Leitherer, S.; Steinrück, H.-G.; Thoss, M.; Clark, T.; Halik, M. Effect of Structure and Disorder on the Charge Transport in Defined Self-Assembled Monolayers of Organic Semiconductors. *ACS Nano* **2017**, *11*, 8747–8757.
2. Calhoun, M. F.; Sanchez, J.; Olaya, D.; Gershenson, M. E.; Podzorov, V. Electronic Functionalization of the Surface of Organic Semiconductors with Self-Assembled Monolayers. *Nat. Mater.* **2008**, *7*, 84–89.
3. Liu, D.; He, Z.; Su, Y.; Diao, Y.; Mannsfeld, S. C. B.; Bao, Z.; Xu, J.; Miao, Q. Self-Assembled Monolayers of Cyclohexyl-Terminated Phosphonic Acids as a General Dielectric Surface for High-Performance Organic Thin-Film Transistors. *Adv. Mater.* **2014**, *26*, 7190–7196.
4. Zhang, X.; Du, X.; Huang, X.; Lv, Z. Creating Protein-Imprinted Self-Assembled Monolayers with Multiple Binding Sites and Biocompatible Imprinted Cavities. *J. Am. Chem. Soc.* **2013**, *135*, 9248–9251.
5. Prieto-Simón, B.; Saint, C.; Voelcker, N. H. Electrochemical Biosensors Featuring Oriented Antibody Immobilization Via Electrografted and Self-Assembled Hydrazide Chemistry. *Anal. Chem.* **2014**, *86*, 1422–1429.
6. Feyzizarnagh, H.; Haushalter, E. F.; Grams, E. K.; Cameron, B. D.; Yoon, D.-Y.; Kim, D.-S. Protein Sensing with Aptamer Immobilized on an Antifouling Binary Self-Assembled Monolayer. *Ind. Eng. Chem. Res.* **2015**, *54*, 4072–4077.

7. Bandyopadhyay, D.; Prashar, D.; Luk, Y.-Y. Anti-Fouling Chemistry of Chiral Monolayers: Enhancing Biofilm Resistance on Racemic Surface. *Langmuir* **2011**, *27*, 6124–6131.

8. Rodriguez Emmenegger, C.; Brynda, E.; Riedel, T.; Sedlakova, Z.; Houska, M.; Alles, A. B. Interaction of Blood Plasma with Antifouling Surfaces. *Langmuir* **2009**, *25*, 6328–6333.

9. Filip, J.; Popelka, A.; Bertok, T.; Holazova, A.; Osicka, J.; Kollar, J.; Ilcikova, M.; Tkac, J.; Kasak, P. Ph-Switchable Interaction of a Carboxybetaine Ester-Based Sam with DNA and Gold Nanoparticles. *Langmuir* **2017**, *33*, 6657–6666.

10. Ye, H.; Wang, L.; Huang, R.; Su, R.; Liu, B.; Qi, W.; He, Z. Superior Antifouling Performance of a Zwitterionic Peptide Compared to an Amphiphilic, Non-Ionic Peptide. *ACS Appl. Mater. Interfaces* **2015**, *7*, 22448–22457.

11. Lee, T. R.; Barriet, D.; Moore, H. J. Structure and Properties of Fluorinated Organic Thin Films: Implications for Mems Devices. *NDSI Digest* **2005**, *2*, 93.

12. Bhushan, B.; Kasai, T.; Kulik, G.; Barbieri, L.; Hoffmann, P. Afm Study of Perfluoroalkylsilane and Alkylsilane Self-Assembled Monolayers for Anti-Stiction in Mems/Nems. *Ultramicroscopy* **2005**, *105*, 176–188.

13. Colorado, R., Jr.; Lee, T. R. Wettabilities of Self-Assembled Monolayers on Gold Generated from Progressively Fluorinated Alkanethiols. *Langmuir* **2003**, *19*, 3288–3296.

14. Fukushima, H.; Seki, S.; Nishikawa, T.; Takiguchi, H.; Tamada, K.; Abe, K.; Colorado, R.; Graupe, M.; Shmakova, O. E.; Lee, T. R. Microstructure,

Wettability, and Thermal Stability of Semifluorinated Self-Assembled Monolayers (Sams) on Gold. *J. Phys. Chem. B* **2000**, *104*, 7417–7423.

15. Castner, D. G.; Grainger, D. W. *Fluorinated Surfaces, Coatings, and Films*; American Chemical Society: 2001; Vol. 787. p. 260.

16. Zenasni, O.; Jamison, A. C.; Lee, T. R. The Impact of Fluorination on the Structure and Properties of Self-Assembled Monolayer Films. *Soft Matter* **2013**, *9*, 6356–6370.

17. Herrero, E.; Buller, L. J.; Abruña, H. D. Underpotential Deposition at Single Crystal Surfaces of Au, Pt, Ag and Other Materials. *Chem. Rev.* **2001**, *101*, 1897–1930.

18. Graupe, M.; Koini, T.; Kim, H. I.; Garg, N.; Miura, Y. F.; Takenaga, M.; Perry, S. S.; Lee, T. R. Wettability and Friction of Cf_3-Terminated Monolayer Films on Gold. *Mater. Res. Bull.* **1999**, *34*, 447–453.

19. Graupe, M.; Takenaga, M.; Koini, T.; Colorado, R., Jr.; Lee, T. R. Oriented Surface Dipoles Strongly Influence Interfacial Wettabilities. *J. Am. Chem. Soc.* **1999**, *121*, 3222–3223.

20. Zenasni, O.; Marquez, M. D.; Jamison, A. C.; Lee, H. J.; Czader, A.; Lee, T. R. Inverted Surface Dipoles in Fluorinated Self-Assembled Monolayers. *Chem. Mater.* **2015**, *27*, 7433–7446.

21. Porter, M. D.; Bright, T. B.; Allara, D. L.; Chidsey, C. E. D. Spontaneously Organized Molecular Assemblies. 4. Structural Characterization of *N*-Alkyl Thiol Monolayers on Gold by Optical Ellipsometry, Infrared Spectroscopy, and Electrochemistry. *J. Am. Chem. Soc.* **1987**, *109*, 3559–3568.

22. Jennings, G. K.; Laibinis, P. E. Underpotentially Deposited Metal Layers of Silver Provide Enhanced Stability to Self-Assembled Alkanethiol Monolayers on Gold. *Langmuir* **1996**, *12*, 6173–6175.

23. Laibinis, P. E.; Whitesides, G. M.; Allara, D. L.; Tao, Y. T.; Parikh, A. N.; Nuzzo, R. G. Comparison of the Structures and Wetting Properties of Self-Assembled Monolayers of *N*-Alkanethiols on the Coinage Metal Surfaces, Copper, Silver, and Gold. *J. Am. Chem. Soc.* **1991**, *113*, 7152–7167.

24. Castner, D. G.; Hinds, K.; Grainger, D. W. X-Ray Photoelectron Spectroscopy Sulfur 2p Study of Organic Thiol and Disulfide Binding Interactions with Gold Surfaces. *Langmuir* **1996**, *12*, 5083–5086.

25. Ishida, T.; Hara, M.; Kojima, I.; Tsuneda, S.; Nishida, N.; Sasabe, H.; Knoll, W. High Resolution X-Ray Photoelectron Spectroscopy Measurements of Octadecanethiol Self-Assembled Monolayers on Au(111). *Langmuir* **1998**, *14*, 2092–2096.

26. Heister, K.; Johansson, L. S. O.; Grunze, M.; Zharnikov, M. A Detailed Analysis of the C 1s Photoemission of N-Alkanethiolate Films on Noble Metal Substrates. *Surf. Sci.* **2003**, *529*, 36–46.

27. Chinwangso, P. Self-Assembled Monolayers Generated from Custom-Tailored Spiroalkanedithiols Offer Unprecedented Multi-Component Interfaces. Ph.D., University of Houston, 2009.

28. Pflaum, J.; Bracco, G.; Schreiber, F.; Colorado Jr, R.; Shmakova, O. E.; Lee, T. R.; Scoles, G.; Kahn, A. Structure and Electronic Properties of Ch3- and Cf3-Terminated Alkanethiol Monolayers on Au(111): A Scanning Tunneling

Microscopy, Surface X-Ray and Helium Scattering Study. *Surf. Sci.* **2002**, *498*, 89–104.

29. Barriet, D.; Lee, T. R. Fluorinated Self-Assembled Monolayers: Composition, Structure and Interfacial Properties. *Curr. Opin. Colloid Interface Sci.* **2003**, *8*, 236–242.

30. Marquez, M. D.; Zenasni, O.; Jamison, A. C.; Lee, T. R. Homogeneously Mixed Monolayers: Emergence of Compositionally Conflicted Interfaces. *Langmuir* **2017**, *33*, 8839–8855.

31. Kim, H. I.; Koini, T.; Lee, T. R.; Perry, S. S. Systematic Studies of the Frictional Properties of Fluorinated Monolayers with Atomic Force Microscopy: Comparison of CF_3- and CH_3-Terminated Films. *Langmuir* **1997**, *13*, 7192–7196.

32. Holger, S.; Vancso, G. J. Afm Study on Lattice Orientation and Tribology of Sams of Fluorinated Thiols and Disulfides on Au(111): The Influence of the Molecular Structure. *ACS Symp. Ser.* **2001**, *787*, 15–30.

33. Tamada, K.; Ishida, T.; Knoll, W.; Fukushima, H.; Colorado, R., Jr.; Graupe, M.; Shmakova, O. E.; Lee, T. R. Molecular Packing of Semifluorinated Alkanethiol Self-Assembled Monolayers on Gold: Influence of Alkyl Spacer Length. *Langmuir* **2001**, *17*, 1913–1921.

34. Ishida, T.; Nishida, N.; Tsuneda, S.; Hara, M.; Sasabe, H.; Knoll, W. Alkyl Chain Length Effect on Growth Kinetics of N-Alkanethiol Self-Assembled Monolayers on Gold Studied by X-Ray Photoelectron Spectroscopy. *Jpn. J. Appl. Phys.* **1996**, *35*, L1710–L1713.

35. Chen, I. W. P.; Chen, C.-C.; Lin, S.-Y.; Chen, C.-h. Effect of Underpotentially Deposited Adlayers on Sulfur Bonding Schemes of Organothiols Self-Assembled on Polycrystalline Gold: Sp or Sp3 Hybridization. *J. Phys. Chem. B* **2004**, *108*, 17497–17504.

36. Snyder, R. G.; Strauss, H. L.; Elliger, C. A. Carbon-Hydrogen Stretching Modes and the Structure of N-Alkyl Chains. 1. Long, Disordered Chains. *J. Phys. Chem.* **1982**, *86*, 5145–5150.

37. MacPhail, R. A.; Strauss, H. L.; Snyder, R. G.; Elliger, C. A. Carbon-Hydrogen Stretching Modes and the Structure of N-Alkyl Chains. 2. Long, All-Trans Chains. *J. Phys. Chem.* **1984**, *88*, 334–341.

38. Thuo, M. M.; Reus, W. F.; Nijhuis, C. A.; Barber, J. R.; Kim, C.; Schulz, M. D.; Whitesides, G. M. Odd−Even Effects in Charge Transport across Self-Assembled Monolayers. *J. Am. Chem. Soc.* **2011**, *133*, 2962–2975.

39. Baghbanzadeh, M.; Simeone, F. C.; Bowers, C. M.; Liao, K.-C.; Thuo, M.; Baghbanzadeh, M.; Miller, M. S.; Carmichael, T. B.; Whitesides, G. M. Odd–Even Effects in Charge Transport across N-Alkanethiolate-Based Sams. *J. Am. Chem. Soc.* **2014**, *136*, 16919–16925.

40. Jiang, L.; Sangeeth, C. S. S.; Nijhuis, C. A. The Origin of the Odd–Even Effect in the Tunneling Rates across Egain Junctions with Self-Assembled Monolayers (Sams) of N-Alkanethiolates. *J. Am. Chem. Soc.* **2015**, *137*, 10659–10667.

41. Frey, S.; Heister, K.; Zharnikov, M.; Grunze, M.; Tamada, K.; Colorado, R.; Graupe, M.; Shmakova, O. E.; Lee, T. R. Structure of Self-Assembled

Monolayers of Semifluorinated Alkanethiols on Gold and Silver Substrates. *Isr. J. Chem.* **2000**, *40*, 81–97.

42. Research on CD_3-Terminated FSAMs has determined the CH_3 symmetric and antisymmetric stretching vibrations for these types of FSAMs are at 2963 and 3022 cm^{-1}.

43. Lee, S.; Puck, A.; Graupe, M.; Colorado, R.; Shon, Y.-S.; Lee, T. R.; Perry, S. S. Structure, Wettability, and Frictional Properties of Phenyl-Terminated Self-Assembled Monolayers on Gold. *Langmuir* **2001**, *17*, 7364–7370.

44. Jańczuk, B.; Białłopiotrowicz, T. Surface Free-Energy Components of Liquids and Low Energy Solids and Contact Angles. *J. Colloid Inter. Sci.* **1989**, *127*, 189–204.

45. Fowkes, F. M.; Riddle Jr, F. L.; Pastore, W. E.; Weber, A. A. Interfacial Interactions between Self-Associated Polar Liquids and Squalane Used to Test Equations for Solid—Liquid Interfacial Interactions. *Colloid Surface* **1990**, *43*, 367–387.

46. Smallwood, I. M. *Handbook of Organic Solvent Properties*; John Wiley & Sons: New York, 1996.

47. Yaws, C. L. *Chemical Properties Handbook Physical, Thermodynamic, Environmental, Transport, Safety, and Health Related Properties for Organic and Inorganic Chemicals*; McGraw-Hill: New York, 1999.

48. Nelson, R. D.; Lide, D. R.; Maryott, A. A. Selected Values of Electric Dipole Moments for Molecules in the Gas Phase. Natl. Stnds. Ref. Data Ser.: Natl. Bur. Stnds. 10, 1967.

49. Riddick, J. A.; Bunger, W. B.; Sakano, T. K. *Organic Solvents*; Fourth ed.; John Wiley & Sons: New York, 1986.

50. Rizk, H. A.; Elanwar, I. M. Dipole Moments of Glycerol, Isopropyl Alcohol, and Isobutyl Alcohol. *Can. J. Chem.* **1968**, *46*, 507–513.

51. Du, Q.; Superfine, R.; Freysz, E.; Shen, Y. R. Vibrational Spectroscopy of Water at the Vapor/Water Interface. *Phys. Rev. Lett.* **1993**, *70*, 2313–2316.

52. Du, Q.; Freysz, E.; Shen, Y. R. Surface Vibrational Spectroscopic Studies of Hydrogen Bonding and Hydrophobicity. *Science* **1994**, *264*, 826.

Chapter 6: Conclusions

6.1. Conclusions

Self-assembled monolayers (SAMs) enjoy use in a variety of applications. The ability to chemically modify the adsorbates used in generating SAMs, specifically by incorporating fluorine atoms, gives thin films with hydrophobic and oleophobic properties as well as reduced adhesion and friction coefficients. The latter features make fluorinated thin films attractive candidates for a variety of applications. The focus of this dissertation is on the partially fluorinated alkanethiols on gold that give thin films with surface dipoles, FC–HC and HC–FC, and methods used to modulate them either through synthetic means or via modification to the metal substrate. All of the generated SAMs were characterized with the following techniques: ellipsometry, to measure thickness; X-ray photoelectron spectroscopy (XPS), to determine chemical composition; polarization-modulation infrared reflection-absorption spectroscopy (PM-IRRAS), to determine relative crystallinity of the films; and contact angle goniometry, to probe the interfacial dipoles.

Chapter 2 introduced a new type of partially fluorinated adsorbate of the form $CH_3(CF_2)(CH_2)_{11}SH$, where n = 10 – 13; **H1F6HnSH**, that bear a HC-FC dipole at the interface. The H1F6HnSH SAMs were evaluated and compared to a series of CF_3-terminated alkanethiols, **F1HmSH**, and normal alkanethiols of the same carbon count. The H1F6HnSH FSAMs proved to have alkyl spacers with the same crystallinity as the CF_3-termianted and normal alkanethiol SAMs. The

larger vdW diameter of the fluorinated segment compared to the hydrocarbon portion of the FSAMs cause the films to have a lower packing density than both the CF_3 and hydrocarbon SAMs. Further analysis of the FSAMs with various contacting liquids, polar and nonpolar, gave substantial insight into the effect the inverted HC-FC dipole has on the interfacial energy of the films. The contact angle values of the nonpolar liquids show that the H1F6HnSH SAMs are more oleophobic than the hydrocarbon SAMs, likely arising from exposure of the underlying CF_2 at the interface. The H1F6HnsH were also more wettable with polar liquids than the hydrocarbon and CF_3-terminated analogs. The enhanced wettability of the H1F6HnSH is likely arising from the presence of the HC-FC dipole and the difference in the sizes of the methyl group atop the fluorinated segment. An observed odd-even effect is also seen with the polar protic contacting liquids that is opposite for the aprotic liquids on the H1F6HnSH films due to a combination of dipole-dipole interactions and H-bonding within the contacting liquids that restrict the molecular organization/reorientation of the liquid molecules within the interfacial region of the liquid drop in response to the dipoles at the liquid− SAM interface.

To further explore the effect of the HC-FC dipole, chapter 3 examines a series of partially fluorinated alkanethiols with a progressively extended alkyl chain atop six fluorocarbons and an alkyl spacer of 11 hydrocarbons, $H(CH_2)_n(CF_2)_6(CH_2)_{11}SH$, where n = 1 – 7; HnF6H11SH. In this series, the HC-FC dipole is systematically buried into the film. The corresponding Monolayers were formed using a THF / EtOH mixture. Analysis with XPS showed that the

packing density of the SAMs increases as the top alkyl chain is extended. The increased vdW interactions between the top alkyl chains are likely causing the increase in the packing density. Consequently, due to the smaller vdW diameter of the alkyl chain compared to the fluorinated segment, a slight disorder is induced between the fluorocarbons. Nonetheless, the FSAMs appear to be well ordered with the alkyl chains being in a *trans*-extended conformation. An odd-even effect is observed in the C-H stretching vibrations of the methyl groups, except for the H1F6H11SH, that is the opposite of trend is observed in the hydrocarbon SAMs of the same carbon counts suggesting the orientation of the terminal methyl group is opposite in the HnF6H11SH FSAMs. Furthermore, the total number of carbons in the top alkyl chain dictates this trend as oppose to the total carbon number in chains in SAMs of normal alkanethiols. Wettability studies using a variety of liquids, polar and nonpolar, found that the effect of the dipole is diminished after 3 hydrocarbons in the top chain, and for the longer chains an odd-even effect is observed that is the opposite of the hydrocarbon SAMs; an observation that further corroborates the analysis made from the surface IR spectra.

To further modulate the dipole present in CF_3-terminated FSAMs, chapter 4 explores the use of an electrochemically modified gold substrate with silver as a means for altering the geometrical orientation of the adsorbates and their terminial dipoles. Specifically, a monolayer of silver was generated via underpotential deposition (UPD), and subsequently used to make SAMs from the CF_3-termianted alkanethiols. The resulting films were compared to their hydrocarbon analogs on

both gold and UPD Ag substrates. Alkanethiols on gold bind with a different geometry on silver substrates. For the UPD Ag, we anticipated the adsorbates to have similar binding geometry as alkanethiols on bulk silver. Analysis of the FSAMs and the hydrocarbon SAMs supported the latter assumption. All of the SAMs formed on the UPD Ag had thicker films, ~ 3Å, than those on gold due to the more upright orientation by which adsorbates assemble on the UPD Ag surface. This orientation of the chains on the UPD Ag surfaces also led to a higher packing density for both types of SAMs, as determined by XPS. Although the SAMs on UPD Ag are thicker and more tightly packed, their relative crystallinity is similar to the SAMs on Au. Wettability studies using several contacting liquids showed odd-even effects for the SAMs on UPD Ag that were the opposite of those observed on Au surfaces. The reversal of the odd-even effect in the wettability data was attributed to a change in the orientation of the terminal groups for the SAMs on UPD Ag.

Chapter 5 is a continuation from the work done in the previous chapter. In chapter 4, we were able to modulate the dipole of the CF_3-termianted SAMs by the incorporation of a monolayer of silver (UPD Ag). In chapter 5, we used Au and UPD Ag substrates to make SAMs with an HC-FC dipole using the H1F6HnSH series. The H1F6HnSH SAMs on UPD Ag also resulted in thicker films than the SAMs on the Au substrate. Monolayers on the UPD Ag substrates had higher packing densities than the corresponding SAMs on Au, that likely arise from the more upward orientation of the molecules on the former substrate. In the IR spectra of the C-H stretching region, an odd-even effect is observed with

the vibrations associated with the methylenes. This observation can be attributed to a reorientation of the molecules on the surface in order to reduce the overall energy of the SAM assembly. The wettability of the FSAMs in addition to the characterization of the SAMs using ellipsometry and PM-IRRAS indicate that the orientation of the SAMs on the electrochemically treated substrates is different from the evaporated Au surface making it difficult to interpret how the HC-FC dipole is modulated on these types of substrates.

Appendix 1. List of Publications and Presentations

A.1. List of Publications

1. **Marquez, M. D**.; Jamison, A. C.; Zenasni, O.; Lee, T. R. Homogenously Mixed Monolayers: The Emergence of Compositionally Conflicted Interfaces. *Langmuir* **2017**, *33*, 8839–8850.

2. Chinwangso, P.; Lee, H. J.; Jamison, A. C.; **Marquez, M. D.**; Lee, T. R. Structure, Wettability, and Thermal Stability of Organic Thin Films on Gold Generated from the Molecular Self-Assembly of Unsymmetrical Oligo(ethylene glycol) Spiroalkanedithiols. *Langmuir* **2017,** *33*, 1751–1762.

3. Shakiba, A.; Zenasni, O.; **Marquez, M. D.**; Lee, T. R. Advanced Drug Delivery via Self-Assembled Monolayer-Coated Nanoparticles. *AIMS Bioengineering*, Submitted **2016**.

4. Xie, M.; Wang, S.; Singh, A.; Cooksey, T. J.; **Marquez, M. D.**; Bhattarai, A.; Kourentzi, K.; Robertson, M. L. Fluorrophore Exchange Kinetics in Block Copolymer Micelles with Varying Solvent-Fluorophore and Solvent-Polymer Interactions. *Soft Matter* **2016**, *12*, 6196–6205

5. Zenasni, O.; **Marquez, M. D**.; Jamison, A. C.; Lee, H. J.; Czader, A.; Lee, T. R. Inverted Surface Dipoles in Fluorinated Self–Assembled Monolayers. *Chem. Mater.* **2015**, *27*, 7433–7446.

6. Zenasni, O.; Jamison, A. C.; **Marquez, M. D**.; Lee, T. R. Self–Assembled Monolayers on Gold Generated from Terminally Perfluorinated Alkanethiols

Bearing Propyl Vs. Ethyl Hydrocarbon Spacers. *J. Fluorine Chem*. **2014**, *168*, 128–136.

A.2. List of Presentations

1. **Marquez, M. D**.; Rodriguez, D.; Zenasni, O.; Lee, T. R. Reversing the Odd-Even Effects in Self-Assembled Monolayers Using UPD Silver. Poster Presentation at the 254th ACS National Meeting, Washington, D.C., **2017**.

2. Rodriguez, D.; **Marquez, M. D**.; Zenasni, O.; Baldelli, S.; Lee, T. R. Sum Frequency Generation Spectroscopy of Terminally Fluorinated Self-Assembled Monolayers on UPD Silver and Bare Gold Substrates. Poster Presentation at the 254th ACS National Meeting, Washington, D.C., **2017**.

3. Yu, T.; **Marquez, M. D.**; Zenasni, O.; Lee, T. R. Polymer Mimics Using Cyclohexyl-Termianted Derivatives as Organic thin-Films. Poster Presentation at the 254th ACS National Meeting, Washington, D.C., **2017**.

4. Ghanbaripour, R.; Zenasni, O.; **Marquez, M**.; Lee, T. R. Synthesis and Characterization of Methyl-Partially Fluorinated Alkanethiols. Poster Presentation at the 254th ACS National Meeting, Washington, DC, **2017**.

5. **Marquez, M. D**.; Zenasni, O.; Lee, T. R. Inverted Surface Dipoles in Fluorinated Self-Assembled Monolayers. Poster Presentation at University of Houston International Symposium on Chemical Sciences, Houston, TX, **2017**.

6. **Marquez, M. D.**; Rodriguez, D.; Zenasni, O.; Lee, T. R. Inverted Interfacial Dipoles Fluorinated Self-assembled monolayers on UPD silver. Poster presentation at the 72nd ACS Southwest Regional Meeting, Galveston, TX, **2016**.

7. Castilleja, D. J.; **Marquez, M. D.**; Zenasni, O.; Lee, T. R. Lattice Characterization of Fluorinated Alkanethiols via Atomic Force Microscopy.

Poster presentation at the 72nd ACS Southwest Regional Meeting, Galveston, TX, **2016**.

8. Yu, T; **Marquez, M. D.**; Lee, T. R. Synthesis and Characterization of Petafluorophenyl-Terminated Self-Assembled Monolayers on Gold. Poster presentation at the 72nd ACS Southwest Regional Meeting, Galveston, TX, **2016**.

9. **Marquez, M. D.**; Zenasni, O.; Lee, T. R. Wettability and Packing Structure of Partially Fluorinated [illegible]-Alkylated Self-Assembled Monolayers. Sci-Mix poster presentation at the 251st ACS National Meeting & Exposition, San Diego, CA, **2016**.

10. **Marquez, M. D.**; Zenasni, O.; Lee, H. J.; Lee, T. R. Synthesis and Characterization of Partially Fluroinated Self-Assembled Monolayers Having and Inverted Surface Dipole. Oral presentation at the 249th ACS National Meeting & Exposition, Denver, CO, **2015**.

11. **Marquez, M. D.**; Zenasni, O.; Lee, H. J.; Lee, T. R. Synthesis and Characterization of Partially Fluroinated Self-Assembled Monolayers Having and Inverted Surface Dipole. Sci-Mix poster presentation at the 249th ACS National Meeting & Exposition, Denver, CO, **2015**.

12. Zenasni, O.; **Marquez, M. D.**; Lee, T. R. Probing the Effect of the HC-FC Dipole on the Properties of Thin Films Formed from Hydrocarbon-Terminated Perfluorinated Alkanethiols. Oral presentation at the 249th ACS National Meeting & Exposition, Denver, CO, **2015**.

13. Zenasni, O.; **Marquez, M. D.**; Lee, T. R. Alkyl –Capped Partially Fluorinated Alkanethiols: Unique Adsorbates for Generating Self –Assembled Monolayers on Gold Poster presentation at the 247th ACS National Meeting & Exposition, Dallas, TX, **2014**.

14. Zenasni, O.; **Marquez, M. D.**; Lee, T. R. Synthesis of Unique Adsorbates for the Preparation of Self –Assembled Monolayers Having an Inverted Surface Dipole. Poster presentation at the 247th ACS National Meeting & Exposition, Dallas, TX, **2014**.

15. Singh, A.; **Marquez, M**.; Piemonte, R.; Madsen, L. A.; Robertson, M. L. Structure and Dynamics of Block Copolymer Micelles in the Presence of Co-Solvents. Poster presentation at the 247th ACS National Meeting & Exposition, Dallas, TX, **2014**.

16. Singh, A.; **Marquez, M. D.**; Robertson, M. L. Dynamic Processes in Diblock Copolymer Micelles with a Semi –Crystalline Core. Poster presentation at the 245th ACS National Meeting & Exposition, New Orleans, LA, **2013**.